GENOME-WIDE ANALYSIS OF ENDOCYTIC RECYCLING IN *S. CEREVISIAE*

by

Helen Elizabeth Burston

B.Sc.
Simon Fraser University, 2005

A THESIS SUBMITTED IN PARTIAL FULFILLMENT OF THE REQUIREMENTS FOR THE DEGREE OF

DOCTOR OF PHILOSOPHY

in

The Faculty of Graduate Studies

(Medical Genetics)

THE UNIVERSITY OF BRITISH COLUMBIA
(Vancouver)

July 2011

ABSTRACT

The process of endocytic recycling, in which cell surface proteins are internalized and re-delivered to the plasma membrane, is essential in all eukaryotes for maintaining plasma membrane composition and regulating the surface levels of signaling receptors. The applicability of *Saccharomyces cerevisiae* as a model to study endocytic recycling is a subject of debate, as there appears to be critical differences between yeast and mammalian cells. For example, while clathrin and its adaptors are critical for uptake in mammals, they do not seem to be essential in yeast. Endocytic recycling has not been comprehensively studied on a genetic level in yeast, and only limited cargo have been considered, making it difficult to accurately assess the similarity between the two systems. Furthermore, the transport of SNARE proteins is poorly understood, but appears to involve specialized mechanisms. This study uses a genome-wide screening approach to systematically and quantitatively identify genes required for the endocytic recycling of the yeast SNARE protein Snc1, homologous to the mammalian VAMP2/synaptobrevin.

Endocytic defects for mutants of many yeast homologs of mammalian endocytosis genes were identified, for the first time. Significantly, a cargo-selective and partially-redundant role for clathrin and its adaptors yAP1801 and yAP1802 was identified. The lipid phosphatase Inp52 was found to mediate AP180 release from endocytic vesicles. Additionally, the previously uncharacterized protein Ldb17, homologous to the mammalian endocytic protein SPIN90, was identified as a new component of the endocytic machinery, and regulates both coat and actin dynamics at endocytic sites.

Factors regulating Snc1 recycling were also identified, including the variant clathrin adaptor AP-1R. This is the first reported function for this complex. The previously uncharacterized protein Ima1 was found to be a putative enzyme that specifically binds to AP-1R, and may have activity related to AP-1R function.

Overall, this study demonstrates that endocytic recycling in yeast and mammals is more similar than previously appreciated, and identifies new factors in this process. Furthermore, it raises awareness of the degree of cargo-selectivity underlying this pathway, and demonstrates quantitative methods that can be further applied to future studies in both systems.

PREFACE

List of publications generated from work presented in this dissertation:

1. CHAPTER 2:

Burston HE, Maldonado-Báez L, Davey M, Montpetit B, Schluter C, Wendland B, and Conibear E. (2009) Regulators of Yeast Endocytosis Identified by Systematic Quantitative Analysis. Journal of Cell Biology. 185(6):1097-110.
A re-formatted version of this publication is included as chapter 2.

Contributions
I was responsible for the writing of the manuscript, all experiments and data analysis, with the exception of the following:

The primary, E-Mapping, and cargo-specificity screens for Invertase activity were carried out by Michael Davey (Conibear lab). Data resulting from these screens were analyzed by Elizabeth Conibear, in collaboration with Jochen Brumm and Jenny Bryan (University of British Columbia).

Figure 2.7 (A-F, H) and **Figure A2 (A-D)**: Live cell microscopy and TIRF analysis were carried out by Lymarie Maldonado-Báez and Beverly Wendland (Johns Hopkins University)

Figure A2 (E, G, and H): Co-immunoprecipitations and Yeast-two-hybrid analyses were carried out by Benjamin Montpetit (University of Berkley)

2. CHAPTER 3:
Burston HE, Tam C, Davey M, Raghuram N, Maldonado-Báez L, Wendland B, and Conibear E. (2010). The Alternate AP-1R Clathrin Adaptor Mediates Snc1 Endocytic Recycling. ***A re-formatted version of this manuscript (in preparation) is included as chapter 3.***

Contributions

I was responsible for the writing of this manuscript, and for the design, implementation, and analyses of all experiments, with the following exceptions:

Figure 3.1 (B): live cell imaging and TIRF analysis was carried out by Lymarie Maldonado-Báez and Beverly Wendland (Johns Hopkins University)

Figure 3.3 (B, C): Co-immunoprecipitations were carried out by Chris Tam (University of British Columbia)

Figure 3.3 (D) and **3.5 (D)**: Yeast-two-hybrid experiments and Invertase assays were carried out by Nandini Raghuram (University of British Columbia)

TABLE OF CONTENTS

ABSTRACT ii
PREFACE iii
TABLE OF CONTENTS v
LIST OF TABLES viii
LIST OF FIGURES ix
LIST OF ILLUSTRATIONS x
LIST OF SYMBOLS AND ABBREVIATIONS xi
ACKNOWLEDGEMENTS xiii
DEDICATION xiv
CHAPTER 1. INTRODUCTION AND LITERATURE REVIEW 1
1.1. Foreward: Membrane protein transport in the endosomal system 2
1.1.1. Endocytic trafficking in cellular function and human disease 2
1.1.2. Overview of intracellular transport and the regulation of vesicle formation 3
1.1.2. Markers of organelle identity and the specificity of vesicular transport 4
1.1.4. Coat proteins mediate vesicle formation 6
1.2. Clathrin adaptors are key regulators of cellular transport 8
1.2.1. Heterotetrameric clathrin adaptors: structure and function 8
1.2.2. Physiological importance of clathrin adaptors 9
1.2.3. Recruitment and un-coating of AP complexes: membrane phospholipids 9
1.2.4. AP appendage domains interact with multiple regulators 10
1.2.5. Mechanisms of AP cargo recognition 11
1.2.6. Non-canonical cargo sorting signals are recognized by CLASPS 12
1.3. Transport of SNARE proteins 13
1.3.1. Alternative sorting mechanisms regulate SNARE transport 13
1.3.2. What is the role of palmitoylation in SNARE transport? 14
1.4. Endocytosis and endocytic recycling pathways 15
1.4.1. Yeast as a model for endocytic recycling 15
1.4.2. Do yeast and mammals share common mechanisms of endocytosis? 16
1.4.3. A comparison of the endosomal system in yeast and mammalian cells 17
1.5. Yeast functional genomics: a tool to dissect trafficking pathways 19
1.5.1. Systems biology approaches to study membrane transport 19
1.5.2. Phenotypic screening in yeast to identify transport components 21
1.6. Research objectives and hypotheses 22
1.6.1. A new approach for identifying endocytic recycling components in yeast 22
1.7. Illustrations 24

CHAPTER 2. REGULATORS OF YEAST ENDOCYTOSIS IDENTIFIED BY SYSTEMATIC QUANTITATIVE ANALYSIS. 27
2.2. Introduction 28
2.3. Results 30
2.3.1. A Snc1-based quantitative assay for endocytic recycling 30
2.3.2. Genetic interaction mapping clusters functionally related genes 31
2.3.3. Integration of genetic and physical interaction data identifies complexes required for Snc1 transport 32
2.3.4. Clathrin and clathrin assembly proteins are required for Snc1 endocytosis 33
2.3.5. Systematic analysis of cargo specificity 34
2.3.6. Ldb17 is a new regulator of yeast endocytosis that is transiently recruited to cortical patches 35
2.3.8. Aberrant actin distribution in LDB17 mutants 37
2.4. Discussion 37
2.4.1. Role for clathrin adaptors in yeast endocytosis 38
2.4.2. Identification of novel components of the yeast endocytic machinery 39
2.5. Materials and methods 40
2.6. Figures and Tables 44
CHAPTER 3: THE YEAST VARIANT AP-1R CLATHRIN ADAPTOR AND IMA1 ARE REQUIRED FOR SNC1 ENDOCYTIC RECYCLING[1] 53
3.1. Synopsis 54
3.2. Introduction 54
3.3. Results 56
3.3.1. A role for the variant AP-1R complex in endocytic recycling 56
3.3.2. AP-1R mediates intracellular recycling 57
3.3.3. AP-1R and Ima1 localize to Golgi/endosomal compartments 57
3.3.4. Ima1 and AP-1R are not required for the transport of AP-1-dependent cargo 58
3.3.5. Ima1 specifically binds the AP-1R C-terminal domain 59
3.3.6. Ima1 is not required for AP-1R recruitment or interaction with cargo 60
3.3.7. Ima1 is a conserved protein with a consensus α/β hydrolase catalytic motif 61
3.3.8. The Ima1 GXSXG catalytic motif is required for normal Snc1 surface levels 62
3.4. Discussion 63
3.4.1. AP-1R mediates Snc1 intracellular recycling 63
3.4.2. Apm2 binds to Snc1 as cargo 63
3.4.3. Distinct sorting functions for AP-1/AP-1R 64
3.4.4. AP-1/AP-1R localize to similar intracellular compartments 65
3.4.5. Role of Ima1 in AP-1R regulation 65
3.4.6. Ima1 has putative enzymatic activity 67

3.5. Materials and methods 68
3.6. Figures 73
CHAPTER 4: DISCUSSION AND FUTURE DIRECTIONS 81
4.1. Overview 82
4.2.1. Role of clathrin and yeast AP180 homologs in Snc1 endocytosis 83
4.2.2. How is yAP180 recruited to endocytic sites? 83
4.2.3. Role of synaptojanin in yAP180 vesicle un-coating 85
4.2.4. How does yAP180 recognize Snc1 for internalization? 87
4.2.5. Does AP-2 mediate endocytosis in yeast? 88
4.2.6. Role of actin and its regulators in Snc1 internalization 89
4.3. Regulators of Snc1 recycling: AP-1R and Ima1 91
4.3.1. What is the role of AP-1R in Golgi/endosomal recycling? 91
4.3.2. What is the Snc1 recycling signal recognized by AP-1R? 94
4.3.3. How do AP-1 and AP-1R regulate distinct sorting pathways? 95
4.3.4. Do AP-1 and AP-1R localize to different lipid domains? 96
4.3.5. Ima1 is a putative enzyme and binds the Apm2 C-terminal domain 97
4.3.6. Is Ima1 important for the generation of lipids required for AP-1R function? 100
4.3.7. Determination of Ima1 substrates 100
4.3.8. Investigating the role of TMC04 in higher cells 101
4.4. Genetic interaction profiling to identify complexes and pathways required for Snc1 transport 102
4.4.1. Phenotypic profiling and the construction of genetic interaction networks 102
4.4.2. Endocytic processes are part of a broader cellular context 104
4.4.3. Assessing the role of essential genes in Snc1 transport 105
4.4.4. Relationships between endocytic recycling factors; implications in disease 106
4.4.5. Future perspectives 107
4.4. Illustrations 109
BIBLIOGRAPHY 111
APPENDIX A: Supplemental material for chapter 2 130
APPENDIX B: Supplemental material (chapter 3) 221

LIST OF TABLES

Table 2.1. Predicted yeast endocytic genes identified in the screen..... 45
Table A1. Plasmids and yeast strains used in this study.....130
Table A2. Full list of mutants with cell surface GSS levels greater to or equal to the median value for all strains.....162
Table B.1. Plasmids and yeast strains used in this study.....221

LIST OF FIGURES

Figure 2.1. Genome-wide screen for endocytic recycling mutants..... 44
Figure 2.2. Endocytosis mutants have related genetic interaction profiles..... 46
Figure 2.3. Integration of genome-wide genetic and physical interaction data identifies pathways and complexes..... 47
Figure 2.4. Yeast AP180 homologs have a conserved role in Snc1 internalization..... 48
Figure 2.5. Cargo sorting defects of yap1801Δ yap1802Δ mutants..... 49
Figure 2.6. Cargo specificity of genes required for Snc1 endocytosis..... 50
Figure 2.7. Ldb17 is required for proper coat and actin dynamics..... 51
Figure 3.1. AP-1R is required for correct sorting of Snc1..... 73
Figure 3.2. AP-1R and Ima1 localize to Golgi and endosomal compartments..... 74
Figure 3.3. Ima1 associates functionally and physically with AP-1R..... 75
Figure 3.4. Ima1 is not required for Apm2 membrane recruitment or cargo binding..... 77
Figure 3.5. Ima1 contains putative catalytic residues, required for Snc1 sorting..... 78
Figure 3.6. Overexpression of Ima1 does not affect Snc1 palmitoylation..... 80
Figure A1. Full hierarchical clustering of the genetic interaction data..... 218
Figure A2. Characterization of LDB17 mutants and identification of Ldb17-interacting proteins..... 219

LIST OF ILLUSTRATIONS

Illustration 1.1. Intracellular compartments and transport pathways. 24
Illustration 1.2. Steps in clathrin-coated vesicle formation and transport. 25
Illustration 1.3. Clathrin Adaptor (AP) structure 26
Illustration 1.4. Comparison of endocytic recycling compartments and pathways in yeast and mammalian cells. 26
Illustration 4.1. New factors required for Snc1 endocytic recycling. 109
Illustration 4.2. AP-1R transport function: Model 1 110
Illustration 4.3. AP-1R transport function: Model 2 110

LIST OF SYMBOLS AND ABBREVIATIONS

AAK1	Adaptor-associated kinase 1
ABE	Acyl-biotin exchange
ABPP	Activity-based protein profiling
AD	Alzheimer's disease
ALP	Alkaline phosphatase
ANTH	AP180 Amino-terminal homology domain
AP	Adaptor Protein
AP-1R	AP-1 related
APP	Amyloid precursor protein
ARF	ADP Ribosylation Factor
ARH	Autosomal recessive hypercholesterolemia
BAR	Bin/Amphiphysin/Rvs domain
BFA	Brefeldin A
CCV	Clathrin-coated vesicle
CLASP	Clathrin-associated sorting protein
CPY	Carboxypeptidase Y
DAB2	Disabled2
DEP	Dishevelled, egl-10, and pleckstrin domain
DUF	Domain of unknown function
Dvl	Dishevelled
E-Map	Epistatic miniarray profiling
EGF	Epidermal growth factor
EH	Eps15 homology domain
ENTH	Epsin amino terminal homology domain
ER	Endoplasmic reticulum
ERC	Endocytic recycling compartment
ESCRT	Endosomal sorting required for transport
FP	Fluorophosphonate
GAE	Gamma-adaptin ear domain
GAP	GTPase-activating protein
GAT	GGA and tom1 domain
GDP	Guanosine di-phosphate
GEF	Guanine nucleotide exchange factor
GGA	Golgi-localized, gamma-ear containing, ARF-binding
GLUT4	Insulin-sensitive glucose transporter 4
GPCR	G Protein-coupled receptor
GSS	GFP-Snc1-Suc2
GTP	Guanosine triphosphate
HD	Huntington's disease
Hip1/Hip1R	Huntington interacting/Huntington interacting-related protein
HPS	Hermansky Pudlak syndrome
Ima1	Interacts with μ adaptin 1
LacZ	β-galactosidase
LatA	Latrunculin A
LBPA	Lysobisphosphatidic acid
MVB	Multivesicular body
NGSS	3x NPFxD-GFP-Sso1-Suc2

NPF	Nucleation promoting factor
PA	Phosphatidic acid
PC	Phosphatidylcholine
PE	Phosphatidylethanolamine
PH	Pleckstrin homology domain
PIPK	Phosphatidylinositol phosphate kinase
PLD	phospholipase D
PRD	Proline-rich domain
PS	Phosphatidylserine
Ptb	Phosphotyrosine-binding domain
PX	Phox homology domain
RNAi	RNA interference
SH3	SRC homology domain
SNARE	Soluble NSF attachment protein receptor
SNC1	Suppressor of the Null allele of CAP 1
SORL1	Sortilin-related receptor 1
TfR	Transferrin receptor
TGN	Trans-Golgi network
TMCO4	Transmembrane and coiled-coil domain 4
TS	Temperature-sensitive
VAMP	Vesicle-associated membrane protein
VHS	Vps-27, Hrs and STAM domain
VPS	Vacuolar protein sorting
WASP	Wiskott-Aldrich syndrome protein
Y2H	Yeast two-hybrid

ACKNOWLEDGEMENTS

First, and foremost, I extend my greatest gratitude to Dr. Elizabeth Conibear. Throughout my degree, Liz has been a constant source of support, guidance, and friendship. Her wisdom and unrelenting enthusiasm is truly inspirational, and she is, and will always be my ultimate mentor.

I am grateful to my colleagues in the Conibear lab, past and present. They have offered support, guidance, and expertise during the course of this work, and it would not have been possible without them. I would like to thank Mike Davey and Cayetana Schluter for their assistance in the design and implementation of many experiments, and for countless helpful discussions. I would also like to thank Benjamin Montpetit, Chris Tam, and Nicole Quenneville for their ongoing advice, encouragement, and career mentorship, and Karen Lam for her support, and for the critical reading of this dissertation. I am also amazed by the talent of the two undergraduate students, whom I had the opportunity to supervise during my degree. Thank you to Nandini Raghuram and Sarah Konefal for your incredible work ethic and enthusiasm.

I would also like to thank our collaborators, Dr. Beverly Wendland and Dr. Lymarie Maldonado-Báez, who have been instrumental in the work presented here. Dr. Nick Davis and Dr. Amy Roth have also contributed many insights and have aided in the development of experimental approaches.

I extend my gratitude to my graduate committee: Dr. Michael Kobor, Dr. Phil Hieter, and Dr. Pamela Hoodless, for their ongoing support and advice, and for the critical reading of this dissertation.

Finally, I would like to thank NSERC and the Michael Smith Foundation for providing generous financial contributions.

DEDICATION

To my family and the many people whom have helped me along the way. Thank you for your support and encouragement.

CHAPTER 1. INTRODUCTION AND LITERATURE REVIEW

1.1. Foreward: Membrane protein transport in the endosomal system

1.1.1. Endocytic trafficking in cellular function and human disease

In every eukaryotic cell, proteins are directed to the appropriate location by membrane transport pathways. These pathways facilitate communication within the cell, and between the cell and its environment, maintaining cell homeostasis and function (Schu, 2001; Van Vliet et al., 2003). Endocytosis allows cells to internalize extracellular material, ligands, and plasma membrane proteins. This removal of membrane from the cell surface by endocytosis is balanced by recycling pathways that return many of these proteins and lipids back to the plasma membrane. These endocytic recycling pathways control the composition of the plasma membrane and contribute to diverse cellular processes, including nutrient uptake, cell adhesion and junction formation, cell migration, cytokinesis, cell polarity, and signal transduction (Jovic et al., 2010; Grant and Donaldson, 2009).

Many human diseases caused by changes in cellular homeostasis arise through compromised membrane trafficking within the endosomal system (Howell et al., 2006; Aridor and Hannan, 2000 and 2002). Endocytosis has a major role in neuronal function, as it is required for synaptic vesicle (SV) recycling within the pre-synaptic compartment (Jung and Haucke, 2007; Girard et al., 2005). It also regulates the activity-dependent exo-endocytic trafficking of postsynaptic receptors, allowing for the fine-tuning of signal strength during neurotransmission and plasticity-associated changes, uptake of growth factors in the pre-synapse, and sculpting of synaptic structure (Sheng and Kim, 2002; Dickman et al., 2006). Disturbance of trafficking is implicated in severe neurodegenerative disorders like Alzheimer's disease (AD), which is characterized by deposition of amyloid β (Aβ) plaques in the brain (reviewed in Mayeux and Hyslop, 2008; Selkoe, 2001). Endosomes appear to be one of the major sites of Aβ generation and several reports indicate that altered endocytic trafficking may play role in development of AD. For instance, the neuronal sortilin-related receptor SORL1 directs trafficking of amyloid precursor protein into recycling pathways and prevents it from accumulating in the compartments generating Aβ (Andersen et al., 2005; Shah and Yu, 2006). Mutations in SORL1 are associated with both inherited and sporadic cases of Alzheimer's disease (Mayeux and Hyslop, 2008). Impaired trafficking has also been shown to contribute to the pathogenesis of Huntington's disease (HD). HD is characterized by the mutant protein huntingtin, which

aggregates and affects membrane trafficking in neurons, leading to neurodegenerative changes (Berman and Greenamyre, 2006; Caviston and Holzbaur, 2009). Abnormal trafficking of the insulin-sensitive glucose transporter GLUT4 has been identified as a possible mechanism of disease in patients with type 2 diabetes. In some of these patients, GLUT4 accumulates in dense membrane compartments, suggesting that defects in GLUT4 membrane trafficking may be involved in the pathogenesis of insulin resistance (Bouché et al., 2004; Karylowski et al., 2004).

Membrane traffic is also intimately connected to infection and immunity. Viruses and bacteria often use the endocytic pathway of host cells for invasion (Mercer et al., 2010; Lin and Guttman, 2010). In addition, large DNA viruses such as adenovirus, herpes simplex virus, Epstein-Barr virus, and cytomegalovirus have evolved sophisticated mechanisms to evade host immune surveillance by perturbing the membrane traffic of host cells, thereby preventing antigen presentation of their own products (Ohno, 2006; Ohmura-Hoshino et al., 2006).

Despite the importance of these pathways, the molecular mechanisms governing their function remain poorly understood. A better understanding membrane transport is therefore crucial for our understanding of human disease, and the development of targeted treatments.

1.1.2. Overview of intracellular transport and the regulation of vesicle formation

The secretory and endocytic pathways of eukaryotic cells connect membrane-bound organelles, whose primary function is to modify newly-synthesized proteins and deliver them to the appropriate location, and to regulate the uptake and turnover of cell surface proteins (Munro, 2004; van Vliet et al., 2003). Each of these organelles is functionally specialized, and contains a unique composition of proteins and lipids pertinent to its function (Munro, 2004). Vesicular transport pathways are essential for maintaining organelle composition and identity. The transport of cellular material between organelles is highly organized and regulated. A large number of factors ensure that each protein is accurately delivered to its appropriate location, thus preventing the inappropriate mixing of cellular compartments.

The main compartments of the secretory and endocytic pathway are the endoplasmic reticulum (ER), Golgi apparatus, plasma membrane, and endosomal compartments (Illustration 1.1). Following delivery to the cell surface, proteins are internalized by endocytosis, and reach early endosomes, where they are then either recycled back to the

cell surface directly or by retrograde transport through the TGN, or targeted for degradation in the vacuole (Munro, 2004). Recycling of cell surface proteins is essential in all organisms to maintain the composition of the plasma membrane, by balancing the removal of proteins by endocytosis. This process, called endocytic recycling is the focus of this dissertation.

Proteins are transported as 'cargo' within membrane-bound vesicles, which shuttle them between organelles. The selective incorporation of cargo into forming vesicles is mediated by protein coats, which are assemblies of proteins that are recruited from the cytosol. Vesicle coats recognize various components of the target membrane, including sorting signals present in the cytosolic domain of cargo proteins. Transport between each compartment is mediated by distinct sets of coats and sorting signals, which confer specificity to these pathways (Bonifacino and Lippincott-Schwartz, 2003). The steps of cargo recognition and vesicle formation will be described in more detail below.

1.1.2. Markers of organelle identity and the specificity of vesicular transport

Vesicle transport is a precise process that requires the specific recognition of cellular membranes by components of the trafficking machinery. How do these components ''know'' how to reach a particular cellular destination? Most internal organelles have 'signposts' of identity to distinguish them from other organelles. The main components specifying organelle identity include specific GTPases of the Rab/Arf family, SNARE proteins, and membrane lipids (Reviewed in Behnia and Munro, 2005).

GTPases

The small GTPases of the Rab/Arf family are molecular switches that can alternate between a membrane-associated GTP-bound active form and a cytosolic GDP-bound inactive form. The activity of these GTPases is controlled by proteins that regulate their GDP/GTP cycle. These include guanine nucleotide exchange factors (GEFs), which replace GDP by GTP, and GTPase-activating proteins (GAPs), which stimulate GTP hydrolysis. There are more than 60 different Rabs in mammalian cells, and fewer in lower eukaryotes. Each organelle is enriched for a particular subset of these Rabs (Segev, 2010; Pereira-Leal and Seabra, 2001). Regulatory GEFs/GAPs also show a restricted distribution, which increases the functional specificity of their cognate GTPases by allowing specific and rapid control of their activity at these compartments (Kawasaki et al., 2005; Itzen and Goody, 2010).

Membrane phospholipids

Phosphoinositide phospholipids (PIs) are also enriched on one or a small subset of organelles. PI(4,5)P_2 is enriched at the plasma membrane, PI3P at endosomal compartments, PI(3,5)P_2 at the vacuole, and PI4P at the Golgi. Much like GTPases, localized synthesis and turnover of these lipids is regulated by specific factors, namely PI kinases and phosphatases, which are also spatially restricted to a subset of organelles. This ensures that the steady state concentration of each PI species varies between organelles. Many components of the vesicle coat have domains that recognize these PI species. These domains include pleckstrin homology (PH), phox homology (PX), epsin amino terminal homology (ENTH) and AP180 amino-terminal holomology (ANTH) domains (Reviewed in De Matteis and Godi, 2004).

SNARE proteins

The selectivity of membrane transport is also provided in part by SNARE proteins, which catalyze the fusion of the opposing membranes of the vesicle and target membrane. Functionally, SNAREs are classified into v-SNAREs, which associate with the vesicle, and t-SNAREs, which are present on the target compartment. Specific interaction between v-SNAREs on an incoming transport vesicle with t-SNAREs on the target membrane is the central event of the docking and fusion process (Pelham, 2001). As each SNARE is restricted to a subset of specific compartments, SNAREs contribute to the specificity of the fusion process. There are 25 members of this family in *S. cerevisiae* and 36 in *Homo sapiens*, most of which are small membrane proteins (Pelham, 2001; Hong, 2005)).

The major, N-terminal portion of the SNARE protein is exposed in the cytoplasm, followed by a single membrane-spanning region and a few amino acids that face either the lumen of an intracellular compartment or the extracellular space. The core feature of SNAREs is the evolutionarily conserved SNARE motif, which is present in all family members. During membrane fusion, SNAREs assemble into a four helical bundle via interactions between specific residues within their SNARE domains. SNAREs can also be classified based on the residue contributed to this interaction. While Q SNAREs contribute a glutamine residue to the core layer of the assembled complex, R SNAREs contribute an arginine residue. The assembly of SNARE motifs of cognate v- and t-SNAREs generates a trans-SNARE complex bridging two membranes, which brings the lipid bilayers in close proximity and drives membrane fusion. Following fusion, the v- and t-SNAREs are present

on the same membrane, and the complex is thus called a cis-SNARE complex. The cis-complex is dissembled by ATP-hydrolysis generated by the coordinated activity of two proteins: SNAP and NSF. The SNAREs are then returned to the donor membranes (Ungar and Hughson, 2003; Brunger, 2005)

In addition to SNAREs, tethering complexes have a major role in the specificity of vesicle fusion with the target membrane. Tethering factors are the initial connection, or tether, between an intracellular trafficking vesicle and its target membrane (Barlowe 1997, Cao et al., 1998). Tethering complexes recognize the features of both the originating upstream compartment and the downstream target compartment, including SNARE proteins of both compartments, as well as activated Rab proteins and phospholipids.

Coincidence detection

Individually, Rab/Arf GTPases, SNAREs and phosphoinositides are not sufficient to explain the degree of specificity achieved in vesicle transport. The precision of this process requires the simultaneous recognition of multiple determinants. Coat recruitment at the donor membrane is achieved through combinatorial recognition of an activated Arf GTPase, specific phospholipids, and cargo. Similarly, Rab, SNAREs and membrane lipids all contribute to tether recruitment and SNARE assembly at the target membrane. Hence, organelle identity is more precisely defined by the combination of these restricted components. The process by which the vesicular transport machinery recognizes multiple determinants at a given membrane is often referred to in the literature as 'coincidence detection' (Carlton and Cullen, 2005).

1.1.4. Coat proteins mediate vesicle formation

The biogenesis of transport vesicles is initiated through the recruitment of large multi-subunit protein complexes termed coats. These coats control both cargo selection and deformation of the lipid bilayer into a budding vesicle. There are three well-defined vesicle coats: COPI, COPII, and clathrin, each of which are involved in distinct transport pathways (Bonifacino and Lippincott-Schwartz, 2003; Kirchhausen, 2000). COPI mediates both intra-Golgi transport and retrograde transport from the Golgi to the ER, while COPII functions in anterograde ER to Golgi traffic. Clathrin was the first coat to be identified, and is the best characterized, both structurally and biochemically. Clathrin coats are considerably more complex than the COPI/COPII coats, as they participate in multiple post-Golgi transport pathways, including receptor-mediated endocytosis, and several sorting pathways between

the TGN and endosomes (Kirchhausen, 2000). To fulfill its role in each of these pathways, clathrin associates with an additional subset of regulatory proteins.

The clathrin-coated vesicle itself is a three-layered structure, consisting of an outer clathrin layer, an inner membrane layer and an adaptor protein layer sandwiched between the two (Brodsky et al., 2001; Edeling et al., 2006). Clathrin is a large hetero-hexameric protein complex composed of three heavy chains and three light chains. Clathrin molecules self-assemble to make a spherical ''clathrin lattice'' structure, a polyhedron made of regular pentagons and hexagons. The clathrin lattice serves as a mechanical scaffold but is unable to bind directly to the membrane. Adaptor protein (AP) complexes are required for recruitment of clathrin. These complexes interact directly with components of the lipid bilayer, cargo, and clathrin, and thus link clathrin to the membrane and to the specific cargo to be transported (Robinson, 2004). Both clathrin and its adaptors interact with many additional regulatory components.

The formation and delivery of clathrin-coated vesicles is divided into 5 major steps: initiation, coated pit formation, vesicle budding, uncoating, and vesicle fusion (Illustration 1.2, Ritter and Wendland, 2009; Ungewickell and Hinrichsen, 2007). Initiation is thought to begin by the recruitment of APs to specific membrane domains where they recruit cargo proteins. Clathrin then binds to these docked AP/cargo complexes, and polymerizes to form the coat. Further stabilization of the budding site is achieved through enhanced affinity of APs with membrane and cargo, and the recruitment of accessory proteins. As clathrin polymerizes, accessory proteins that include BAR (Bin/amphiphysin/Rvs) domain-containing proteins, such as amphiphysin and endophilin, promote the membrane curvature required for vesicle budding. The crescent-shaped BAR domain has a highly positively charged concave surface, contributing to electrostatic interactions that aid membrane deformation. Further deformation of the membrane and polymerization of clathrin leads to a coated vesicle attached to the plasma membrane by a narrow neck, which pinches off to form a free coated vesicle. Once the vesicle is formed, the clathrin coat is removed. This allows the vesicle to fuse with its target membrane and deliver its cargo, and ensures that coat proteins are returned to the soluble pool to initiate new rounds of coat assembly (Ritter and Wendland, 2009).

1.2. Clathrin adaptors are key regulators of cellular transport

1.2.1. Heterotetrameric clathrin adaptors: structure and function

There are three main AP complexes (AP-1, AP-2, and AP-3) in most organisms, including yeast, while higher organisms also have AP-4. Each of these complexes regulates distinct vesicle transport pathways, localizes to different compartments, and binds distinct sets of cargo (Boehm and Bonifacino, 2002). AP-2 mediates the formation of endocytic CCVs from the plasma membrane. AP-1 regulates transport between the TGN and endosomes, although it is not clear in which direction it operates. AP-3 traffics cargo from the TGN to the yeast vacuole, or the mammalian lysosome, and is involved in the biogenesis of lysosome-like organelles. The function of AP-4 is not well understood, but it appears to be involved in TGN to endosome trafficking (Robinson, 2004).

All APs share a similar hetero-tetrameric structure, consisting of two large subunits of 100–130 kDa (β and one of either α, γ, δ, or ε), a medium-sized subunit of ~50 kDa (μ1–4 in AP1–4, respectively) and a small subunit of ~20 kDa (σ1–4 in AP1–4, respectively), (Illustration 1.3). The large subunits are divided into an N-terminal core domain, which assembles with the medium and small subunits, and a C-terminal appendage domain, which is connected to the core by an unstructured hinge. Each subunit and domain mediates distinct sets of regulated interactions pertinent to AP function. The core domain of the large subunits (α, γ, δ, and ε) is required for binding to the target membrane. The other large subunit (β) contains a clathrin box within its hinge, and is required for the recruitment of clathrin. The medium (μ) subunits have a direct role in the recognition of cargo sorting signals, while the small (σ) subunit is mainly involved in complex stability. Together with regions of the large subunits, the small subunits also bind to cargo sorting signals that are distinct from those recognized by the medium subunit. Interactions between APs and their binding partners are dynamic, weak, and under strict spatiotemporal control, ensuring that vesicles form at the correct time and place, and can be rapidly disassembled once the vesicle has formed (Owen et al., 2004).

Some AP complexes can exist as different isoforms that have different sorting functions. Exchange of the large, medium, and small subunits are all observed in mammals (Owen et al., 2004; Nakatsu and Ohno, 2003). Mammals have two isoforms of both AP-1 and AP-3, which differ by the inclusion of an alternate medium subunit. These are expressed in a cell-type specific manner. AP-3B is expressed exclusively in neurons, and is involved in synaptic vesicle biogenesis (Newell-Litwa et al., 2009). AP-1B is expressed only in polarized

epithelial cells, and mediates sorting to the basolateral membrane (Traub and Apodaca, 2003). From these studies, it is clear that exchange of the medium subunit can dramatically affect the sorting function of each complex. Two isoforms of the AP-1 complex also exist in yeast, containing the alternate medium subunits Apm1 or Apm2. While the Apm1-containing complex has a well-established role in the clathrin-mediated sorting of the Chitin synthase Chs3 and the α-factor modification enzyme Ste13 between the endosomes and Golgi (Valdivia et al, 2002; Foote and Nothwehr, 2006), no role has been established for the alternate Apm2-containing complex (Stepp et al., 1995).

1.2.2. Physiological importance of clathrin adaptors

The physiological importance of AP complexes is illustrated by studies in multiple organisms. Knockout of AP-1A or AP-2 results in embryonic lethality in *C. elegans* and mice, indicating that they are essential for normal development (Ohno, 2006). Mutations in AP-3A underlie the autosomal recessive disorder Hermansky-Pudlak syndrome 2 (Dell'Angelica et al., 1999). This disease is characterized by defective transport to lysosome-related organelles, including melanosomes and platelet dense granules, and results in clinical features including albinism, platelet storage pool deficiency, defective immune function, and bleeding defects (Huizing and Gahl, 2002 and Huizing et al., 2002). In mice, knockout of the neuronal-specific AP-3B causes epileptic seizures and neurotransmission defects, as a result of mis-regulation of synaptic vesicle formation (Nakatsu et al., 2004; Seong et al., 2005). In addition to demonstrating the critical role of APs, these studies illustrate that different phenotypic consequences can result from deficiency of closely related AP isoforms. The physiological importance of AP complexes has driven considerable research into their function. The mechanisms regulating AP membrane recruitment, cargo recognition, and un-coating are described below.

1.2.3. Recruitment and un-coating of AP complexes: membrane phospholipids

Interaction with membrane phospholipids appears to be an early event in the recruitment and activation of APs at their target membranes. Accordingly, the control of phosphoinositide levels by kinases and phosphatases is important in regulating AP recruitment and uncoating (Edeling et al., 2006). For example, higher rates of endocytic internalization by AP2 are associated with increased levels of $PI(4,5)P_2$, caused by overexpression of the type I phosphatidylinositol 4-phosphate 5-kinase h (PIP5KIh) (Krauss et al., 2006) . There is a good correlation between $PI(4,5)P_2$ levels, association of AP-2 with

the cell surface, and the number of clathrin coated structures (Gaidarov and Keen, 1999; Padrón et al., 2003;) Conversely, synaptojanin 1, which hydrolyses PtdIns(4,5)P_2 to PtdIns(4)P, promotes the dissociation of AP-2 from the membrane of CCVs following budding. In mice knockout studies, the absence of synaptojanin 1 leads to 100% mortality within 2 weeks of birth, elevated steady-state levels of PI(4,5)P_2, an increased number of clathrin-coated vesicles in presynaptic terminals, and increased synaptic depression in hippocampal slices (Cremona et al., 1999). The Golgi contains the main cellular pool of PI(4)P, generated by the phosphorylation of PtdIns by the type II alpha phosphatidylinsositol 4-kinase PI4KII (D'Angelo et al., 2008). In both yeast and mammalian cells, PI4KII homologs are involved in sorting at the late Golgi (De Matteis and D'Angelo, 2007). AP-1 has been shown to bind directly to PI(4)P in mammalian cells, and reduction of PI(4)P levels results in the redistribution of AP-1 from Golgi compartments to the cytosol (Wang et al., 2003).

1.2.4. AP appendage domains interact with multiple regulators

The appendage domains of the large AP subunits serve as a major interaction hub for various regulatory proteins that help drive rapid assembly of AP-containing vesicles and aid in cargo recognition. These proteins, called "accessory" factors, fall into three categories: regulatory proteins, mechanical/assembly proteins, and alternate adaptors (Traub, 2005). Examples of regulatory proteins include the kinases AAK1, and GAK, which phosphorylate the μ subunit of AP-2 and AP-1, respectively. These phosphorylation events are required for productive association of AP-1 and AP-2 with cargo.

Mechanical/assembly proteins act during and after cargo recognition to synchronize interactions between adaptors and other components of the vesicle formation machinery, and may also contribute directly to the vesicle budding event. Although there seem to be multiple mechanisms involved, interaction of clathrin with these proteins appears to increase the intrinsic curvature and rigidity of coated vesicles at the membrane. Many of these proteins are lipid-binding proteins that contribute to membrane deformation (Lundmark and Carlsson, 2010). A well-studied example is epsin, an ENTH domain protein, which inserts a hydrophobic helix into the membrane, leading to membrane curvature (Horvath et al., 2007). Proteins containing BAR domains facilitate the membrane bending required at late stages of vesicle formation. These include amphiphysin1 and Sorting nexin 9 (SNX9) (Itoh and De Camilli, 2006).

Alternate sorting adaptors or CLASPs link a subset of cargo to AP complexes. Most

CLASPs identified to date interact with the AP appendage domain. Mechanisms of AP cargo recognition and the role of CLASPs are discussed below.

1.2.5. Mechanisms of AP cargo recognition

Most signals recognized by AP complexes consist of short, linear sequences of amino acid residues present in the cytosolic domain of cargo proteins. Two of the most widely-used and best understood signals conform to YXXΦ 'Tyrosine' motif (in which X represents any amino acid and Φ represents a large hydrophobic residue) and [D/E]XXXL[L/I] 'acidic dileucine' motif. All APs recognize YXXΦ motifs, and some additionally bind dileucine motifs (Heilker et al., 1999; Bonifacino and Traub, 2003). Examples of YXXΦ-containing cargo include mammalian LAMPs, the Transferrin receptor and CD63, and yeast Yck3 (Bonifacino and Traub, 2003; Sun et al., 2004). Dileucine-based cargo includes mammalian tyrosinase and GLUT4, and yeast ALP and Gap1 (Bonifacino and Traub, 2003).

The medium (μ) subunit of each AP interacts with a distinct but overlapping set of YXXΦ signals, as defined by deviation in the residues other than the critical tyrosine. This partially explains how each is able to recognize a different subset of YXXΦ-based cargo. The μ subunit is organized into two main domains, separated by a flexible linker. The N-terminal domain assembles with the core complex, while the C-terminal domain contains the YXXΦ binding site (Owen et al., 2004). The C-terminal domain is further divided into two β-sandwich subdomains (A and B). Subdomain A is folded to create a cargo-binding pocket. The critical Y and Φ residues fit into hydrophobic pockets on the surface of this domain, and binding is mediated through both hydrogen bonding and backbone interactions (Edeling et al., 2006, Brodsky et al., 2001). Structural studies have demonstrated that in order to efficiently bind cargo, the μ subunit undergoes a large-scale rearrangement relative to the rest of the complex. In the inactive form, the YXXΦ binding site on the μ subunit is occluded by interaction with the large subunit (closed form), and is freed from this occlusion by the movement of the C-terminal cargo binding domain (open form). This rearrangement occurs following binding of the complex to membrane lipids, and is stabilized by phosphorylation of a specific threonine residue within the unstructured linker of μ2 by the kinase AAK1, and by association with cargo. This complex rearrangement is thought to couple cargo binding to membrane attachment, therefore preventing inappropriate interactions the complex and cytosolic proteins (Jackson et al., 2010).

The dileucine signal is structurally distinct from the tyrosine-based signal, and binds to the AP complex in a unique manner. The interaction surface is primarily positioned on the small (σ) subunit. Similarly to the recognition of tyrosine-based signals by the μ subunit, interaction of dileucine-based signals requires a structural rearrangement of the complex. In this case, the binding site on the σ subunit is blocked by the large β subunit, which must shift to expose the binding site. This shift may be mediated through phosphorylation of a tyrosine residue on the β subunit, and is less dramatic than the large-scale movement of the μ subunit relative to the core. Dileucine-based peptides can engage in binding while the tyrosine binding site remains in a closed conformation (Huang et al., 2003).

It seems that cargo recognition is not a mandatory step in AP recruitment, as APs with mutated cargo binding sites still assemble into CCVS. Cargo binding has, however, been shown to enhance the membrane affinity of APs. It is likely that cargo capture occurs concomitantly with coat polymerization. The numerous simultaneous contacts that APs can establish with other factors and accessory proteins serve to explain how APs can associate with the membrane before binding to cargo. It also appears that cargo load is dynamically monitored in the forming vesicle by APs and their regulators, in order to prevent unproductive budding (Traub, 2009). For example, overexpression of the transferrin receptor (TfR), a well-studied AP-2 cargo, decreases the number buds that abort prior to formation or scission (Loerke et al., 2009).

1.2.6. Non-canonical cargo sorting signals are recognized by CLASPS

Not all cargo sorting motifs conform to the YXXΦ or [D/E]XXXL[L/I] based motif. In fact, there a broad range of alternative sorting signals. These include variants of the tyrosine and dileucine motifs, but can also involve various post-translational modifications, including phosphorylation or ubiquitination. These signals are not recognized directly by AP complexes, but by a family of AP-associated monomeric adaptors called clathrin-associated sorting proteins (CLASPs), which link APs to cargo containing these alternative signals. Although they share little overall sequence homology with APs, all have a clathrin-binding box, and/or AP interaction sequences that mediate interaction with the clathrin heavy chain and the AP appendage domain, and contain binding sites for membrane phospholipids (reviewed in Traub, 2009 and Maldonado-Baez and Wendland, 2006).

The phosphotyrosine-binding (Ptb) CLASPs, including β-arrestins, recognize [FY]XNPX[YF] signals. These mediate internalization of phosphorylated GPCR, by recruiting

activated receptors to pre-existing AP-2 containing endocytic pits. ARH and disabled2 (DAB2) recognize the tyrosine-based FXNPXY signal within the LDL receptor, and mediate its internalization. The epsin superfamily is another subset of CLASPs, which includes AP180/CALM, epsin1, and Hip1/Hip1R. Each of these has structurally related ENTH/ANTH domains, and primarily recognizes ubiquitylated cargo. These include the yeast epsin homologs Ent1 and Ent2, which mediate internalization of monoubiquitinated cargo, which is the primary internalization signal in yeast (Maldonado-Baez and Wendland, 2006).

Another family of Golgi regulatory adaptors is the Golgi-localized, gamma-ear containing, ARF-binding (GGA) proteins. There are two forms of Gga in yeast (Gga1 and Gga2), which are thought to be largely redundant, and three forms of Gga in mammalian cells, which may have unique sorting roles. These monomeric ubiquitously-expressed proteins have 4 modular domains (VHS, GAT, a hinge and GAE) that essentially recapitulate all of the functional attributes of AP-1 and AP-2. The VHS domain binds to DXXLL-type acidic cluster sorting signals in mammalian cells, and recognizes the receptor Vps10 in yeast. The GAT domain is required for membrane recruitment by activated Arf1 and PI4P at the Golgi, and interacts with ubiquitylated cargo. Clathrin binding is mediated by a variant of the clathrin box motif that is present in the hinge region of Gga. Finally, the GAE domain interacts with accessory proteins that are involved in cargo selection and membrane binding (reviewed in Ghosh and Kornfeld, 2004 and Bonifacino, 2004). Gga proteins are required for sorting of proteins, including the SNARE Pep12, from the Golgi to the late endosome (Black and Pelham, 2000).

The use of multiple adaptors provides plasticity to allow precise temporal control in the face of high traffic volumes, ensuring that cargo do not compete with each other for inclusion into coated vesicles (Sorkin, 2004; Traub, 2003). Alternate adaptors can be regulated to alter the sorting of individual cargo, without affecting the sorting of other cargo by the main AP complexes.

1.3. Transport of SNARE proteins

1.3.1. Alternative sorting mechanisms regulate SNARE transport

SNARE proteins are critical regulators of vesicle fusion. An important concept is that SNAREs themselves must be accurately transported in the cell. To ensure that a vesicle can fuse with its target membrane, sufficient amounts of the correct v-SNARE must be incorporated into a vesicle during formation, and its cognate t-SNARE must be correctly

sorted to its target membrane. Following fusion, SNAREs must also be recycled back to the donor compartment in order for fusion processes to continue (Miller et al., 2007). Some SNAREs interact with directly with AP complexes through canonical motifs, including the TGN-localized VAMP4, which binds to AP-1 through a dileucine-based signal (Peden et al., 2001). Most SNAREs, however, lack the canonical motifs recognized by adaptor proteins. Recent studies have demonstrated that SNARE sorting often involves recognition by unconventional adaptors, and novel methods of cargo interaction.

In both yeast and mammals, epsin family proteins interact with various SNAREs involved in the late endocytic pathway. In mammals, enthoprotin, also called epsinR (Wasiak et al., 2002) interacts with the Q- SNARES vti1b, syntaxin 7 and syntaxin 8, involved in late endosome/lysosome transport (Chidambaram et al., 2004 and 2008). The yeast epsinR homolog Ent3 binds the related SNAREs Vti1, Pep12 and Syn8, which participate in fusion with the late endosome (Chidambaram et al., 2004). The localization of Vti1 and Pep12 is dependent on Ent3 together with the partially redundant Ent5, indicating that the cargo-sorting function of Ent3 is conserved in yeast and extends to more than one SNARE (Chidambaram et al., 2008). The clathrin-mediated endocytic retrieval of VAMP7 from the plasma membrane requires the protein Hrb1 (HIV Rev-binding protein), (Pryor et al., 2008). Hrb1 is an ArfGAP, which binds both the AP-2 appendage domain and clathrin, demonstrating the properties of an alternate adaptor.

For SNAREs, the transport signal recognized by adaptors can consist of a folded epitope instead of a short cytosolic motif. The ENTH domain of EpsinR interacts with the N-terminus of vti1b via a conformational motif, which includes at least two turns and one helix of epsinR and amino acid residues from three helices of vti1b (Miller et al., 2007). VAMP7 binds Hrb1 through its N-terminal longin domain, a highly structured region of 120 amino acids (Pryor et al., 2008). These studies demonstrate that mechanistically novel interactions occur between given SNARE/adaptor pairs. These specific mechanisms may ensure that there is no competition between SNAREs and standard motif-containing cargo for inclusion in a nascent vesicle. This is important, as a vesicle must include both cargo and SNAREs to be productively delivered to the target membrane (Miller et al, 2007). As the proper sorting of SNAREs is critical to the integrity of essential transport processes, there is considerable interest in uncovering how they are recognized and transported.

1.3.2. What is the role of palmitoylation in SNARE transport?

Several SNARE proteins are post-translationally modified by palmitoylation, the

reversible addition of palmitate to a cysteine via thioesterification (Roth et al., 2006). SNAREs lacking transmembrane regions require palmitoylation for membrane anchoring (Dietrich et al., 2005; Veit et al., 1996). Many integral membrane SNAREs are also palmitoylated, but the functional consequences of these modifications are not clear (Roth et al., 2006). There is growing evidence that this could regulate the trafficking of these transmembrane SNAREs. For example, palmitoylation of the yeast SNARE Tlg1, which mediates endosome to Golgi transport, protects it from ubiquitination and subsequent degradation in the vacuole (Valdez-Taubas and Pelham, 2005). The mammalian endosomal SNARE syntaxin7 is also palmitoylated. While it normally localizes to early and late endosomes, preventing syntaxin7 palmitoylation leads to its accumulation on the cell surface (He and Linder, 2009). Several studies have highlighted regulatory effects of palmitoylation on either retention or anterograde trafficking of proteins at the ER–Golgi or protein cycling within the endosomal/lysosomal system (Linder and Deschenes, 2007; Greaves et al., 2009). Palmitoylation can also aid in the partitioning of proteins into cholesterol-rich membrane subdomains, and in changing protein orientation and thus affecting protein-protein interactions that could regulate trafficking (Linder and Deschenes, 2007).

The mechanisms by which palmitoylation regulates the dynamics of SNARE transport are an important unresolved issue in the field. It remains unclear if palmitoylation directly affects the recognition of SNAREs by components of the transport machinery, and whether the consequences of this modification are generally applicable to all SNARES.

1.4. Endocytosis and endocytic recycling pathways

1.4.1. Yeast as a model for endocytic recycling

The protein families that mediate vesicle trafficking are conserved from yeast to mammals, as is the compartmentalization throughout the cell from the endoplasmic reticulum to the plasma membrane. Yeast has therefore been used as a model for both genetic and biochemical analyses to study transport processes for decades (Bock et al., 2001). These studies have revealed that identifying the transport machinery and their pathway relationships in yeast can inform relationships between gene products in mammalian cells. Despite this, there do appear to be some important differences between transport in yeast and mammalian cells, especially in mechanisms regulating endocytosis

and recycling. The similarities and differences in these pathways, and possible explanations for these discrepancies are discussed below.

1.4.2. Do yeast and mammals share common mechanisms of endocytosis?

Elegant studies in both yeast and mammalian systems have revealed an intricate network of endocytic regulatory proteins, and have used novel methods to investigate their dynamics at endocytic sites. This has revealed that most components of the endocytic machinery are highly conserved from yeast to humans. These studies also show that actin polymerization has an important role in the endocytic process (Engqvist-Goldstein and Drubin, 2003). Most progress in defining the order and timing of endocytic internalization events has resulted from real-time, live cell fluorescence microscopy. A striking feature revealed by these studies is that proteins fall into discrete groups based on their dynamic relationship to clathrin-coated structures, which is also conserved in both mammalian cells and yeast (Kaksonen et al., 2005; Perrais and Merrifield, 2005).

In yeast, four protein modules cooperate to drive the distinct stages of endocytic vesicle formation, based on their dynamic localization. The early coat complex is the first to arrive which recruit cargo and establish the endocytic site. The late coat module is then recruited, followed by components of the actin polymerization machinery including the Arp2/3 complex and its activators. An actin network is formed by the Arp2/3 complex, which then drives the rapid internalization of the vesicle. Finally, the vesicle scission machinery pinches the vesicle off the membrane, and coat components are released (Kaksonen et al., 2005; Toret et al., 2008). Despite the similar timeline of recruitment of endocytic homologs in yeast and mammals, there appear to be some critical differences in their relative importance. The endocytic adaptor AP-2 is required for endocytosis in mammals, but appears to be dispensable for uptake in yeast. Targeted disruption of AP-2 is lethal in mammalian cells (Mitsunari et al., 2005), and has been shown to block the uptake of multiple cargo, including the transferrin receptor (Conner and Schmid, 2003), as well as a population of lysosome-associated membrane proteins that traffic via the plasma membrane (Janvier and Bonifacino, 2005). Yeast AP-2 deletion mutants, however, are viable, and have no defects in the internalization of commonly studied endocytic cargo, including Ste6 (Burston et al., 2009; Conibear, 2010).

Actin is an essential component of the cytoskeleton, and localizes to endocytic sites in both yeast and mammalian cells (Engqvist-Goldstein and Drubin, 2003). The importance of dynamic actin regulation in endocytic vesicle formation seems to differ between yeast and

mammals. In yeast, actin and actin-regulatory proteins are essential for this process. Treatment with inhibitors of actin polymerization, such as latrunculin, or deletion of actin-regulatory proteins blocks endocytosis completely in yeast. Actin is required to drive invagination and post-scission movement of the newly formed vesicle (Kaksonen et al., 2006). In mammalian cells, actin appears to be less important, as blocking polymerization results in only partial endocytic defects (Engqvist-Goldstein and Drubin, 2003).

Finally, the GTPase dynamin has a key role in the scission of endocytic vesicles in mammalian cells. Upon GTP-binding, it self-assembles into a ring-like collar around the neck of deeply invaginated, mature coated pits. Subsequent GTP hydrolysis causes constriction of this collar, which facilitates vesicle fission. Dynamin was not previously thought to play a role in yeast endocytosis, although a recent study has suggested that it may be involved (Smaczynska-de Rooij et al., 2010).

1.4.3. A comparison of the endosomal system in yeast and mammalian cells

The basic organization of the endosomal system in mammalian cells is now fairly well defined. It has functionally and physically distinct compartments, which includes early/sorting endosomes, recycling endosomes, lysosomes, and the TGN (Illustration 1.4.). The sorting endosome is the first destination for endocytosed cargo. Sorting events initiated at this compartment determine the subsequent fate of internalized proteins, directing them for either recycling to the plasma membrane, delivery to the trans-Golgi network, or for degradation. The sorting endosomes have a characteristic morphology, consisting of thin tubular extensions, and vesicular structures. These endosomes contain distinct membrane subdomains, in which cargo are concentrated for different downstream transport steps. Proteins targeted for recycling have been shown to cluster within tubules, while those destined for degradation are concentrated within the vesicular structures. There are multiple routes back to the cell surface from sorting endosomes. Molecules are delivered directly back to the plasma membrane either through an intermediate compartment called the endocytic recycling compartment, or can alternatively pass through the Golgi from sorting endosomes prior to surface redelivery. Each of these pathways has different kinetics of transport. Proteins targeted for degradation are transported from sorting endosomes, which mature into compartments called the multivesicular body (MVB), and subsequently reach lysosomes. The first step in targeting these proteins for lysosomal degradation is often the ubiquitination of their cytoplasmic domain. These ubiquitinated receptors are recognized by the ESCRT (endosomal sorting required for transport) complex

at the MVB, which sorts them for delivery to later compartments. The ESCRT complex invaginates the endosomal membrane to form the internal vesicles of the MVB. Fusion of the limiting membrane of the MVB with the lysosome ultimately delivers the internalized vesicles to the lumen for degradation.

Most mammalian endocytic compartments can be distinguished based on specific lipid composition. Sorting and recycling endosomes contain high amounts of PI(3)P, while later compartments are enriched in $PI(3,5)P_2$ and the lipid lysobisphosphatidic acid (LBPA). As different endocytic compartments are quite distinct in mammalian cells, most approaches used to study them are based on morphology, and there are a variety of markers available for proteins and lipids at each of these compartments, also facilitating their study (Gruenberg, 2003)

Yeast cells share many conserved recycling components and mechanisms with mammalian cells (Illustration 1.4.; left). In yeast, however, the morphological distinction between different endocytic compartments is more elusive than in mammals, and LBPA has not been detected in yeast. It is not clear whether yeast has distinct populations of endosomes, or if subdomains with different lipid compositions exist on these organelles, like those in mammals (Russell et al., 2006). Due to the difficulty in discerning endosomal components in yeast, most compartments have traditionally been defined by genetic analysis, through identifying mutants that lead to the mistargeting of cargo known to transit through the endosomal system. Despite the apparent differences, some key aspects of these sorting pathways appear to be remarkably conserved. In fact, the molecular machinery involved in sorting at the MVB was first identified in yeast. Loss of the ESCRT machinery results in a readily identifiable phenotype: the accumulation of endosomal membranes resulting from the failure in the formation of MVB luminal vesicles (Raymond et al., 1992).

Despite progress in identifying components of the late endocytic (MVB) pathway, the early endocytic pathway has not been as well characterized in yeast (Pelham, 2002). Several proteins have been used as markers to study these recycling pathways. For example, the pheromone-induced endocytosis of Ste3 results in its recycling back to the plasma membrane (Chen and Davis 2000, 2002), while the chitin synthase Chs3 translocates between sites of chitin deposition on the cell surface and endosomes (Ziman et al. 1998; Valdivia et al., 2002).

Another marker that has been used to study endocytic recycling in yeast is the exocytic v-SNARE Snc1, which is involved in fusion of Golgi-derived secretory vesicles with

the plasma membrane, and recycles through early endosomes to the Golgi before redelivery to the cell surface. The localization of GFP-Snc1 has typically been used to identify genes required for its early endosomal recycling. In wild-type cells, Snc1 is localized at the plasma membrane with some punctate staining of internal structures, and has been found to either accumulate in intracellular structures or is enhanced at the plasma membrane in various recycling mutants (Lewis et al. 2000; Galan et al. 2001). Multiple proteins have been implicated in Snc1 recycling, based on the effects of deleting these proteins on the localization of GFP-Snc1. These include the sorting nexin, Snx4, which interacts specifically with the endosome-enriched PI3P (Hettema et al., 2003), and the Arf-GAP Gcs1, which binds directly to Snx4 (Robinson et al., 2006). This process also requires Rcy1, the Ypt31/32 GTPases that facilitate Golgi export and act upstream of Rcy1 (Chen et al., 2005), and components of the coatomer coat complex (Robinson et al., 2006). Importantly, the recycling of Snc1 is not blocked by loss of the MVB sorting machinery, including the ESCRT and retromer complexes, suggesting that Snc1 transits through a distinct endosomal population (Lewis et al., 2000; Schluter et al., 2008; Hettema et al., 2003). The Snc1 recycling pathway has not previously been genetically well characterized, and in most cases, the relationships between genes required for this pathway are not well understood.

To understand the similarities and differences between these sorting pathways in yeast and other organisms, it will be important to develop new methods to better define these early sorting steps. It is likely that the development and application of novel technologies to study these pathways in yeast will help resolve these differences, and lead to a better understanding of endosomal sorting in eukaryotic cells.

1.5. Yeast functional genomics: a tool to dissect trafficking pathways

1.5.1. Systems biology approaches to study membrane transport

The work described in this dissertation uses yeast functional genomics to study mechanisms regulating endocytic recycling. This approach identifies protein complexes and pathways that are coordinately required in a broad cellular context. By considering the requirements for endocytic recycling on a genome-wide level, we aim to elucidate basic principles that may not be apparent at the level of individual components, and to understand how individual genes and pathways are connected to carry out a common process on the level of a whole organism.

S. cerevisiae is an important model system for the development of large-scale genomic and proteomic technologies, due to its compact genome and relatively simple genetics. The yeast genome was the first eukaryotic genome to be successfully sequenced, and over the last decade, numerous genomic methodologies have been developed to identify functions for the roughly 5800 genes in yeast. A collection of ~4800 yeast mutant strains, comprised of systematic knock-out disruptions of all non-essential genes, is available in haploid (MATa and MATα), homozygous and heterozygous diploid strains (Giaever et al., 2002). The deletion collection has allowed for a variety of "reverse genetics" investigations, leading to the discovery of novel components in genetic pathways and protein complexes (Scherens and Goffeau, 2004). In recent years, additional genome wide collections have been developed, allowing for studies of over-expression, localization, protein-protein interactions, and essential genes (Boone et al., 2007). Finally, yeast is easy to manipulate for cell biological and biochemical studies, providing a robust system for functional genomics.

Genetic interactions, which represent the modulation of the phenotype of one mutation by the presence of a second mutation, have long been used as a tool to dissect the functional relationships among sets of genes (Guarente, 1993; Kaiser and Schekman, 1990). Classically, researchers have looked for strong qualitative differences between observed phenotypes of double mutants and the phenotypes of the two related single mutants. For example, a relationship referred to as synthetic lethality is observed when two mutations are not lethal when present individually but, when combined, result in an inviable organism. Synthetic sick/ lethal, or negative, interactions have been used as evidence that two genes act in independent but complementary pathways. Strong negative genetic interactions, in which the double mutant phenotype is stronger than the phenotype of either single mutant, often suggests that these genes work in parallel/redundant pathways. On the other hand, a positive interaction, in which a normally deleterious mutation has no additive effect in the context of a second mutation, often identifies genes that act in the same pathway or complex. Investigating these interactions has provided a wealth of data about functional relationships between genes in yeast (Collins et al., 2010). In recent years, technology has developed allowing genetic interactions to be evaluated on a large scale. Genes that are closely related in function often share highly similar patterns of genetic interactions. Thus, the pattern of genetic interactions of each mutant can be considered as a phenotypic signature. Genes that share similar signatures can be identified and grouped, a useful method for identifying functionally related genes (Schuldiner *et al.*, 2005; Tong *et al.*,

2004). One problem with this approach is that with 6000 genes in the yeast genome, a complete genetic interaction map requires accurately evaluating 18 million double mutant phenotypes, which is beyond the capacity of most studies. The E-MAP (Epistatic miniarray profiling) approach provides a shortcut, in which pairwise interactions are measured among a rationally chosen subset of genes, predicted to to have a shared function in a given process (Schuldiner *et al.*, 2005; Collins et al., 2010). The subset of genes can be selected based on multiple criteria, including shared protein localization (Schuldiner *et al.*, 2005), or protein-protein interaction data (Collins et al., 2007).

1.5.2. Phenotypic screening in yeast to identify transport components

Genetic approaches are a well-established, commonly used approach to evaluate gene function for a wide variety of cellular pathways. In yeast, genetic screens have been immensely successful for discovering genes involved in the secretory, Golgi, endosomal and vacuolar transport pathways (Raymond et al., 1996; Novick et al., 1980; Bankaitis et al., 1996). Characterization of mutants discovered in these screens has revealed roles in cargo sorting, vesicle budding, and tethering/fusion, emphasizing the power of this approach to discover genes with direct roles in trafficking. In recent years, genetic screens have been developed which focus on phenotypes directly related to trafficking. This involves detection of missorting of specific cargo proteins within different transport pathways in the genome-wide deletion collection, allowing for systematic identification of the pathway requirements. Many genes, for example, have been identified that are required for the sorting of the CPY receptor Vps10, between the Golgi and late endosome through these phenotypic screening methods. While in the Golgi, Vps10 binds newly synthesized pro-CPY, and together, Vps10 and pro-CPY are transported to the late endosome. At the late endosome, CPY dissociates from Vps10, and is delivered to the vacuole, where it matures and functions. In the absence of Vps10, or other factors required for transport of pro-CPY, this pathway is blocked, resulting in the missorting of pro-CPY to the extra-cellular space. CPY secretion can be detected based on a colony overlay assay, in which yeast colonies are grown on a nitrocellulose membrane, and secreted pro-CPY is detected by western blotting. Identifying mutants in the genome-wide collection has that lead to pro-CPY secretion have been a well-used screening approach to identify genes involved in Golgi/vacuolar transport (Bonangelino et al., 2002; Schluter et al., 2008).

Despite the progress in yeast functional genomics, over 20% of all yeast genes remain functionally uncharacterized (Peña-Castillo and Hughes, 2007). Furthermore, many

yeast homologs of mammalian genes known to be involved in characterized transport steps have not yet been shown to be functionally important. A prime example is the discrepancy between the requirement for many yeast and mammalian endocytosis genes, as previously described (Conibear, 2010). One explanation for this discrepancy is that deletion of many of these genes may lead to a weak phenotype in yeast that is undetectable by standard assays of transport defects. This issue necessitates the development of novel quantitative strategies, which are sensitive enough to detect these mild defects.

1.6. Research objectives and hypotheses

1.6.1. A new approach for identifying endocytic recycling components in yeast

The endocytic recycling pathway of Snc1 appears to involve many genes not required for the transport of other recycling cargo (Kama et al., 2007; Robinson et al., 2006). It is therefore expected that developing a functional genomics approach to dissect the Snc1 recycling pathway in yeast could identify previously unrecognized endocytic recycling factors, and generate insight into their functional relationships. Snc1 was selected as a reporter for endocytic recycling due to the similarity of its sorting pathway to that of mammalian VAMP2/synaptobrevin. In mammalian neuronal cells, VAMP2 mediates the fusion of synaptic vesicles with the presynaptic membrane, and is required for neurotransmitter release. Its recycling allows continued rounds of synaptic vesicle fusion, and sustained neurotransmission (Grote et al., 1995). As defects in pathways of synaptic vesicle formation and recycling are prominent in a variety of neurological disorders, systematically characterizing the genes required for its sorting pathway will aid in the identification of causal variants in human disease, and ultimately will contribute to the development of drugs that are targeted to correct the resulting defects.

The work described in this dissertation uses a genome-wide phenotypic screen to identify components involved in Snc1 endocytic recycling based on quantitative genome-wide techniques to measure the localization of the Snc1 in the genome-wide deletion collection. In this study, a reporter for Snc1 recycling was created by fusing the sucrose converting enzyme invertase, encoded by the gene *SUC2*, to the C-terminus of GFP-Snc1. The invertase portion is exposed to the extracellular space, allowing detection of plasma membrane localization by whole colony assays of invertase activity. The identification of transport defects in the genome-wide collection relies on densitometry measurements of cell surface invertase activity in each mutant. This provides a sensitive and quantitative

assay, which is compatible with high-throughput approach.

The following chapters are based on our genome-wide phenotypic assay for increased Snc1 surface levels. The goal of this screen was to identify genes regulating Snc1 endocytosis and recycling in a systematic and non-biased manner. Due to its sensitive and quantitative nature, we anticipated that it would reveal functions for genes that were previously uncharacterized due to weak mutant phenotypes or cargo-specific functions.

By evaluating the transport pathway of Snc1, we also aimed to address the mechanisms regulating the sorting of SNARE proteins, one of the least understood issues in the field. We anticipated that we would identify novel factors required for Snc1 sorting, including cargo-specific adaptor proteins and regulators that are not required for the uptake or recycling of other proteins. Chapter 2 is focused on genes required for the endocytosis of Snc1 from the plasma membrane, and the downstream analysis of novel components regulating this process. Chapter 3 is an extension of the results of the primary screen, and investigates the function of the previously uncharacterized clathrin adaptor AP-1R and its interacting protein Ima1 in Snc1 endosomal recycling.

1.7. Illustrations

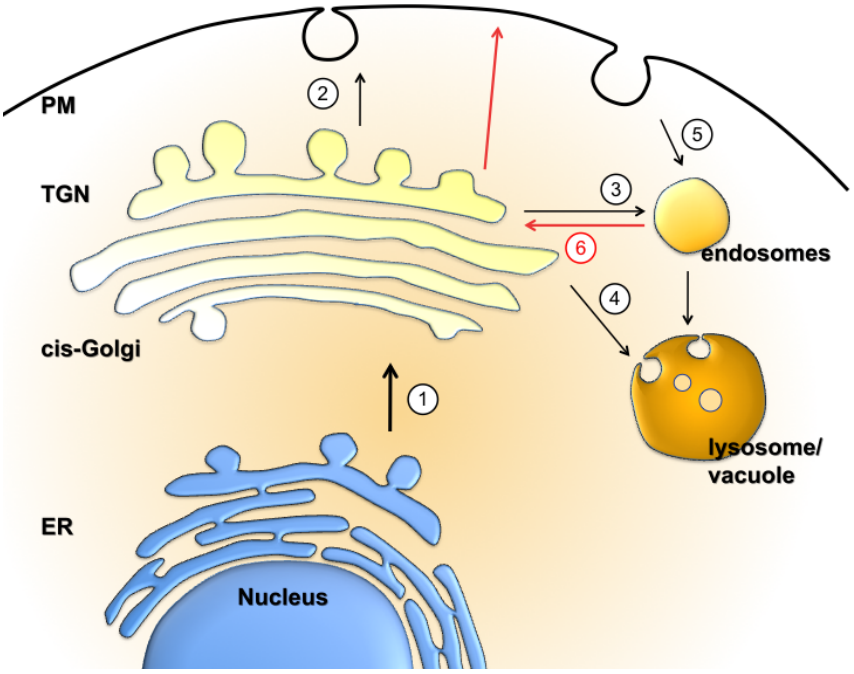

Illustration 1.1. Intracellular compartments and transport pathways.

Following synthesis in the endoplasmic reticulum (ER), proteins are transported to the Golgi **(1)**. The last compartment of the Golgi (the trans-Golgi network) sorts cargo for delivery to multiple possible destinations. From the TGN, proteins move by anterograde transport to the plasma membrane **(2)**, or are diverted to endosomes **(3)**, or to the vacuole for targeted degradation **(4)**. Following cell surface delivery, some proteins are retrieved through endocytosis **(5)**, and are recycled back to the surface via the endosomes and Golgi (Endocytic recycling, **(6)**).

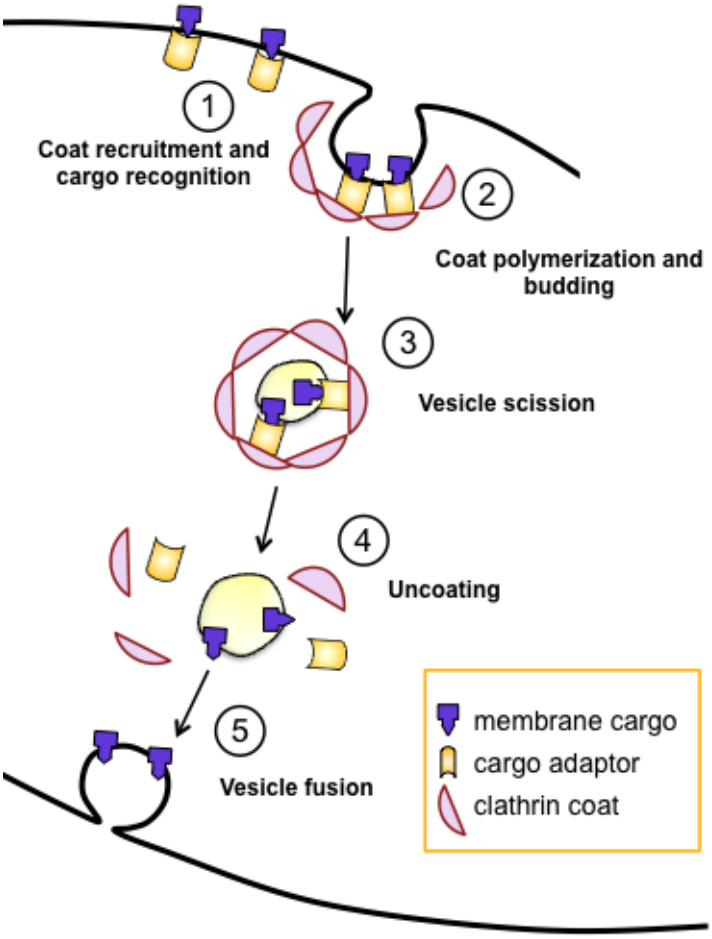

Illustration 1.2. Steps in clathrin-coated vesicle formation and transport.

Vesicle formation is initiated when adaptor proteins are recruited to the donor membrane and bind transmembrane cargo **(1)**. Adaptor/cargo complexes then recruit components of the clathrin coat, leading to its polymerization. These include BAR domain proteins, which promote the membrane curvature required for budding **(2)**. The vesicle is internalized, and pinches off of the target membrane **(3)**. Adaptors and other components are subsequently removed from the vesicle **(4)**. Finally, the uncoated vesicle fuses with the target membrane, delivering its cargo **(5)**.

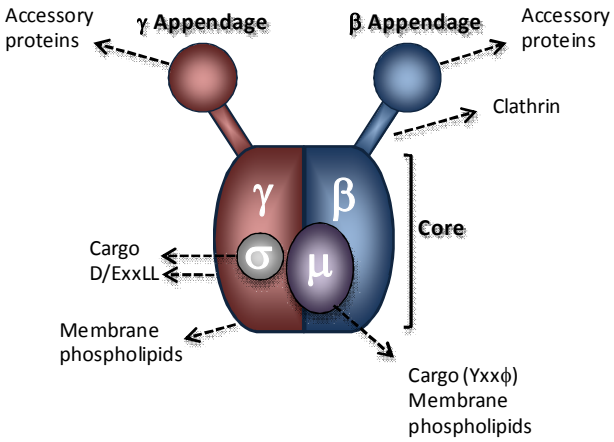

Illustration 1.3. Clathrin Adaptor (AP) structure

Structure of the heterotetrameric AP-1 complex. The complex consists of two large subunits (γ and β1), one medium subunit (μ1), and one small subunit (σ1). The large subunits are divided into a core domain, which assembles with the medium and small subunits, and appendage domains, connected to the core by flexible hinges. Each subunit interacts with a different subset of transport components, as indicated.

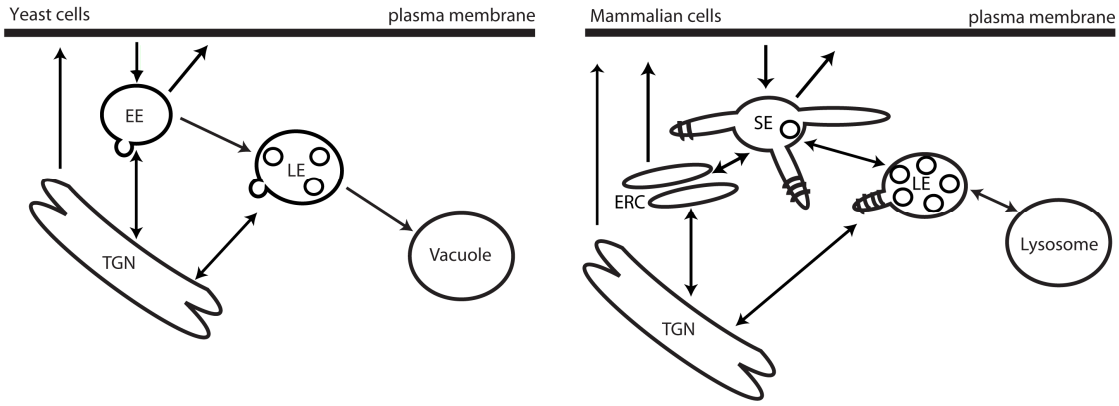

Illustration 1.4. Comparison of endocytic recycling compartments and pathways in yeast and mammalian cells. Following endocytosis, yeast cell surface proteins are transported the the early endosome (EE), from which they can recycle back to the plasma membrane directly, or by passing throught the TGN. Alternatively, they can be targeted to the vacuole for degradation through transport to the late endosome (LE). In mammalian cells, internalized proteins first reach the sorting endosome (SE), from which they can take a variety of routes back to the surface. They are either recycled directly back from early endosomes (rapid recycling), or can pass through the intermediate endocytic recycling compartment (ERC, slow recycling). They can also recycle by passing through the TGN from the endocytic recycling compartment. Proteins targeted for degradation are transported through late endosomes (LE), to the lysosome, the mammalian equivalent of the yeast vacuole.

CHAPTER 2. REGULATORS OF YEAST ENDOCYTOSIS IDENTIFIED BY SYSTEMATIC QUANTITATIVE ANALYSIS. [1]

[1] A version of this chapter has been published as: Burston HE, Maldonado-Baez L, Davey M, Montpetit B, Schluter C, Wendland B, and Conibear E. (2008) Regulators of yeast endocytosis identified by systematic quantitative analysis. *Journal of Cell Biology*. 185 (6): 1097-1111.

2.1. Synopsis

This chapter describes the screening approach used to identify genes involved in the Snc1 endocytic recycling pathway, and focuses on genes that were identified to play a role in yeast endocytosis, and the relationships between them. The main goal of this study was to explain why internalization defects have not been shown for many yeast homologs of mammalian endocytosis genes. This is a question that has puzzled many in the field, leading to the hypothesis that internalization in yeast and mammals utilizes fundamentally different mechanisms. Multiple explanations have been advanced to account for these differences. First, deletion of yeast endocytic homologs may have internalization defects that have not yet been detected, due to weak defects that cannot be measured by standard assays, which may be a result of functional redundancy. Second, many of these genes may be important only for a subset of endocytic cargo. To overcome these limitations, a quantitative approach was developed to systematically assess endocytic defects across the genome, using a novel enzymatic reporter based on Snc1. This revealed roles for many of these yeast endocytic homologs, as well as other previously uncharacterized genes. Genetic interaction mapping was used to place these genes into functional modules containing known and novel endocytic regulators. Hypothesis-driven downstream analysis was then used to functionally characterize novel regulators. In addition, an array-based comparison of two different reporters containing distinct internalization signals was carried out in order to evaluate cargo specificity on a large scale.

This study demonstrates that clathrin and the yeast AP180 clathrin adaptor proteins have a cargo-specific role in Snc1 internalization. Additionally, low dye binding 17 (*LDB17*) is shown to be a novel conserved component of the endocytic machinery. Ldb17 is recruited to cortical actin patches before actin polymerization and regulates normal coat dynamics and actin assembly. Collectively, these findings highlight the conserved machinery and reveal novel mechanisms that underlie endocytic internalization. They also illustrate that parallel mechanisms regulate the internalization of Snc1 in yeast and mammalian cells.

2.2. Introduction

Clathrin-mediated endocytosis selects proteins at the plasma membrane for internalization in membrane-bound vesicles. In mammalian cells, cargo is initially concentrated at endocytic sites by adaptor proteins that promote clathrin recruitment and assembly. A variety of adaptors, such AP2, AP180/CALM, epsins, arrestins and Dab2, recognize different endocytic motifs and select distinct classes of cargo (Maldonado-Baez

and Wendland, 2006). The subsequent recruitment of accessory factors including WASP, dynamin, and amphiphysin stimulates actin polymerization, resulting in membrane deformation and vesicle scission (Smythe and Ayscough, 2006).

Studies in yeast have demonstrated conserved endocytic modules are recruited to sites of internalization in a similar temporal sequence (Kaksonen et al., 2005; Newpher et al., 2005; Perrais and Merrifield, 2005). Clathrin and adaptors are part of the early coat module that establishes the initial site of uptake, while the late coat module (Sla1/Sla2/End3/Pan1) couples coat formation to actin polymerization through recruitment and stimulation of yeast WASP (Las17) and Myo5. This activates the Arp2/3 complex to form an actin network that, stabilized by the actin regulatory module (Cap1/2, Sac6, Abp1), promotes rapid inward movement of the internalizing vesicle. Finally, the amphiphysins Rvs161/167 are thought to drive scission of endocytic vesicles from the plasma membrane. Recycling of the endocytic machinery by vesicle uncoating requires additional proteins, including the synaptojanin homolog Inp52.

This sequence of events, defined by live cell imaging studies, suggests endocytic processes are largely conserved. However, striking differences in the functional requirement for certain regulatory proteins argue that internalization may be differentially regulated in yeast and mammalian cells. For example, the dynamic regulation of actin polymerization is essential for uptake in yeast but not in most mammalian cell types (Engqvist-Goldstein and Drubin, 2003; Smythe and Ayscough, 2006). Conversely, clathrin has an important role in higher cells yet loss of yeast clathrin causes only partial reduction in receptor internalization, and yeast homologs of major clathrin adaptor proteins such as AP2 and AP180 are not required for the uptake of known cargo (Huang et al., 1999; Wendland and Emr, 1998). A number of other yeast genes are homologous to components of the mammalian endocytic machinery, yet do not lead to observable endocytosis defects when mutated (Engqvist-Goldstein and Drubin, 2003; Kaksonen et al., 2005). Some of these factors may have functionally redundant homologs, or have cargo-specific roles. Additional, unrecognized factors may also regulate cargo uptake in yeast. To better understand the endocytic process in both yeast and mammalian cells, it will be important to identify the complete set of structural and regulatory proteins, and systematically define their specific roles.

The yeast VAMP2/synaptobrevin homolog Snc1, which regulates the fusion of exocytic vesicles at the cell surface, is a widely studied endocytic cargo protein. After

delivery to the plasma membrane of the growing bud, it is rapidly internalized and transported to endosomal and Golgi compartments, where it is incorporated into new secretory vesicles (Lewis et al., 2000). Here, we perform a genome-wide analysis of Snc1 localization in yeast to uncover genes with functional roles in endocytosis, and quantify their relative contribution to this process. We identify functions for known and novel proteins not previously shown to be required for uptake, and demonstrate that the yeast AP180 homologs and clathrin have a cargo-specific role in Snc1 internalization. In addition, we describe an endocytic function for the previously uncharacterized protein Ldb17.

2.3. Results

2.3.1. A Snc1-based quantitative assay for endocytic recycling

To quantify defects in endocytosis on a genome-wide scale, we developed an enzymatic assay based on the cell surface localization of a Snc1 reporter. The enzyme invertase (encoded by *SUC2*) was fused to the extracellular C-terminus of Snc1, and GFP was appended to its intracellular N-terminus, creating the chimeric protein GSS (GFP-Snc1-Suc2; Fig. 2.1 A). Cell surface GSS levels can be determined by a colorimetric invertase activity assay, using cell-impermeant reagents (Darsow et al., 2000). By fluorescence microscopy, GSS displayed a polarized distribution at the plasma membrane of small buds similar to Snc1 (Fig. 2.1 B; Lewis et al., 2000), which has been attributed to a cycle of localized exocytosis followed by rapid endocytosis that prevents diffusion away from the site of new growth (Valdez-Taubas and Pelham, 2003). In support of this model, when the Snc1 endocytosis signal was mutated, the polarization of GSS was lost and the level of invertase activity at the plasma membrane increased (Fig. 2.1 B and data not shown). Both Snc1 and GSS were mislocalized to the vacuole in *vps51Δ* mutants (data not shown), demonstrating that they follow a similar recycling pathway back to the cell surface (Conibear et al., 2003).

We introduced the GSS reporter into two independent genome-wide collections of viable deletion mutants, and measured its cell surface level for each mutant in parallel, using a large-scale plate-based invertase assay (Fig. 2.1 C). Mutants were ranked according to their median invertase activity score, determined by automated image densitometry (Fig. 2.1 D and Table A2). Mutants with increased cell-surface GSS included well-characterized endocytosis-defective strains such as *rvs161Δ* and *vrp1Δ*. Other predicted endocytosis genes were enriched in the top 400 hits (Table 2.1), including many not previously shown to cause defects in cargo uptake when deleted such as yeast homologs of AP180 (*yap1801*

and *yap1802*), epsin (*ent1*), tropomyosin (*tpm1*), type I myosin (*myo5*), synaptojanin (*inp52*), coronin (*crn1*), and syndapin (*bzz1*). We generated a "gold standard" list of 33 proteins that have been localized to sites of endocytosis by time-lapse live cell microscopy that were also represented in the haploid deletion collections we evaluated (Newpher et al, 2005; Maldonado-Baez et al., 2008; Toret et al., 2008; D. Drubin, personal communication). Of these, 23 were found in the top 400 hits, representing a significant degree of enrichment ($p < 2.2 \times 10^{-16}$, Fisher exact test). This set of ~400 top-scoring mutants was chosen for further analysis. Mutants with cell-surface GSS levels significantly lower than wildtype (e.g., *snx4Δ, vps51Δ*) were also identified in the screen. This class of mutants, which may have impaired endosomal recycling, will be described in more detail elsewhere.

2.3.2. Genetic interaction mapping clusters functionally related genes

The large number of mutants with elevated surface invertase activity suggested many distinct processes influence GSS reporter distribution. To functionally dissect these processes, we analyzed GSS surface levels in 374 top-scoring deletion mutants in pairwise combination with a panel of 81 deletion mutants that affect a variety of protein trafficking pathways. Genes that co-function within individual complexes and pathways can be identified in large scale genetic interaction analyses based on two characteristic properties (Schuldiner et al., 2006). When loss of one gene disrupts a pathway or complex, loss of a second gene in the same pathway has no further effect, and the double mutant phenotype is less than would be expected under an additive model of genetic interaction. In addition, genes with related functions share similar patterns of genetic interactions and can be identified by cluster analysis.

In typical applications, such as synthetic lethal analysis, the double mutant array is analyzed using cell viability as the phenotypic readout. Here, we quantified the GSS surface distribution to analyze the ~33,000 double mutants of our 374 x 81 array. Hierarchical clustering grouped genes according to their pattern of genetic interactions (Fig. 2.2 A and Fig. A1, see Materials and Methods for details). Strikingly, many clusters were enriched for genes that act together (Fig. 2.2 B). Endocytosis genes were found in two distinct clusters, whereas other gene groupings corresponded to distinct processes (see below). We observed that mutants deleted for two different endocytic genes (eg. *vrp1* and *inp52*) often had lower cell surface levels of GSS than would be expected under an additive model of genetic interaction, consistent with a function in the same pathway or complex. In contrast, mutants disrupted for both endocytosis (*vrp1, rvs167*) and recycling (*snx4, cvt20/snx42*)

genes had cell surface GSS levels greater than expected under the additive null model. This is consistent with previous observations that endocytic defects are epistatic to defects in the Snx4-dependent recycling of Snc1 (Lewis et al., 2000).

2.3.3. Integration of genetic and physical interaction data identifies complexes required for Snc1 transport

To comprehensively identify pathways that regulate Snc1 distribution, we integrated our genetic interaction results with genome-wide physical interaction datasets (see Materials and Methods for details). In a network analysis, genes are represented as "nodes" (circles) linked by "edges" (lines) that indicate an experimental observation such as a physical interaction. To generate a network from the genetic interaction data, pairwise correlation scores were calculated for all genes in the array, and genes were linked by an edge if their correlation score was greater than a threshold value. The resulting network connects genes that share similar patterns of genetic interaction, and thus may represent components of pathways and complexes. Physical interaction networks were then created for the same set of genes, where edges represent interactions observed in high throughput yeast two-hybrid or mass spectrometry experiments. Highly connected sets of genes in each network were identified and integrated, and significant gene clusters were assigned to subcellular compartments based on the localization of their constituent proteins (Huh et al., 2003).

The resulting map (Fig. 2.3) provides a visual representation of the processes contributing to GSS localization and an indication of their relative importance. The size of each node is proportional to the phenotype of the corresponding deletion mutant, whereas edges represent either a physical interaction or a genetic correlation extracted from genome-wide data. Four major clusters, containing a total of 20 genes, mapped to the plasma membrane. The largest of these groupings was enriched for genes with known or predicted roles in endocytosis (*SLA1*, *ABP1*, *INP52*, *EDE1*, *YAP1802*, *RVS161*, *RVS167, CRN1,* and the *INP52*-overlapping ORF *YNL105W*). Additional genes implicated in endocytosis or actin regulation were found in three other clusters at the plasma membrane. These findings highlight the importance of known endocytic regulators in Snc1 trafficking, and predict an endocytic role for uncharacterized genes in these clusters, such as *LDB17* (see below).

A number of well-characterized protein complexes that function at intracellular organelles or regulate transcription or translation were also identified by our integrative network analysis (Fig. 2.3). Some have established roles in actin assembly or protein

transport, such as the cytosolic Prefoldin/GimC complex, which acts as a co-chaperone in actin folding (Siegers et al., 1999). ESCRT mutants are known to exhibit increased cell surface levels of receptors, which has been attributed to enhanced recycling from endosomal compartments (Davis et al., 1993). Chromatin remodeling complexes have also been implicated in regulating vesicle transport at endosomes (Schluter et al., 2008), although the mechanism remains unclear. Mutant strains lacking components of the Sin3/Rpd3 histone deacetylation complex, including Dep1 and Ume6, had particularly strong phenotypes. These proteins regulate the expression of phospholipid biosynthesis genes such as *OPI3*, *INO1*, and *CHO2* (Elkhaimi et al., 2000; Lamping et al., 1994), which were among the top hits in our screen (Table S1). The regulation of plasma membrane lipid composition may also explain the identification of RIM pathway components, which mediate the cellular response to lipid asymmetry and other stimuli (Ikeda et al., 2008).

2.3.4. Clathrin and clathrin assembly proteins are required for Snc1 endocytosis

Our network analysis suggested 20 genes, in four major clusters, are involved in Snc1 uptake at the plasma membrane. To confirm the results of the large-scale plate-based assay, cell-surface GSS levels in these 20 mutants were quantified by a liquid-based invertase activity assay (Fig. 2.4 A). Most had elevated GSS levels that correlated well with values derived from the large-scale densitometry data. The significant internalization defect of *yap1802* mutants was surprising, as previous studies have not identified a clear role for AP180 homologs in yeast (Huang et al., 1999; Wendland et al., 1999). Yap1802 shares 43% sequence identity with Yap1801, which was also recovered by the genome-wide screen (Table A2). By microscopy, the polarized distribution of Snc1 at the bud was largely maintained in *yap1801* or *yap1802* single mutants, but Snc1 was evenly distributed at the cell surface of *yap1801 yap1802* double mutants (Fig. 2.4 B). This strong defect in internalization is consistent with a functionally redundant role for the yeast AP180 proteins in Snc1 uptake.

In mammalian cells, the ubiquitous AP180 homolog CALM participates in clathrin-mediated endocytosis, and interacts with the AP-2 adaptor complex (Meyerholz et al., 2005). Deletion of clathrin heavy or light chain (*CHC1* or *CLC1*), but not AP-2 (*APL1*), also caused a strong Snc1 localization defect (Fig. 2.4 B and data not shown). Surprisingly, no defect was seen when the major clathrin-binding site in Yap1802 (Wendland and Emr, 1998) was deleted in a strain lacking Yap1801 (Fig. 2.5 A), suggesting that Yap1802

contains additional clathrin binding sites, or that additional proteins can bridge the interaction.

In contrast to Snc1 endocytosis, loss of Yap1801 and Yap1802 singly or in combination does not alter ligand-induced down-regulation of the a-factor/Ste2 complex (Huang et al., 1999). We found loss of Yap1801/2 had little effect on the internalization of a distinct endocytic cargo, Ste6-GFP (Fig. 2.5 B). Defects may be more apparent for Snc1, which depends on continuous rounds of internalization and recycling to maintain its polarized distribution, compared to Ste6, which is delivered to the vacuole following internalization (Kelm et al., 2004). To determine if Yap1801/2 are generally required for the uptake of proteins subject to endocytic recycling, we appended the well-characterized Sla1-dependent NPFxD endocytosis signal to the t-SNARE GFP-Sso1 to create a different recycling reporter, NPF-Sso1 (Valdez-Taubas and Pelham, 2003). Like Snc1, NPF-Sso1 has a polarized distribution that depends on endocytosis. Consistent with previous results, we found the localization of NPF-Sso1 to be similar to that of Snc1 in wild type cells, but completely depolarized in *sla1* mutants (Fig. 2.4 B). Its polarized distribution was maintained in *yap1801 yap1802* double mutants, suggesting Yap1801/2 are specifically required for Snc1 internalization.

We created a chimeric version of the NPF-Sso1 reporter by fusing invertase to the NPF-GFP-Sso1 C-terminus and adding two additional NPFxD motifs to further enhance internalization (Fig. 2.4 C), and measured cell surface levels of the resulting NGSS (3xNPF-GFP-Sso1-Suc2) and GSS reporters (Fig. 2.4 D). Internalization of GSS was blocked by mutation of the Snc1 endocytic signal, whereas NPF-dependent internalization of NGSS was abolished in a *sla1* mutant, as expected. Combined deletion of *YAP1801* and *YAP1802* dramatically increased levels of GSS at the cell surface, whereas NGSS surface levels were unaffected. Taken together, these results indicate Yap1801 and Yap1802 act as cargo-specific adaptors for the clathrin-mediated endocytosis of Snc1.

2.3.5. Systematic analysis of cargo specificity

To determine if other genes identified in our genome-wide screen have cargo-specific functions, we re-introduced the GSS and NGSS reporters in parallel into our array of top-scoring deletion mutants. Invertase activity values for each mutant, normalized to the array median, were determined from 6 independent mutant arrays per reporter and converted into relative sorting scores. The ranked differences between NGSS and GSS sorting scores for each mutant indicated that deletion of *YAP1802* and *INP52* had the

greatest specific effect on GSS (Fig. 2.6 A). By measuring cell surface reporter levels in liquid culture (Fig. 2.6 B), we confirmed *inp52* mutants (rank=2) exhibited a highly significant degree of cargo specificity whereas a lower-ranking mutant (*ldb17*) that fell below the 2SD cutoff did not.

A cargo-specific role for the synaptojanin homolog Inp52, a PI(4,5)P2 phosphatase required for recycling of coat proteins after vesicle budding is complete (Toret et al., 2008), was unexpected. Because the membrane association of Yap1801/2 is mediated by PI(4,5)P_2-binding ANTH domains, we considered the possibility that elevated PI(4,5)P_2 levels in *inp52* mutants lead to retention of Yap1801/2 on budded vesicles. Consistent with this hypothesis, Yap1801/2-GFP were observed on cytosolic patches *inp52* mutants, but not in wild type cells (Fig. 2.6 C). Likewise, loss of Inp52 resulted in cytoplasmic aggregates of the ANTH domain protein Sla2-GFP, but had no effect on Sla1-GFP localization, as previously reported (Fig. 2.6 C, (Toret et al., 2008)). Prolonged association of Yap1801/2 with budded vesicles would be expected to reduce levels available for GSS internalization, which may explain the apparent cargo specificity of the *inp52* deletion.

2.3.6. Ldb17 is a new regulator of yeast endocytosis that is transiently recruited to cortical patches

Mutation of the uncharacterized gene *LDB17* (Low Dye Binding 17; Corbacho et al., 2005) caused a strong GSS localization defect (Fig 2.3 and Fig 2.4 A) that, in contrast to *yap1801 yap1802* and *inp52* mutants, was not strongly cargo-specific (Fig. 2.6 B). We confirmed both Snc1 and NPF-Sso1 lost their polarized distributions in *ldb17* mutants (Fig. 2.6 D), and a weak internalization defect was also observed for Ste6-GFP (Fig. 2.5 B), suggesting Ldb17 is a general component of the endocytic machinery. Although an endocytic role for Ldb17 has not previously been described, it has a PTHR13357 domain also found in the mammalian protein SPIN90 (Fig. 2.6 E), which has been implicated in clathrin-mediated endocytosis in fibroblasts (Kim et al., 2007; Kim et al., 2006). Most organisms, including yeast and human, contain a single PTHR13357 family member, indicating Ldb17 and SPIN90 may have orthologous functions.

To help define the role of Ldb17 in endocytosis, we analyzed its recruitment to sites of internalization using two-color time-lapse fluorescence microscopy. Although difficult to visualize due to its low abundance (Ghaemmaghami et al., 2003), GFP-tagged Ldb17 was observed in faint puncta at the cell surface where it showed partial overlap with mRFP-tagged forms of the late coat component Sla1, the Type I myosin Myo5 and the F-actin-

binding protein Abp1 (Fig. 2.7 A-C), consistent with transient co-localization. Kymograph analysis showed Ldb17 joined pre-existing Sla1 patches just prior to the onset of Sla1 inward movement and Myo5 recruitment (Fig. A2 A-C). Myo5 patches appeared ~1-3 s after Ldb17 patches, whereas Ldb17 dissociated from the membrane ~4-6 s prior to Abp1 disassembly. These results allow us to place Ldb17 on the temporal map of the endocytic process (Fig. 2.7 D): Ldb17 is maximally recruited after assembly of the late coat components, immediately prior to the recruitment of the Myosin module, which precedes the actin-driven inward movement of the invaginating membrane.

The coat module assembles at endocytic sites prior to the onset of actin polymerization, and its components are recruited before the appearance of F-actin. Treatment with the actin monomer-sequestering drug Latrunculin A (LatA) resulted in the expected complete delocalization of Abp1, whereas the membrane localization of Ldb17 was dramatically enhanced (Fig. 2.7 E). The endocytic coat components Sla1 and Sla2 show similar LatA-resistant cortical localization (Ayscough et al., 1997). This indicates actin is not required for the membrane recruitment of Ldb17, and is consistent with a role for Ldb17 at late stages of coat assembly.

2.3.7. Sla1 contributes to membrane recruitment of Ldb17

The F-actin-independent localization of Ldb17 suggests other factors regulate its recruitment to sites of endocytosis. We found the C-terminal Proline-Rich Domain (PRD) of Ldb17 was important for its localization at the cell periphery (Figs. A2 D, left panels, and 2.6 F). Many endocytic proteins contain SH3 domains that recognize specific PRD sequences and contribute to the assembly of the endocytic network. We confirmed by co-immunoprecipitation that the yeast syndapin homolog Bzz1 binds Ldb17 in a PRD-dependent manner (Fig. A2 E), as predicted in a large-scale study (Tong et al., 2002). Surprisingly, membrane localization of Ldb17-GFP was enhanced in *bzz1* mutants (Figs. A2 D and 6 F) and simultaneous loss of Bzz1 and the Ldb17 PRD had additive effects on cell surface GSS levels (Fig. A2 F), indicating Bzz1-PRD interactions are not involved in Ldb17 recruitment.

To identify additional PRD binding partners, we used yeast two-hybrid analysis to screen a panel of 16 SH3 domains from proteins implicated in endocytosis or actin regulation (Tong et al., 2002). SH3 domains from Sla1, Lsb3, and Lsb4 all exhibited PRD-dependent interactions with Ldb17 (Fig. A2 G and H). Because Lsb3 and Lsb4 are known binding partners of Sla1 (Dewar et al., 2002; Gavin et al., 2006), their interactions with

Ldb17 may be indirect. Interestingly, loss of Sla1 had an effect similar to loss of the PRD; by live-cell microscopy, the lifetime of Ldb17 at the cell surface was reduced from 9 sec to 5 sec (Fig. 2.7 F). Taken together, these results suggest Sla1 binds the Ldb17 PRD to enhance its membrane association at endocytic sites, whereas Bzz1 is important for its release.

2.3.8. Aberrant actin distribution in *LDB17* mutants

Based on the timing of its recruitment, we hypothesized Ldb17 may link coat formation to actin polymerization, as has been suggested for other components of the late coat module. Consistent with this, the actin module protein Abp1 was found in a smaller number of larger, brighter clusters in *ldb17Δ* cells compared to wildtype cells (Fig. 2.7 G), similar to the large actin clumps found in *sla1Δ* mutants (Kaksonen et al., 2005). Actin polymerization is required for internalization of the Sla1-containing late coat module; in cells treated with LatA or lacking the Arp2/3 activator Las17, Sla1 patches remain immobile at the cell surface (Ayscough et al., 1997; Sun et al., 2006). Sla1 was similarly stabilized at the membrane in the absence of Ldb17 (Fig. 2.7 H), suggesting Ldb17 plays a role in the dynamic regulation of actin polymerization required for the internalization of Sla1-containing endocytic vesicles.

2.4. Discussion

We have developed a genome-wide screening method that provides a systematic and quantitative analysis of genes required for the endocytic recycling of Snc1, the yeast VAMP2 homolog. In addition to well-established endocytic regulators, this screen uncovered phenotypes for deletion mutants of predicted endocytosis genes for which no cargo uptake defects had previously been observed. The mammalian homologs of many of these genes also have endocytic roles, underscoring the conserved nature of endocytic processes in eukaryotic cells (Engqvist-Goldstein and Drubin, 2003; Kaksonen et al., 2005; Smythe and Ayscough, 2006).

Collectively, our results highlight the sensitive nature of our reporter assay and reinforce the importance of dynamic actin regulation for the endocytic process. Multiple regulators of the actin cytoskeleton were identified in our screen, including the actin binding proteins Abp1 and Crn1 (coronin homolog), the Actin Capping complex (Cap1/2), and the Cap1/2 binding protein twinfilin (Twf1). Lack of sufficiently sensitive assays and study of limited cargo may have prevented detection of endocytic phenotypes for these mutants in previous studies (Kubler and Riezman, 1993). In addition, redundancy of the

endocytic machinery may account for the weak but significant phenotypes resulting from loss of individual myosin-I (Myo5) and epsin (Ent1) isoforms (Lechler et al., 2000; Maldonado-Baez and Wendland, 2006; Wendland et al., 1999).

2.4.1. Role for clathrin adaptors in yeast endocytosis

The severe defect in Snc1 uptake caused by loss of Yap1801 and Yap1802, homologs of the mammalian clathrin assembly factor AP180/CALM, represents the first demonstration of a unique role for these proteins in yeast endocytosis. Studies in mammalian cells, worms, and flies all support a requirement for AP180 and its homologs in the internalization of VAMP/Synaptobrevin. It mediates the selective uptake of this SNARE in worms, and appears to regulate the internalization of additional proteins in flies (Bao et al., 2005; Nonet et al., 1999).

AP180-like proteins may cooperate with other adaptors for the uptake of certain cargo. For example, a redundant role with the epsins in the internalization of the yeast pheromone receptor Ste3 was recently reported (Maldonado-Baez et al., 2008). AP180/CALM contains multiple binding sites for AP2, Eps15, and clathrin (Maldonado-Baez and Wendland, 2006; Wendland and Emr, 1998). A quantitative analysis of synaptobrevin localization in selected *C. elegans* mutants using the pH-sensitive synaptobrevin-GFP fusion protein synaptopHluorin demonstrated its surface levels were enhanced in both AP180 and AP2 mutants (Dittman and Kaplan, 2006), suggesting the interaction between AP180 and AP2 is functionally important in worms. In contrast, our results show Yap1801/2 does not require AP2 to mediate Snc1 internalization in yeast, consistent with a recent study that saw little effect of mutating the AP2 binding site of CALM on synaptobrevin uptake in mammalian cells (Harel et al., 2008).

The specific requirement for Yap1801/2 in Snc1 endocytosis suggests they may act as adaptors to recruit Snc1 into a clathrin-coated pit. Internalization signals recognized by AP180-like monomeric adaptors have yet to be described (Maldonado-Baez and Wendland, 2006) and, like most SNAREs, Snc1 lacks canonical adaptor sorting motifs such as YxxF or D/ExxxL/E. Instead, SNARE proteins appear to use specialized sorting signals that differ from those of other cellular cargo (Chidambaram et al., 2004; Miller et al., 2007). The V40A M43A mutations that reduce Snc1 endocytosis could impair a Yap1801/2 recognition site; however, this remains to be determined, as we have not been able to demonstrate a direct physical interaction between Yap1801/2 and Snc1.

2.4.2. Identification of novel components of the yeast endocytic machinery

Our systematic analysis of cargo specificity did not identify additional adaptor proteins that were clearly specific for Snc1. Instead, we discovered loss of the syntaptojanin homolog Inp52 affected uptake of the Snc1 reporter more strongly than a reporter that uses a Sla1-dependent NPFxD signal. This can be explained by the differential recognition of $PI(4,5)P_2$ by Yap1801/2 and Sla1. High levels of $PI(4,5)P_2$ resulting from loss of Inp52 prevented efficient recycling of Yap1801/2, which is predicted to reduce its availability for further rounds of internalization. However, no such effect was seen for Sla1, consistent with previous reports (Toret et al., 2008).

In contrast to the cargo-specific role of Yap1801/2, we found the previously uncharacterized gene *LDB17* plays a broad role in regulating endocytosis. Ldb17 is transiently recruited to Sla1-containing cortical patches shortly before the onset of actin polymerization, and its membrane association is stabilized by interactions between its PRD and the Sla1 SH3 domain. The aberrant actin assembly and increased lifetime of Sla1 patches in *ldb17Δ* mutants suggest Ldb17 helps trigger the dynamic actin rearrangements that precede coat disassembly.

Ldb17 may link coat assembly to the activation of the Arp2/3 complex through interactions with Sla1 and Arp2/3 activators, or act more directly. The C-terminal region of SPIN90 most similar to Ldb17 is sufficient to promote the WASP-independent activation of Arp2/3-mediated actin polymerization in vitro (Kim et al., 2007). The Arp2/3 and actin binding motifs present in SPIN90 are only partially conserved in Ldb17, and we did not observe binding of Ldb17 to the Arp2/3 complex and the yeast WASP homolog Las17 in vivo (unpublished results). However, we identified an interaction between the Ldb17 PRD and the Bzz1 SH3 domain that mirrors the PRD-dependent binding of the Ldb17-related protein SPIN90 to the mammalian Bzz1 homolog syndapin (Kim et al., 2006). The conserved interaction of syndapin-like proteins with proline-rich regions in Ldb17 and SPIN90, despite the different placement of the interacting domains, suggests these proteins may fulfill related roles. Further work will be needed to clarify the function of these conserved proteins in regulating actin polymerization and endocytosis.

Overall, our results suggest that endocytic processes are generally more similar in yeast and higher cells than previously believed, and underscores Snc1 transport in yeast as a model for synaptobrevin recycling at the synapse. Characterization of other genes identified in our screen may yield additional endocytosis factors. Due to the functional

redundancy of the endocytic machinery in all eukaryotes, many regulatory proteins are likely to have weak mutant phenotypes that can only be discovered by more sensitive and quantitative approaches. Future application of our genome-wide analysis to different reporter proteins may identify alternative cargo-specific machinery and further define the complexity of endocytic systems.

2.5. Materials and methods

Construction of plasmids and yeast strains

Plasmids and yeast strains used in this study, and details of their construction, are listed in Table S2. Unless otherwise indicated, plasmids were constructed by homologous recombination after co-transforming yeast with linearized vector and DNA fragments bearing 50-55bp homology, and recovering recombinant plasmids in *Escherichia coli*. Oligonucleotide sequences are available upon request. The *MATa* yeast strain BY4741 and its gene deletion derivatives were obtained through Open Biosystems (Huntsville, AL). Unless otherwise stated, gene disruptions and tagging of genomic ORFs were carried out by transformation of a PCR product containing a drug selection marker, flanked by 50-55bp of homology to the region of interest.

Genome wide screening

The GFP-Snc1-Suc2 (GSS) reporter was introduced into MATa and MAT*alpha* knockout collections using the SGA procedure (Tong and Boone, 2006). Query strains containing the GSS reporter and a gene deletion marked with NAT^R were mated to a 384-colony knockout array that contained 374 mutants identified in the genome-wide analysis (top 402 hits minus 28 mitochondrial mutants) and controls (wild type, blank, *ent3*, and *rvs161*). Double mutant haploid strains containing the GSS reporter were selected on –LEU –URA +G418 +clonNAT plates.

Manipulation and screening of the resulting colony arrays was performed essentially as described (Burston et al., 2008). Colony arrays on 384-array stock plates were pinned four times to YPF plates creating 1536-arrays using a Virtek automated colony arrayer (BioRad, Hercules, CA). Digital images of colony arrays subjected to the invertase overlay assay (Darsow et al., 2000) were acquired using an Epson 2400 flat-bed scanner. Local normalization was carried out using National Institute of Health ImageJ software (http://rsb.info.nih.gov/ij/) with the local normalization plugin

(bigwww.epfl.ch/sage/soft/localnormalization) to correct for differences in intensity resulting from uneven distribution of reagents. Densitometry on corrected images used the spot-finding program GridGrinder (gridgrinder.sourceforge.net) and values were subjected to background subtraction and filtered to eliminate absent or very slow-growing strains. As densitometry values are inverted during analysis, reported values are inversely correlated with cell surface levels of the reporter. Therefore, these values were subtracted from the median value for all strains to give a score where a high value represents a high level of the reporter. The invertase overlay assay was carried out twice on each knockout collection; average values were used to generate the final ranking.

Genetic Interaction and Network Analysis

In an additive model of genetic interaction, the phenotype of the double mutant strain (P_{XY}) can be expressed as: $P_{XY} = P_{WT} + E_X + E_Y + E_{GI}$, where P_{WT} is the wild type phenotype, E_X is the effect of the first mutation, E_Y is the effect of the second mutation and E_{GI} is the genetic interaction effect. In a genetic interaction matrix, all double mutants in a given row or column have a mutation in the same "array" gene (row) or "query" gene (column). Assuming genetic interactions are rare, and positive and negative interactions are equally common, dividing double mutant phenotype values (P_{XY}) in each column by the mean of that column removes the effect of the query mutation ($P_{wt} + E_Y$). Subsequently dividing values in each row by the row-wise mean removes the effect of the array mutation (E_X), leaving only the genetic interaction effect, E_{GI}.

We applied a modified version of this data pre-processing strategy to the matrix of raw double mutant invertase activity values. Rows with more than 20% missing observations were removed. Remaining values were divided by row- and column-wise medians, and values in each row and column were scaled so the sum of the squares of the values in each row or column was 1.0. Although these manipulations do not preserve the numerical value of E_{GI} they optimize clustering of functionally related groups by emphasizing patterns of genetic interactions. Cluster 3.0 software (http://bonsai.ims.u-tokyo.ac.jp/~mdehoon/software/cluster/software.htm) was used to perform average linkage hierarchical clustering using an uncentered correlation similarity metric on both horizontal and vertical axes, and results were presented using Java Treeview (http://jtreeview.sourceforge.net/), where ordering of genes on both axes reflects the similarity of their genetic interaction profiles, and cluster relationships are indicated by

trees. The resulting heat map (Fig. A1) does not provide a true quantitative measure of genetic interaction, but instead approximates the direction of the genetic interaction effect for each double mutant where yellow is negative (less than expected under the additive null model), and blue positive (greater than expected).

A network of correlated genetic interaction profiles was generated using the ARACNE algorithm (Margolin et al., 2006) with a threshold of 0.015. The MCODE plugin for Cytoscape (Bader and Hogue, 2003; Shannon et al., 2003) was used to identify densely-connected gene clusters in synthetic genetic data and physical interaction networks from SGD (www.yeastgenome.org) and WI-PHI (Kiemer et al., 2007), which were then integrated. The size of each node (gene) was mapped to the strength of the endocytic defect in Cytoscape based on the results from the genome-wide analysis in Table A2.

Liquid invertase assay

The liquid invertase assay was modified from (Darsow et al., 2000). Strains expressing GSS or NGSS reporters were grown for 20 h in 2ml YP fructose (OD_{600} ≈10). After dilution to 3 OD600/mL, 5µl of each culture was mixed with 55µl 0.1M NaOAc buffer pH4.9 in a 96 well microtiter plate. Subsequent steps were carried out with a VICTOR^3 1420 multilabel plate reader system (PerkinElmer, Waltham, Massachusetts). 13µl of freshly prepared 0.5M ultra pure sucrose was added to each well, and the plate was incubated for 5min at 30°C. Next, 100µl of glucostat reagent (0.1M K_2HPO_4 pH7.0, 347.1 U Glucose Oxidase, 2.6 ng/ml Horseradish Peroxidase, 102.6 nM N-ethyl-maleimide, 0.15 mg/ml O-Dianisidine) was added to each well, and the plate incubated for 5 min at 30°C. Finally, 100µl of 6N HCl was added to each well to stop the reaction. The absorbance at 540nm was used to determine glucose concentration by comparison to a glucose standard curve (range from 5-50nM glucose). Results are reported as nM glucose produced per 1 OD_{600} of culture.

Live cell imaging

Yeast cells expressing GFP-tagged proteins were grown to mid-log phase and were viewed directly in minimal selective media at room temperature using a Plan-Apochromat 100x 1.40 NA oil-immersion objective on a Zeiss Axioplan 2 fluorescence microscope (Carl Zeiss, Thornwood, NY). Images were captured with a CoolSNAP camera (Roper Scientific, Tuscan, AZ) using MetaMorph 6.1 software (Molecular Devices, Downingtown, PA) and adjusted using Adobe Photoshop CS. Alternatively, cells were grown to early log phase on

rich medium plates at 30°C and placed in 200 ml minimal media on Concavalin A-coated 8 well Lab-Tek coverglass bottom dishes (Nalge Nunc, Rochester, NY). Images were collected at room temperature with a 3i Marianas microscope (Intelligent Imaging Innovations, Denver, CO) equipped with an alpha Plan-Fluar 100x 1.46 NA objective and a Zeiss TIRF slider. Single color widefield GFP images were acquired using 488 nm laser excitation and a GFP dichroic and emission filter (Semrock, Rochester, NY). Two-color and RFP images were acquired with 488nm and/or 561nm laser excitation, with GFP and RFP emission split between two Cascade II 512 cameras with an Optical Insights Dual Cam (Photometrics, Germany) equipped with the D520/30m D630/50m splitting optics (Mag Biosciences). Exposure times varied from 600-750ms as follows: Ldb17-GFP single experiments, 750ms; two-color Ldb17/Myo5, 750ms; Ldb17/Sla1, 750ms; Lbd17/Abp1, 750ms for Ldb17 and 650 for Abp1. TetraSpeck 100nm beads (Invitrogen) were used to align the two channels and for subsequent registration in software. Slide-Book 4.2® software (Intelligent Imaging Innovations, Denver, CO) was used for image acquisition and dual channel image registration. Kymographs and montages were created using ImageJ software with Kymograph plugins (http://www.embl.de/eamnet/html/kymograph.html).
Live-cell imaging experiments with LAT-A treatment were performed by incubating cells from early-log phase cultures in a final concentration of 200 mM LAT-A dissolved in DMSO for 30 min at 30°C.

Co-immunoprecipitation

30 OD_{600} cell pellets made from flash-frozen log phase cells were lysed by vortexing with glass beads in 200ul lysis buffer (100mM NaCl pH 8.0, 2mM EDTA, 0.5% Tween-20 + PMSF) and incubated with mouse αHA (1:1000 ABM) and 30ul Protein G-Sepharose (75% slurry in PBS). Co-precipitating proteins were identified by western blotting with mouse αGFP (1:1000, Roche) and HRP-labelled secondary antibodies (BioRad). Blots were developed with ECL (Pierce, Rockford, IL) and and luminescent images were captured with a Fluor S Max Multi-imager.

2.6. Figures and Tables

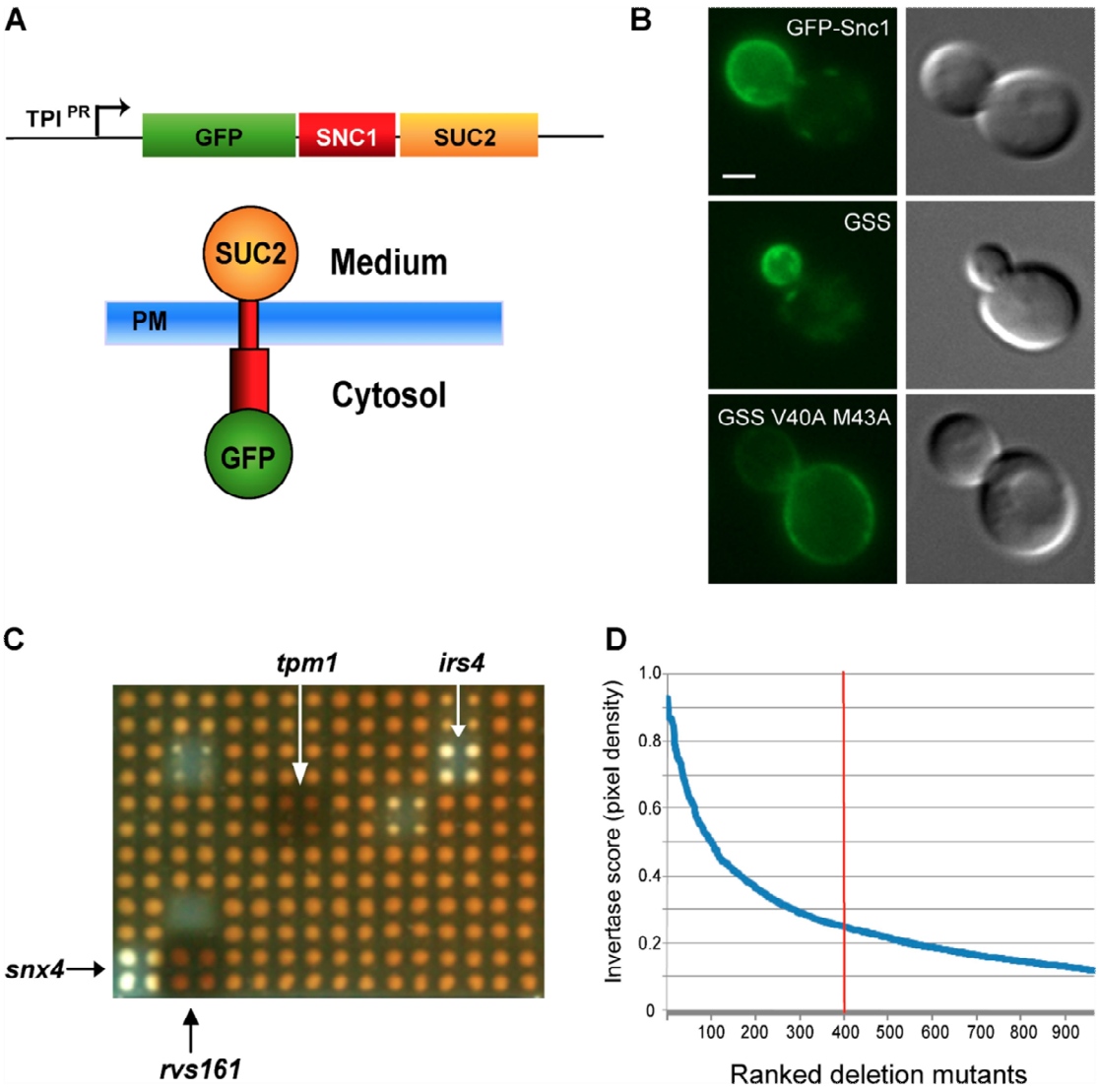

Figure 2.1. Genome-wide screen for endocytic recycling mutants.

(A) Schematic of the GFP-Snc1-Suc2 (GSS) reporter. At the plasma membrane (PM), the Suc2 (invertase) portion is accessible to the extracellular space. **(B)** Localization of GFP-Snc1, GSS, and an endocytosis-defective form of GSS containing snc1V40A,M43A mutations (Scale bar, 2μm). **(C)** Representative portion of the yeast knockout array tested using the invertase activity overlay assay. Mutants defective in Snc1 endocytosis exhibit increased surface invertase activity relative to wildtype cells, and appear dark. Mutants with high (*tpm1* and *rvs161*) or low (*snx4* and *irs4*) levels of cell surface invertase activity are indicated. **(D)** Relative cell surface invertase activities of top 1000 mutants. Red line indicates threshold used to designate top hits.

Table 2.1. Predicted yeast endocytic genes identified in the screen

			Previously reported requirement for:	
Name	Rank[a]	Homologue	Patch dynamics[b]	Internalization[c]
RVS161	1	Bin3/amphiphysin	Yes	Yes
VRP1	4	WIP	Yes	Yes
RVS167	8	Bin1/amphiphysin	Yes	Yes
SLA1	12	SH3 domain	Yes	Yes
ARC18	18	Arp2/3 complex	Yes	Yes
YAP1801	29	AP180	No	No
EDE1	31	Eps15	Yes	Yes
YAP1802	42	AP180	No	No
CAP1	45	Actin-capping complex	Yes	No
TPM1	52	Tropomyosin	No	No
ABP1	54	Abp1	Yes	No
MYO5	61	Type 1 myosin	No	No
INP52	68	Synaptojanin	Yes	No
YIR003w	78	ND	No	ND
CAP2	127	Actin-capping complex	Yes	No
TWF1	155	Cofilin-like repeats	No	No
SAC6	209	Fimbrin	Yes	Yes
SYP1	216	ND	No	ND
BBC1	231	ND	Yes	No
ENT1	281	Epsin	No	No
END3	315	ND	Yes	Yes
LSB3	338	ND	No	ND
CRN1	365	Coronin	No	No
AIP1	368	WDR1	No	ND
BZZ1	383	Syndapin	No	No
PKH2	396	PDK1	ND	No

ND, not determined
[a]See Table A1.
[b]Kaksonen et al., 2005
[c]Internalization of FM4-64 or cargo proteins. See Engqvist-Goldstein and Drubin (2003), Kaksonen et al. (2005), and Moseley and Goode (2006).

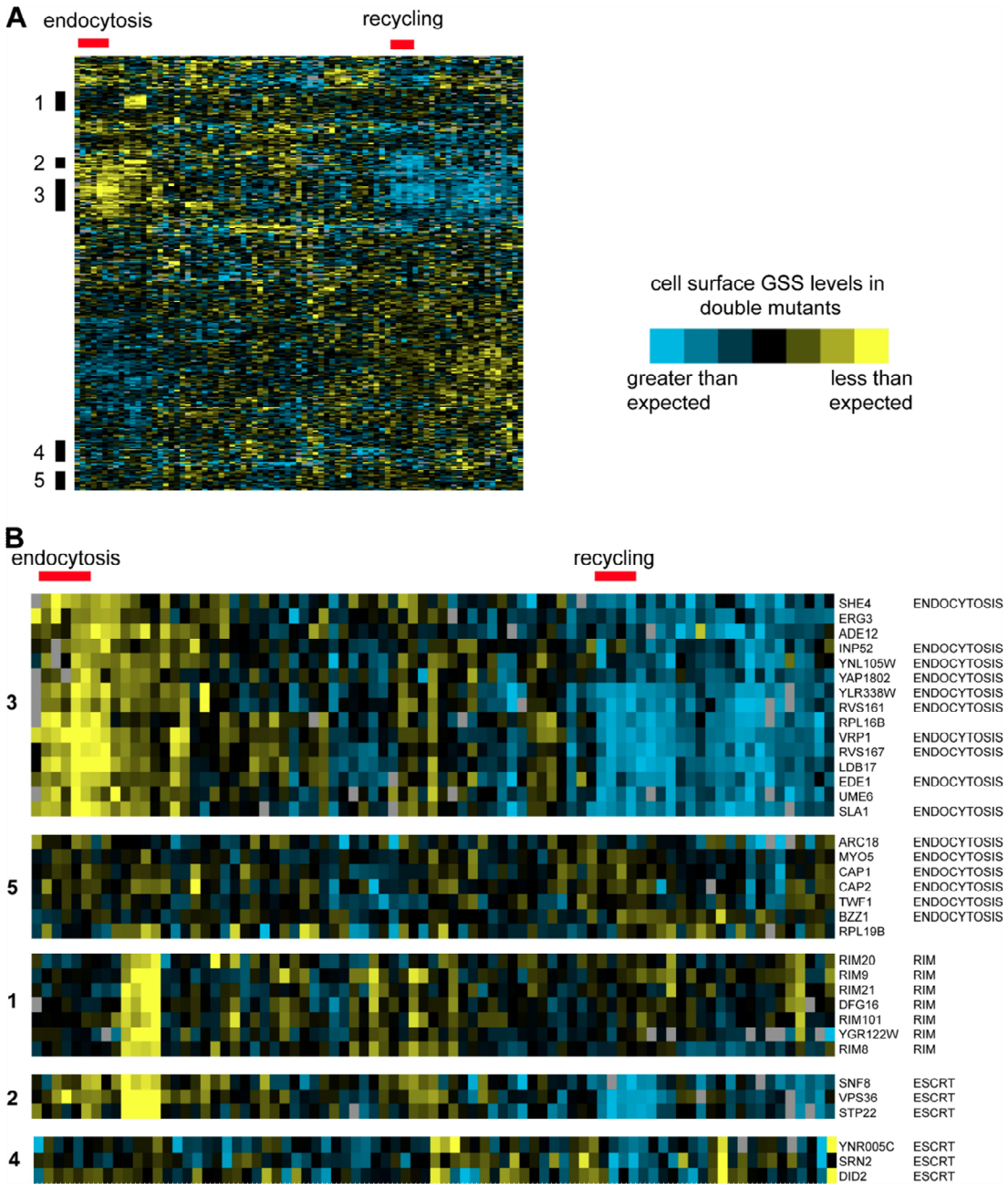

Figure 2.2. Endocytosis mutants have related genetic interaction profiles.

(A) Hierarchical clustering was used to analyze the invertase activity values of double mutant strains generated by crossing top-scoring mutants from the primary screen (y-axis) to 81 diverse trafficking mutants (x-axis). Yellow indicates lower than expected levels of GSS at the cell surface, while blue indicates higher than expected levels (see Methods and Materials for details). **(B)** Detailed view of clusters showing names of genes and highly represented pathways/complexes. Clusters are numbered to indicate their relative position on the heatmap in (A). Red bar indicates gene clusters on the Y-axis enriched in endocytosis or recyling genes. See Fig. A1 for a detailed view of gene names and cluster relationships.

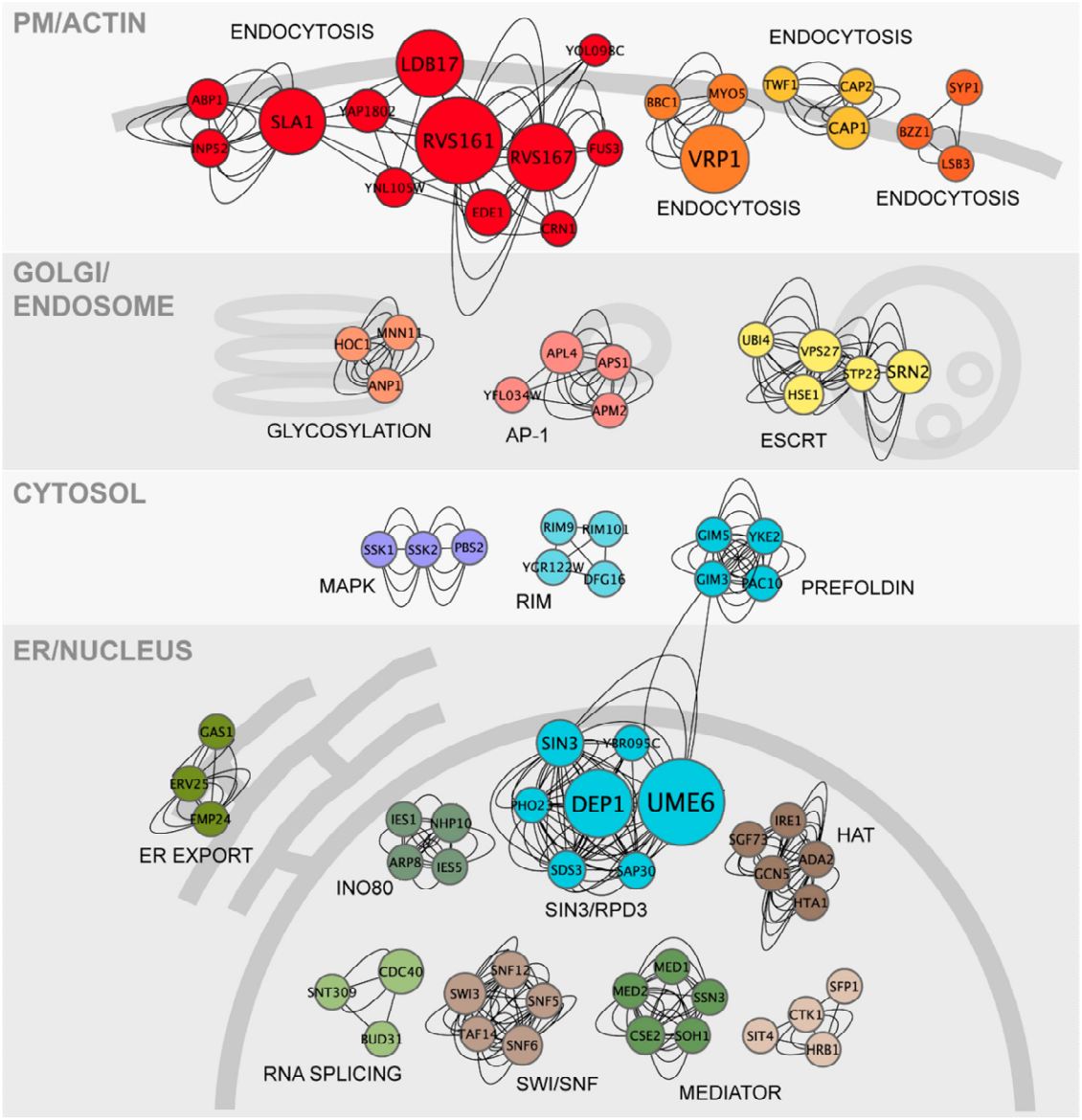

Figure 2.3. Integration of genome-wide genetic and physical interaction data identifies pathways and complexes.

Significant genes clusters contributing to GSS localization were mapped based on integrated physical and genetic interaction networks. Array genes are represented as nodes (where relative size is proportional to GSS surface levels in the corresponding deletion mutant), and are connected by edges that represent either a physical interaction or a genetic correlation extracted from genome-wide data. Clusters were assigned to subcellular compartments based on the localization of their constituent proteins.

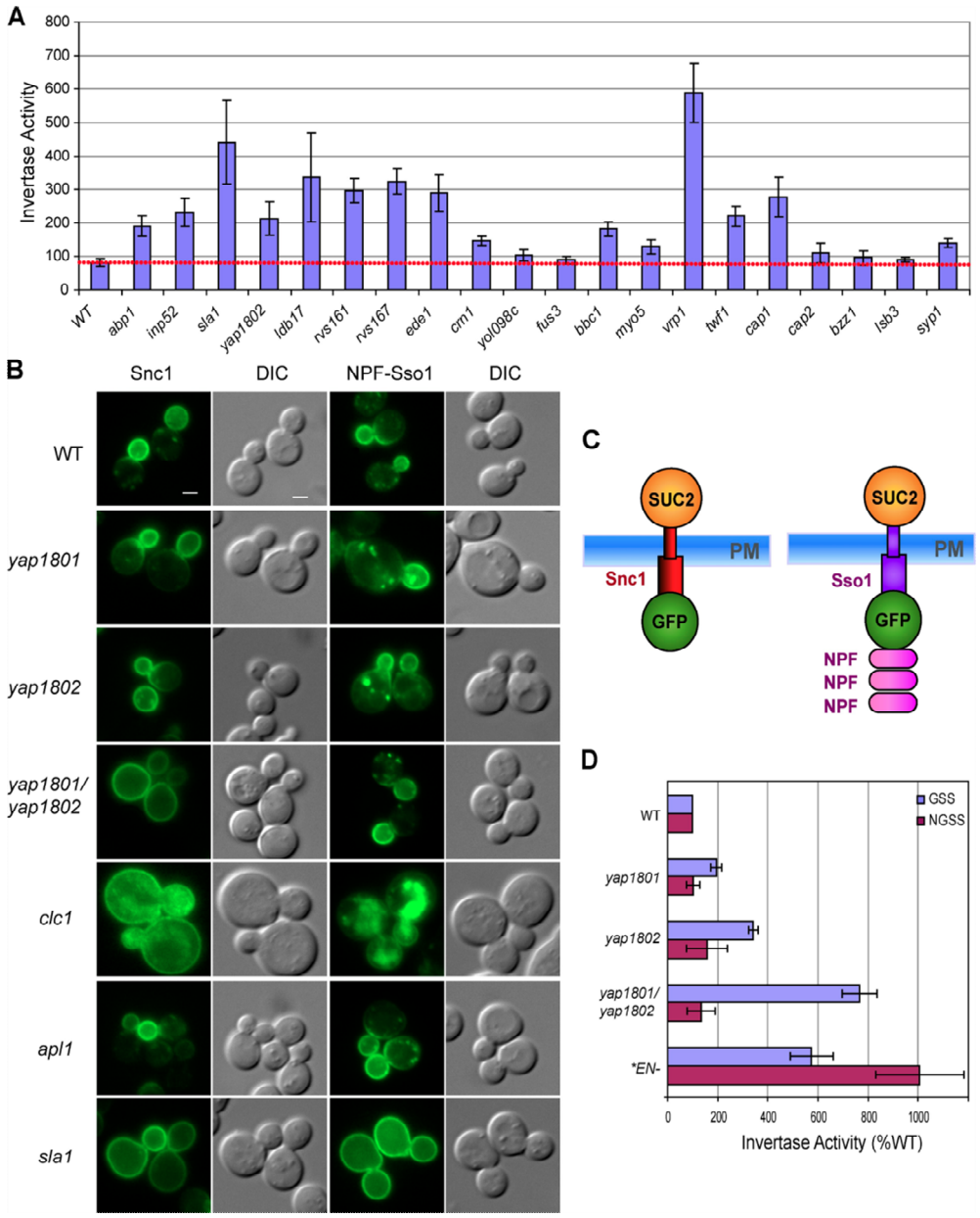

Figure 2.4. Yeast AP180 homologs have a conserved role in Snc1 internalization.

(A) Quantification of cell surface GSS levels in WT and candidate endocytic mutants by the liquid invertase assay. Invertase activity represents relative surface levels of the GSS reporter, quantified as nmol glucose released/OD600 (mean of at least 3 experiments ± SD). **(B)** Localization of GFP-tagged Snc1 and NPF-Sso1 in WT and mutant strains (Scale bar, 2μm). **(C)** Schematic of the GFP-Snc1-Suc2 (GSS) and 3xNPF-GFP-Sso1-Suc2 (NGSS) reporters. **(D)** Relative cell surface levels of GSS and NGSS reporters measured by liquid invertase assay in mutant strains (mean of 3 experiments +/- SD). Results for each reporter are expressed as % invertase activity relative to WT. Different endocytosis defective controls (*EN-) were used for each reporter. GSS: endocytosis defective GSS (snc1V40A M43A) reporter in WT cells. NGSS: NGSS in sla1 mutant strain.

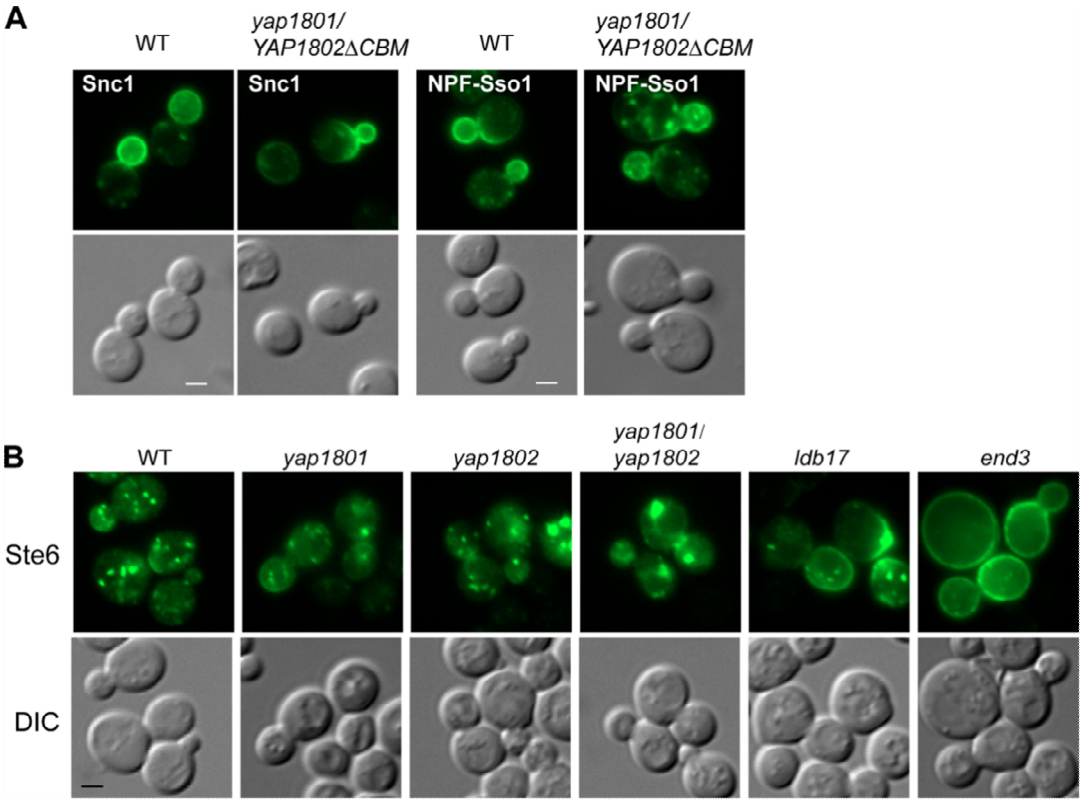

Figure 2.5. Cargo sorting defects of yap1801Δ yap1802Δ mutants.

(A) The Yap1802 C-terminal clathrin-binding motif (CBM) is not required for Snc1 internalization. Localization of GFP-tagged Snc1 and NPF-Sso1 in WT and yap1801/ yap1802ΔCBM mutants. **(B)** Deletion of *YAP1801* and *YAP1802* does not prevent internalization of Ste6-GFP, whereas loss of LDB17 results in a slight increase in cell surface Ste6-GFP. Localization of Ste6-GFP is shown in wild type (WT) and indicated mutants.

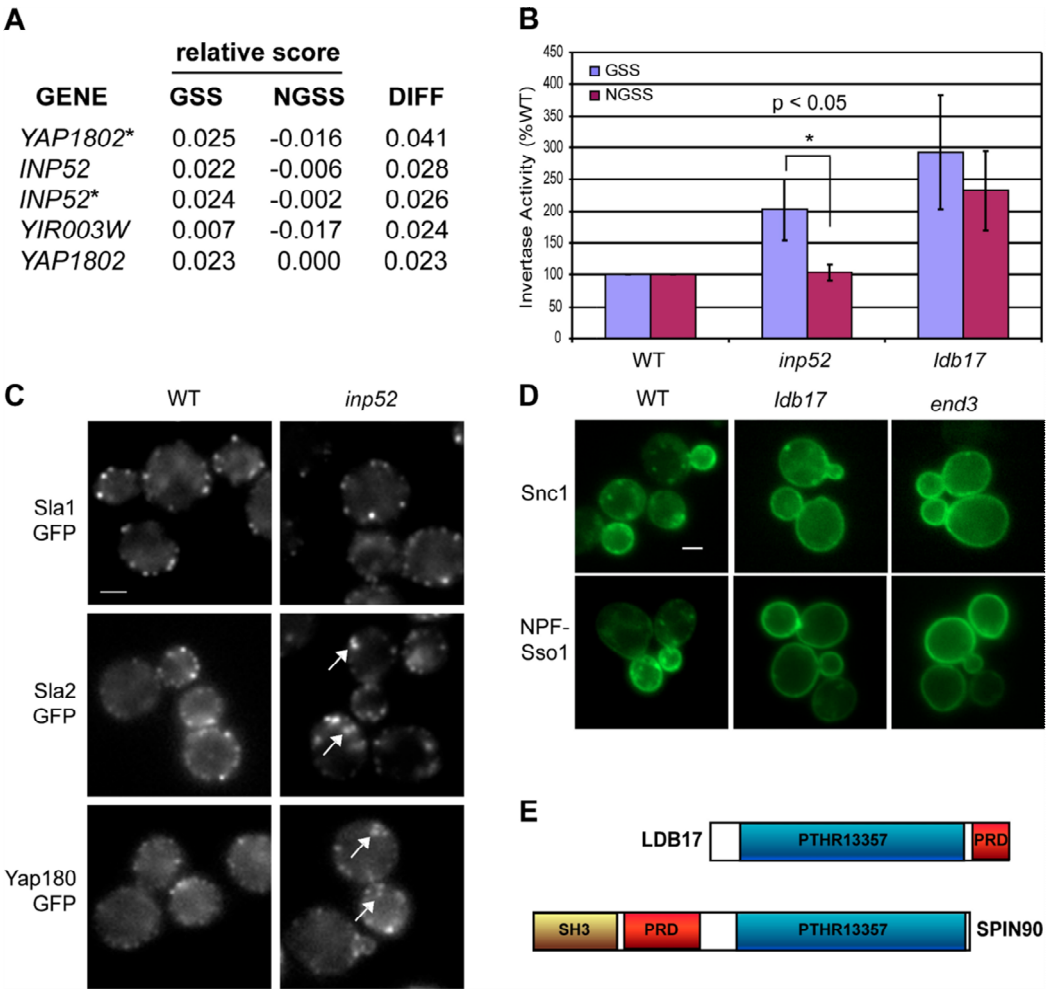

Figure 2.6. Cargo specificity of genes required for Snc1 endocytosis.

(A) Array-based analysis of cargo specificity. The difference (DIFF) in cell surface levels of GSS and NGSS reporters was determined for each mutant by subtracting normalized invertase activity scores measured in parallel analyses of mutant arrays. Mutants with differences greater than 2SD ($p<0.05$) from the mean are shown. * indicates loss of gene function by deletion of an overlapping open reading frame **(B)** Relative cell surface levels of GSS and NGSS reporters measured by liquid assay in inp52 and ldb17 mutants. Results for each reporter are expressed as % invertase activity relative to appropriate WT control (*$p < 0.05$). **(C)** Yap180 and Sla2 are present on internal puncta in inp52 strains. Wild type and inp52 mutants expressing Sla1-GFP, Sla2-GFP or both Yap1801-GFP and Yap1802-GFP were examined by live cell microscopy. Arrows indicate internal patches. **(D)** Localization of GFP-tagged Snc1 and NPF-Sso1 in WT, ldb17, and end3 strains. Scale bar, 2μm. **(E)** Ldb17 shares homology with the mammalian SPIN90 and contains a PRD. The conserved PTHR13357 domain is indicated (blue region).

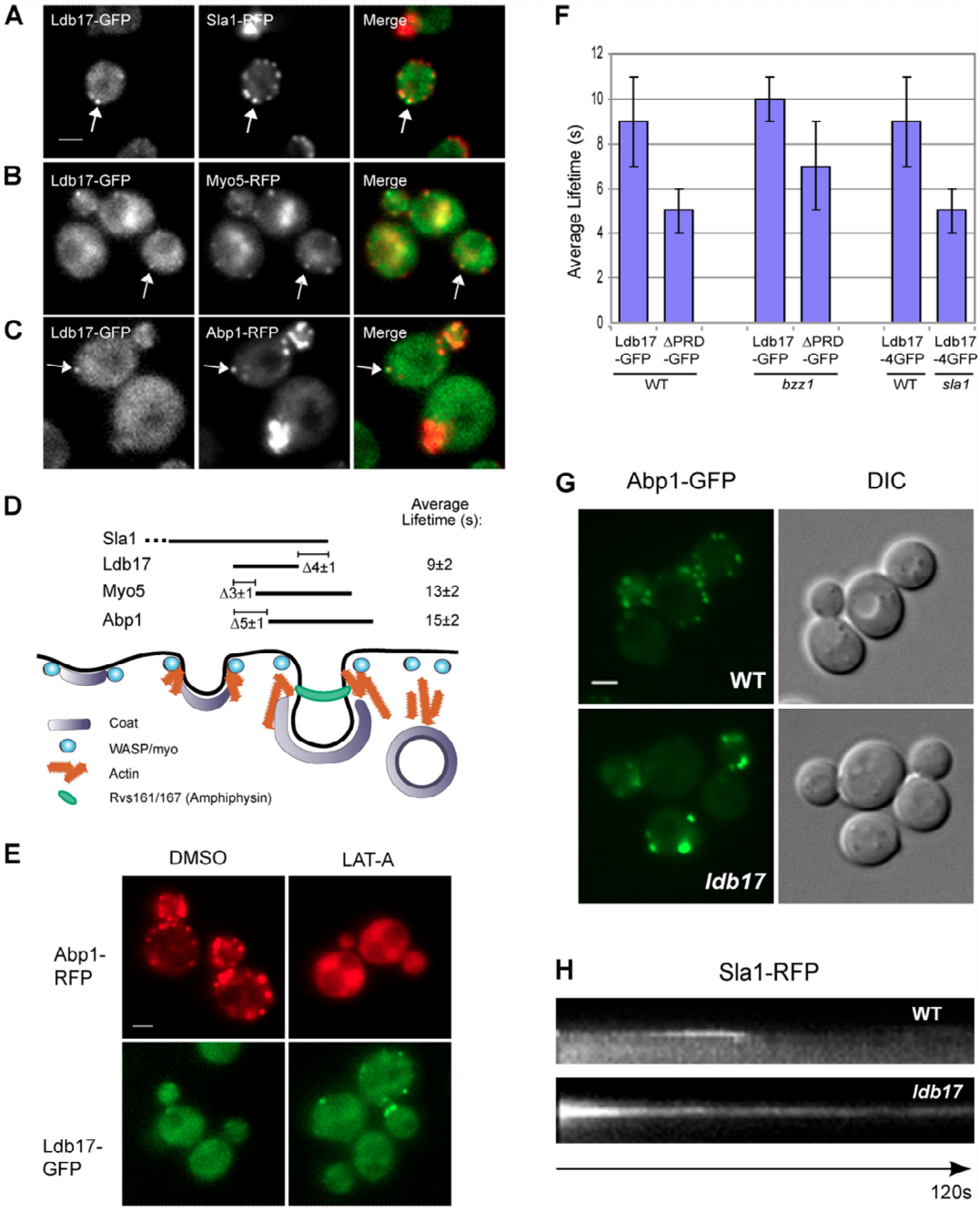

Figure 2.7. Ldb17 is required for proper coat and actin dynamics

(A-C) Colocalization of Ldb17-GFP with Sla1-RFP, Myo5-RFP, and Abp1-RFP. Representative single frames from GFP and RFP channels are shown together with merged images. Arrows indicate cortical patches containing both Ldb17 and RFP-tagged proteins. **(D)** Schematic diagram, adapted from (Kaksonen et al., 2005), illustrating the timing of Ldb17 recruitment to cortical patches relative to markers of the late coat (Sla1), WASP/myo

(Myo5) and actin (Abp1) modules, based on kymograph analysis of 10 patches for each GFP/RFP pair (see Fig. S3 A-C). The average difference in the timing of Ldb17 arrival or disappearance (+/- SD, in seconds) relative to other markers is indicated, together with the total average lifetime of Ldb17, Myo5, and Abp1 patches. **(E)** Localization of Ldb17-GFP and Abp1-RFP in cells treated with DMSO (left panels), or 200 μM LAT-A (right panels), for 30 min at 30°C. **(F)** Lifetime of GFP-tagged Ldb17 and/or Ldb17ΔPRD at cortical patches in WT, bzz1 and sla1. Lifetimes were measured for at least 10 patches/strain. **(G)** Reduced number and increased brightness of actin patches in ldb17 cells, as assessed by microscopy of Abp1-GFP. (H) Kymograph representation of time-lapse wide-field fluorescence microscopy showing extended lifetime of Sla1-RFP at endocytic patches in *ldb17Δ* mutants, as compared to wild type cells over 120s. Scale bar, 2μm.

CHAPTER 3: THE YEAST VARIANT AP-1R CLATHRIN ADAPTOR AND IMA1 ARE REQUIRED FOR SNC1 ENDOCYTIC RECYCLING[1]

[1]Burston HE, Tam C, Davey M, Raghuram N, Maldonado-Báez L, Wendland B, and Conibear E. (2010). Chapter 2 is a version of a manuscript in preparation.

3.1. Synopsis

In this chapter, the results of the primary genome-wide screen described in Chapter 2 were extended to identify factors required for Snc1 intracellular recycling. This identified a requirement for a previously uncharacterized variant of the AP-1 complex in this process, which we have named AP-1R (AP-1 related). AP-1R differs from the well-characterized AP-1 complex only by the alternate inclusion of the medium subunit. The work presented in this chapter demonstrates that AP-1R and AP-1 have distinct functions in endosomal recycling, and the mechanisms regulating the specificity of AP-1R in Snc1 transport are investigated.

Inclusion of alternate medium subunits has been shown to alter the sorting function of AP complexes (Gonzalez and Rodriguez-Boulan, 2009; Gan et al., 2002). However, it is not well understood how subunit exchange can confer novel functions to these complexes. Recent findings suggest that differential interactions between the medium subunit with cargo, regulatory proteins, and membrane lipids may underlie these differences (Fields et al., 2007 and 2010; Ang et al., 2003). Consistent with findings from these previous studies, this work demonstrates that AP-1 and AP-1R participate in different regulatory interactions. The previously uncharacterized gene *YFL034w* was identified as an AP-1R-specific regulator, and has putative enzymatic activity required for AP-1R function. Yfl034w has been predicted to physically interact with AP-1R components in genome-wide studies (Krogan et al., 2006; Gavin et al., 2006), and here, it is shown to interact preferentially with AP-1R versus AP-1. Yfl034w is therefore referred to as Ima1 in this work (Interacts with μ adaptin 1). Collectively, this study provides insight into the differential interactions that occur between alternate AP medium chains and regulatory proteins. It also reinforces the idea that SNARE transport is mediated by specialized components of the vesicle formation machinery.

3.2. Introduction

The process of endocytic recycling is essential for maintaining the composition of the plasma membrane, and also in the regulation of nutrient uptake, cell polarity, and signal transduction (Jovic et al., 2010; Grant and Donaldson, 2009). The AP-1 adaptor complex plays a key role in endocytic recycling, and mediates sorting between the trans-Golgi network and endosomes (Reusch et al., 2002). AP-1 is a member of the heterotetrameric clathrin adaptor complexes, and consists of four adaptin subunits: γ1 and β1, which interact

with accessory proteins, and μ1 and σ1. The μ1 adaptin mediates cargo and membrane binding, while σ is involved both in complex stability, and cargo recognition (Mattera et al., 2011).

AP-1 exists as variant isoforms, which differ through the alternate inclusion of one subunit. In many cases, these variants mediate distinct sorting functions. Mammalian cells express 3 isoforms of the small σ1 subunit (σ1A-C). Although deletion of the large subunits are embryonic lethal, specific deletion of σ1B in mice results in defects in the recycling of synaptic vesicles (Glyvuk et al., 2010). These mice exhibit a severe reduction in the number of synaptic vesicles at hippocampal boutons, and the endosomal accumulation of vesicle components. Most organisms also express AP-1 variants that differ by inclusion of alternate medium subunits. Mammalian polarized epithelial cells express the ubiquitous AP-1A (containing μ1A), as well as the epithelial-specific AP-1B (containing μ1B). While AP-1A mediates Golgi/endosomal sorting, AP-1B functions at recycling endosomes, and directs the transport of a distinct set of cargo to the basolateral domain (Gan et al., 2002). Although the mechanisms underlying this alternate specificity have not been well characterized, this subunit exchange may confer the ability of each complex to interact with a distinct set of cargo, lipids, and regulators (Fields et al., 2007 and 2010; Ang et al., 2003).

Two alternate forms of the AP-1 complex have also been identified in yeast, which share the large γ and β (Apl2, Apl4) and small σ (Aps1) chains, differing only by the alternate inclusion of either Apm1 or Apm2 as the medium μ subunit (Stepp et al., 1995). The characterized AP-1 complex, which incorporates Apm1, has a well-established role in transport of cargo, including Chs3 (Chitin Synthase 3) and Ste13 between Golgi and endosomes (Valdivia et al., 2002; Foote and Nothwehr, 2006). No sorting role has previously been identified for the Apm2-containing complex. Early studies suggested that the Apm1 and Apm2-containing complexes are biochemically and functionally distinct; they co-fractionate with separate clathrin-coated vesicle populations, and while deletion of *APM1* enhances the defects in growth and α-factor processing in combination with a temperature-sensitive allele of clathrin light chain, deletion of *APM2* does not (Stepp et al., 1995).

A screening approach to identify regulators of the yeast Snc1/synaptobrevin endocytic recycling pathway was previously reported (Chapter II/Burston et al., 2009). Through this approach, a role for the alternate AP-1 clathrin adaptor complex containing Apm2 (AP-1R; AP-1-related) in the regulation of Snc1 cell surface levels was revealed.

The work reported in this chapter demonstrates that AP-1R is involved in Snc1 intracellular transport, and that AP-1 and AP-1R mediate different sorting pathways. Additionally, a requirement for the previously uncharacterized gene, *YFL034w* in AP-1R-mediated Snc1 recycling was identified. Yfl034w binds specifically to AP-1R vs. AP-1, and we have therefore named it *IMA1* (interacts with mu Adaptin 1). Furthermore, this work demonstrates that Ima1 is a putative enzyme of the serine hydrolase family, conserved among eukaryotes, and its catalytic activity may be required for Snc1 transport. This finding is significant, as a growing body of research has identified interactions between AP medium subunits with various enzymatic regulators, although this is the first study to investigate this in yeast.

3.3. Results

3.3.1. A role for the variant AP-1R complex in endocytic recycling

In the genome-wide screen to identify genes required for the intracellular recycling pathway of the yeast synaptobrevin homolog Snc1 (described in Chapter 2), deletion mutants of 3 subunits of the AP-1 complex resulted in increased Snc1 surface levels. These results were surprising, as the subunits that were identified (Apl4, Aps1, and Apm2, table A2) are components of the functionally uncharacterized AP-1 isoform, AP-1R. Interestingly, loss of the uncharacterized gene *YFL034w*/*IMA1* also led to increased Snc1 surface levels. Ima1 has been predicted to bind AP-1R components in multiple high-throughput interaction studies (Krogan et al., 2006; Gavin et al., 2006). Furthermore, AP-1R components and *IMA1* shared similar genetic interaction profiles with a panel of trafficking mutants representing various sorting pathways, and were highly-connected based on our network analysis (Burston et al., 2009). Collectively, these results suggest that Ima1 and AP-1R may share a related role in Snc1 transport.

To verify that loss of AP-1R components leads to increased surface levels of GSS, these results were quantified in liquid culture (Fig. 3.1, A). Loss of *APM2* and *APL4* led to GSS surface levels significantly greater than WT. Although this phenotype was reproducible, it was weak. The increased GSS surface levels in *apm2Δ* mutants were lower than in *yap1801Δ* mutants. As described in chapter 2, yAP1801 is an endocytic adaptor required for Snc1 internalization, which is partially redundant with its homolog, yAP1802. This defect was specifically due to loss of AP-1R, as deletion of the AP-1 specific subunit, *APM1,* did not result in increased Snc1 surface levels.

3.3.2. AP-1R mediates intracellular recycling

As Snc1 maintains a steady state surface localization through continuous rounds of endocytosis and redelivery through endosomal recycling, the increased surface levels of Snc1 in the absence of AP-1R could reflect either a defect in the rate of endocytosis or an increase in the rate of surface recycling. An endocytic role for AP-1R would be surprising, as AP-1 has a well-established role in intracellular sorting, and localizes to Golgi and endosomal compartments (Valdivia et al., 2002; Fernández and Payne, 2006). However, as no requirement for the endocytic adaptor AP-2 in Snc1 internalization was identified in the primary screen, it was considered possible that AP-1R may have a role in endocytosis. Whether AP-1R could be detected at endocytic sites was determined by comparing the localization of Apm2 with that of the endocytic AP-2 medium chain, Apm4 in cells treated with LAT-A, which permits the visualization of cortical actin patches. While Apm4 co-localized with Clc1 in coated pits at the plasma membrane, Apm2 did not. Instead, it localized to intracellular compartments (Fig. 3.1 B, upper). In very few cases, however, Apm2 was observed in close proximity to cortical patches. The kinetics of these surface patches was further investigated. While Apm4 retained co-localization with clathrin at the plasma membrane over the course of the TIRF experiment, Apm2 showed dynamic activity in relation to these cortical clathrin-containing patches (Fig. 3.1 B lower). These results suggest that Apm2 is mostly present in intracellular compartments, consistent with a role for AP-1R in the intracellular recycling of Snc1, and not in endocytosis.

3.3.3. AP-1R and Ima1 localize to Golgi/endosomal compartments

As Apm2 localized to motile intracellular structures, the identity of these structures, and whether they contain clathrin was investigated. AP-1 has previously been shown to localize to Golgi/endosomal compartments (Valdivia et al., 2002). To determine if this is also the case for AP-1R, fluorescence microscopy was used to compare the localization of Apm2-GFP relative to Sec7-RFP, a marker of late Golgi and endosomal compartments (Franzusoff et al., 1991). Consistent with a role in Golgi/endosomal sorting, substantial overlap was observed between Apm2-GFP and Sec7-RFP (Fig. 3.2 A). Apm2-containing structures also showed overlap with intracellular clathrin patches (Fig. 3.2 B).

The distinct sorting roles of AP-1 and AP-1R could reflect a different localization of the two complexes. To investigate whether AP-1 and AP-1R have non-overlapping distributions, the localization of Apm1 and Apm2 were compared. Consistent with previous findings, Apm1 localized to Golgi/endosomal membranes. Direct co-localization of Apm1-

RFP and Apm2-GFP revealed substantial overlap of Apm2-GFP and Apm1-RFP at these compartments (Fig. 3.2 C). Together with the functional invertase assays, AP-1 and AP-1R likely have non-overlapping sorting roles, and that this cannot likely be explained based purely on differential localization of the two complexes, as assessed by this study.

As Ima1 was also identified by our screening approach, and is a predicted binding partner of AP-1R, this suggested that it may be involved in AP-1R function. If this were the case, Ima1 would likely localize to compartments consistent with AP-1 function. Although Apm2 and Ima1 could not be co-localized directly due to the low expression of both proteins, Ima1-GFP shared a similar extent of co-localization with both Apm1 and intracellular clathrin as did Apm2 (Fig. 3.2 D and E), suggesting that Ima1 and AP-1R localize to similar compartments, and that Ima1 may have a role in AP-1R-mediated transport.

3.3.4. Ima1 and AP-1R are not required for the transport of AP-1-dependent cargo

Since Ima1 localized to compartments consistent with AP-1 function, the next question to be addressed is whether Ima1 functions specifically with AP-1R, or with both forms of AP-1. If Ima1 functions specifically with AP-1R, it could suggest a regulatory role, and may contribute to the specific sorting function of the complex.

The relative importance of Ima1 in AP-1R versus AP-1-mediated trafficking was investigated by determining if Ima1 is required for sorting of AP-1-dependent cargo. AP-1 is required for the endosomal transport of the chitin synthase Chs3 (Valdivia, 2002), and when deleted, can restore the cell surface translocation of Chs3 from late Golgi/endosomes in *chs6Δ* cells, in which this pathway is blocked. It has previously been shown that Apm2 does not contribute to this sorting role (Valdivia et al., 2002). We therefore compared the requirement for AP-1R and Ima1 in Chs3 transport using a previously established assay to measure Chs3 surface levels, based on the fluorescence levels observed for cells grown on media containing Calcofluor white (CW). While deletion of AP-1 (*APM1*, *APL2*), restored WT cell surface levels of Chs3 in *chs6Δ* cells, deletion of either AP-1R (*APM2*) or *IMA1* did not lead to an obvious restoration (Fig. 3.3, A). Furthermore deletion of *APM2* did not affect Chs3 surface levels in combination with deletion of either *APM1* or *IMA1*. These results suggest that Ima1 functions preferentially with AP-1R, and has a minor, if any role in AP-1 transport.

3.3.5. Ima1 specifically binds the AP-1R C-terminal domain

If Ima1 localization overlaps with both AP-1 and AP-1R, how does Ima1 specifically contribute to AP-1R function? One explanation is that Ima1 may bind preferentially to AP-1R vs. AP-1, as demonstrated in multiple genome-wide studies. To investigate this, the ability for Ima1-GFP to co-immunoprecipitate Apm2-HA versus Apm1-HA was assessed. Ima1-GFP co-precipitated exclusively with Apm2-HA, while no interaction was observed with Apm1-HA (Fig. 3.3, B). This confirmed that Ima1 interacts preferentially with the AP-1R vs. the AP-1 complex, and may therefore play a role in AP-1R regulation.

Most AP-1 regulators interact with the appendage domain formed by the Gamma subunit (GAE domain, Page et al., 1999; Hirst et al., 2003), although a few have been found to bind to the Beta appendage (Edeling et al., 2006). It was therefore evaluated whether Ima1 interacts with the AP-1 Gamma appendage. Interestingly, Ima1-GFP co-purified with Apl4-HA from yeast cell lysates, and this interaction was maintained in the absence of the Apl4 GAE appendage domain, suggesting that Ima1 binds to the AP-1R core complex (Fig. 3.3 C). Although the role of the Beta appendage in mediating this interaction was not tested, it is likely that Ima1 interacts with the AP-1R core complex, since Ima1 interacted preferentially with AP-1R vs. AP-1, and these complexes differ only by the alternate inclusion of Apm1 and Apm2.

To better define the interaction between Ima1 and AP-1R, a Yeast Two-Hybrid assay was carried out between Ima1 and Apm2, which confirmed the interaction between the full-length proteins. Based on structural homology to other μ adaptin chains, Apm2 is divided into an N-terminal domain, required for incorporation into the AP complex, and a C-terminal domain, which contains regions for both membrane recruitment and tyrosine-based cargo binding (Collins et al., 2002). To potentially narrow down the role of Ima1 in AP-1R regulation, further yeast-two hybrid assays were used to identify the regions involved in this interaction. This demonstrated that the Ima1 N-terminal domain (residues 1-262) interacted with the Apm2 C-terminal domain (Fig. 3.3 D). As Ima1 binding does not require the presence of the Apm2 N-terminal domain, which mediates its assembly into the AP-1 complex, Ima1 likely interacts directly with Apm2, and not through another complex subunit. Based on structural analysis, the C-termini of adaptor μ chains can be further divided into distinct subdomains (A and B). Subdomain A forms the tyrosine-binding pocket, while subdomain B contains regions shown to interact with specific membrane lipids and regulatory factors (Owen and Evans, 1998, Heldwein et al., 2004). Further Apm2

truncations revealed a minimal binding region of residues 389-562, which constitutes the B domain, and lacks subdomain A. This indicates that Ima1 does not interact with Apm2 as a typical cargo through the tyrosine-binding pocket, but may associate with it through a region which, by analogy to other μ subunits, contains sites for multiple regulatory and lipid interactions (Fields et al., 2010; Owen and Evans, 1998; Heldwein et al., 2004).

3.3.6. Ima1 is not required for AP-1R recruitment or interaction with cargo

The work described above demonstrates that Ima1 is both functionally and physically associated with AP-1R, and may regulate the sorting function of this AP complex. There are multiple mechanisms by which Ima1 may regulate AP-1R. Ima1 may be important for the recruitment of AP-1R to Golgi/endosomal membranes, or may be an alternate cargo adaptor, linking Apm2 to Snc1.

To determine if Ima1 is required for AP-1R membrane recruitment, fluorescence microscopy was used to compare Apm2-GFP localization in WT and *ima1Δ* cells. No significant differences in the number of Apm2 membrane puncta in the absence of Ima1 were observed (Fig 3.4 A). To rule out any subtle defects in Apm2 membrane association in the absence of *IMA1*, subcellular fractionation was used to compare the distribution of Apm2-HA in WT and *ima1Δ* cells. Apm2 was enriched in the high-speed (P100) membrane fraction, containing vesicles and small organelles, in both WT and *ima1Δ* cells, consistent with the microscopy results (Fig. 3.4 B). These studies demonstrate that Ima1 is not important for the membrane recruitment or stabilization of AP-1R.

An alternate possibility is that Ima1 may be important for AP-1R cargo recognition. AP medium subunits bind directly to signals within the cytosolic domain of their respective cargo (Robinson et al., 2004, Owen et al., 2004). Since Snc1 does not contain canonical AP-binding tyrosine or dileucine motifs, Ima1 may be a non-conventional adaptor, bridging the interaction between Snc1 and Apm2. We sought to determine whether Apm2 physically interacts with Snc1 and subsequently, whether Ima1 is required for this interaction. A GST-tagged Snc1 cytosolic domain was expressed in bacterial cells, and it was determined whether Apm2 could be co-precipitated from yeast cell lysates on a GST-binding column. Apm2-TAP was pulled down by Snc1-GST, and this interaction was stronger than that between Apm2-TAP and GST alone (Fig. 3.4 C). This indicates that Apm2 binds to Snc1 through its cytosolic domain, typical of adaptor-cargo binding mechanisms. This interaction was maintained in the absence of IMA1. However, a very weak interaction was identified

between Ima1-TAP and GST-Snc1 (Fig. 3.4 C), suggesting that Ima1 may be physically associated with the Apm2-Snc1 adaptor-cargo complex.

3.3.7. Ima1 is a conserved protein with a consensus α/β hydrolase catalytic motif

The results described above suggest that Ima1 is not critical for either AP-1R recruitment or cargo binding. In order to form alternate hypotheses regarding Ima1 function, its molecular properties were further investigated. Ima1 contains a C-terminal DUF726 domain, which is also present in a large number of uncharacterized eukaryotic proteins, from yeast to humans (Fig. 3.5 A). The DUF726 domain is predicted to conform to an α/β hydrolase fold, a catalytic domain found in a wide range of eukaryotic enzymes, including thioesterases, lipases, acetyltransferases, and peptidases (reviewed in Holmquist, 2000; Nardini and Dijkstra, 1999). A BLAST search and sequence alignment revealed that that this domain within Ima1 is highly conserved among eukaryotes. A characteristic feature of all α/β hydrolases is the presence of a conserved catalytic triad consisting of a nucleophile (generally a serine within the context of a G-X-S-X-G motif), an acidic residue (D or E), and a histidine. The residues surrounding the active site are also well conserved, to preserve its structural features. Based on these homology studies, a potential catalytic triad was identified within the Ima1 C-terminal domain, which was 100% conserved. The conserved residues consist of S759 (within the motif GFSIG), D817, and H858.

Ima1is predicted to be a trans-membrane protein, according to its hydrophobicity profile (TMHMM Server v. 2.0 http://www.cbs.dtu.dk/services/TMHMM, accessed on January 17, 2011). If this were the case, however, the putative enzymatic domain would be contained within the predicted membrane-spanning region, which would not permit the association of this activity to potential substrates. To examine whether Ima1 is likely to be integral to the membrane, as predicted, subcellular fractionation was used. This showed that Ima1 is present mostly in the soluble S100 fraction (Fig. 3.5 B). The punctate membrane localization of Ima1 observed by microscopy suggests that it is likely peripherally membrane associated through weak or transient interactions with other membrane components.

These studies were followed up by determining whether the membrane association of Ima1 is influenced by treatment with Brefeldin A (BFA). BFA is a fungal metabolite which blocks the GTP exchange and membrane recruitment of Arf1, therefore causing protein transport defects at the ER and Golgi, and the mislocalization of proteins whose recruitment to these membranes depend on Arf1 (Donaldson et al., 1992). Upon brief treatment of cells

with 100ug/mL BFA, Ima1 membrane localization was lost (Fig. 3.5 C). This suggests that Ima1, like many other clathrin coat-associated proteins, is localized either directly by Arf1 or indirectly through interaction with Arf1-dependent components, and that Ima1 is likely dynamically recruited from the cytosol to sites of AP-1R function. Together, the findings that the putative catalytic domain of Ima1 is not likely membrane spanning, and that Ima1 interacts with Apm2 through its N-terminal domain, supports that the putative catalytic residues may be accessible for binding to substrates and carrying out catalysis at these sites.

3.3.8. The Ima1 GXSXG catalytic motif is required for normal Snc1 surface levels

To investigate whether the conserved predicted catalytic site identified in Ima1 is required for Snc1 sorting, the motif GFSIG containing the catalytic serine nucleophile was mutated to AFAIA by site-directed mutagenesis. The ability of this mutant construct (Ima1^{CM} *catalytic mutant*) to restore normal Snc1 surface levels *ima1Δ* cells was assessed by a plate-based invertase assay (Fig. 3.5 D). Loss of *IMA1* led to a significantly increased level of Snc1, as compared to WT cells in this assay. This increase was partially complemented by introduction of a plasmid expressing WT *IMA1* (pIMA1), as Snc1 surface levels were lowered relative to *ima1Δ*. This complementation was not complete, likely because the final screening media (YPF) does not allow for plasmid selection. Introduction of a plasmid expressing the catalytic mutant (p*IMA1*^{CM}) however, did not complement the Snc1 sorting defect to any degree. This suggests that Ima1 may have catalytic activity required for its role in Snc1 sorting by AP-1R.

The serine hydrolases include thioesterases, which catalyze the depalmitoylation of proteins (Zeidman et al., 2009). Snc1 is palmitoylated at a single cysteine residue, adjacent to its transmembrane domain, although the effects of this modification are unknown (Couve et al., 1995; Valdez-Taubas and Pelham, 2005). Since cycles of protein palmitoylation and depalmitoylation have been shown to regulate the transport of SNARE proteins (Valdez-Taubas and Pelham, 2005; He and Linder, 2009), one possibility is that Ima1 might have a role in Snc1 depalmitoylation, which may, in turn be required for its transport by AP-1R. No increase in Snc1 palmitoylation was observed when *IMA1* was overexpressed, as assessed using the Acyl-biotin exchange assay (Fig. 3.6 A and B). This suggests that Ima1 does not likely have a direct role in its depalmitoylation.

As serine hydrolases catalyze a diverse array of reactions, future work should focus on identifying the biologically relevant substrates of Ima1, which will further our understanding of the role of Ima1 in AP-1R-mediated transport.

3.4. Discussion

3.4.1. AP-1R mediates Snc1 intracellular recycling

In this study we identified a specific requirement for AP-1R in the endocytic recycling of the yeast synaptobrevin homolog Snc1, the first identified role for this complex. The co-localization of AP-1R with intracellular clathrin at Golgi/endosomal compartments supports a role for AP-1R in Snc1 recycling, and not internalization. Although the precise role of AP-1R in this pathway remains to be determined, the increase in cell-surface Snc1 in the absence of AP-1R may reflect re-routing of Snc1 along an alternate bypass pathway with faster recycling kinetics than that of the AP-1R-mediated pathway.

AP-1 has also been shown to play a role in the transport of the *S. pombe* synaptobrevin homolog, Syb1 (Kita et al. 2004; Ma et al., 2009). Deletion of both the medium chain Apm1, homologous to yeast Apm1, and the small chain of the AP-1 complex resulted in the accumulation of Syb1 in Golgi/endosomes. In addition, loss of fission yeast Apm1 function causes defects in cellular processes such as secretion, cytokinesis, vacuole fusion, and cell wall integrity. Deletion of AP-1 in *S. cerevisiae*, however, results in no discernible phenotypes and does not cause the intracellular accumulation of Snc1. Despite these differences, both of these studies support the role of AP-1 in the endosomal sorting of synaptobrevin. While Ima1 is present in *S. pombe*, Apm2 does not have considerable homology to either of the two AP-1 medium subunits. In the future, it would be interesting to determine if the fission yeast Ima1 homolog plays a role in AP-1-mediated sorting of Syb1.

3.4.2. Apm2 binds to Snc1 as cargo

A significant finding of this study is that Apm2 interacts with the Snc1 cytosolic domain, which is consistent with the well-established role of AP medium subunits in cargo recognition. Like most SNAREs, Snc1 does not contain tyrosine or di-leucine motifs. In mammalian cells, only VAMP4 and VAMP7 contain recognizable di-leucine-based motifs (Peden et al. 2001). Multiple adaptor complexes have now been shown to interact with SNAREs of the VAMP family, and a growing body of research suggests that most of these interactions are mediated by nonconventional mechanisms. The use of folded regulatory

domains, rather than the commonly used short, linear motifs, and specialized components of the transport machinery appears to be the paradigm for sorting SNAREs into post-Golgi transport vesicles (Miller et al., 2007; Chidambaram et al., 2004). As the fidelity of vesicle fusion processes in the cell requires appropriate amounts of SNAREs at their correct locations, these specialized mechanisms are likely in place to ensure that the transport of SNAREs are not vulnerable to competition from standard motif-containing cargo, and that sufficient amounts of the correct SNAREs are incorporated into CCVs for transport.

The *in vitro* binding assays used in this study could not resolve whether Apm2 interacts directly with Snc1, or if additional factors are required to bridge this interaction. If this interaction is direct, it must be mediated by non-conventional sorting signals. Apm2 may recognize Snc1 through a folded epitope. Structural studies would therefore be insightful in the understanding of how this interaction is mediated. The primary screen identified a weak requirement for the epsins Ent1 and Ent4, suggesting the possibility that they bridge the interaction between Apm2 and Snc1. As discussed, epsins are known to function as alternate sorting adaptors, and have been shown to bridge the interactions between SNAREs and AP complexes. In yeast, Ent1 is partially redundant with Ent2 for internalization (Wendland et al., 1999). Ent3/5 are required for endosome to Golgi recycling of both Chs3 and Snc1, and bind to multiple SNAREs, including Vti1 and Pep12 (Chidambaram et al., 2004), while Ent4 mediates transport from the Golgi to the vacuole (Deng et al., 2009). Whether one or more epsins bridges the interaction between Apm2 and Snc1 should be a priority in future work.

3.4.3. Distinct sorting functions for AP-1/AP-1R

These results support that the two alternate AP-1 complexes in yeast have largely non-overlapping functions. Deletion of AP-1R, but not AP-1, results in increased Snc1 surface levels. Conversely, deletion of AP-1R has no effect on the recycling of Chs3, which is mediated by AP-1 (Valdivia et al. 2002). As *APM1* mutants, but not *APM2* mutants display synthetic phenotypes in combination with a temperature sensitive allele of *CLC1* (Stepp et al., 1995), it has been suggested that Apm2 may function in a non-clathrin-mediated pathway. This seems unlikely, however, as Apm2 co-fractionates with clathrin-coated vesicles (Stepp et al., 1995), and the results reported here demonstrated that Apm2 co-localizes with intracellular clathrin. As Apm1 and Apm2 have distinct co-fractionation profiles with clathrin, they likely function in different clathrin-mediated pathways.

Alternate forms of AP-1, formed by medium subunit exchange have been identified in other organisms, including *C. elegans* and mammalian polarized epithelial cells. In both examples, these complexes have largely non-overlapping roles. In *C. elegans*, disruption of *UNC-101* (the μ1 homolog), and mutation of the alternate medium chain Apm1 have distinct effects on viability (Shim et al., 2000). In polarized epithelial cells, the ubiquitously expressed AP-1A mediates TGN to endosome transport of the proprotein convertase furin, while the epithelial cell-specific AP-1B is required for the polarized targeting of the transferrin and LDL receptors from recycling endosomes. These complexes are not functionally interchangeable, as introduction of AP-1A cannot complement the sorting defects of AP-1B-deficient polarized cells, and vice versa.

3.4.4. AP-1/AP-1R localize to similar intracellular compartments

The non-redundant cargo-specific functions of AP-1A and AP-1B in polarized cells have been partially explained by their differential localization to distinct membrane domains. Although mammalian AP-1A and AP-1B were first shown to share a similar localization, further studies revealed by immunoelectron microscopy that they define partially distinct subdomains, with AP-1A localizing to the Golgi, and AP-1B localizing to a perinuclear region immediately adjacent to the Golgi (Fölsch et al., 2003).

Despite their specificity for distinct cargo, however, substantial overlap in the localization of Apm1 and Apm2 to Golgi/endosomal compartments was observed, suggesting that the two complexes may recognize distinct sets of cargo from a common membrane. This overlap was not complete, however. A small proportion of Apm2 puncta did not co-localize with Apm1, and it is therefore possible that AP-1R facilitates Snc1 recycling through a distinct endosomal population or membrane domain. Further studies may help to resolve whether there are small-scale differences in AP-1 and AP-1R localization. Currently, these studies are limited by the incomplete understanding of endosomal organization in yeast. It is not known if there are functionally distinct populations of early endosomes, or if endosomal membranes contain subdomains, with different compositions.

3.4.5. Role of Ima1 in AP-1R regulation

In this study, Ima1 was identified as a specific regulator of AP-1R. Deletion of *IMA1* resulted in increased Snc1 surface levels, and it shared a similar genetic interaction profile with AP-1R components based on E-MAP studies (Burston et al., 2009). Both Ima1 and AP-

1R localize to Golgi/endosomal compartments. Furthermore, a preferential and likely direct interaction between Ima1 with Apm2, but not Apm1 was demonstrated.

The interaction between Apm2 with Ima1 was surprising, as most AP-regulatory proteins associate with the appendage domains of the large subunits (Page et al., 1999; Hirst et al., 2003). A few recent studies, however, have reported that the medium subunit also participates in regulatory interactions. Many μ-binding regulators are enzymes that have important roles in lipid regulation. Some of these regulators are themselves tyrosine-based cargo proteins, and bind to the canonical μ binding pocket. For example, the lipid kinase PIPKI gamma-p90 interacts with the AP-2 μ subunit. (Kahlfeldt et al., 2010). Binding to AP-2 μ stimulates the kinase activity of PIPKI gamma-p90, facilitating localized PI(4,5)P_2 synthesis activity at endocytic sites. The increased PI(4,5)P_2, in turn leads to enhanced AP-2 recruitment to these sites. This interaction is therefore cooperative, and enhances the activity of both the adaptor and the regulator in a positive feedback loop.

The interaction between Ima1 and Apm2 is mediated through the N-terminal 162 amino acids of Ima1. Within the Apm2 μ2 C-terminal region, Ima1 binds subdomain B, and does not require its tyrosine motif-binding site. Interestingly, this region is quite divergent between Apm1 and Apm2, suggesting that it could contribute to the sorting specificity of the two complexes due to differential interaction with Ima1. In regions where μ1 homologs contain negatively charged residues, the corresponding residues in μ2 homologs are often positively charged and vice-versa. A recent study identified a patch of three positively charged residues within the corresponding region of the mammalian AP-1B μ1-B subunit, which are conserved among μ1-B homologs, but not with those of μ1-A homologs (Fields et al., 2010). This patch was required for the differential recruitment of AP-1R complexes to PI(3,4,5)P_3-rich recycling endosomes, and upon mutation of these residues to the corresponding residues in μ1-A, this localization was lost, resulting in missorting of AP-1B-dependent cargo. Furthermore, AP-1B expression was required for the localization of PIPKI-gamma90, which generates PI(3,4,5)P_3 at recycling endosomes. This indicates that there is interdependence in the function of both AP-1B, and PIPKI-gamma90. It was proposed that AP-1B either binds PI(3,4,5)P_3 directly, or that it is recruited by an unidentified protein that requires PI(3,4,5)P_3 for its localization.

Since Ima1 binds to the region of Apm2 which by analogy to other μ subunits, contains residues important for lipid binding, it was hypothesized that Ima1 could be required for the membrane localization of AP-1R. However, no decrease in membrane

binding of AP-1R in *ima1Δ* cells was observed by either microscopy or subcellular fractionation. The possibility still remains that Ima1 is required for recruitment of AP-1R to the small population of compartments that do not contain Apm1. It is also possible that Ima1 is necessary for recruitment of AP-1R to specialized lipid domains within membrane compartments containing both complexes.

This study also demonstrated that Ima1 is not required for Apm2 cargo binding. The *in vitro* approach that was taken, which assessed the binding of Apm2 from cell lysates to an immobilized GST-Snc1 construct, suggesed that Ima1 does not form a direct link between Apm2 and Snc1, and is not required for any modification of Apm2 necessary for this binding. It remains to be determined whether Ima1 is required for the interaction between Apm2 and Snc1 *in vivo*, as no reproducible interaction between these proteins was detected by coimmunoprecipitation. These results are consistent with a weak and transient interaction between Apm2 and Snc1 *in vivo*, as has been shown by multiple other studies for adaptors and their respective cargo.

It remains possible that Ima1 is required for a later step in AP-1R function, such as vesicle formation or un-coating. Investigating these possibilities is of priority for future studies.

3.4.6. Ima1 has putative enzymatic activity

The only previous study investigating the function of Ima1 was based on its interaction with the P0 subunit of the ribosomal stalk, which is translocated to the cell surface by unknown mechanisms (Aruna et al., 2004). The precise role of Ima1 in this process, however, has not been further investigated.

Our homology studies revealed that Ima1 is conserved among eukaryotes, and is a member of the α/β-hydrolase family. This is a catalytic domain found in a wide-range of enzymes, including esterases, lipases, acetyltransferases, and peptidases, containing a unique structural fold, and encompassing a catalytic triad, consisting of the residues (Ser, Cys, or Asp), Asp/Glu, and His. We identified a putative catalytic site in Ima1, conforming to this consensus. This site is characteristic of serine hydrolases, and is 100% conserved among all considered sequences. Serine hydrolases are generally cytoplasmically localized, and show transient recruitment to their sites of activity. Although Ima1 is predicted to be a transmembrane protein, this work demonstrates that it is mainly cytosolic, and that it is likely has a dynamic localization to Golgi/endosomal compartments. The conserved Ima1 catalytic residues appear to be required for Snc1 sorting, as a mutant version in which these

residues were mutated to alanine was unable to complement Snc1 surface levels in *ima1Δ* cells. An important challenge in the future will be to characterize the precise enzymatic activity of Ima1 and to identify its biologically relevant substrates. Based on its binding to the Apm2 B domain, Ima1 may play a role in lipid remodeling at Golgi/endosomal compartments. A full understanding of Ima1 function will require the identification of its substrates, and a better understanding of the organization of endosomal membranes in yeast.

In conclusion, this work has identified a role for the previously uncharacterized AP-1R complex in Snc1 recycling, a function distinct from AP-1. Furthermore, Ima1 was specifically required for AP-1R-mediated transport, and has putitive enzymatic activity related to this function. These findings fit with a growing body of research suggesting that alternate isoforms carry out distinct sorting functions through participating in differential interactions with sorting determinants, and provide new evidence that AP medium subunits are the target of interactions by enzymatic regulators.

3.5. Materials and methods

Construction of plasmids and yeast strains

Plasmids and yeast strains constructed for this study, and details of their construction, are listed in Table B1. Unless otherwise indicated, plasmids were constructed by homologous recombination after cotransforming yeast with linearized vector and DNA fragments bearing 50–55-bp homology, and recovering recombinant plasmids in *E. coli*. The MATa yeast strain BY4741 and its gene deletion derivatives were obtained through Thermo Fisher Scientific. Unless otherwise stated, gene disruptions and tagging of genomic ORFs were performed by transformation of a PCR product containing a drug selection marker, flanked by 50–55 bp of homology to the region of interest.

Liquid invertase assay

The liquid invertase assay used in this study is modified from that previously described (Darsow et al., 2000). Strains expressing either the GSS construct were inoculated into 2ml YP fructose cultures and allowed to grow for 20 hours to saturation (OD 600 ≈10). Cultures were diluted to 3OD/mL, and 5µl was mixed with 55µl 0.1M NaOAc buffer pH4.9 inside a well of a 96 well microtiter plate. With the use of a Victor3 multilabel counter and injectors (PerkinElmer, Waltham, Massachusetts), 13µl of freshly prepared 0.5M ultra pure sucrose was added to each well, and the plate was incubated for 5min. at 30°C. Following

sucrose incubation, 100µl of glucostat reagent (0.1M K2HPO4 pH 7.0, 347.1 U Glucose Oxidase, 2.6 ng/ml Horseradish peroxidase (HRP), 102.6 nM N-ethylameide (NEM), 0.15 mg/ml O-Dianisidine) was added to each well, and the plate incubated for an additional 7min. at 30°C. Finally, 100µl of 6N HCL was added to each well to stop the reaction. The absorbance of each well at 540nm was measured and used to determine glucose concentration. Results are reported as nM glucose produced per 1 OD600 of culture. Glucose standards (ranging from 5-50nM) and blanks were included in each experiment to ensure accurate measurements that were within the linear range.

Calcofluor white screening

Knockout strains were plated in 1,536-array format onto YPD plates containing 50 µg/ml CW (Sigma-Aldrich), using a Virtek automated colony arrayer (Bio-Rad Laboratories). After incubation at 30°C for 3 d, white-light images were acquired using a flat-bed scanner (model 2400; Epson), and fluorescent-light images were captured with a Fluor S Max MultiImager (Bio-Rad Laboratories) using the 530DF60 filter and Quantity One software (version 4.2.1; Bio-Rad Laboratories). The open-source spot-finding program GridGrinder (http://gridgrinder.sourceforge.net) was used for the densitometry of digital images. Average growth and fluorescence values from two independent screens were calculated for each strain using Excel (Microsoft).

Fluorescence microscopy

Indirect immunofluorescence microscopy, fluorescent microscopy of yeast cells expressing GFP-tagged proteins were carried out as described (Conibear and Stevens, 2000, 2002). Cells were viewed using a 100x oil-immersion objective on a Zeiss Axioplan2 fluorescence microscope, and images were captured with a CoolSnap camera using MetaMorph software and adjusted using Adobe Photoshop. Immunofluorescence experiments involving BFA were carried out by incubating cells from early-log phase cultures in a final concentration of 100ug/mL BFA for 10 minutes. Two color widefield images were acquired and processed as described in chapter 2. Exposure times varied from 600-750ms. TIRF images were collected with a 3i Marianas microscope (Intelligent Imaging Innovations, Denver, CO) equipped with an alpha Plan-Fluar 100x 1.46 NA objective and a Zeiss TIRF slider (Carl Zeiss, Thornwood, NY). Images were acquired with 488nm and/or 561nm laser excitation, with GFP and RFP emission split between two Cascade II 512

cameras with an Optical Insights Dual Cam with an exposure time of 750ms. TetraSpeck 100nm beads (Invitrogen) were used to align the two channels and for subsequent registration in software. Slide-Book 4.2® software (Intelligent Imaging Innovations, Denver, CO) was used for image acquisition and dual channel image registration. Montages were created using the National Institute of Health ImageJ software (http://rsb.info.nih.gov/ij/) with the Kymograph plugins installed (http://www.embl.de/eamnet/html/kymograph.html).

Live-cell imaging experiments involving LAT-A treatments were performed by incubating cells from early-log phase cultures in a final concentration of 200 μM LAT-A dissolved in DMSO for 30 min at 30°C. LAT-A treated early-log phase cultures were used for the total internal reflection microscopy (TIRF) experiments. For each TIRF experiment 200 μL of treated cells were spotted onto Conconavalin A-coated 8 well Lab-Tek dishes (Nalge Nunc, Rochester, NY).

Co-immunoprecipitation

Log phase cells were converted to spheroplasts and stored at -85°C (Conibear and Stevens, 2000). Spheroplasts from 20OD600 of cells were resuspended in 1mL lysis buffer (600mM Sorbitol, 50mM KH2PO4 pH7.5, 50mM NaCl, 1.5%TX-100), on ice for 10 minutes. Lysates were incubated with 40ul IgG sepharose (75% slurry) for 2.5 hours, rotating at 4°C. The pellets were washed two times with 1ml lysis buffer (50mM KH2PO4 pH 7.5, 75mM NaCl, 1.5% TX100), and were subjected to SDS-PAGE. Co-precipitated proteins were detected by Western blotting with antibodies to GFP (mouse mαGFP 1:1000, Roche #1814460, monoclonal) HA (mouse mαHA 1:1000, Abcam #ab16918, monoclonal) or TAP (rabbit α-TAP 1:5000, Open biosystems #cab1001 polyclonal) followed by HRP-labelled secondary antibodies (GAR-HRP Biorad #170-6515 or GAM-HRP Biorad #170-5047). Blots were developed with ECL and exposed to X-ray film (X-OMAT LS, Kodak).

In vitro Snc1-GST binding assays

Truncated Snc1 lacking its transmembrane domain cloned into vector pETGEXCT (Sharrocks, 1994, gift from Anne Spang). Snc1-GST was expressed and purified from in E. coli BL21 using standard procedures. Bacterial Induction of GST proteins and immobilization on glutathione: Cells were grown at 37°C to mid-log phase, and expression was induced at 30°C by addition of 1mM IPTG for 3 hours. 3 OD pellets were frozen at

stored at -85°C. Cell pellets were lysed by sonication in PBS, on ice (in the presence of protease inhibitors). Bacterial lysates were incubated with 20 ul of 50% glutathione Sepharose 4B for 1 hour at 4°C, while rotating. Unbound proteins were removed with three washes in PBS. Incubation of yeast lysates with immobilized GST proteins: Yeast lysates were prepared as described above. Lysates were incubated with GST proteins immobilized on glutathione sepharose beads for 2.5 hours at 4°C, while rotating (total volume of 1mL; NaCl adjusted to 150mM). Following incubation, beads were washed two times with cold lysis buffer. Samples were heated to 70°C in SDS sample buffer, and eluted proteins were analyzed by SDS-PAGE and Western Blotting, as described above.

Yeast two-hybrid screening

PJ694a strains carrying pOAD-based vectors were mated to PJ694alpha strains carrying pOBD2-based plasmids expressing the indicated full length and truncation proteins (Tong et al. 2002). Positive two-hybrid interactions were scored on minimal media lacking histidine (containing 5mM 3-AT) or adenine after growth at 30°C for 5 days.

Subcellular fractionation

Fractionation of organelles was performed by differential centrifugation of cell lysates as described by Conibear and Stevens (2000). 20 OD_{600} of exponentially growing cells were spheroplasted, lysed and centrifuged for 5 min at 500 g to remove unbroken cells. The supernatant was centrifuged for 10 min at 13,000 g to generate the membrane pellet fraction (P13), and the supernatant (S13) was centrifuged at 100,000 g for 60 min generating the P100 pellet fraction and S100 supernatant. The membrane pellets were re-suspended in 300ul sample buffer. Proteins in the S100 fraction were precipitated by the addition of TCA to a final concentration of 5%, collected by centrifugation for 5 min at 13,000 g, washed twice with acetone, air dried and resuspended in 300ul sample buffer. The proteins in 10ul of each fraction were separated by 15% SDS-PAGE, transferred to nitrocellulose, and were subjected to western blotting, as described above.

Invertase plate assay

Colony arrays of strains containing an integrated version of the GSS reporter plus the indicated pRS415-based plasmids were spotted on SC-LEU plates in 96-array format. This array was then replicated to 384-array and then 1536-array formats on the same

media. For screening, the 1536 array was replicated to YPF plates. The invertase assay was carried out as described in chapter 2.

Snc1 palmitoylation assay

Snc1 palmitoylation was assessed by acyl-biotin exchange (Politis et al., 2005), using a modified version of the Drisdel and Green method (Drisdel and Green, 2004). Ima1 overexpression was carried out from GAL-based plasmids with a 4-hour galactose-induction period. Overnight cultures grown in SC-URA+2% raffinose, and were then grown to early log phase, at which point they were transferred to either SC-URA +2% galactose or SC-URA +2% raffinose media for the 4 hour induction period. Denatured protein extracts were prepared from Snc1-GFP–expressing cells by glass bead lysis either with or without *IMA1* overexpression. Extracts were subjected to the three steps of acyl-biotinyl exchange protocol. The epitope-tagged Snc1 was immunoprecipitated with anti-GFP antibodies, and the resulting samples were run on a 10% SDS gel. Western blotting was then carried out with either anti–biotin-HRP or anti-GFP antibodies.

3.6. Figures

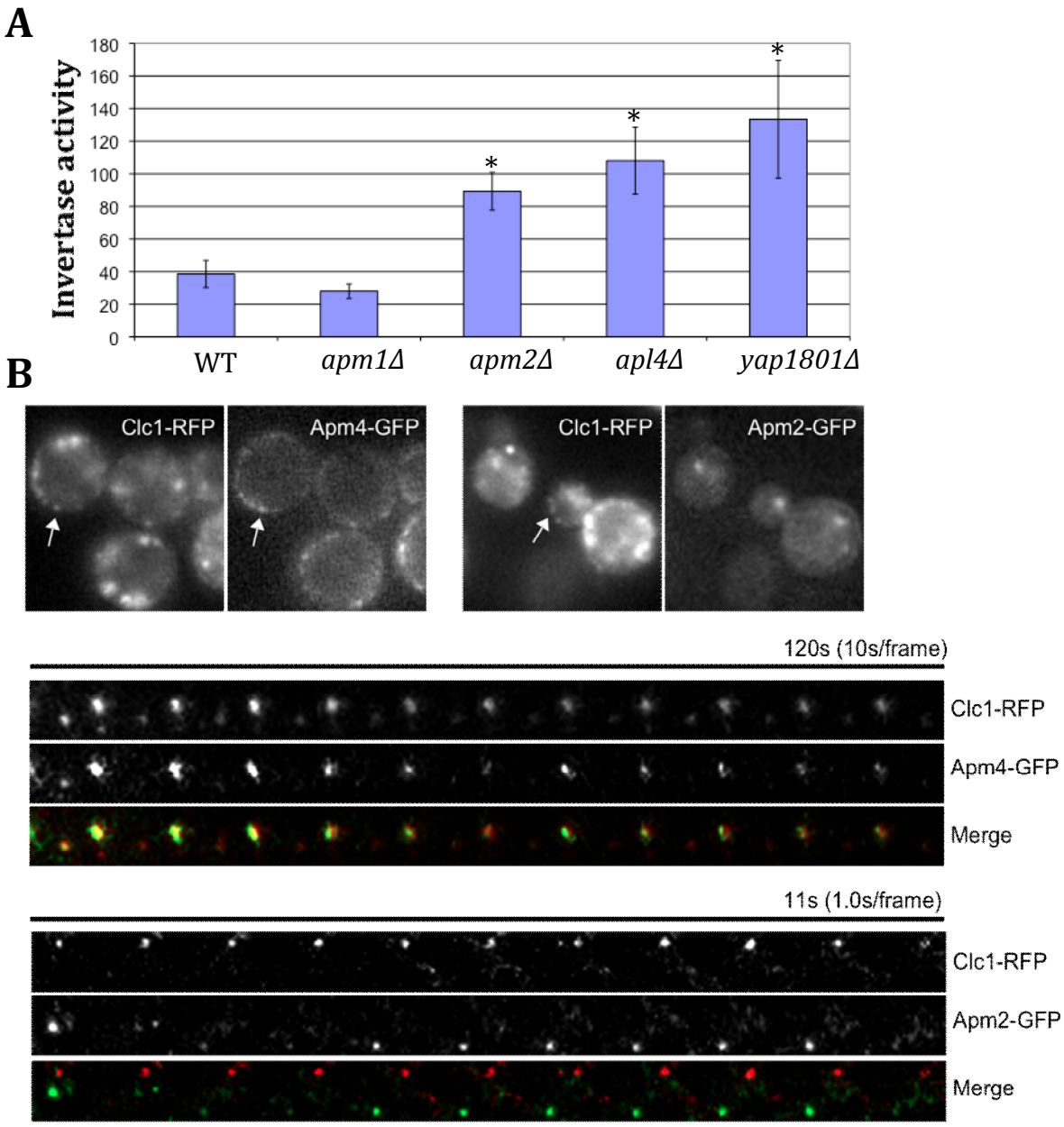

Figure 3.1. AP-1R is required for correct sorting of Snc1

(A) Quantification of cell surface levels of the Snc1 reporter (GSS) at the cell surface in AP-1R deletion strains by invertase assay of liquid cultures. Invertase activity is reported as nmol glucose release/OD600, and the mean +/-SD of 5 independent experiments is shown. * P<0.001 by student t-test, as compared with WT. **(B)** Co-localization of Apm4-GFP and Apm2-GFP with Clc1-RFP at cortical actin patches in LAT-A-treated cells by wide-field microscopy (upper panels). Lower panels show TIRF microscopy and kymograph analysis of Apm2-GFP or Apm4-GFP relative to a single cortical clathrin patch marked by Clc1-RFP (*sla2Δ* cells)

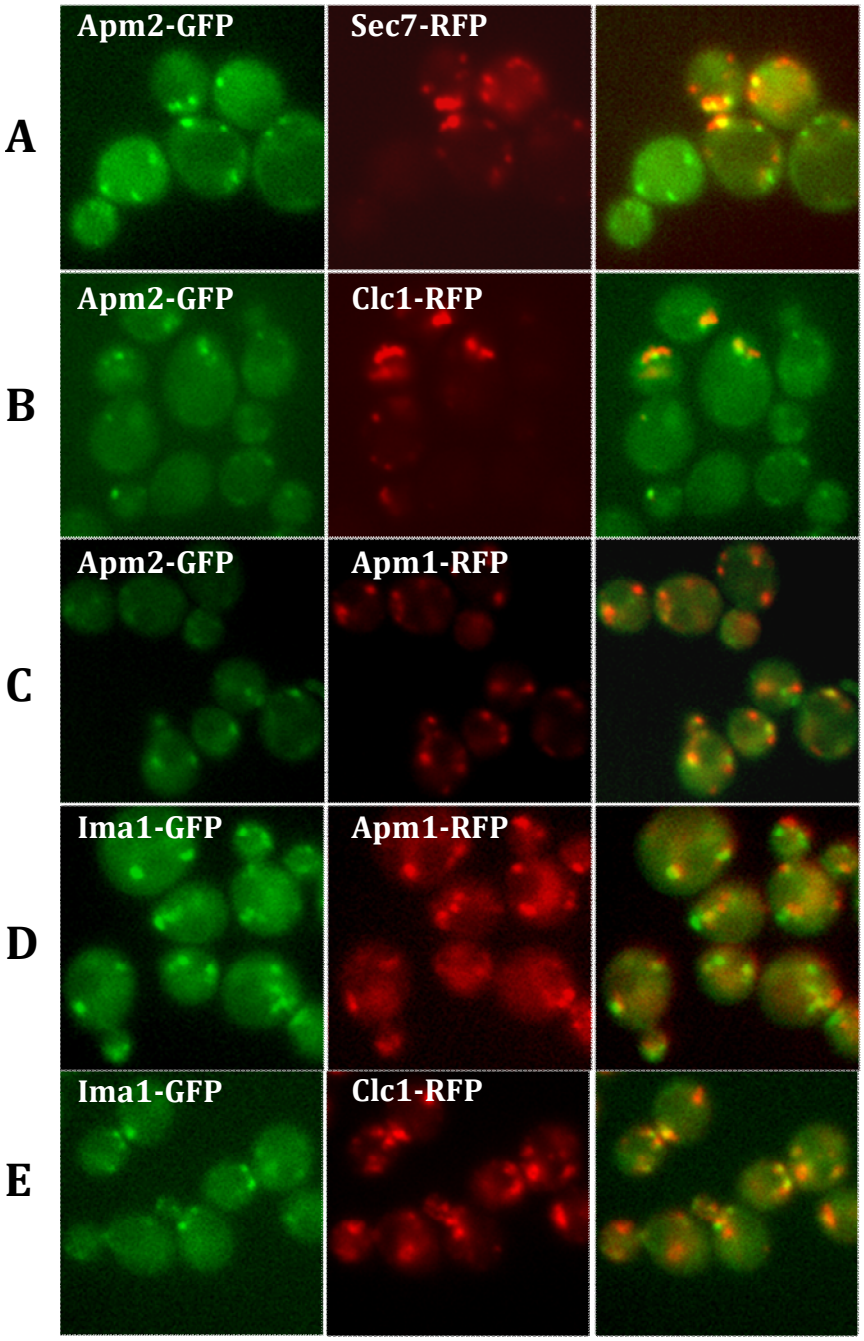

Figure 3.2. AP-1R and Ima1 localize to Golgi and endosomal compartments

Co-localization of Apm2-GFP or Ima1-GFP with the RFP-tagged markers Sec7-RFP (late Golgi), Clc1-RFP (clathrin), and Apm1-RFP (AP-1).

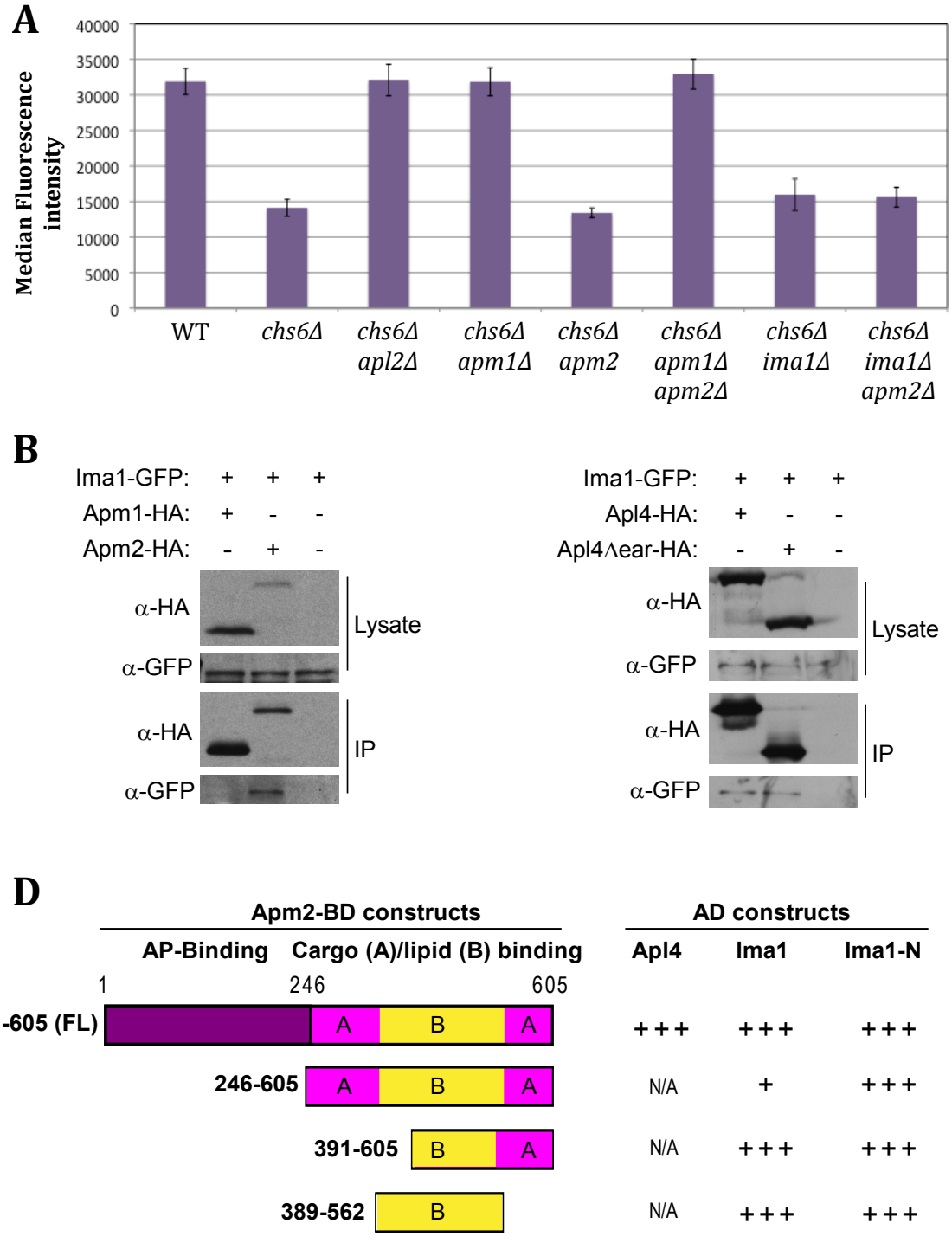

Figure 3.3. Ima1 associates functionally and physically with AP-1R

(A) Chs3 surface levels were quantified in *chs6Δ* cells in combination with mutations in AP-1 or AP-1R components and *IMA1*, based on Calcoflour White fluorescence assay. Results are reported as spot median pixel intensity, as assessed by densitometry.

(B) Ima1 preferentially interacts with Apm2 versus Apm1 by co-immunoprecipitation. Cells were grown to midlog phase and were processed for immunoprecipitation (see Materials and Methods). Immunoprecipitation (IP) was performed with anti-GFP antibodies, whereas Western blotting was performed with both anti-HA and anti-GFP antibodies. **(C)** Ima1 interaction does not require the Apl4 GAE domain. Immunoprecipitation was carried out as in (B). **(D)** Yeast two-hybrid assay between full-length Apm2-GAD and Ima1-GBD, and between full-length and N-terminal domain of Ima1 (1-262) with the indicated Apm2 truncations. Apl4-GBD was used as a positive control for the expression of Full length Apm2. The relative strength of interaction is indicated, as qualitatively assessed by growth on SC-HIS supplemented with 5mM 3AT.

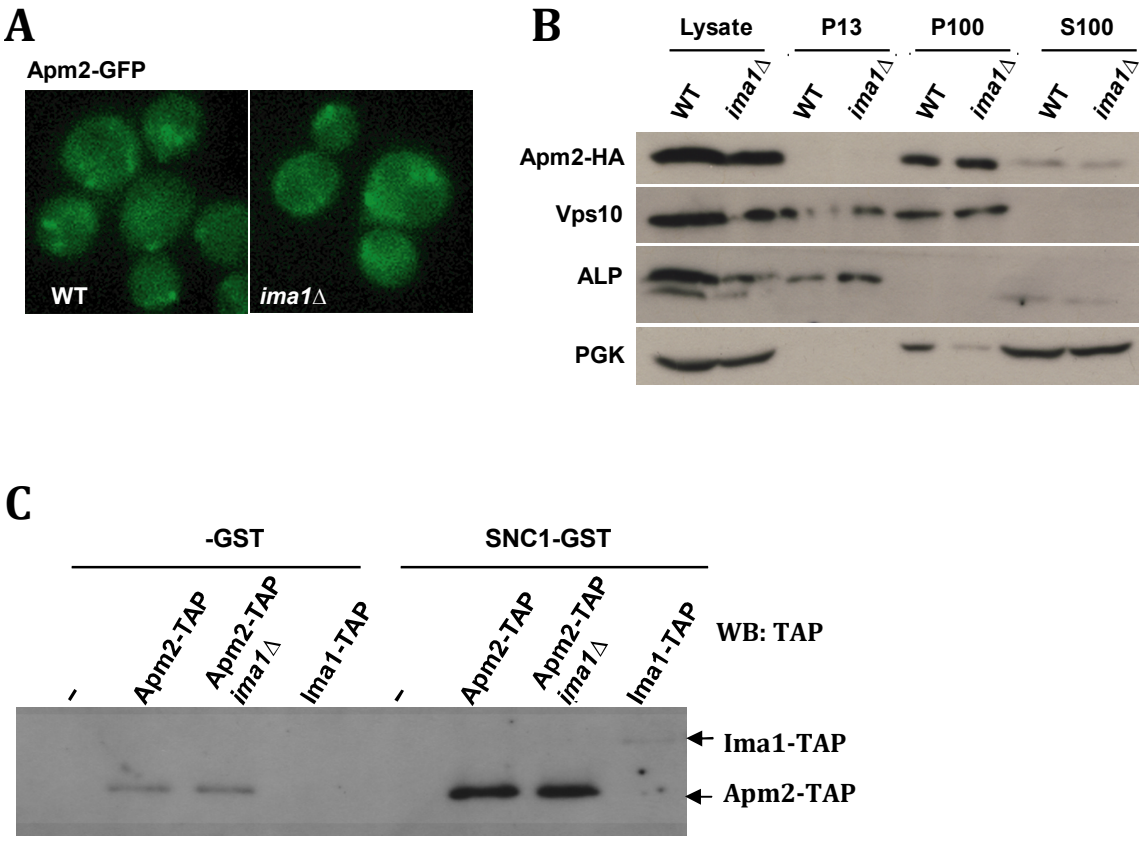

Figure 3.4. Ima1 is not required for Apm2 membrane recruitment or cargo binding

(A) Localization of Apm2-GFP in WT vs. *ima1Δ* cells. **(B)** Membrane association of Apm2-3HA in WT versus *ima1Δ* cells, assessed by subcellular fractionation. Apm2 is enriched in the high speed membrane fraction (P100). Markers of subcellular fractions are Vps10 (Golgi), ALP (vacuole), and PGK (cytosol). **(C)** Apm2-3HA binds to immobilized GST-Snc1 in vitro, and does not require *IMA1*. Purified recombinant GST-Snc1 or GST alone were incubated with lysates prepared from Apm2-3HA WT or Apm2-3HA *ima1Δ* cells, and a GST-pull down assay was performed. Samples were subjected to SDS-PAGE and analyzed by immunoblotting with anti-HA antibodies. Ima1 interacts weakly with GST-Snc1, as assessed on the same blot.

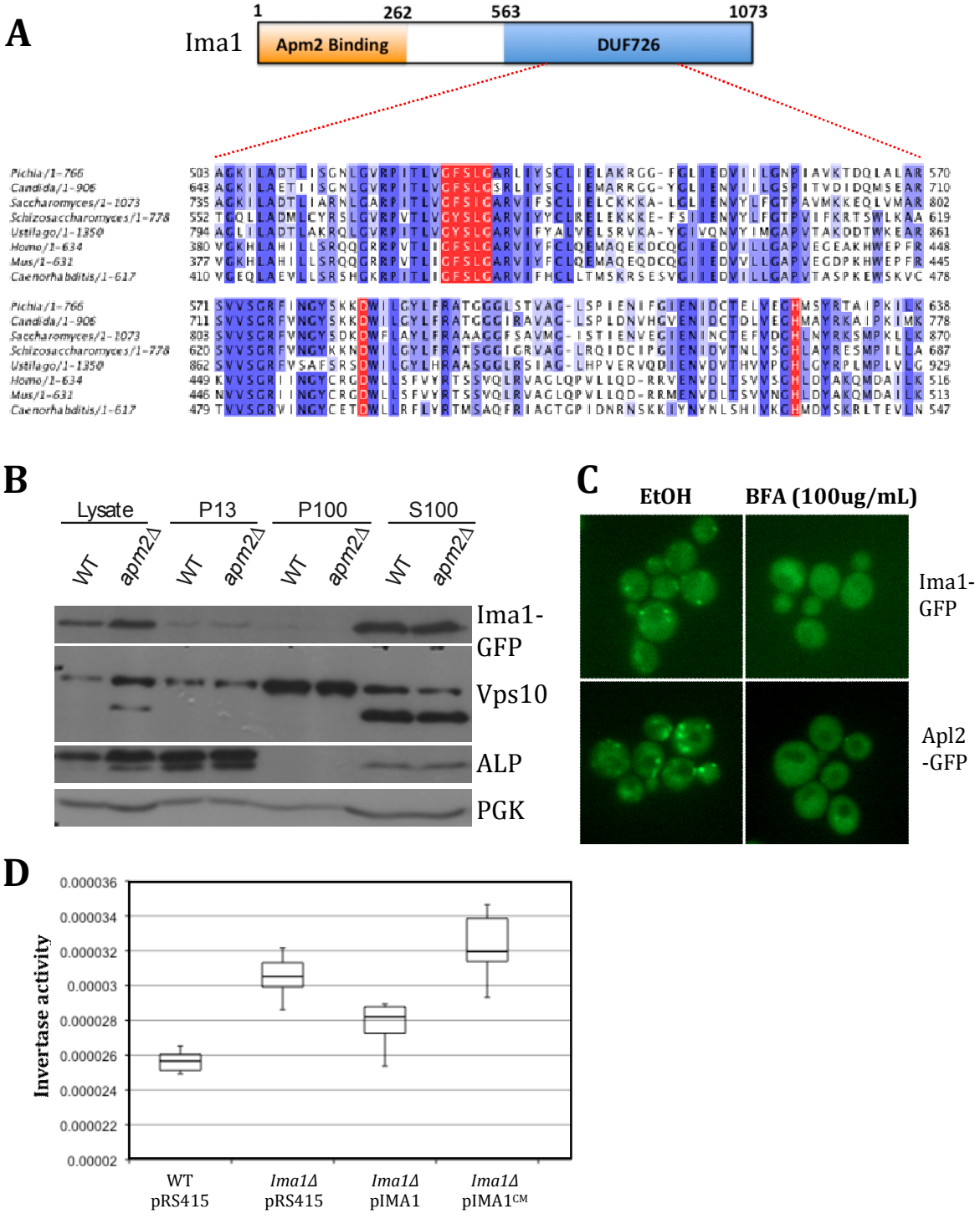

Figure 3.5. Ima1 contains putative catalytic residues, required for Snc1 sorting

(A) Schematic of Ima1, indicating N-terminal Apm2-binding domain, and DUF726 domain (top) Sequence alignment of Ima1 C-terminal domain with conserved homologs, highlighting the conserved catalytic triad residues (bottom) **(B)** Subcellular fractionation of

Ima1). Control markers for other subcellular fractions are Vps10 (P100; light membrane fraction), ALP (P13; heavy membrane fraction), and PGK (S100; soluble fraction). **(C)** Microscopy of Ima1-GFP in cells treated with BFA (100ug/mL, 10 min). Apl2-GFP is included as a control for peripheral membrane association. **(D)** Quantification of GSS surface levels in WT versus *ima1Δ* cells, containing plasmids for the expression of WT *IMA1*, *IMA*^{CM} (catalytic mutant) or empty vector (pRS415). (invertase overlay assay; n=7 replicates per group). pRS415-based plasmids were introduced into a background strain expressing the GFP-Snc1-Suc2 (GSS) reporter, and were selected for based on growth on –LEU plates. Strains were arrayed onto YPF plates in 1536 format, and were assessed for GSS surface levels as described in chapter 2 (genome-wide screening, materials and methods). Boxes represent upper and lower quartiles.

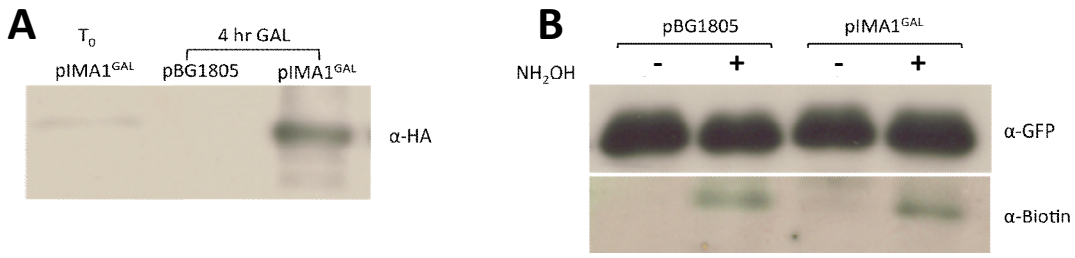

Figure 3.6. Overexpression of Ima1 does not affect Snc1 palmitoylation

(A) *IMA1* GAL-induced overexpression. GAL-inducible plasmids expressing Ima1 (pIMA1^{GAL}) or empty vector control (pBG1805) were introduced into WT cells. Cells grown overnight in SC + 2% raffinose were diluted and grown to mid-log phase (T_0), at which point they were grown for 4 hours in SC + 2% galactose for 4 hours. Overexpression of Ima1 was detected by immunoblotting to HA. **(B)** Snc1 palmitoylation status was assessed by Acyl-Biotin Exchange (ABE) in strains expressing GFP-Snc1 (endogenously tagged), and overexpressing either *IMA1* (pIMA1^{GAL}) or empty vector control (pBG1805) (4h gal induction, as described in A). Cells were were subjected to the acyl-biotin exchange reaction. Protein extracts were treated with (+) or without (-) hydroxylamine (NH_2OH). Anti-GFP precipitates were blotted with anti-biotin and anti-GFP to detect palmitoylated and total Snc1, respectively.

CHAPTER 4: DISCUSSION AND FUTURE DIRECTIONS

4.1. Overview

The overall goal of this work was to identify the requirements for the endocytic recycling pathway of Snc1, the yeast VAMP2 homolog. Towards this goal, a sensitive and quantitative assay was used to systematically identify genes required for this pathway, on a genome-wide level. Genetic and bioinformatic approaches were used to infer functional relationships between top candidates, and to guide downstream molecular analysis of these genes. Through this work, multiple genes were identified that were predicted to function in endocytosis and recycling, but have not previously been shown to have sorting defects. A model that encompasses the findings from this work is proposed in illustration 4.1

Chapter 2 investigated the mechanisms regulating Snc1 endocytosis. This study identified roles for many yeast homologs of mammalian endocytosis genes, including clathrin and the yeast AP180 clathrin adaptors. The results showed that yAP1801 and yAP1802 are partially redundant in Snc1 internalization. Furthermore, they have a cargo-selective function: combined deletion selectively blocked internalization of Snc1, but not other endocytic cargo. Similarly, the synaptojanin Inp52 also had a cargo-selective function, likely through its role in the uncoating of AP180 from endocytic vesicles. This study also identified a requirement for the previously uncharacterized protein Ldb17 in the regulation of coat and actin dynamics at endocytic sites.

Chapter 3 focused on characterizing components required for Snc1 intracellular recycling, and demonstrated a role for the AP-1 complex variant, AP-1R in this process, and for the previously uncharacterized protein Ima1. The results support that the closely related AP-1 and AP-1R have cargo-specific functions in Golgi/endosomal transport. Ima1 was found to be a regulator of AP-1R function, and is specifically associated with AP-1R both functionally and physically, but not AP-1. It is therefore likely to contribute to the specificity of the AP-1R complex. Ima1 is highly conserved in eukaryotes, and has predicted enzymatic residues that are required for normal Snc1 surface levels.

Collectively, these studies show that considerable functional redundancy and weak endocytic defects at least partially explain the lack of observable defects for these components in previous studies, and demonstrate that endocytic mechanisms in yeast and man are more similar than previously appreciated. These studies are also consistent with the view that sorting of SNARE proteins is subject to highly specific mechanisms, and that the use of unconventional adaptors may be widespread for these recognition events.

Although this work has generated insight into mechanisms regulating Snc1 endocytic recycling, it also encourages new questions. How is AP180 recruited to endocytic sites, and what is the mechanism by which Inp52 contributes to AP180 uncoating? The signals in Snc1 that mediate its interaction with the endocytic machinery and with AP-1R also remain to be identified. These questions, methods to address them, and ways to apply the insight generated here to future studies, are discussed in this chapter.

4.2. Mechanisms regulating Snc1 internalization

4.2.1. Role of clathrin and yeast AP180 homologs in Snc1 endocytosis

A requirement for clathrin and its adaptors in the internalization of Snc1 was a highly significant finding. This study revealed that the yeast AP180 clathrin adaptor homologs yAP1801/1802 have a partially redundant role in Snc1 internalization. While individual deletion of yAP1801 or yAP1802 led to a relatively weak endocytic defect, combined deletion of yAP1801/1802 completely blocked internalization. Furthermore, yAP180 was not required for the uptake of other commonly studied endocytic cargo. The partial redundancy and cargo-specificity of these adaptors serve to explain why endocytic defects have not previously been identified for yAP1801 and yAP1802. This was significant because although clathrin contributes to the total number of endocytic sites and to the stability of endocytic complexes, no cargo has previously been shown to be dependent on clathrin or its adaptors for internalization in yeast (Newpher et al., 2005; Drubin et al., 2005). This discrepancy has remained unexplained in the field for decades, as it contrasts with the essential role for clathrin in mammalian cells.

There are many important questions raised by our work on yAP180 that should be addressed in future studies. What are the mechanisms regulating its recruitment to endocytic sites, and release from endocytic vesicles? Does AP180 bind to cargo directly, or through additional bridging interactions? In this study, some of these questions were addressed. In the context of our findings, future approaches that would be useful in further addressing these questions are discussed below.

4.2.2. How is yAP180 recruited to endocytic sites?

We identified a strong requirement for clathrin in Snc1 uptake, but found that AP180 does not need to bind to clathrin directly to carry out internalization, as deletion of its clathrin binding site did not prevent Snc1 uptake. This suggested that AP180 might be

linked to clathrin through additional proteins. Although CLASPs generally bind to AP-2 for recruitment to endocytic sites (Maldonado-Báez and Wendland, 2006), we did not identify a requirement for AP-2 in Snc1 uptake. It thus remains unclear how yAP180 is recruited. The requirement for clathrin and AP-2 for AP180 recruitment appears to differ between organisms, and thus remains unclear. In *C. elegans*, it is likely that AP180 works with AP-2 to direct internalization, as a similar increase in surface levels was shown in AP180 and AP-2 mutants (Dittman and Kaplan, 2006). In mammalian cells, however, the AP-2 binding sites within AP180 have only a minor contribution, suggesting that other factors regulate the recruitment of AP180 to endocytic sites (Harel et al., 2008).

Although mutation of the known yAP180 clathrin-binding motif did not prevent Snc1 uptake, it remains possible that yAP180 contains additional clathrin binding motifs yet to be identified. Mammalian AP180/CALM contains multiple clathrin binding motifs (Legendre-Guillemin et al., 2004). Whether the yAP180 clathrin binding mutant actually blocks interaction with clathrin has not been determined, and should be assessed in future studies.

Is yAP180 recruited to sites of internalization through association with proteins other than clathrin and AP-2? AP180 proteins contain binding sites for not only clathrin and AP-2, but also for $PI(4,5)P_2$ (the ANTH domain), and for EH domain motif-containing proteins (NPF motifs) (Maldonado-Báez and Wendland, 2006). It is therefore possible that yAP180 is recruited by lipid binding, or by EH-domain proteins. Interaction between the AP180 NPF motifs with EH-domain-containing scaffolding proteins seems to be important in mammalian cells: AP180 interacts with the EH-domain proteins eps15 and intersectin. In yeast, the yAP180 NPF motifs bind to the EH-containing epsins (Ent1 and Ent2), and to yeast homologs of eps15 (Ede1) and intersectin (Pan1) (Maldonado-Báez L, and Wendland, B., 2006; Wendland and Emr, 1998; Aguilar et al., 2003; Miliaras and Wendland, 2004). These EH domain proteins interact with multiple components of the endocytic machinery, and may be important in AP180 recruitment. Additionally, Ent1, Ent2, and Ede1 all contain clathrin binding sites, and may therefore link AP180 to clathrin.

How could the role of Ent1/2, Ede1, and Pan1 in the recruitment of yAP180 be determined? A first approach could be to investigate whether mutation of the AP180 NPF motifs causes defects in Snc1 internalization using the invertase assay, or microscopy. If strong defects were observed, this would suggest an important function for association between the AP180 NPF motifs and one or more of these EH-motif containing proteins.

Further studies could help determine which of these proteins are important. This could be accomplished by assessing the effects of mutating the EH-motifs in each of these proteins on Snc1 internalization. Our screen results demonstrated that *ede1Δ* mutants have a relatively weak defect in Snc1 internalization, similar to that of the *yap1801Δ* and *yAP1802Δ* single mutants. This demonstrates that Ede1 alone is not likely to be the only requirement for yAP180 recruitment. Ent1 mutants had an even weaker phenotype, but Ent1 has been shown to be partially redundant with Ent2. Although *ent1Δ/ent2Δ* mutants are inviable (Wendland et al., 1999), assessment of Snc1 sorting in *ent2Δ* mutants in combination with a temperature sensitive *ENT1* allele could reveal a role for these proteins in AP180 function. *PAN1* is an essential gene and was not assessed in our primary screen. The role of Pan1 could therefore also be assessed through the use of temperature sensitive alleles, overexpression studies, or through mutation of its EH motifs. If mutation of any of these proteins is found to result in a strong endocytic defect, their effects on yAP180 endocytic patch recruitment could be evaluated by TIRF microscopy. AP180 recruitment could alternatively be mediated though $PI(4,5)P_2$ binding through its ANTH domain. A similar strategy could therefore assess the effects of ANTH domain deletion on Snc1 internalization.

Although we may find that individual deletion of the NPF motifs, or the ANTH domain impairs the AP180 Snc1 sorting function, mutation of these domains may not be enough. Since adaptors bind to multiple components simultaneously for membrane recognition, often mutations in multiple motifs are required to observe recruitment defects (Motley et al., 2006). Therefore, the combinatorial effects of these mutations on yAP180 recruitment may also need to be assessed by the methods described above.

4.2.3. Role of synaptojanin in yAP180 vesicle un-coating

By screening for additional cargo-specific factors, a requirement for the $PI(4,5)P_2$ lipid phosphatase, synaptojanin (Inp52) was identified. Loss of *INP52* resulted in a cargo-specific internalization defect that was similar to the *yap1802Δ* mutant. Further work showed that deletion of *INP52* caused the accumulation of yAP180 on cytosolic vesicles, likely explaining the similar cargo-specific defect in Snc1 internalization that we observed for both *yAP180* and *INP52* mutants.

Inp52 has previously been shown to localize to endocytic patches, and to specifically control the dissociation of proteins that bind $PI(4,5)P_2$ through ANTH or ENTH domains, including Sla1, and Ent1/2, respectively (Sun, Y., 2007). The ability of Inp52 to hydrolyze $PI(4,5)P_2$ is important to release these ANTH/ENTH domain proteins from the vesicle,

following fission. This led us to propose that the similar cargo-specific defects observed in the absence of either *INP52* or *yAP180* is a result of failed disassembly of yAP180 from internalized vesicles. An alternate explanation is that this accumulation is due to inappropriate recruitment of yAP180 to internal compartments. To distinguish between these possibilities, yAP180-GFP patches could be tracked in *inp52Δ* mutants by TIRF microscopy. A similar approach was used to demonstrate that in *inp52Δ* mutants, Sla2 patches are internalized normally, but that Sla2 remains associated with these vesicles following scission (Sun et al., 2007). This showed that loss of Inp52 causes prolonged association of Sla2 with endocytic vesicles, and does not cause inappropriate recruitment of Sla2 to internal compartments.

Loss of *INP52* did not completely block internalization of Snc1, as it showed a similar defect as a *yap1802Δ* single mutant, which is considerably weaker than the defect observed in *yap1801Δ/1802Δ* double mutants. This suggests that Inp52 may be partially redundant, and that other factors may facilitate PI(4,5)P_2 hydrolysis in its absence. In addition to Inp52, yeast expresses the related synaptojanin Inp51, which also localizes to endocytic sites, and Inp53, which is involved in sorting at the TGN (Bensen et al., 2000). Inp53 is recruited to cortical actin patches under conditions of hyperosmotic stress (Ooms et al., 2000). None of these genes are essential for growth; however a triple deletion of *INP51*, *INP52*, and *INP53* is lethal (Stolz et al., 1998). Although loss of Inp52, but not Inp51, has previously been shown to result in the accumulation of ENTH/ANTH domain containing proteins, this could be due to the lower expression level of Inp51 relative to Inp52. Our results suggest that Inp52 function may be partially substituted by Inp51 and possibly Inp53 for Snc1 internalization. To investigate this, it could be tested whether combined deletion of *INP51/INP52* or *INP51/INP53* results in a more severe internalization defect than a single INP52 deletion. The effect of the triple mutant could also be tested in *inp51Δ/inp53Δ/inp52^{ts}* cells at a non-permissive temperature (Stefan et al., 2002).

It will be important to carry out these studies to better understand how AP180 and synaptojanin may function together in higher cells. The synaptojanins are evolutionarily conserved from yeast to humans, and their regulation of PI(4,5)P_2 turnover at the cell surface is critical for cellular function, and relevant to human disease (Liu Y, Bankaitis VA, 2010). Synaptojanin 1 null mice die shortly after birth and present neurological defects and accumulate clathrin-coated vesicles at nerve endings, due to failed disassembly of these coats (Cremona O., 1999, Kim WT., 2002). Interestingly, increased synaptojanin 1 activity is

directly associated with the brain dysfunction and cognitive defects manifested in some Down's sydrome patients. Synaptojanin1 resides in a genomic region present in trisomic rearrangement in Ts65Dn mice, a model for Down's syndrome. In these mice, homoeostasis of $PI(4,5)P_2$ is disrupted. Restoring the Synaptojanin gene to disomy in these mice is alone is sufficient to correct these altered levels of $PI(4,5)P_2$, and the neurological defects observed in this model (Voronov SV, 2008). Synaptojanin 2 functions in non-neuronal cells, and its disruption inhibits internalization of the epidermal growth factor and transferrin receptors, and has been shown to disrupt the formation of clathrin coated vesicles in lung carcinoma cells (Hill E., 2001, Malecz N., 2000, Rusk N., 2003). Although defects in both synaptojanin and AP180 result in coated vesicle accumulation and neurological defects in multiple model organisms, it is unknown if synaptojanin contributes directly to the un-coating of AP180 proteins at the synapse. The studies in yeast described here, could contribute important insight into the coordinated roles of synaptojanin and AP180 proteins, and guide future studies in mammalian cells.

4.2.4. How does yAP180 recognize Snc1 for internalization?

Another outstanding question regarding yAP180 function is whether it interacts directly with Snc1, or indirectly through additional factors. An interaction between yAP180 and Snc1 could not be detected *in vivo*. This is consistent with other studies, which have generally failed to detect interactions between adaptors and their cargo *in vivo*, due to their weak and transient nature. Generally, interactions between adaptors and their cargo have been more successful by *in vitro* methods using recombinant proteins. An *in vitro* approach may therefore aid in determining whether yAP180 interacts directly with Snc1, or whether other proteins bridge this interaction.

If an interaction between AP180 and Snc1 were to be identified though these studies, the next step would be to identify the Snc1 sorting signal, as the signal recognized by AP180 has not yet been identified in any organism. Two cytosolic residues have been defined that are required for internalization of both Snc1 and Vamp2. In Snc1, mutation of V40A and M43A cause a complete endocytic block (Grote E., 1995, 2000; Lewis et al., 2000). Although these residues are located on the same face of the amphipathic helix that binds to t-SNAREs, they are not required for SNARE complex assembly or function. Currently, no sorting adaptor has been shown to bind to this motif. It is also unknown whether these residues independently mediate internalization, or if they are part of a larger conformational epitope required for recognition by AP180 or other adaptors.

Whether the V40M43A mutation blocks the interaction between Snc1 and AP180 could be tested *in vitro*. An alternate approach would be to identify putative Snc1 sorting signals by error-prone PCR to introduce random mutations in its cytosolic domain. The effects of these mutations on Snc1 internalization could be tested systematically using our GSS invertase assay. If candidate endocytic mutants are identified, they could then be tested individually for binding to yAP180 *in vitro*. If a non-continuous set of mutations is found to block internalization, this could suggest that Snc1 is recognized by a conformational epitope. To further investigate this, structural studies, like those carried out to determine the interaction surface of the SNARE Vti1 recognized by the epsin adaptor, would likely be required.

Currently, there is no evidence from our studies, or those of others, that yAP180 binds directly to Snc1; it is possible that other proteins could bridge this interaction. yAP180 interacts with multiple endocytic proteins, as previously discussed. It would therefore be useful to test if deletion of yAP180 binding partners, such as the epsins, blocks its interaction with Snc1. A larger scale approach could also be used to identify binding partners of the Snc1 endocytic signal *in vitro*. For example, total cell lysates could be passed through a GST-Snc1 column, and the purified components separated by SDS-PAGE. The identity of each co-purifying protein could be identified by mass spectroscopy. To identify proteins that bind to the endocytic signal, the profiles of binding partners could be compared between GST-Snc1 and GST-Snc1^{V40M43A} mutant. For example, if a protein is present in the WT, but not the mutant purification, it may be a candidate bridging protein. A similar approach was recently used to identify and compare the profiles of effectors for all 60 mammalian Rab proteins (Kanno et al., 2010).

4.2.5. Does AP-2 mediate endocytosis in yeast?

A requirement for AP-2 in yeast endocytosis has not yet been identified, in contrast to the essential role for this complex in mammalian endocytosis. Targeted disruption of AP-2 leads to embryonic lethality in mice (Mitsunari T, 2005), and has been shown to block the uptake of multiple cargo including the transferrin receptor (Conner, S. D., and S. L. Schmid. 2003), as well as a population of lysosome-associated membrane proteins that traffic via the plasma membrane (Janvier and Bonifacino, 2005). Yeast AP-2 deletion mutants, however, are viable, and have no clear defects in the internalization of commonly studied endocytic cargo. This has led to the suggestion that AP-2 is unimportant for endocytosis in yeast (Sorkin, 2004; Yeung et al., 1999). Could considering a broader range of cargo help us

identify an endocytic role for AP-2?

One recent study has shown that AP-2 also shows cargo-specific internalization defects, which may serve to explain this discrepancy. A large-scale screen demonstrated that mutants lacking any of the four AP-2 subunits are resistant to K28, a virally encoded yeast killer toxin that enters the cells via endocytosis by binding to its unidentified receptor. AP-2 mutants have a strong defect in uptake of K28 from the media, but do not affect the uptake of other endocytic markers, including the peptide cargo α-factor and of the lipophilic dye FM4-64 (Carroll et al., 2006). The authors thus proposed that AP-2 has a strong but cargo-specific effect on K28 endocytosis. This study also showed that AP-2 is recruited to endocytic sites concurrent with clathrin and other early coat components, suggesting that it likely has a direct role in uptake.

In contrast to what was previously believed, both this study and our screen for regulators of Snc1 internalization demonstrate that clathin and its associated adaptors are important in both yeast and mammalian cells. Our understanding of these similarities has only become clear through the study of cargo proteins that have not been previously studied by genome-wide methods in yeast. Further large-scale functional screens using additional non-conventional cargo will aid in the identification of proteins recognized by AP-2 and cargo-specific adaptors, and of new adaptor-related proteins required for internalization.

4.2.6. Role of actin and its regulators in Snc1 internalization

The results from our screen re-enforced the importance of dynamic actin regulation in the yeast endocytic process. We identified multiple regulators of the actin cytoskeleton, for which no endocytic defects have previously been shown. Abp1 and Crn1 are actin-binding proteins, and promote the activity of the Arp2/3 complex, a key regulator of actin polymerization. The actin capping proteins Cap1/2 are thought to function in polymerization by limiting monomer addition to recently assembled ends, and increasing local polymerization rates (Kim K., 2004; 1990; Kaksonen M., 2005). We also identified a novel regulator of actin dynamics, Ldb17, and demonstrated that it is an important link between cargo selection and the regulation of actin polymerization. The absence of Ldb17 resulted in defects in both vesicle internalization and actin morphology. The mechanism by which Ldb17 promotes actin polymerization, however, is currently undefined.

Does Ldb17 promote actin polymerization through direct regulation of the Arp2/3 complex, or does it function indirectly in this regulation? Like Ldb17, its mammalian

homolog, SPIN90, interacts with multiple components of the vesicle coat, and with the actin regulatory machinery. SPIN90 has been proposed to carry out a similar role as Ldb17, linking coat and actin dynamics (Kim et al., 2005, 2006 (1), 2007, 2009). SPIN90 stimulates actin polymerization both directly and indirectly, through binding to components of the Arp2/3 complex, as well as to its activators, including N-WASP (Kim et al., 2006; Lee et al., 2006). The results of this study suggest that Ldb17 does not likely have a direct effect in Arp2/3 regulation. Ldb17 did not bind to Las17, the yeast homolog of N-WASP or the Arp2/3 complex, likely because the regions important for binding to N-WASP and Arp2/3 in SPIN90 are only partially conserved in Ldb17. This suggests that Ldb17 interacts with additional regulators to stimulate actin polymerization in yeast. Interestingly, interactions were identified between the Ldb17 PRD with the SH3 domain-containing proteins Sla1, Lsb3, and Lsb4. These proteins bind to Las17, and are important in stimulating actin polymerization. Additionally, the PRD of Ldb17 interacts with the SH3 domain of Bzz1, the yeast syndapin homolog, and this interaction is required for membrane release of Ldb17. Bzz1 interacts directly with Las17 via its SH3 domain, and with other components of the actin polymerization machinery (Soulard et al., 2002 and 2005). These factors could thus be important in forming a link between Ldb17 and Arp2/3 regulation.

Whether Ldb17 can promote actin polymerization and the requirement for its interacting factors in this process could be assessed in future studies. The role for actin polymerization factors is often tested in vitro, and there are a variety of commercially available in vitro actin polymerization assays. One of these assays is based on the enhanced fluorescence of pyrene-conjugated actin that occurs during polymerization, which can be detected using fluorimetry (Blader et al., 1999). In this assay, purified Ldb17 could be added to the reaction mixture in the presence of Arp2/3, to determine if it has a direct effect on actin polymerization. Ldb17 could also influence actin polymerization indirectly, through its association with Bzz1, Sla1, or Lsb3/4, which could be tested by addition of these factors in combination with Ldb17.

Yeast is an important model for understanding protein sorting in higher cells, and the underlying mechanisms that govern vesicle formation are generally well conserved. Our work and that of other groups has provided explanations for some of the apparent discrepancies between endocytic processes in yeast and man. This study has highlighted that specific mechanisms are in place for the endocytosis of different cargo proteins, which is true in both mammalian and yeast systems. Each internalization pathway shows distinct requirements for clathrin, actin regulators, and lipids, and the use of these distinct pathways may also change in response to the context of the cellular environment. Different cell types in mammals also appear to use specialized sorting mechanisms to suit their specific functions. Elucidating the unique and conserved features of these processes will be essential in understanding the fundamental principles that underlie cargo selection, membrane deformation, and vesicle scission in all organisms and cell types.

4.3. Regulators of Snc1 recycling: AP-1R and Ima1

4.3.1. What is the role of AP-1R in Golgi/endosomal recycling?

In addition to the clathrin adaptor AP180, we identified a requirement for the alternate AP-1 isoform, AP-1R in Snc1 transport. In contrast to the endocytic role of yAP180, AP-1R is involved in the intracellular recycling of Snc1. Deletion of AP-1R components leads to a weak, yet reproducible increase in cell-surface localized Snc1. Based on its co-localization with intracellular clathrin, and Golgi/endosomal markers, we have concluded that AP-1R likely functions in Snc1 intracellular recycling, and not in endocytosis. How does loss of AP-1R lead to increased levels of Snc1 at the surface? As all trafficking pathways in the cell are part of a network, and their interconnected nature allows cargo to follow alternate "bypass" routes, the increase in cell surface levels suggests that deletion of AP-1R allows Snc1 to transit to the plasma membrane by an alternate recycling bypass pathway, with faster recycling kinetics than the normal route. We considered different mechanisms by which this might occur, which are discussed below and shown in illustrations 4.2 and 4.3.

Model 1: AP-1R mediates sorting to an intermediate compartment prior to surface delivery.

In this first model (Illustration 4.2), AP-1R is present on endosomes, and promotes Snc1 recycling at these compartments. The recycling pathway regulated by AP-1R may be a 'slow' route, whereby AP-1R may transport Snc1 from endosomes to either the Golgi, or perhaps another intermediate compartment prior to cell surface delivery. In the absence of AP-1R, Snc1 may be diverted along to a more rapid and direct recycling route, in which it bypasses the Golgi/intermediate compartment, and is recycled directly from endosomes. As discussed in chapter 3, this bypass ability has been observed for other recycling cargo in yeast, including Chs3, which is able to recycle directly to the cell surface from early endosomes or the Golgi in the absence of AP-1 (Valdivia et al., 2002).

In mammalian cells, there are at least two main types of recycling pathways to the cell surface, each of which has different kinetics. The rapid recycling route mediates transport of cargo such back to the plasma membrane from either early endosomes or an earlier stage in the endocytic pathway. The so-called slow recycling route transports cargo from the early endosome to an intermediate endocytic recycling compartment (ERC), before re-delivery to the plasma membrane. Kinetic studies measuring the recycling rates of the transferrin receptor (TfR) show that it follows both pathways. Whether TfR follows the fast or slow pathway appears to be determined largely at the early endosome. This endosomal compartment contains several Rab GTPases, including Rab4 and Rab5. For TfR to undergo fast recycling, it must be quickly sorted away from Rab5, into a specialized Rab4-containing microdomain on the early endosome. These GTPases likely recruit different regulators that sort cargo either directly back to the cell surface or to the recycling endosome (Grant and Donaldson, 2009).

The characterization of the mammalian endocytic system raises important questions about the nature of endosomal organization in yeast. Currently, it is not clear whether yeast have kinetically distinct recycling pathways, or different populations of endosomes like those in mammals. The current view of protein recycling in yeast is much simpler, in that cargo is thought to pass only through one type of endosome, and is returned to the plasma membrane following direct retrieval to the Golgi. Furthermore, it is not known whether the early endosome contains distinct microdomains that are important for directing proteins to different locations. Differential inclusion of AP-1 and AP-1R into distinct microdomains of a common membrane would be consistent with the overlap of these complexes at endosomal

compartments, and could thus explain their different sorting function.

Snc1 has previously been shown to recycle to the plasma membrane through bypass pathways in the absence of components required for it normal recycling itinerary. Mutation of certain components of the COPI B coat (*sec27-1* and *sec28*), for example, results in increased surface levels of GFP-Snc1, and enrichment at bud sites. This implies that Snc1 retrieval and recycling through early endosomes to the Golgi may require COP1B (Robinson et al. 2006), and that loss of this complex results in retargeting of Snc1 to the plasma membrane. Despite the established role of the COPI coat in intra-Golgi and Golgi-ER retrograde transport, studies in both yeast and mammalian cells also describe a post-Golgi transport role for COPI (Whitney *et al.,* 1995; Aniento *et al.,* 1996; Gu and Gruenberg, 2000; Faure *et al.,* 2004). It would be interesting to test the relationship between AP-1R and COP1B in Snc1 intracellular recycling. Although most components of this coat are essential, and therefore would not have been present in our screen, a strong requirement was identified for Sec28, the only non-essential COP1B component. Genetic interaction studies between AP-1R and COPIB components could be used to determine whether they work in the same or parallel recycling pathways. Snc1 surface levels could be compared in double mutant AP-1R/COP1B strains, using the invertase assay, but would require the use of temperature-sensitive alleles of most COP1B components.

Model 2: AP-1R sorts Snc1 into a specific class of secretory vesicles

In contrast to an endosomal sorting role, AP-1R may function at the Golgi, and mediate inclusion of Snc1 into secretory vesicles (Illustration 4.3). There are two populations of vesicles that are targeted to the plasma membrane in yeast, each of which is enriched for distinct cargo. As these vesicles have distinct densities (dense and light), they can be distinguished based on subcellular gradient separation in *sec6Δ* mutants, which prevent their fusion with the plasma membrane. Snc1 is normally contained in the lighter vesicle fraction, as is the SNARE Tlg1, which partners with Snc1 in the fusion of vesicles derived from early endosomes with the Golgi (Harsay E., and Bretscher A., 1995). AP-1 is involved in the sorting of cargo into the light fraction, and in the absence of AP-1, both Chs3 and Tlg1 are missorted from the light to the dense fraction (Valdivia et al., 2002). It would be interesting to test whether AP-1R is required for Snc1 incorporation into light vesicles, which could be done by determining if deletion of AP-1R shifts the incorporation of Snc1 from the light to the dense exocytic vesicle population by subcellular fractionation. How

can this model explain the increased levels of Snc1 in the absence of AP-1R? This could occur if the dense vesicle fraction can carry relatively more cargo than the light fraction over a given time frame. Dense vesicles may have faster kinetics of transport. One way that this could occur is if dense vesicles are transported directly to the cell surface, while light vesicles require an intermediate transport through endosomes prior to cell surface delivery. Alternatively, dense and light vesicles could both arise from the Golgi: dense vesicles, however, could carry a higher concentration of cargo, have or have higher fusion efficiency at the cell surface than the lighter fraction.

Model 3: AP-1R has indirect effects on Snc1 recycling

Although localization studies suggest a role for AP-1R at Golgi/endosomal compartments, this is not sufficient to conclude that AP-1R has a direct role in Snc1 intracellular recycling. Indirect effects resulting in increased Snc1 surface levels could reflect a variety of indirect mechanisms. For example, a partial defect in endocytosis could be a result of the mislocalization of a component required for Snc1 internalization in the absence of AP-1R. It is also possible that the total cellular levels of Snc1 are increased in AP-1R mutants. Deletion of AP-1R may lead to either increased transcription or decreased degradation of Snc1. These indirect effects should be considered in future studies.

4.3.2. What is the Snc1 recycling signal recognized by AP-1R?

In this study, an interaction between AP-1R and GST-Snc1 was identified vitro, but the Snc1 signal recognized by AP-1R for recycling remains to be determined. Whether AP-1R recognizes Snc1 directly or indirectly is also unknown.

Like the signal required for Snc1 endocytosis the Snc1 recycling signal could be a yet unrecognized short cytosolic motif or a conformational epitope, consisting of a combination of folded residues. Furthermore, Snc1 is both palmitoylated and ubiquitinated, post-translational modifications that have been found to affect the sorting of multiple other SNARE proteins (Valdez-Taubas and Pelham; He and Linder, 2009). It is unlikely that the Snc1 sorting signal is a post translational modification, however, as the GST-Snc1 construct used for our *in vitro* assay was isolated from *E. Coli*, which lacks the machinery required for these modifications. This suggests that the Snc1 sorting signal is likely an intrinsic part of the Snc1 cytosolic domain. To identify residues in Snc1 that are important for AP-1R recognition, alanine-scanning mutagenesis could be used to systematically replace regions of Snc1 with alanine. The effects of these mutations on preventing the interaction between Apm2 and Snc1 could then be tested in vitro.

It will also be important to determine whether the interaction between Apm2 and Snc1 is direct or indirect. The identification of a putative Snc1 recycling signal could help resolve this. To identify potential bridging proteins, for example, the co-purification profiles of GST-tagged WT Snc1 vs. Snc1 containing a mutated recycling signal could be compared by mass spectroscopy.

An outstanding question in the field is whether Snc1 is transported as part of a trans or cis-SNARE complex. It is possible that Apm2 may bind to other SNAREs in complex with Snc1 at the Golgi/endosomes, including the functionally redundant t-SNAREs Tlg1 and Tlg2. Our in vitro Snc1 binding assay could be used to determine if Tlg1/2 is also present in the pulldown between Snc1 and Apm2, by blotting with anti-Tlg1 antibodies. If this is found to be the case, it could be interesting to test whether Snc1 and Tlg need to be in a SNARE complex to bind Apm2. Snc1 and Tlg interact though critical residues in their SNARE domain. While Snc1 provides an arginine residue, Tlg1/2 provide a glatamine. Mutation of either the Snc1 arginine or the Tlg glutamine prevents assembly of these proteins. Our *in vitro* assay could therefore be used to determine if Snc1 binding to Apm2 is prevented in a TlgQ>A mutant strain, and if mutation of the Snc1 arginine shows the same effects. If these mutations prevent interaction between Apm2 and Snc1, this would provide evidence that AP-1R sorts Snc1 as part of a trans-SNARE complex.

4.3.3. How do AP-1 and AP-1R regulate distinct sorting pathways?

As AP-1 and AP-1R show considerable co-localization to Golgi/endosomal compartments, it is unclear how they mediate largely non-overlapping transport functions. In mammalian cells, AP-1A localizes to the TGN, wheras AP-1B localizes to the perinuclear recycling endosomes, adjacent to the TGN. This is not clearly the case for AP-1 and AP-1R in yeast, although, they may localize to slightly different membrane domains.

Studies in mammalian cells suggest that exchange of the medium subunit may confer alternate specificity to AP-1A and AP-1B by providing a novel interaction surface, which is able to associate with distinct sets of lipids and also with regulatory proteins. AP-1B specifically facilitates the recruitment of exocyst subunits Exo70 and Sec8, which mediate tethering and fusion from recycling endosomes to the cell surface (Fölsch et al., 2003). The SNARE protein cellubrevin has also recently been shown to be required for AP-1B-dependent sorting, and co-localizes with AP-1B within recycling endosomes (Fields et al., 2007).

Although these alternate complexes are not analogous to AP-1 and AP-1R in yeast based strictly on homology, important insights about the differential functions of AP-1 and AP-1R may be gained from these mammalian studies. Apm2 is considerably larger than Apm1, and is only 30% identical on the amino acid level. Inclusion of Apm2 therefore may confer alternate specificity to AP-1 through facilitating differential interaction with regulators, including Ima1, and possibly different membrane lipids. These ideas are expanded upon in the following sections.

4.3.4. Do AP-1 and AP-1R localize to different lipid domains?

Although we found that Apm1 and Apm2 show considerable overlap at Golgi/endosomal compartments, this overlap was not complete. This could suggest that AP-1R mediates Snc1 transport at these unique sites, or that the localization of these complexes may be more different than can be appreciated based on the resolution of techniques used in this study.

The differential localization of mammalian AP-1A and AP-1B has been at least explained by the differential preferences of the medium subunits for membrane lipids. While μ1A binds the Golgi-enriched PI(4)P, μ1B binds PI(3,4,5)P_3, enriched in recycling endosomes. Interestingly, a patch of only three amino acids within the μ1B C-terminal B domain was found to be necessary for its recruitment to recycling endosomes. Switching this patch with the analogous residues of μ1A both inhibited the ability for AP-1B to localize to recycling endosomes, and resulted in the mis-targeting of AP-1B-dependent cargo. This suggests that differences in the lipid binding domains of these similar μ subunits are important for their differential targeting and sorting function (Fields et al., 2010).

The analogous regions in Apm1 and Apm2 differ substantially, suggesting that this site may contribute to the distinct sorting functions of AP-1 and AP-1R. This may also be explained by the ability of this region in Apm2 to associate with specific phospholipid domains. In the future, it would be interesting to determine whether AP-1 and AP-1R localize to slightly different Golgi/endosomal sub-domains. These studies will rely on a better understanding of membrane domains and their corresponding lipids within these compartments in yeast. Powerful microscopy techniques and novel assays to detect these small-scale localization differences will likely be required. It could, however, be investigated whether replacing these residues in Apm2 with the analogous residues in Apm1 result in the mis-sorting of Snc1. If this is the case, this would be evidence that these complexes may be differentially targeted, by analogy to the mammalian AP-1 complexes.

4.3.5. Ima1 is a putative enzyme and binds the Apm2 C-terminal domain

This study demonstrated that AP-1 and AP-1R participate in differential regulatory interactions, and the previously uncharacterized protein Ima1 was identified as a specific regulator of AP-1R. Deletion of *IMA1*, which shares a similar genetic interaction profile with AP-1R components, also resulted in increased Snc1 surface levels. Furthermore, Ima1 binds specifically to AP-1R vs. AP-1, and co-localizes to similar intracellular compartments.

Ima1 is not critical for the early steps of AP-1R vesicle formation, including membrane recruitment or cargo binding. It may act at a later stage of AP function, possibly as a mediator of vesicle formation, or AP-1R un-coating. As Apm2 has previously been shown to co-fractionate with clathrin-coated vesicles by gel filtration (Stepp et al., 1995), the role of Ima1 in Apm2 vesicle inclusion could be tested by this method. This would involve comparing the quantity of Apm2 included in vesicles in the presence or absence of Ima1. Decreased abundance of Apm2 vesicles in *ima1Δ* cells would provide evidence for a role for Ima1 in Apm2 vesicle formation. Conversely, an increased abundance of these vesicles would suggest a role for Ima1 in AP-1R vesicle dissociation.

An interesting finding is that Ima1 interacts with the Apm2 C-terminus, but not through the Apm2 tyrosine-binding pocket (subdomain A). Rather, it binds to subdomain B, which has been shown by recent studies to associate with membrane lipids lipids and may be a target of regulatory interactions (Fields et al., 2010; Owen and Evans, 1998; Heldwein et al., 2004). Evidence was provided that Ima1 may have enzymatic function related to AP-1R function. The Ima1 C-terminal domain is remarkably conserved among eukaryotes, and contains a putative enzymatic motif, which is characteristic of serine hydrolases. The Ima1 catalytic mutant failed to complement Snc1 surface levels in *ima1Δ* cells, suggesting that this motif may have catalytic activity required for AP-1R-mediated sorting. Subcellular fractionation revealed that this enzymatic domain is not integral to the membrane, as predicted. Together with the finding that the Ima1 N-terminal region binds to Apm2, it is conceivable that the Ima1 C-terminal enzymatic domain may be accessible to its substrates at sites of AP-1R function.

The finding that Ima1 is a candidate enzyme that binds to the Apm2 B-domain is interesting, as recent studies in mammalian cells have shown that the μ subunit is an important target of regulation. These studies are changing the canonical view of μ subunit function, in which their primary role is to bind tyrosine-based cargo. Interaction between the μ subunit and specific lipids and lipid-regulatory enzymes is one recurrent theme of

these studies. While some of these regulatory enzymes bind to the tyrosine cargo-binding site in a canonical manner, others bind to regions that are distinct from this site, like Ima1. Interestingly, the subdomain B has been shown to regulate some of these interactions. For example, differences in the B domain of AP-1A μ1 and AP-1B μ2 confer differential localization of these complexes in polarized cells (Fields et al., 2010). Understanding the mechanisms by which these μ-binding proteins regulate AP function could thus inform us how Ima1 may contribute to AP-1R sorting, and how we can best direct future experiments to identify this role. These mechanisms are reviewed below.

AP complexes – Interactions with lipids and lipid-regulatory enzymes

AP complexes can influence lipid metabolism, and can specifically participate in the generation of lipids that recruit them to their target membranes, through interaction with lipid regulatory enzymes. APs and lipid regulators have been shown to interact in positive feedback loops; binding of an enzyme to its target AP has been shown to stimulate enzymatic activity, which can result in the localized generation of phospholipids (Fields et al., 2010; Kahlfeldt et al., 2010). In turn, the increased lipids generated through this binding leads to further AP recruitment and membrane stabilization. The μ subunit appears to be an important target for these interactions, and multiple μ subunits have now been shown to bind lipid kinases. PI(3,4,5)P_3 enrichment at recycling endosomes is required for recruitment of AP-1B. In turn, PI(3,4,5)P_3 accumulation is dependent on the recruitment of the lipid kinase PIPKI-p90 to recycling endosomes by AP-1B (Fields et al., 2010). PIPKI-p90 interacts directly with μ1B via a tyrosine-based motif, and this interaction stimulates the kinase activity of the enzyme. Furthermore, μ-binding enzymes can have additional roles in AP regulation. PIPKI-p90, for example, also binds to E-cadherin, an AP-1B-specific cargo. The dual interaction supports that PIPK serves as both a scaffold, linking E-cadherin to AP-complexes, and a regulator of spatially restricted lipid generation (Ling et al., 2007).

PIPKI-p90 also binds directly to AP-2 μ2, and is required for the generation of PI(4,5)P_2 during endocytosis (Bairstow et al, 2006; Krauss et al., 2006). The mechanism of this interaction is unclear. One study has suggested that PIPKI-p90 interacts with the cargo-binding pocket of μ2 through a tyrosine motif (Bairstow et al, 2006). In contrast, a second study has shown that this interaction is not dependent on the tyrosine motif, and may therefore involve a site of μ2 that does not include the cargo-binding pocket (Krauss et al., 2006). Endocytic cargo protein binding to μ2 leads to a potent stimulation of PIPK activity. These data thus identify a positive feedback loop consisting of endocytic cargo proteins, AP-

2μ, and PIPK type I, which may provide a specific pool of $PI(4,5)P_2$ dedicated to clathrin/AP-2-dependent receptor internalization. The mechanism by which binding of PIPKI to the μ subunit stimulates its kinase activity remains to be determined.

The AP-2 μ subunit has also recently been shown to interact directly with phospholipase D (PLD1), a receptor-associated signaling protein and this facilitates the membrane recruitment of AP2 and the endocytosis of epidermal growth factor receptor (EGFR). PLD catalyzes the hydrolysis of phosphatidylcholine (PC) to choline and phosphatidic acid (PA) (Lee et al., 2009). Interestingly, like Ima1, PLD is also a serine hydrolase. The PLD1-μ2 interaction requires the binding of PLD1 with phosphatidic acid, its own product. A model was proposed, in which auto-regulatory interactions beween PLD1 and PA promote μ2 binding, which subsequently facilitates EGFR endocytosis in response to receptor activation. It has been hypothesized that PA, in turn, stimulates a phosphoinositide kinase to generate $PI(4,5)P_2$ at the plasma membrane. It was therefore suggested that PA generation by PLD1 activation is a key molecular event that causes the local accumulation of $PI(4,5)P_2$ through direct activation of a kinase and enhancing the AP-2/kinase pathway by placing these two molecules in close proximity to facilitate EGFR endocytosis.

Members of the Dishevelled family of proteins have been found to bind directly to AP-2 μ2 in both mammals and C. elegans. Dishevelled (Dvl) functions as an adaptor between AP-2 and other components of the Wnt signaling pathway. This interaction is required for internalization of the Wnt signaling protein Frizzled. The interaction between Dvl and AP2 μ is bipartite, and requires simultaneous association of the Dvl DEP domain and a tyrosine-based signal. The tyrosine-based signal interacts with the μ2 cargo binding pocket, while the DEP domain binds at one end of the elongated, C-terminal domain of μ2. This domain:domain interface further reinforces that parts of the μ2 surface distinct from the tyrosine-motif pocket can help recruit specific receptors or adaptors into a clathrin coated pit. It is also considered likely that other parts of this surface may also have partners, as yet unidentified. The incorporation of two interaction modes into one cargo molecule further suggests that combinatorial recognition (and combinatorial cargo addressing) may be more widespread than previously suspected (Yu et al., 2007 and 2010). Wnt signaling stimulates the production of $PI(4,5)P_2$ through Frizzled and Dvl, which activates the lipid kinases phosphoinositide kinases 4 and 5. (MacDonald et al., 2009; Qin et al., 2009). This further supports the direct role for lipids and lipid-regulatory enzymes in driving the membrane recruitment and function of AP complexes.

4.3.6. Is Ima1 important for the generation of lipids required for AP-1R function?

What is the enzymatic function of Ima1, and could it regulate the generation of lipids important in AP-1R-mediated sorting? The finding that Ima1 binds to the Apm2 B domain suggests this possibility, in light of the work described in the previous section. The serine hydrolase family includes many proteins that can influence lipid metabolism, including esterases and lipases. Confirming that Ima1 is a serine hydrolase and identifying its potential substrates could help elucidate how it contributes to AP-1R function. Experimental strategies to dissect its enzymatic function are discussed below.

The first step will be to verify that Ima1 is a serine hydrolase, as predicted based on homology. To address this central question, we can take advantage of a chemical strategy referred to as activity-based protein profiling (ABPP) that uses active site-directed probes to profile the functional state of enzymes. ABPP probes label active enzymes by binding covalently to the active site. They bind enzymes only in their active state, but not their inactive precursor or inhibitor-bound forms. ABPP probes remain covalently bound to the active site, and in this way impede catalytic activity. These probes contain a tag or label, such as biotinylation, providing a means to detect them (Barglow and Cravatt, 2007; Heal et al., 2011). Fluorophosphonate (FP) probes have been developed that target active serine hydrolases (Simon and Cravatt., 2010). In order to determine if Ima1 is a serine hydrolase, the FP probe would be added to cell lysates. Ima1 would then be affinity purified, and western blotting would be carried out to determine if the probe was incorporated by detection with anti-biotin. As the probe only labels active enzymes, we could test whether mutation of the potential catalytic residues prevents probe incorporation.

Other questions that could be addressed by ABPP are whether AP-1R binds the active or inactive form of Ima1, and whether binding to AP-1R stimulates Ima1 enzymatic activity. Since FP probes inhibit enzymatic activity, whether Apm2 preferentially co-immunoprecipitates with the labeled or non-labeled form of Ima1 could be investigated. Whether binding to AP-1R stimulates Ima1 enzymatic activity could also be evaluated, by comparing the amount of probe that is incorporated into Ima1 upon deletion or over-expression of *APM2*.

4.3.7. Determination of Ima1 substrates

If Ima1 were confirmed to be a serine hydrolase by the studies described above, it would next be important to identify its biologically relevant substrate. Serine hydrolases comprise a large class of enzymes, incuding proteases, esterases, lipases, peptidases, and

aminases, and therefore have diverse substrate specificity. In recent years high-throughput screening assays have been developed to identify substrates of hydrolytic enzymes. The majority of these assays are based on screening an enzyme in question against a library of structurally diverse synthetic substrates. Upon reaction with the enzyme, its substrates release a colored or fluorescent product, permitting their identification. Many of these substrates are now commercially available, and can be tested in parallel in 96-well microtiter plates. This method, called enzyme activity fingerprinting (Reymond, 2008), has been used to classify different types of enzymes, including lipases, proteases, and peptidases, and to differentiate between closely related enzymes within these groups (Wahler et al., 2002; Konarzycka-Bessler and Bornscheuer, 2003). By screening a diverse library of these compounds in the presence of Ima1, we may be able to refine the class of enzyme to which Ima1 belongs, by identifying which of these substrates it reacts with. This could help us to identify potentially biologically relevant substrates. By doing so, we may be able to decipher whether Ima1 has a role in the remodeling of lipid membranes, and which lipids are potential substrates. This would be beneficial in understanding the role of lipid regulation in endosomal sorting, and could help us formulate directed hypotheses about how Ima1 activity may regulate the AP-1R sorting pathway.

4.3.8. Investigating the role of TMC04 in higher cells

Identifying the enzymatic activity and substrates of Ima1 could help us understand the potential role of its mammalian homolog TMCO4. Like most other mammalian serine hydrolases, the role of TMCO4 remains uncharacterized. Although serine hydrolases make up 1% of the mammalian proteome, nearly half of them remain completely uncharacterized with respect to substrates and functions. Of the enzymes that have been characterized, many have been shown to have important biological functions. They are important targets of several pharmaceutical agents, including proteases involved in the coagulation cascade, and amidases required for the metabolism of signaling molecules. Widely used drugs targeted against specific human serine hydrolases include Angiomax for cardiovascular disease, Xenical for obesity, and Aricept and Cognex for Alzheimer's disease, as well as drugs in development for diabetes, arthritis, and cancer (Baxter et al., 2004). It is of great interest in the field to gain a more complete understanding of these enzymes, and our work on Ima1 may contribute important insight into the function of TMCO4.

One perplexing issue is that while Ima1 is highly conserved in all organisms, Apm2 is not. Apm2 is unique as a medium chain, as it is considerably larger than, and shares only

30% homology to other μ subunits. This may suggest that although AP-1R is not conserved strictly based on similarity, it may carry out an analogous role to an AP complex in higher cells. Alternatively, Ima1 may have evolved to carry out function unrelated to AP-mediated sorting in multi-cellular organisms. To investigate these possibilities, methods such as mass spectroscopy could be used to identify TMCO4-interacting factors in mammalian cells. A more directed approach could also be used to determine if Ima1 interacts with specific AP complex components by co-immunoprecipitation.

4.4. Genetic interaction profiling to identify complexes and pathways required for Snc1 transport

4.4.1. Phenotypic profiling and the construction of genetic interaction networks

Genetic interaction profiling was used to screen the top candidates from the primary screen against a panel of query mutants in multiple trafficking pathways. This analysis allowed these candidates to be classified based on shared genetic interactions with these query genes, and enabled discovery of a set of genes enriched for functions in Snc1 endocytic transport. In this case, the cell surface levels of the GSS reporter in each double mutant served as a quantitative phenotypic readout. These results re-enforce the power of genetic interaction profiling in identifying genes that are highly influential to a given biological process after performing a genomic screen, and how these genes are interrelated.

Many previous studies have used genetic interaction profiling to infer functional relationships between genes required for a given process (reviewed in Boone et al., 2007). In the vast majority of these studies, however, growth is used as a phenotypic readout. The resulting networks from these studies therefore leave out processes that have no effect on cell viability or growth (Dixon et al., 2009). The quantitative nature of our assay was beneficial in overcoming this limitation, allowing for more precise determination of phenotypes directly related to Snc1 transport, and the accurate assessment of their genetic relationships.

This study took advantage of recent advances in technology, which have made it possible to measure large numbers of genetic interactions systematically and in parallel (Dixon et al., 2009). An E-Mapping approach was used to determine the genetic interaction profile between the top candidates from the primary screen, and a selected panel of mutants representing a variety of intracellular transport pathways, instead of the whole genome. This approach has several advantages beyond decreasing the number of

interactions that require analysis. It also increases the signal to noise ratio because the frequency of genetic interactions is higher between genes acting in related pathways, and provides a richer set of patterns for analysis. In previous studies, this subset of genes has been selected based on multiple criteria, including shared protein localization (Schuldiner *et al.*, 2005), or protein-protein interaction data (Collins et al., 2007). This selection process has multiple limitations. Selecting genes based purely on either of these criteria would miss important regulatory factors, such as signaling proteins, which may mediate strong effects on spatially distant processes. As large-scale protein interaction data suffers from a high degree of false positive and false negative interactions (Szilágyi et al., 2005), starting with this dataset may miss important factors, or may include factors that are not relevant to the process in question. For example, the interactions found in two independent genome-wide Y2H studies in S. cerevisiae show little overlap and are estimated to have a 50% false-positive rate (von Mering et al., 2002; Ito et al., 2001).

We took advantage of the E-Mapping approach to investigate the profile of genetic interactions of our top candidates, in combination with a panel of query mutants with established function in diverse intracellular transport pathways. In our approach, we selected our gene set based on a sensitive and quantitative assay. By selecting our gene set based on this criteria, we avoided many of the limitations that have been observed in other less stringent methods such as protein localization or interaction data. Furthermore, an integrative approach, which incorporated both genetic and physical interaction data, was used to refine the network of genes important for regulating Snc1 surface levels into discrete complexes and pathways. Integration of multiple data sets have generally been shown to add to the confidence of inferred related functions, and reduce the noise associated with individual genome-scale approaches. By using this integrative approach, we were able to conceive strong hypotheses about the function of uncharacterized genes, based on both a shared genetic interaction profile, and physical interaction with other well-studied genes.

Despite the insight generated by this study, this screening approach had important limitations. First, there could have been errors in the deletion collections. It is widely known that these mutant arrays are subject to genetic changes as a result of manipulation and selective pressure, including aneuploidy and second site mutations (Rancati et al., 2008; Yuen et al., 2007). As a multi-step selection process was required to generate double mutants for the interaction analysis, undesired mutations and rearrangements could have

been introduced. This would lead to false interpretation of the phenotypic data for some of these genes. A gene involved in Snc1 transport could have been missed, for example, if a second site mutation suppressed the defect caused by deletion of the gene in question (false negative). A gene with no role in this process could also be falsely interpreted to perturb this process if a second site mutation occurs in a functionally relevant gene (false positive). Screening two independent genome wide collections and averaging the results for both helped address this issue. Furthermore, many candidates were also verified by independent knockout or complementation.

4.4.2. Endocytic processes are part of a broader cellular context

The systems-level approach allowed us to identify factors involved in Snc1 endocytic recycling, and also to determine how these factors are interrelated in a broad cellular context. This work revealed surprising diversity among the processes involved. In addition to cellular transport, we identified proteins involved in roles including signaling, chromatin modification, transcription and translation, and lipid regulation. The role of some of these components can be readily explained by the current knowledge of the regulation of intracellular transport pathways, such as the critical role of actin polymerization and phospholipid distribution. We identified a strong requirement for the cytosolic prefoldin-GimC complex, which acts as a co-chaperone in actin folding (Siegers et al., 1999). Some of the transcripional/translational factors identified regulate the expression of specific phospholipid species known to be important for endocytic processes Ikeda et al., 2008). Some identified genes, however, have molecular functions that are not immediately reconcilable with membrane trafficking, including various signaling proteins. Recent studies have uncovered a wealth of evidence that endocytic transport and signaling are deeply integrated in the cellular program, and that these processes are closely connected. (Scita and Di Fiore, 2010; Sorkin and von Zastrow, 2009).

Despite evidence for connections between transport and other cellular processes, a caveat of our study is that the increased surface levels of our Snc1 reporter could be an indirect result of increased expression in some mutant strains. Although we did not directly address this issue, the effect of our candidates on GSS reporter expression will be important to address in future studies. This could be accomplished by creating a transcriptional reporter, in which the upstream regions of the GSS integration site are fused with LacZ. Expression of this reporter could be evaluated by a B-galactosidase assay in candidate mutants. Increased B-galactosidase levels in these mutants could inform us whether these

mutants are involved in the transciption of Snc1.

4.4.3. Assessing the role of essential genes in Snc1 transport

Another important limitation of this screening approach is that it considered the ~5000 non-essential genes, but not the ~1000 essential genes in yeast. Therefore, our view of Snc1 endocytic recycling is incomplete. Essential genes, by definition, encode critical cellular functions that are not buffered by redundant functions or pathways (Ben-Aroya et al., 2010). Inclusion of essential genes would be expected to have a significant impact on the size and complexity of our Snc1 sorting network, as multiple studies have demonstrated that they exhibit significantly more genetic interactions than nonessential genes, and the essential network is therefore significantly denser than the nonessential network. (Davierwala et al, 2005). Furthermore, essential genes tend to be more highly conserved in evolution; 38% of essential yeast proteins have easily identifiable counterparts in humans, versus 20% for nonessential genes (Ben-Aroya et al., 2010). Inclusion of essential genes could have therefore improved our study by adding to the connectivity between relevant pathways, and by expediting the analysis of critically important genes involved in endocytic recycling.

As many genome-wide studies have faced this limitation, this issue has prompted the development of genome-wide collections that facilitate the investigation of essential gene function. Most notably, temperature-sensitive (ts) mutants have been used with great success to analyze essential genes, and current work is in progress to develop ts alleles covering the yeast genome. Ts mutations are typically missense mutations, which retain the function of a specific essential gene at standard (permissive) temperatures, but lack that function at a defined high (non permissive) temperature. These mutants therefore facilitate analysis of physiologic changes that follow controlled inactivation of a gene by shifting cells to a non-permissive temperature. A subset of 250 ts mutants, including alleles for all uncharacterized essential genes and genes with human counterparts, is now ready for distribution (Ben-Aroya et al., 2008 and 2010). A complete set of these genes is expected to be available shortly, and will be tested for a role in Snc1 endocytic transport. Another approach involves the replacement of the native promoter of each gene with one that can be rapidly repressed. This includes the use of the tetracycline (tet)-regulatable promoter (Mnaimneh et al., 2004). In this system, the expression of each gene is controlled by a promoter that can be shut off by adding the tetracycline analog doxycyline, to the growth medium. Currently, TetO-promoter alleles have been created for over two-thirds of all

essential yeast genes. A major advantage of this system is that the native open reading frame of each gene is maintained. The addition of doxycycline to the growth media has also been shown to have little effect on yeast physiology at concentrations used for promoter shutoff. These genes have been developed for two-thirds of all yeast essential genes.

4.4.4. Relationships between endocytic recycling factors; implications in disease

A better understanding of the machinery regulating the selective transport of proteins within the endosomal system, and their relationships is critical for deciphering the genetic causes of diseases relating to trafficking malfunction. One feature common among diseases of intracellular transport is the considerable underlying genetic heterogeneity, which is a direct result of the complex regulatory mechanisms involved in these pathways. Many of these transport diseases present common clinical phenotypes, but are due to defects in seemingly unrelated gene products. As a result of this heterogeneity, it is difficult to carry out studies based purely on clinical phenotypes because of variable underlying mutations. More complete knowledge of how candidate genes could be related will therefore aid in the interpretation of the results from studies investigating diseases of intracellular transport (Howell et al., 2006; Olkkonen and Ikonen, 2006).

This study demonstrated unanticipated links between factors required for endocytic recycling. One example is the coordinated roles of yAP180 and synaptojanin in Snc1 internalization. Neurological defects are observed in the absence of both AP180 and synaptojanin in mouse models, although these defects have not previously been linked (Cao et al., 2010; Kim et al., 2002). Altered levels of clathrin regulatory proteins, including dynamin I, AP180, and synaptophysin have been observed in AD patients and mouse models, as compared to controls, suggesting that malfunctioning of clathrin dynamics may contribute to disease pathology. This example illustrates how a better understanding of relationships between transport factors could generate a more complete picture of the mechanisms underlying disorders of intracellular transport.

Therapeutic intervention for the manipulation of endocytic transport pathways could provide a means for treating diseases resulting from defects in these transport processes. In Alzheimer's patients, for example, defective transport of amyloid precursor protein (APP) in axons leads to the generation of AB plaques and the progression of neurodegenerative disease (Mayeux and Hyslop, 2008). Manipulating the transport of AB-containing vesicles in the endosomal system may therefore facilitate clearance of accumulated APP. There has been some significant progress towards this goal. It has been

found that APP processing to its plaque producing form is enhanced by inhibition of cholesterol transport, and that treatments that restore normal cholesterol levels and enhance APP transport to rab7-positive late endosomes may reduce aberrant APP processing (Stein et al., 2003; Huttunen et al., 2009). Furthermore, many cancers result from the increased recycling of growth factor receptors to the cell surface (Hyun and Ross., 2004; Rao et al., 2003). Implementing therapies that result in receptor down-regulation through shifting the balance between recycling and degradation may therefore positively impact outcomes. It is therefore of interest to develop gene therapies that effectively target the specific pathway in question, without significantly affecting other important transport steps. Current work in the field aims to develop therapies that selectively block or enhance Rab protein function, or stimulate cofactors that shunt cargo along the desired pathway, including increased expression at the cell surface, or down-regulation via enhancing degradation. This approach would benefit significantly from a greater understanding of cargo-specific cellular transport pathways, which was an important issue addressed by this study.

4.4.5. Future perspectives

The main theme that has been highlighted by this work is that many genes involved in endocytic recycling remain unidentified, due to functional redundancy, or cargo-specific effects. These findings highlight the importance of considering multiple cargo proteins, and the development of highly sensitive quantitative assays to detect defects in this transport process. Future application of our genome-wide analysis to different reporter proteins is expected to aid in the identification of additional cargo-specific machinery. Furthermore, the effects of different environmental conditions should also be considered. The endocytosis of some cargo is directly regulated by environmental conditions, including many nutrient and amino acid transporters, whose cell surface expression is regulated based on external nutrient availability (Nikko and Pelham, 2009). Studies of the same cargo under different conditions may help us determine if genes involved in their uptake are context-dependent.

Although the vast majority of functional genetic screens have been carried out in yeast, with the advent of RNAi and other knockdown techniques, it is expected that it will not be long before these types of screens could be applied to multi-cellular systems. Our quantitative phenotypic and genetic interaction approaches will provide considerable guidance in the identification of transport components in higher cells, and the relationships between them. Together, the emerging development of technology to study genetic

interactions in mammalian cells, combined with the analytical methods used in this study, could provide us with considerable insight into how defects in cellular transport pathways can contribute to human disease. Furthermore, application of these studies to different cell types could provide insight into the similarities and differences in endocytic transport in cell types that contain specialized organelles and pathways, such as neurons and polarized epithelial cells.

4.4. Illustrations

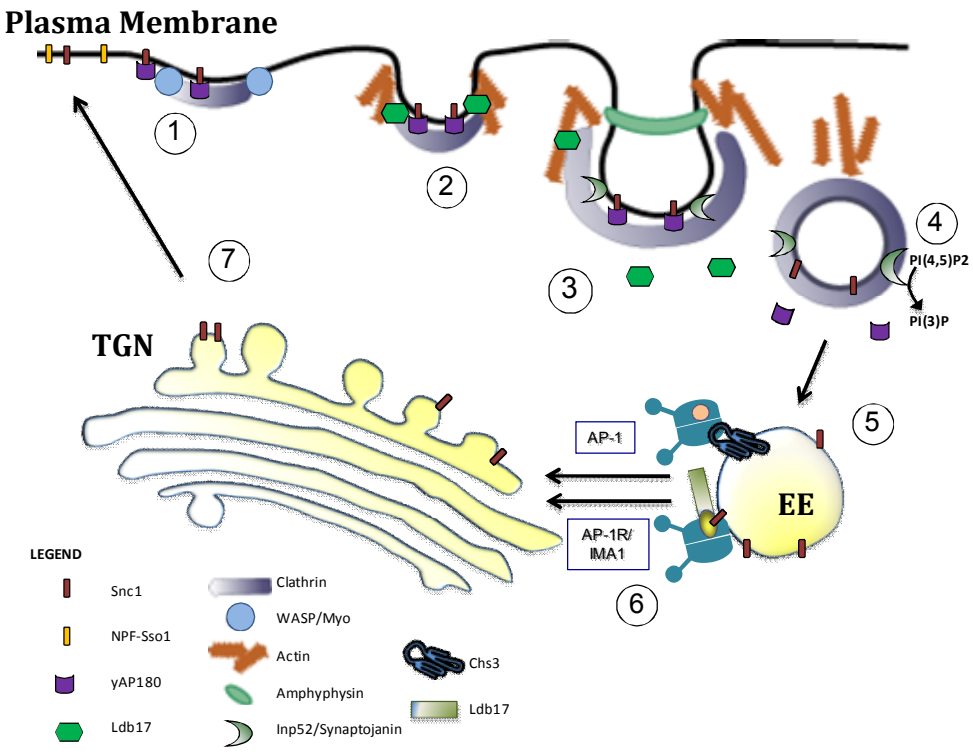

Illustration 4.1. New factors required for Snc1 endocytic recycling.

A proposed model summarizing the findings from this study regarding the functional requirements for clathrin and the clathrin adaptors yAP180s and Ldb17 in Snc1 internalization and AP-1R/Ima1 in Snc1 recycling. (1) yAP180 is recruited to the plasma membrane by combinatorial recognition of the membrane lipid PI(4,5)P2 and cargo. Snc1, but not all endocytic cargo (including NPF-Sso1) is recognized by yAP180 for internalization. Additional components of the early coat complex are subsequently recruited and clathrin assembly begins (2) Late coat components are then recruited, including components of the actin polymerization machinery. Ldb17 joins the late coat complex, just before the onset of actin polymerization, and is required for both normal coat and actin dynamics. (3) Actin polymerization begins, and the vesicle begins to internalize. (4) Inp52/synaptojanin mediates the hydrolysis of PI(4,5)P2 to PI(3), leading to uncoating of yAP180. (5) The free vesicle fuses with the early endosome to which it delivers Snc1. (6) Snc1 is recognized by AP-1R, possibly at the early endosome. Ima1 associates with the AP-1R-specific medium subunit Apm2. AP-1R/Ima1 mediate Snc1 recycling to the Trans Golgi Network (TGN), from which it is Snc1 is subsequently re-delivered to the plasma membrane.

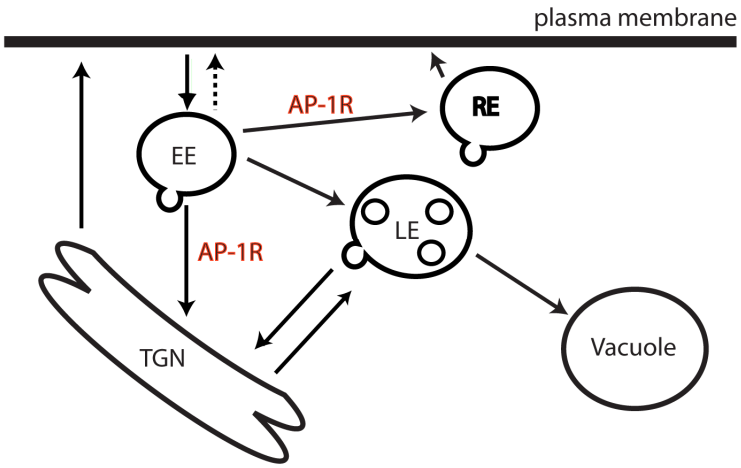

Illustration 4.2. AP-1R transport function: Model 1

In this model, AP-1R is present on early endosomes (EE), and directs internalized Snc1 to either the TGN or an intermediate recycling endosome (RE), from which Snc1 recycles back to the cell surface. In the absence of AP-1, Snc1 may avoid transport through these intermediate compartments and recycle back to the surface direcly from EEs (hatched arrow).

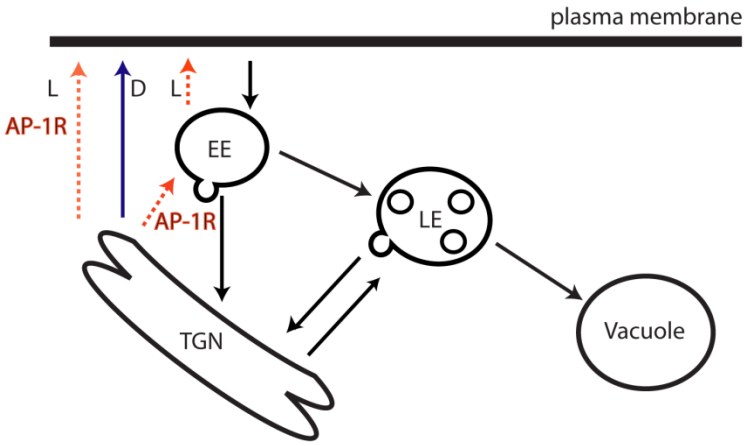

Illustration 4.3. AP-1R transport function: Model 2

In this model, AP-1R may function at the TGN to incorporate Snc1 into the light vesicle fraction, which may arise either directly from the TGN or from early endosomes (EE) (L: red arrows). In the absence or AP-1R, Snc1 may be missorted into the dense vesicle fraction (D: blue arrows).

BIBLIOGRAPHY

Aghamohammadzadeh and Ayscough. Differential requirements for actin during yeast and mammalian endocytosis. Nat Cell Biol (2009) vol. 11 (8) pp. 1039-42

Aguilar et al. The yeast Epsin Ent1 is recruited to membranes through multiple independent interactions. J.Biol.Chem. (2003) vol. 278 (12) pp. 10737-43

Andersen et al. Neuronal sorting protein-related receptor sorLA/LR11 regulates processing of the amyloid precursor protein. Proc.Natl.Acad.Sci.U.S.A. (2005) vol. 102 (38) pp. 13461-6

Ang et al. The Rab8 GTPase selectively regulates AP-1B-dependent basolateral transport in polarized Madin-Darby canine kidney cells. J.Cell Biol. (2003) vol. 163 (2) pp. 339-350

Aniento et al. An endosomal beta COP is involved in the pH-dependent formation of transport vesicles destined for late endosomes. J.Cell Biol. (1996) vol. 133 (1) pp. 29-41

Aridor and Hannan. Traffic jams II: an update of diseases of intracellular transport. Traffic (2002) vol. 3 (11) pp. 781-90

Aridor and Hannan. Traffic jam: a compendium of human diseases that affect intracellular transport processes. Traffic (2000) vol. 1 (11) pp. 836-51

Aruna et al. Identification of a hypothetical membrane protein interactor of ribosomal phosphoprotein P0. J Biosci (2004) vol. 29 (1) pp. 33-43

Ascough. Endocytosis: Actin in the driving seat. Curr.Biol. (2004) vol. 14 (3) pp. R124-6

Ayscough et al. High rates of actin filament turnover in budding yeast and roles for actin in establishment and maintenance of cell polarity revealed using the actin inhibitor latrunculin-A. J.Cell Biol. (1997) vol. 137 (2) pp. 399-416

Bader and Hogue. An automated method for finding molecular complexes in large protein interaction networks. BMC Bioinformatics (2003) vol. 4 pp. 2

Bairstow et al. Type Igamma661 phosphatidylinositol phosphate kinase directly interacts with AP2 and regulates endocytosis. J Biol Chem (2006) vol. 281 (29) pp. 20632-42

Bankaitis et al. Isolation of yeast mutants defective in protein targeting to the vacuole. Proc.Natl.Acad.Sci.U.S.A. (1986) vol. 83 (23) pp. 9075-9

Bao et al. AP180 maintains the distribution of synaptic and vesicle proteins in the nerve terminal and indirectly regulates the efficacy of Ca2+-triggered exocytosis. J Neurophysiol (2005) vol. 94 (3) pp. 1888-903

Barglow and Cravatt. Activity-based protein profiling for the functional annotation of enzymes. Nat Methods (2007) vol. 4 (10) pp. 822-7

Barr. Vesicular transport. Essays Biochem. (2000) vol. 36 pp. 37-46

Baxter et al. Synergistic computational and experimental proteomics approaches for more accurate detection of active serine hydrolases in yeast. Mol Cell Proteomics (2004) vol. 3 (3) pp. 209-25

Becherer et al. Novel syntaxin homologue, Pep12p, required for the sorting of lumenal hydrolases to the lysosome-like vacuole in yeast. Mol.Biol.Cell (1996) vol. 7 (4) pp. 579-94

Behnia and Munro. Organelle identity and the signposts for membrane traffic. Nature (2005) vol. 438 (7068) pp. 597-604

Ben-Aroya et al. Making temperature-sensitive mutants. Meth Enzymol (2010) vol. 470 pp. 181-204

Ben-Aroya et al. Toward a comprehensive temperature-sensitive mutant repository of the essential genes of Saccharomyces cerevisiae. Mol Cell (2008) vol. 30 (2) pp. 248-58

Bensen et al. Synthetic genetic interactions with temperature-sensitive clathrin in Saccharomyces cerevisiae. Roles for synaptojanin-like Inp53p and dynamin-related Vps1p in clathrin-dependent protein sorting at the trans-Golgi network. Genetics (2000) vol. 154 (1) pp. 83-97

Berman and Greenamyre. Update on Huntington's disease. Curr Neurol Neurosci Rep (2006) vol. 6 (4) pp. 281-6

Bishop. Dynamics of endosomal sorting. Int.Rev.Cytol. (2003) vol. 232 pp. 1-57

Black and Pelham. A selective transport route from Golgi to late endosomes that requires the yeast GGA proteins. J.Cell Biol. (2000) vol. 151 (3) pp. 587-600

Blader et al. GCS1, an Arf guanosine triphosphatase-activating protein in Saccharomyces cerevisiae, is required for normal actin cytoskeletal organization in vivo and stimulates actin polymerization in vitro. Mol.Biol.Cell (1999) vol. 10 (3) pp. 581-96

Bock et al. A genomic perspective on membrane compartment organization. Nature (2001) vol. 409 (6822) pp. 839-41

Boehm and Bonifacino. Genetic analyses of adaptin function from yeast to mammals. Gene (2002) vol. 286 (2) pp. 175-86

Bonangelino et al. Genomic screen for vacuolar protein sorting genes in Saccharomyces cerevisiae. Mol Biol Cell (2002) vol. 13 (7) pp. 2486-501

Bonifacino and Glick. The mechanisms of vesicle budding and fusion. Cell (2004) vol. 116 (2) pp. 153-66

Bonifacino. The GGA proteins: adaptors on the move. Nat Rev Mol Cell Biol (2004) vol. 5 (1) pp. 23-32

Bonifacino and Lippincott-Schwartz. Coat proteins: shaping membrane transport. Nat Rev Mol Cell Biol (2003) vol. 4 (5) pp. 409-14

Bonifacino and Traub. Signals for sorting of transmembrane proteins to endosomes and lysosomes. Annu.Rev.Biochem. (2003) vol. 72 pp. 395-447

Boone et al. Exploring genetic interactions and networks with yeast. Nat Rev Genet (2007) vol. 8 (6) pp. 437-49

Botos and Wlodawer. The expanding diversity of serine hydrolases. Curr Opin Struct Biol (2007) vol. 17 (6) pp. 683-90

Bouché et al. The cellular fate of glucose and its relevance in type 2 diabetes. Endocr Rev (2004) vol. 25 (5) pp. 807-30

Brett and Traub. Molecular structures of coat and coat-associated proteins: function follows form. Curr Opin Cell Biol (2006) vol. 18 (4) pp. 395-406

Brodsky et al. Biological basket weaving: formation and function of clathrin-coated vesicles. Annu.Rev.Cell Dev.Biol. (2001) vol. 17 pp. 517-568

Brunger. Structure and function of SNARE and SNARE-interacting proteins. Q.Rev.Biophys. (2005) vol. 38 (1) pp. 1-47

Burston et al. Regulators of yeast endocytosis identified by systematic quantitative analysis. J.Cell Biol. (2009) vol. 185 (6) pp. 1097-110

Cao et al. Changed clathrin regulatory proteins in the brains of Alzheimer's disease patients and animal models. J Alzheimers Dis (2010) vol. 22 (1) pp. 329-42

Carlton and Cullen. Coincidence detection in phosphoinositide signaling. Trends Cell Biol. (2005) vol. 15 (10) pp. 540-7

Carroll et al. A yeast killer toxin screen provides insights into a/b toxin entry, trafficking, and killing mechanisms. Dev Cell (2009) vol. 17 (4) pp. 552-60

Caviston and Holzbaur. Huntingtin as an essential integrator of intracellular vesicular trafficking. Trends Cell Biol. (2009) vol. 19 (4) pp. 147-55

Chen et al. Ypt31/32 GTPases and their novel F-box effector protein Rcy1 regulate protein recycling. Mol Biol Cell (2005) vol. 16 (1) pp. 178-92

Chen and Davis. Ubiquitin-independent entry into the yeast recycling pathway. Traffic (2002) vol. 3 (2) pp. 110-23

Chen and Davis. Recycling of the yeast a-factor receptor. J.Cell Biol. (2000) vol. 151 (3) pp. 731-8

Chidambaram et al. ENTH domain proteins are cargo adaptors for multiple SNARE proteins at the TGN endosome. J.Cell.Sci. (2008) vol. 121 (Pt 3) pp. 329-38

Chidambaram et al. Specific interaction between SNAREs and epsin N-terminal homology (ENTH) domains of epsin-related proteins in trans-Golgi network to endosome transport. J.Biol.Chem. (2004) vol. 279 (6) pp. 4175-9

Collins et al. Quantitative genetic interaction mapping using the E-MAP approach. Meth Enzymol (2010) vol. 470 pp. 205-31

Collins et al. Functional dissection of protein complexes involved in yeast chromosome biology using a genetic interaction map. Nature (2007) vol. 446 (7137) pp. 806-10

Collins et al. Molecular architecture and functional model of the endocytic AP2 complex. Cell (2002) vol. 109 (4) pp. 523-35

Conibear E. Converging views of endocytosis in yeast and mammals. Curr Opin Cell Biol (2010) vol. 22 (4) pp. 513-18

Conibear et al. Vps51p mediates the association of the GARP (Vps52/53/54) complex with the late Golgi t-SNARE Tlg1p. Mol Biol Cell (2003) vol. 14 (4) pp. 1610-23

Conner and Schmid. Differential requirements for AP-2 in clathrin-mediated endocytosis. J.Cell Biol. (2003) vol. 162 (5) pp. 773-9

Corbacho et al. A genome-wide screen for Saccharomyces cerevisiae nonessential genes involved in mannosyl phosphate transfer to mannoprotein-linked oligosaccharides. Fungal Genet Biol (2005) vol. 42 (9) pp. 773-90

Couve et al. Yeast synaptobrevin homologs are modified posttranslationally by the addition of palmitate. Proc.Natl.Acad.Sci.U.S.A. (1995) vol. 92 (13) pp. 5987-91

Cremona et al. Essential role of phosphoinositide metabolism in synaptic vesicle recycling. Cell (1999) vol. 99 (2) pp. 179-88

D'Angelo et al. The multiple roles of PtdIns(4)P -- not just the precursor of PtdIns(4,5)P2. J Cell Sci (2008) vol. 121 (Pt 12) pp. 1955-63

Darsow et al. Invertase fusion proteins for analysis of protein trafficking in yeast. Meth Enzymol (2000) vol. 327 pp. 95-106

Davierwala et al. The synthetic genetic interaction spectrum of essential genes. Nat Genet (2005) vol. 37 (10) pp. 1147-52

Davis et al. Cis- and trans-acting functions required for endocytosis of the yeast pheromone receptors. J.Cell Biol. (1993) vol. 122 (1) pp. 53-65

De Matteis and D'Angelo. The role of the phosphoinositides at the Golgi complex. Biochem.Soc.Symp. (2007) (74) pp. 107-16

De Matteis and Godi. PI-loting membrane traffic. Nat.Cell Biol. (2004) vol. 6 (6) pp. 487-492

Dell'Angelica et al. Altered trafficking of lysosomal proteins in Hermansky-Pudlak syndrome due to mutations in the beta 3A subunit of the AP-3 adaptor. Mol Cell (1999) vol. 3 (1) pp. 11-21

Deng et al. Gga2 mediates sequential ubiquitin-independent and ubiquitin-dependent steps in the trafficking of ARN1 from the trans-Golgi network to the vacuole. J.Biol.Chem. (2009) vol. 284 (35) pp. 23830-41

Derby and Gleeson. New insights into membrane trafficking and protein sorting. Int.Rev.Cytol. (2007) vol. 261 pp. 47-116

Dewar et al. Novel proteins linking the actin cytoskeleton to the endocytic machinery in Saccharomyces cerevisiae. Mol Biol Cell (2002) vol. 13 (10) pp. 3646-61

Dickman et al. Altered synaptic development and active zone spacing in endocytosis mutants. Curr.Biol. (2006) vol. 16 (6) pp. 591-8

Dietrich et al. The SNARE Ykt6 is released from yeast vacuoles during an early stage of fusion. EMBO Rep (2005) vol. 6 (3) pp. 245-50

Dittman and Kaplan. Factors regulating the abundance and localization of synaptobrevin in the plasma membrane. Proc.Natl.Acad.Sci.U.S.A. (2006) vol. 103 (30) pp. 11399-404

Dixon et al. Systematic mapping of genetic interaction networks. Annu Rev Genet (2009) vol. 43 pp. 601-25

Donaldson et al. Brefeldin A inhibits Golgi membrane-catalysed exchange of guanine nucleotide onto ARF protein. Nature (1992) vol. 360 (6402) pp. 350-2

Drees et al. A protein interaction map for cell polarity development. J.Cell Biol. (2001) vol. 154 (3) pp. 549-71

Edeling et al. Molecular switches involving the AP-2 beta2 appendage regulate endocytic cargo selection and clathrin coat assembly. Dev Cell (2006) vol. 10 (3) pp. 329-42

Edeling et al. Life of a clathrin coat: insights from clathrin and AP structures. Nat.Rev.Mol.Cell Biol. (2006) vol. 7 (1) pp. 32-44

Elkhaimi et al. Combinatorial regulation of phospholipid biosynthetic gene expression by the UME6, SIN3 and RPD3 genes. Nucleic Acids Res (2000) vol. 28 (16) pp. 3160-7

Engqvist-Goldstein and Drubin. Actin assembly and endocytosis: from yeast to mammals. Annu.Rev.Cell Dev.Biol. (2003) vol. 19 pp. 287-332

Evans and Owen. Endocytosis and vesicle trafficking. Curr.Opin.Struct.Biol. (2002) vol. 12 (6) pp. 814-821

Fauré et al. ARF1 regulates Nef-induced CD4 degradation. Curr.Biol. (2004) vol. 14 (12) pp. 1056-64

Fernández and Payne. Laa1p, a conserved AP-1 accessory protein important for AP-1 localization in yeast. Mol.Biol.Cell (2006) vol. 17 (7) pp. 3304-17

Fields et al. Phosphatidylinositol 3,4,5-trisphosphate localization in recycling endosomes is necessary for AP-1B-dependent sorting in polarized epithelial cells. Mol.Biol.Cell (2010) vol. 21 (1) pp. 95-105

Fields et al. Phosphatidylinositol 3,4,5-trisphosphate localization in recycling endosomes is necessary for AP-1B-dependent sorting in polarized epithelial cells. Mol Biol Cell (2010) vol. 21 (1) pp. 95-105

Fields et al. v-SNARE cellubrevin is required for basolateral sorting of AP-1B-dependent cargo in polarized epithelial cells. J.Cell Biol. (2007) vol. 177 (3) pp. 477-88

Fölsch et al. The AP-1A and AP-1B clathrin adaptor complexes define biochemically and functionally distinct membrane domains. J.Cell Biol. (2003) vol. 163 (2) pp. 351-62

Fölsch et al. Distribution and function of AP-1 clathrin adaptor complexes in polarized epithelial cells. J.Cell Biol. (2001) vol. 152 (3) pp. 595-606

Foote and Nothwehr. The clathrin adaptor complex 1 directly binds to a sorting signal in Ste13p to reduce the rate of its trafficking to the late endosome of yeast. J.Cell Biol. (2006) vol. 173 (4) pp. 615-26

Franzusoff et al. Localization of components involved in protein transport and processing through the yeast Golgi apparatus. J.Cell Biol. (1991) vol. 112 (1) pp. 27-37

Gabriely et al. Involvement of specific COPI subunits in protein sorting from the late endosome to the vacuole in yeast. Mol Cell Biol (2007) vol. 27 (2) pp. 526-40

Galan et al. Skp1p and the F-box protein Rcy1p form a non-SCF complex involved in recycling of the SNARE Snc1p in yeast. Mol Cell Biol (2001) vol. 21 (9) pp. 3105-17

Gan et al. The epithelial-specific adaptor AP1B mediates post-endocytic recycling to the basolateral membrane. Nat.Cell Biol. (2002) vol. 4 (8) pp. 605-609

Gavin et al. Proteome survey reveals modularity of the yeast cell machinery. Nature (2006) vol. 440 (7084) pp. 631-6

Ghaemmaghami et al. Global analysis of protein expression in yeast. Nature (2003) vol. 425 (6959) pp. 737-41

Ghosh and Kornfeld. The GGA proteins: key players in protein sorting at the trans-Golgi network. Eur.J.Cell Biol. (2004) vol. 83 (6) pp. 257-62

Giaever et al. Functional profiling of the Saccharomyces cerevisiae genome. Nature (2002) vol. 418 (6896) pp. 387-91

Girard et al. Non-stoichiometric relationship between clathrin heavy and light chains revealed by quantitative comparative proteomics of clathrin-coated vesicles from brain and liver. Mol Cell Proteomics (2005) vol. 4 (8) pp. 1145-54

Glyvuk et al. AP-1/sigma1B-adaptin mediates endosomal synaptic vesicle recycling, learning and memory. EMBO J. (2010) vol. 29 (8) pp. 1318-30

Gonzalez and Rodriguez-Boulan. Clathrin and AP1B: key roles in basolateral trafficking through trans-endosomal routes. FEBS Lett. (2009) vol. 583 (23) pp. 3784-3795

Grant and Donaldson. Pathways and mechanisms of endocytic recycling. Nat Rev Mol Cell Biol (2009) vol. 10 (9) pp. 597-608

Greaves et al. The fat controller: roles of palmitoylation in intracellular protein trafficking and targeting to membrane microdomains (Review). Mol Membr Biol (2009) vol. 26 (1) pp. 67-79

Grote et al. A snc1 endocytosis mutant: phenotypic analysis and suppression by overproduction of dihydrosphingosine phosphate lyase. Mol Biol Cell (2000) vol. 11 (12) pp. 4051-65

Grote et al. A targeting signal in VAMP regulating transport to synaptic vesicles. Cell (1995) vol. 81 (4) pp. 581-9

Gruenberg. Lipids in endocytic membrane transport and sorting. Curr Opin Cell Biol (2003) vol. 15 (4) pp. 382-8

Gu and Gruenberg. ARF1 regulates pH-dependent COP functions in the early endocytic pathway. J Biol Chem (2000) vol. 275 (11) pp. 8154-60

Guarente. Synthetic enhancement in gene interaction: a genetic tool come of age. Trends Genet (1993) vol. 9 (10) pp. 362-6

Harel et al. Evidence for CALM in directing VAMP2 trafficking. Traffic (2008) vol. 9 (3) pp. 417-29

Harsay and Bretscher. Parallel secretory pathways to the cell surface in yeast. J.Cell Biol. (1995) vol. 131 (2) pp. 297-310

Hatakeyama et al. Endocytosis of the aspartic acid/glutamic acid transporter Dip5 is triggered by substrate-dependent recruitment of the Rsp5 ubiquitin ligase via the arrestin-like protein Aly2. Mol Cell Biol (2010) vol. 30 (24) pp. 5598-607

He and Linder. Differential palmitoylation of the endosomal SNAREs syntaxin 7 and syntaxin 8. J Lipid Res (2009) vol. 50 (3) pp. 398-404

Heal et al. Activity-based probes: discovering new biology and new drug targets. Chem Soc Rev (2011) vol. 40 (1) pp. 246-57

Heilker et al. Recognition of sorting signals by clathrin adaptors. Bioessays (1999) vol. 21 (7) pp. 558-67

Heldwein et al. Crystal structure of the clathrin adaptor protein 1 core. Proc.Natl.Acad.Sci.U.S.A. (2004) vol. 101 (39) pp. 14108-13

Hettema et al. Retromer and the sorting nexins Snx4/41/42 mediate distinct retrieval pathways from yeast endosomes. EMBO J (2003) vol. 22 (3) pp. 548-57

Hirst et al. EpsinR: an ENTH domain-containing protein that interacts with AP-1. Mol.Biol.Cell (2003) vol. 14 (2) pp. 625-41

Holmquist. Alpha/Beta-hydrolase fold enzymes: structures, functions and mechanisms. Curr.Protein Pept.Sci. (2000) vol. 1 (2) pp. 209-35

Hong. SNAREs and traffic. Biochim.Biophys.Acta (2005) vol. 1744 (3) pp. 493-517

Horvath et al. Epsin: inducing membrane curvature. Int J Biochem Cell Biol (2007) vol. 39 (10) pp. 1765-70

Howell et al. Cell biology of membrane trafficking in human disease. Int.Rev.Cytol. (2006) vol. 252 pp. 1-69

Huang et al. Tyrosine phosphorylation of the beta2 subunit of clathrin adaptor complex AP-2 reveals the role of a di-leucine motif in the epidermal growth factor receptor trafficking. J.Biol.Chem. (2003) vol. 278 (44) pp. 43411-7

Huang et al. Clathrin functions in the absence of heterotetrameric adaptors and AP180-related proteins in yeast. EMBO J (1999) vol. 18 (14) pp. 3897-908

Huh et al. Global analysis of protein localization in budding yeast. Nature (2003) vol. 425 (6959) pp. 686-91

Huizing et al. Hermansky-Pudlak syndrome: vesicle formation from yeast to man. Pigment Cell Res (2002) vol. 15 (6) pp. 405-19

Huizing and Gahl. Disorders of vesicles of lysosomal lineage: the Hermansky-Pudlak syndromes. Curr Mol Med (2002) vol. 2 (5) pp. 451-67

Huttunen et al. Inhibition of acyl-coenzyme A: cholesterol acyl transferase modulates amyloid precursor protein trafficking in the early secretory pathway. FASEB J (2009) vol. 23 (11) pp. 3819-28

Hyun and Ross. HIP1: trafficking roles and regulation of tumorigenesis. Trends Mol Med (2004) vol. 10 (4) pp. 194-9

Ikeda et al. The Rim101 pathway is involved in Rsb1 expression induced by altered lipid asymmetry. Mol Biol Cell (2008) vol. 19 (5) pp. 1922-31

Ito et al. A comprehensive two-hybrid analysis to explore the yeast protein interactome. Proc.Natl.Acad.Sci.U.S.A. (2001) vol. 98 (8) pp. 4569-74

Itoh and De Camilli. BAR, F-BAR (EFC) and ENTH/ANTH domains in the regulation of membrane-cytosol interfaces and membrane curvature. Biochim Biophys Acta (2006) vol. 1761 (8) pp. 897-912

Itzen and Goody. GTPases involved in vesicular trafficking: Structures and mechanisms. Semin.Cell Dev.Biol. (2010)

Jackson et al. A large-scale conformational change couples membrane recruitment to cargo binding in the AP2 clathrin adaptor complex. Cell (2010) vol. 141 (7) pp. 1220-9

Janvier and Bonifacino. Role of the endocytic machinery in the sorting of lysosome-associated membrane proteins. Mol Biol Cell (2005) vol. 16 (9) pp. 4231-42

Jovic et al. The early endosome: a busy sorting station for proteins at the crossroads. Histol Histopathol (2010) vol. 25 (1) pp. 99-112

Jung and Haucke. Clathrin-mediated endocytosis at synapses. Traffic (2007) vol. 8 (9) pp. 1129-36

Kahlfeldt et al. Molecular basis for association of PIPKI gamma-p90 with clathrin adaptor AP-2. J.Biol.Chem. (2010) vol. 285 (4) pp. 2734-2749

Kaiser and Schekman. Distinct sets of SEC genes govern transport vesicle formation and fusion early in the secretory pathway. Cell (1990) vol. 61 (4) pp. 723-33

Kaksonen et al. Harnessing actin dynamics for clathrin-mediated endocytosis. Nat Rev Mol Cell Biol (2006) vol. 7 (6) pp. 404-14

Kaksonen et al. A modular design for the clathrin- and actin-mediated endocytosis machinery. Cell (2005) vol. 123 (2) pp. 305-20

Kaksonen et al. A pathway for association of receptors, adaptors, and actin during endocytic internalization. Cell (2003) vol. 115 (4) pp. 475-87

Kanno et al. Comprehensive screening for novel rab-binding proteins by GST pull-down assay using 60 different mammalian Rabs. Traffic (2010) vol. 11 (4) pp. 491-507

Karylowski et al. GLUT4 is retained by an intracellular cycle of vesicle formation and fusion with endosomes. Mol.Biol.Cell (2004) vol. 15 (2) pp. 870-82

Katzmann et al. Ubiquitin-dependent sorting into the multivesicular body pathway requires the function of a conserved endosomal protein sorting complex, ESCRT-I. Cell (2001) vol. 106 (2) pp. 145-55

Kawasaki et al. Membrane recruitment of effector proteins by Arf and Rab GTPases. Curr.Opin.Struct.Biol. (2005) vol. 15 (6) pp. 681-689

Kelm et al. The internalization of yeast Ste6p follows an ordered series of events involving phosphorylation, ubiquitination, recognition and endocytosis. Traffic (2004) vol. 5 (3) pp. 165-80

Kiemer et al. WI-PHI: a weighted yeast interactome enriched for direct physical interactions. Proteomics (2007) vol. 7 (6) pp. 932-43

Kim et al. Regulation of dendritic spine morphology by SPIN90, a novel Shank binding partner. J.Neurochem. (2009) vol. 109 (4) pp. 1106-17

Kim et al. F-actin binding region of SPIN90 C-terminus is essential for actin polymerization and lamellipodia formation. Cell Commun Adhes (2007) vol. 14 (1) pp. 33-43

Kim et al. Interaction of SPIN90 with syndapin is implicated in clathrin-mediated endocytic pathway in fibroblasts. Genes Cells (2006) vol. 11 (10) pp. 1197-211

Kim and Chang. Ever-expanding network of dynamin-interacting proteins. Mol Neurobiol (2006) vol. 34 (2) pp. 129-36

Kim et al. Interaction of SPIN90 with dynamin I and its participation in synaptic vesicle endocytosis. J Neurosci (2005) vol. 25 (41) pp. 9515-23

Kim et al. Capping protein binding to actin in yeast: biochemical mechanism and physiological relevance. J.Cell Biol. (2004) vol. 164 (4) pp. 567-80

Kim et al. Delayed reentry of recycling vesicles into the fusion-competent synaptic vesicle pool in synaptojanin 1 knockout mice. Proc.Natl.Acad.Sci.U.S.A. (2002) vol. 99 (26) pp. 17143-8

Kirchhausen. Three ways to make a vesicle. Nat.Rev.Mol.Cell Biol. (2000) vol. 1 (3) pp. 187-198

Kita et al. Loss of Apm1, the micro1 subunit of the clathrin-associated adaptor-protein-1 complex, causes distinct phenotypes and synthetic lethality with calcineurin deletion in fission yeast. Mol.Biol.Cell (2004) vol. 15 (6) pp. 2920-31

Konarzycka-Bessler and Bornscheuer. A high-throughput-screening method for determining the synthetic activity of hydrolases. Angew Chem Int Ed Engl (2003) vol. 42 (12) pp. 1418-20

Krauss et al. Stimulation of phosphatidylinositol kinase type I-mediated phosphatidylinositol (4,5)-bisphosphate synthesis by AP-2mu-cargo complexes. Proc.Natl.Acad.Sci.U.S.A. (2006) vol. 103 (32) pp. 11934-9

Krogan et al. Global landscape of protein complexes in the yeast Saccharomyces cerevisiae. Nature (2006) vol. 440 (7084) pp. 637-43

Kübler and Riezman. Actin and fimbrin are required for the internalization step of endocytosis in yeast. EMBO J (1993) vol. 12 (7) pp. 2855-62

Lamping et al. Isolation and characterization of a mutant of Saccharomyces cerevisiae with pleiotropic deficiencies in transcriptional activation and repression. Genetics (1994) vol. 137 (1) pp. 55-65

Lechler et al. Direct involvement of yeast type I myosins in Cdc42-dependent actin polymerization. J.Cell Biol. (2000) vol. 148 (2) pp. 363-73

Lee et al. Determination of EGFR endocytosis kinetic by auto-regulatory association of PLD1 with mu2. PLoS ONE (2009) vol. 4 (9) pp. e7090

Lee et al. SPIN90/WISH interacts with PSD-95 and regulates dendritic spinogenesis via an N-WASP-independent mechanism. EMBO J (2006) vol. 25 (20) pp. 4983-95

Legendre-Guillemin et al. ENTH/ANTH proteins and clathrin-mediated membrane budding. J.Cell.Sci. (2004) vol. 117 (Pt 1) pp. 9-18

Lewis and Pelham. A new yeast endosomal SNARE related to mammalian syntaxin 8. Traffic (2002) vol. 3 (12) pp. 922-9

Lewis et al. Specific retrieval of the exocytic SNARE Snc1p from early yeast endosomes. Mol.Biol.Cell (2000) vol. 11 (1) pp. 23-38

Lin and Guttman. Hijacking the endocytic machinery by microbial pathogens. Protoplasma (2010) vol. 244 (1-4) pp. 75-90

Linder and Deschenes. Palmitoylation: policing protein stability and traffic. Nat Rev Mol Cell Biol (2007) vol. 8 (1) pp. 74-84

Ling et al. Type I gamma phosphatidylinositol phosphate kinase modulates adherens junction and E-cadherin trafficking via a direct interaction with mu 1B adaptin. J.Cell Biol. (2007) vol. 176 (3) pp. 343-53

Liu and Bankaitis. Phosphoinositide phosphatases in cell biology and disease. Prog Lipid Res (2010) vol. 49 (3) pp. 201-17

Loerke et al. Cargo and dynamin regulate clathrin-coated pit maturation. PLoS Biol (2009) vol. 7 (3) pp. e57

Lundmark and Carlsson. Driving membrane curvature in clathrin-dependent and clathrin-independent endocytosis. Semin.Cell Dev.Biol. (2010) vol. 21 (4) pp. 363-70

Ma et al. Deletion mutants of AP-1 adaptin subunits display distinct phenotypes in fission yeast. Genes Cells (2009) vol. 14 (8) pp. 1015-28

MacDonald et al. Wnt/beta-catenin signaling: components, mechanisms, and diseases. Dev Cell (2009) vol. 17 (1) pp. 9-26

Maldonado-Baez and Wendland. Endocytic adaptors: recruiters, coordinators and regulators. Trends Cell Biol. (2006) vol. 16 (10) pp. 505-513

Maldonado-Báez et al. Interaction between Epsin/Yap180 adaptors and the scaffolds Ede1/Pan1 is required for endocytosis. Mol.Biol.Cell (2008) vol. 19 (7) pp. 2936-48

Malecz et al. Synaptojanin 2, a novel Rac1 effector that regulates clathrin-mediated endocytosis. Curr.Biol. (2000) vol. 10 (21) pp. 1383-6

Margolin et al. Reverse engineering cellular networks. Nat Protoc (2006) vol. 1 (2) pp. 662-71

Mattera et al. Conservation and Diversification of Dileucine Signal Recognition by Adaptor Protein (AP) Complex Variants. J.Biol.Chem. (2011) vol. 286 (3) pp. 2022-30

Mayeux and Hyslop. Alzheimer's disease: advances in trafficking. Lancet Neurol (2008) vol. 7 (1) pp. 2-3

Mercer et al. Virus entry by endocytosis. Annu.Rev.Biochem. (2010) vol. 79 pp. 803-33

Meyerholz et al. Effect of clathrin assembly lymphoid myeloid leukemia protein depletion on clathrin coat formation. Traffic (2005) vol. 6 (12) pp. 1225-34

Miller et al. A SNARE-adaptor interaction is a new mode of cargo recognition in clathrin-coated vesicles. Nature (2007) vol. 450 (7169) pp. 570-4

Mitsunari et al. Clathrin adaptor AP-2 is essential for early embryonal development. Mol Cell Biol (2005) vol. 25 (21) pp. 9318-23

Mnaimneh et al. Exploration of essential gene functions via titratable promoter alleles. Cell (2004) vol. 118 (1) pp. 31-44

Moseley and Goode. The yeast actin cytoskeleton: from cellular function to biochemical mechanism. Microbiol Mol Biol Rev (2006) vol. 70 (3) pp. 605-45

Motley et al. Functional analysis of AP-2 alpha and mu2 subunits. Mol Biol Cell (2006) vol. 17 (12) pp. 5298-308

Munro. Organelle identity and the organization of membrane traffic. Nat.Cell Biol. (2004) vol. 6 (6) pp. 469-472

Nakatsu et al. Defective function of GABA-containing synaptic vesicles in mice lacking the AP-3B clathrin adaptor. J.Cell Biol. (2004) vol. 167 (2) pp. 293-302

Nakatsu and Ohno. Adaptor protein complexes as the key regulators of protein sorting in the post-Golgi network. Cell Struct Funct (2003) vol. 28 (5) pp. 419-29

Nardini and Dijkstra. Alpha/beta hydrolase fold enzymes: the family keeps growing. Curr Opin Struct Biol (1999) vol. 9 (6) pp. 732-7

Newell-Litwa et al. Roles of BLOC-1 and adaptor protein-3 complexes in cargo sorting to synaptic vesicles. Mol.Biol.Cell (2009) vol. 20 (5) pp. 1441-53

Newpher et al. In vivo dynamics of clathrin and its adaptor-dependent recruitment to the actin-based endocytic machinery in yeast. Dev Cell (2005) vol. 9 (1) pp. 87-98

Nikko and Pelham. Arrestin-mediated endocytosis of yeast plasma membrane transporters. Traffic (2009) vol. 10 (12) pp. 1856-67

Nonet et al. UNC-11, a Caenorhabditis elegans AP180 homologue, regulates the size and protein composition of synaptic vesicles. Mol Biol Cell (1999) vol. 10 (7) pp. 2343-60

Novick et al. Identification of 23 complementation groups required for post-translational events in the yeast secretory pathway. Cell (1980) vol. 21 (1) pp. 205-15

Ohmura-Hoshino et al. A novel family of membrane-bound E3 ubiquitin ligases. J.Biochem. (2006) vol. 140 (2) pp. 147-54

Ohno. Physiological roles of clathrin adaptor AP complexes: lessons from mutant animals. J.Biochem. (2006) vol. 139 (6) pp. 943-948

Ohno. Overview: membrane traffic in multicellular systems: more than just a housekeeper. J.Biochem. (2006) vol. 139 (6) pp. 941-2

Olkkonen and Ikonen. When intracellular logistics fails--genetic defects in membrane trafficking. J Cell Sci (2006) vol. 119 (Pt 24) pp. 5031-45

Ooms et al. The yeast inositol polyphosphate 5-phosphatases inp52p and inp53p translocate to actin patches following hyperosmotic stress: mechanism for regulating phosphatidylinositol 4,5-bisphosphate at plasma membrane invaginations. Mol Cell Biol (2000) vol. 20 (24) pp. 9376-90

Owen et al. Adaptors for clathrin coats: structure and function. Annu.Rev.Cell Dev.Biol. (2004) vol. 20 pp. 153-191

Owen. Linking endocytic cargo to clathrin: structural and functional insights into coated vesicle formation. Biochem.Soc.Trans. (2004) vol. 32 (Pt 1) pp. 1-14

Owen and Evans. A structural explanation for the recognition of tyrosine-based endocytotic signals. Science (1998) vol. 282 (5392) pp. 1327-32

Padrón et al. Phosphatidylinositol phosphate 5-kinase Ibeta recruits AP-2 to the plasma membrane and regulates rates of constitutive endocytosis. J.Cell Biol. (2003) vol. 162 (4) pp. 693-701

Page et al. Gamma-synergin: an EH domain-containing protein that interacts with gamma-adaptin. J.Cell Biol. (1999) vol. 146 (5) pp. 993-1004

Peden et al. The Di-leucine motif of vesicle-associated membrane protein 4 is required for its localization and AP-1 binding. J.Biol.Chem. (2001) vol. 276 (52) pp. 49183-7

Pelham. Insights from yeast endosomes. Curr Opin Cell Biol (2002) vol. 14 (4) pp. 454-62

Pelham. SNAREs and the specificity of membrane fusion. Trends Cell Biol. (2001) vol. 11 (3) pp. 99-101

Peña-Castillo and Hughes. Why are there still over 1000 uncharacterized yeast genes?. Genetics (2007) vol. 176 (1) pp. 7-14

Pereira-Leal and Seabra. Evolution of the Rab family of small GTP-binding proteins. J Mol Biol (2001) vol. 313 (4) pp. 889-901

Perrais and Merrifield. Dynamics of endocytic vesicle creation. Dev.Cell. (2005) vol. 9 (5) pp. 581-592

Prescott et al. Palmitoylation of the synaptic vesicle fusion machinery. J Neurochem (2009) vol. 110 (4) pp. 1135-49

Pryor et al. Molecular basis for the sorting of the SNARE VAMP7 into endocytic clathrin-coated vesicles by the ArfGAP Hrb. Cell (2008) vol. 134 (5) pp. 817-27

Qin et al. Regulation of phosphatidylinositol kinases and metabolism by Wnt3a and Dvl. J Biol Chem (2009) vol. 284 (34) pp. 22544-8

Rancati et al. Aneuploidy underlies rapid adaptive evolution of yeast cells deprived of a conserved cytokinesis motor. Cell (2008) vol. 135 (5) pp. 879-93

Rao et al. Altered receptor trafficking in Huntingtin Interacting Protein 1-transformed cells. Cancer Cell (2003) vol. 3 (5) pp. 471-82

Raymond et al. Morphological classification of the yeast vacuolar protein sorting mutants: evidence for a prevacuolar compartment in class E vps mutants. Mol.Biol.Cell (1992) vol. 3 (12) pp. 1389-402

Reusch et al. AP-1A and AP-3A lysosomal sorting functions. Traffic (2002) vol. 3 (10) pp. 752-61

Reymond. Substrate arrays for fluorescence-based enzyme fingerprinting and high-throughput screening. Ann N Y Acad Sci (2008) vol. 1130 pp. 12-20

Ritter and Wendland. Clathrin-Mediated Endocytosis. Trafficking Inside Cells: Pathways (2009)

Robinson et al. The Gcs1 Arf-GAP mediates Snc1,2 v-SNARE retrieval to the Golgi in yeast. Mol Biol Cell (2006) vol. 17 (4) pp. 1845-58

Robinson. Adaptable adaptors for coated vesicles. Trends Cell Biol. (2004) vol. 14 (4) pp. 167-174

Rönty et al. Palladin interacts with SH3 domains of SPIN90 and Src and is required for Src-induced cytoskeletal remodeling. Exp Cell Res (2007) vol. 313 (12) pp. 2575-85

Roth et al. Proteomic identification of palmitoylated proteins. Methods (2006) vol. 40 (2) pp. 135-42

Rusk et al. Synaptojanin 2 functions at an early step of clathrin-mediated endocytosis. Curr.Biol. (2003) vol. 13 (8) pp. 659-63

Russell et al. Molecular mechanisms of late endosome morphology, identity and sorting. Curr Opin Cell Biol (2006) vol. 18 (4) pp. 422-8

Scherens and Goffeau. The uses of genome-wide yeast mutant collections. Genome Biol (2004) vol. 5 (7) pp. 229

Schluter et al. Global analysis of yeast endosomal transport identifies the vps55/68 sorting complex. Mol Biol Cell (2008) vol. 19 (4) pp. 1282-94

Schu. Vesicular protein transport. Pharmacogenomics J. (2001) vol. 1 (4) pp. 262-271

Schuldiner et al. Quantitative genetic analysis in Saccharomyces cerevisiae using epistatic miniarray profiles (E-MAPs) and its application to chromatin functions. Methods (2006) vol. 40 (4) pp. 344-52

Schuldiner et al. Exploration of the function and organization of the yeast early secretory pathway through an epistatic miniarray profile. Cell (2005) vol. 123 (3) pp. 507-19

Scita and Di Fiore. The endocytic matrix. Nature (2010) vol. 463 (7280) pp. 464-73

Seaman. Endosome protein sorting: motifs and machinery. Cell Mol Life Sci (2008) vol. 65 (18) pp. 2842-58

Segev. GTPases in Intracellular Trafficking: An Overview. Semin.Cell Dev.Biol. (2010) pp.

Selkoe. Alzheimer's disease: genes, proteins, and therapy. Physiol Rev (2001) vol. 81 (2) pp. 741-66

Seong et al. Genetic analysis of the neuronal and ubiquitous AP-3 adaptor complexes reveals divergent functions in brain. Mol.Biol.Cell (2005) vol. 16 (1) pp. 128-40

Shah and Yu. sorLA: sorting out APP. Mol Interv (2006) vol. 6 (2) pp. 74-6, 58

Shannon et al. Cytoscape: a software environment for integrated models of biomolecular interaction networks. Genome Res (2003) vol. 13 (11) pp. 2498-504

Sheng and Kim. Postsynaptic signaling and plasticity mechanisms. Science (2002) vol. 298 (5594) pp. 776-80

Shim et al. Distinct and redundant functions of mu1 medium chains of the AP-1 clathrin-associated protein complex in the nematode Caenorhabditis elegans. Mol.Biol.Cell (2000) vol. 11 (8) pp. 2743-56

Siegers et al. Compartmentation of protein folding in vivo: sequestration of non-native polypeptide by the chaperonin-GimC system. EMBO J (1999) vol. 18 (1) pp. 75-84

Simon and Cravatt. Activity-based proteomics of enzyme superfamilies: serine hydrolases as a case study. J Biol Chem (2010) vol. 285 (15) pp. 11051-5

Smaczynska-de Rooij et al. A role for the dynamin-like protein Vps1 during endocytosis in yeast. J.Cell.Sci. (2010) vol. 123 (Pt 20) pp. 3496-506

Smythe and Ayscough. Actin regulation in endocytosis. J.Cell.Sci. (2006) vol. 119 (Pt 22) pp. 4589-98

Sorkin and von Zastrow. Endocytosis and signalling: intertwining molecular networks. Nat Rev Mol Cell Biol (2009) vol. 10 (9) pp. 609-22

Sorkin. Cargo recognition during clathrin-mediated endocytosis: a team effort. Curr.Opin.Cell Biol. (2004) vol. 16 (4) pp. 392-399

Soulard et al. The WASP/Las17p-interacting protein Bzz1p functions with Myo5p in an early stage of endocytosis. Protoplasma (2005) vol. 226 (1-2) pp. 89-101

Soulard et al. Saccharomyces cerevisiae Bzz1p is implicated with type I myosins in actin patch polarization and is able to recruit actin-polymerizing machinery in vitro. Mol Cell Biol (2002) vol. 22 (22) pp. 7889-906

Spang. The life cycle of a transport vesicle. Cell Mol.Life Sci. (2008) vol. 65 (18) pp. 2781-2789

Stefan et al. The yeast synaptojanin-like proteins control the cellular distribution of phosphatidylinositol (4,5)-bisphosphate. Mol.Biol.Cell (2002) vol. 13 (2) pp. 542-57

Stein et al. Rab proteins and endocytic trafficking: potential targets for therapeutic intervention. Adv Drug Deliv Rev (2003) vol. 55 (11) pp. 1421-37

Stepp et al. A late Golgi sorting function for Saccharomyces cerevisiae Apm1p, but not for Apm2p, a second yeast clathrin AP medium chain-related protein. Mol Biol Cell (1995) vol. 6 (1) pp. 41-58

Stolz et al. Identification and characterization of an essential family of inositol polyphosphate 5-phosphatases (INP51, INP52 and INP53 gene products) in the yeast Saccharomyces cerevisiae. Genetics (1998) vol. 148 (4) pp. 1715-29

Sun et al. PtdIns(4,5)P2 turnover is required for multiple stages during clathrin- and actin-dependent endocytic internalization. J.Cell Biol. (2007) vol. 177 (2) pp. 355-67

Sun et al. Endocytic internalization in budding yeast requires coordinated actin nucleation and myosin motor activity. Dev.Cell. (2006) vol. 11 (1) pp. 33-46

Sun et al. The yeast casein kinase Yck3p is palmitoylated, then sorted to the vacuolar membrane with AP-3-dependent recognition of a YXXPhi adaptin sorting signal. Mol.Biol.Cell (2004) vol. 15 (3) pp. 1397-406

Szilágyi et al. Prediction of physical protein-protein interactions. Phys Biol (2005) vol. 2 (2) pp. S1-16

Tong and Boone. Synthetic genetic array analysis in Saccharomyces cerevisiae. Methods Mol Biol (2006) vol. 313 pp. 171-92

Tong et al. Global mapping of the yeast genetic interaction network. Science (2004) vol. 303 (5659) pp. 808-13

Tong et al. A combined experimental and computational strategy to define protein interaction networks for peptide recognition modules. Science (2002) vol. 295 (5553) pp. 321-4

Toret et al. Multiple pathways regulate endocytic coat disassembly in Saccharomyces cerevisiae for optimal downstream trafficking. Traffic (2008) vol. 9 (5) pp. 848-59

Traub. Tickets to ride: selecting cargo for clathrin-regulated internalization. Nat.Rev.Mol.Cell Biol. (2009) vol. 10 (9) pp. 583-596

Traub. Common principles in clathrin-mediated sorting at the Golgi and the plasma membrane. Biochim.Biophys.Acta (2005) vol. 1744 (3) pp. 415-437

Traub. Sorting it out: AP-2 and alternate clathrin adaptors in endocytic cargo selection. J.Cell Biol. (2003) vol. 163 (2) pp. 203-208

Traub and Apodaca. AP-1B: polarized sorting at the endosome. Nat Cell Biol (2003) vol. 5 (12) pp. 1045-7

Ungar and Hughson. SNARE protein structure and function. Annu.Rev.Cell Dev.Biol. (2003) vol. 19 pp. 493-517

Ungewickell and Hinrichsen. Endocytosis: clathrin-mediated membrane budding. Curr.Opin.Cell Biol. (2007) vol. 19 (4) pp. 417-25

Valdez-Taubas and Pelham. Swf1-dependent palmitoylation of the SNARE Tlg1 prevents its ubiquitination and degradation. EMBO J (2005) vol. 24 (14) pp. 2524-32

Valdez-Taubas and Pelham. Slow diffusion of proteins in the yeast plasma membrane allows polarity to be maintained by endocytic cycling. Curr.Biol. (2003) vol. 13 (18) pp. 1636-40

Valdivia et al. The yeast clathrin adaptor protein complex 1 is required for the efficient retention of a subset of late Golgi membrane proteins. Dev Cell (2002) vol. 2 (3) pp. 283-94

van Vliet et al. Intracellular sorting and transport of proteins. Prog.Biophys.Mol.Biol. (2003) vol. 83 (1) pp. 1-45

Veit et al. Multiple palmitoylation of synaptotagmin and the t-SNARE SNAP-25. FEBS Lett (1996) vol. 385 (1-2) pp. 119-23

von Mering et al. Comparative assessment of large-scale data sets of protein-protein interactions. Nature (2002) vol. 417 (6887) pp. 399-403

von Mollard et al. The yeast v-SNARE Vti1p mediates two vesicle transport pathways through interactions with the t-SNAREs Sed5p and Pep12p. J.Cell Biol. (1997) vol. 137 (7) pp. 1511-24

Voronov et al. Synaptojanin 1-linked phosphoinositide dyshomeostasis and cognitive deficits in mouse models of Down's syndrome. Proc.Natl.Acad.Sci.U.S.A. (2008) vol. 105 (27) pp. 9415-20

Wahler et al. Enzyme fingerprints of activity, and stereo- and enantioselectivity from fluorogenic and chromogenic substrate arrays. Chemistry (2002) vol. 8 (14) pp. 3211-28

Wang et al. Phosphatidylinositol 4 phosphate regulates targeting of clathrin adaptor AP-1 complexes to the Golgi. Cell (2003) vol. 114 (3) pp. 299-310

Wasiak et al. Enthoprotin: a novel clathrin-associated protein identified through subcellular proteomics. J.Cell Biol. (2002) vol. 158 (5) pp. 855-62

Wei. Hermansky-Pudlak syndrome: a disease of protein trafficking and organelle function. Pigment Cell Res (2006) vol. 19 (1) pp. 19-42

Wendland et al. Yeast epsins contain an essential N-terminal ENTH domain, bind clathrin and are required for endocytosis. EMBO J (1999) vol. 18 (16) pp. 4383-93

Wendland and Emr. Pan1p, yeast eps15, functions as a multivalent adaptor that coordinates protein-protein interactions essential for endocytosis. J.Cell Biol. (1998) vol. 141 (1) pp. 71-84

Whitney et al. Cytoplasmic coat proteins involved in endosome function. Cell (1995) vol. 83 (5) pp. 703-13

Yu et al. Structural analysis of the interaction between Dishevelled2 and clathrin AP-2 adaptor, a critical step in noncanonical Wnt signaling. Structure (2010) vol. 18 (10) pp. 1311-20

Yu et al. Association of Dishevelled with the clathrin AP-2 adaptor is required for Frizzled endocytosis and planar cell polarity signaling. Dev Cell (2007) vol. 12 (1) pp. 129-41

Yuen et al. Systematic genome instability screens in yeast and their potential relevance to cancer. Proc.Natl.Acad.Sci.U.S.A. (2007) vol. 104 (10) pp. 3925-30

Zeidman et al. Protein acyl thioesterases (Review). Mol Membr Biol (2009) vol. 26 (1) pp. 32-41

Ziman et al. Chs6p-dependent anterograde transport of Chs3p from the chitosome to the plasma membrane in Saccharomyces cerevisiae. Mol.Biol.Cell (1998) vol. 9 (6) pp. 1565-76

APPENDIX A: Supplemental material for chapter 2

Table A1. Plasmids and yeast strains used in this study

Type	Name	Description/Genotype	Source	Notes
Plasmid	pCS7	SNC1-GFP in pRS316	(Schluter et al., 2008)[a]	
Plasmid	pCS30	GFP-SNC1-SUC2 in pRS306 (GSS; TPI1 promoter)	This study	Sequences from pGS (Lewis et al., 2000)[b] were PCR-amplified to introduce a SmaI site before the Snc1 stop codon, and subcloning this into XhoI/SmaI-digested pRS306. The resulting plasmid was digested with XbaI/SmaI, end-filled, and ligated to SUC2 sequences on a SmaI-HpaI fragment from pSEYC306 (Darsow et al., 2000)[c]
Plasmid	pMD9	GFP-SNC1(V40A M43A)-SUC2 in pRS306 (GSS en-; TPI1 promoter)	This study	V40A and M43A mutations were introduced into the *SNC1* coding region of pCS30 by site-directed mutagenesis
Plasmid	pHB4	SUC2 5'UTR-ADHpr-NATR-GFP-SNC1-SUC2 (GSS; ADH promoter)	This study	pHB4 was created in a multi-step process. pHB1 was first created by co-transformation of SacI/Kpn1-cut pRS416 with the following PCR products: (1) the NATR selection marker, ADH promoter and yeGFP coding sequence amplified from pYMN9 (Janke et al., 2004)[h] and (2) a 2378 bp fragment amplified from yeast genomic DNA after integration of pCS30, encoding the SNC1-SUC2 fusion and including 458 bp of SUC2 3'UTR. A PCR fragment encoding the

Type	Name	Description/Genotype	Source	Notes
				Nyv1 cytosolic domain (aa 1-229), amplified from yeast genomic DNA, was used to replace the Snc1 cytosolic domain (aa 1-90) by co-transformation with EcoR1-digested pHB1, creating pHB2. To facilitate integration into the SUC2 locus, 252bp of SUC2 5'UTR were amplified by PCR and incorporated upstream of the NATR cassette in BglII-digested pHB2, creating pHB3. This introduced a unique NotI restriction site upstream of the SUC2 5'UTR, such that NotI/SnaB1 digestion of pHB3 (or its derivatives) releases the chimeric reporter and the NATR marker on a cassette that is targeted to the SUC2 locus. pHB4 was then created by co-transforming ClaI/SalI-digested pHB3 with a PCR fragment containing the SNC1 sequence from pCS30.
Plasmid	pMD65	SUC2 5'UTR-ADHpr-NATR-GFP-NPFxD-SSO1 (NPF-Sso1)	This study	pMD51 was created by co-transforming ClaI/SalI-digested pHB3 with a PCR fragment containing the SNC1(V40A M43A) sequence from pMD9. The NPFxD endocytosis signal was appended to the N-terminus of the *SNC1*(V40A M43A) sequence in pMD51 by

Type	Name	Description/Genotype	Source	Notes
				co-transforming SpeI-digested pMD51 with a PCR product encoding MVLTNANPFSD, to generate pMD52. The *SNC1*(V40A M43A) coding sequence was then replaced with that of *SSO1* by co-transforming ClaI/SalI digested pMD52 with a PCR fragment containing the *SSO1* sequence amplified from yeast genomic DNA to create pMD60. pMD65 was made by co-transforming ClaI/SalI-digested pMD52 with a PCR fragment that directed replacement of SNC1-SUC2 sequences with the *SSO1* coding sequence.
Plasmid	pMD69	SUC2 5'UTR-ADHpr-NATR-GFP-3xNPFxD-SSO1-SUC2 in pRS416 (NGSS)	This study	pMD67 was created by insertion of two additional NPFxD motifs N-terminal in tandem with the existing NPFxD motif in pMD52 by synthesizing a PCR product containing 2 VLTNANPFSD motifs by primer extension, using overlapping oligonucleotides with 5' homology to the *ADH* promoter and 3' homology to the NPFxD motif in pMD52. The *SNC1*(V40A M43A) sequence of pMD67 was then replaced with *SSO1* by co-transforming ClaI/SalI digested pMD67 with PCR-amplified *SSO1*,

Type	Name	Description/Genotype	Source	Notes
				resulting in pMD69.
Plasmid	pSM1493	STE6-GFP in pRS426	Huyer et al., 2004[d]	gift from Susan Michaelis
Plasmid	pBW1427	LDB17-4XGFP tagging construct	This study	A plasmid for C-terminal tagging of *LDB17* with 4 tandem copies of GFP+ was created in a multistep process. Site directed mutagenesis was first used to convert the ApaLI site in pGFP+(NAT^R) (Scholz et al., 2000)[e] to an HpaI site, and the SacI site to a PmlI site, generating pBW1395. The 1014bp PmlI/HpaI fragment from pBW1395 was cloned into PmlI-linearized pBW1395 to generate pBW1396, which has two copies of GFP+ flanked by unique HpaI and PmlI sites. The 2028bp PmlI/HpaI 2xGFP+ fragment from pBW1396 was then cloned into PmlI-linearized pBW1396, generating pBW1397, which has four copies of GFP+ flanked by unique HpaI and PmlI sites. PCR amplification and TA cloning was used to clone 349 bp of the *LDB17* 3'UTR immediately following the *LDB17* ORF while introducing flanking BglII/XbaI sites. The 353bp BglII/XbaI fragment was verified by DNA sequencing and ligated into BglII/XbaI-cut pBW1397,

Type	Name	Description/Genotype	Source	Notes
				generating pBW1426. The *LDB17* ORF from nt 10 to 1473 was amplified by PCR, introducing an in-frame PvuII site immediately preceding the stop codon, subjected to TA cloning, and sequenced. The 1352bp PvuII/HpaI fragment was then ligated into HpaI-cut pBW1398, generating the pBW1427, which contains a 6970bp 4xGFP+-NAT^R cassette flanked by *LDB17* sequences that can be released by HpaI/XbaI digestion.
Plasmid	pOAD	pOAD	Uetz et al., 2000[f]	gift from Stan Fields
Plasmid	pOBD2	pOBD2	Uetz et al., 2000[f]	gift from Stan Fields
Plasmid	p3384	Yfr024c(291-373) in pOBD2	Tong et al., 2002[g]	gift from Charlie Boone.
Plasmid	p3388	Abp1(351-592) in pOBD2	Tong et al., 2002[g]	gift from Charlie Boone.
Plasmid	p3390	Bzz1(476-564) in pOBD2	Tong et al., 2002[g]	gift from Charlie Boone.
Plasmid	p3391	Bzz1(562-633) in pOBD2	Tong et al., 2002[g]	gift from Charlie Boone.
Plasmid	p3392	Bzz1(476-633) in pOBD2	Tong et al., 2002[g]	gift from Charlie Boone.
Plasmid	p3497	Myo3(1054-1271) in pOBD2	Tong et al., 2002[g]	gift from Charlie Boone.
Plasmid	p3519	Bem1(51-240) in pOBD2	Tong et al.,	gift from Charlie Boone.

Type	Name	Description/Genotype	Source	Notes
			2002[g]	
Plasmid	p3520	Bem1(1-551) in pOBD2	Tong et al., 2002[g]	gift from Charlie Boone.
Plasmid	p3697	Rvs167(401-482) in pOBD2	Tong et al., 2002[g]	gift from Charlie Boone.
Plasmid	p3699	Sla1(336-435) in pOBD2	Tong et al., 2002[g]	gift from Charlie Boone.
Plasmid	p3700	Sla1(1-150) in pOBD2	Tong et al., 2002[g]	gift from Charlie Boone.
Plasmid	p3735	Sla1(1-435) in pOBD2	Tong et al., 2002[g]	gift from Charlie Boone.
Plasmid	p3737	Sla1(61-150) in pOBD2	Tong et al., 2002[g]	gift from Charlie Boone.
Plasmid	p3755	Ysc84(391-468) in pOBD2	Tong et al., 2002[g]	gift from Charlie Boone.
Plasmid	p3771	Bbc1(1-90) in pOBD2	Tong et al., 2002[g]	gift from Charlie Boone.
Plasmid	p3842	Hof1(576-669) in pOBD2	Tong et al., 2002[g]	gift from Charlie Boone.
Yeast Strain	BY4741	MATa *his3Δ1 leu2Δ0 met15Δ0 ura3Δ0*	Open Biosystems	
Yeast Strain	BY4742	MATa *his3Δ1 leu2Δ0 lys2Δ0 ura3Δ0*	Open Biosystems	
Yeast Strain	HBY280	BY4741 *suc2::GFP-SNC1-SUC2::URA3*	This study	The GSS reporter plasmid pCS30 was linearized with XbaI and integrated at the *SUC2* locus in BY4741 and its knockout derivatives.
Yeast Strain	HBY222	BY4741 *rvs167Δ::KAN suc2::GFP-SNC1-SUC2::URA3*	This study	The GSS reporter plasmid pCS30 was linearized with XbaI and integrated at the *SUC2* locus in BY4741 and its knockout derivatives.
Yeast Strain	CSY448	BY4741 *ldb17Δ::KAN suc2::GFP-SNC1-*	This study	The GSS reporter plasmid pCS30 was

Type	Name	Description/Genotype	Source	Notes
		SUC2::URA3		linearized with XbaI and integrated at the *SUC2* locus in BY4741 and its knockout derivatives.
Yeast Strain	CSY461	BY4741 *bzz1Δ::KAN suc2::GFP-SNC1-SUC2::URA3*	This study	The GSS reporter plasmid pCS30 was linearized with XbaI and integrated at the *SUC2* locus in BY4741 and its knockout derivatives.
Yeast Strain	CSY520	BY4741 *lsb3Δ::KAN suc2::GFP-SNC1-SUC2::URA3*	This study	The GSS reporter plasmid pCS30 was linearized with XbaI and integrated at the *SUC2* locus in BY4741 and its knockout derivatives.
Yeast Strain	CSY453	BY4741 *inp52Δ::KAN suc2::GFP-SNC1-SUC2::URA3*	This study	The GSS reporter plasmid pCS30 was linearized with XbaI and integrated at the *SUC2* locus in BY4741 and its knockout derivatives.
Yeast Strain	CSY451	BY4741 *abp1Δ::KAN suc2::GFP-SNC1-SUC2::URA3*	This study	The GSS reporter plasmid pCS30 was linearized with XbaI and integrated at the *SUC2* locus in BY4741 and its knockout derivatives.
Yeast Strain	HBY277	BY4741 *myo5Δ::KAN suc2::GFP-SNC1-SUC2::URA3*	This study	The GSS reporter plasmid pCS30 was linearized with XbaI and integrated at the *SUC2* locus in BY4741 and its knockout derivatives.
Yeast Strain	HBY282	BY4741 *fus3Δ::KAN suc2::GFP-SNC1-SUC2::URA3*	This study	The GSS reporter plasmid pCS30 was linearized with XbaI and integrated at the *SUC2* locus in BY4741 and its knockout derivatives.
Yeast	HBY278	BY4741 *ede1Δ::KAN*	This	The GSS reporter

Type	Name	Description/Genotype	Source	Notes
Strain		*suc2::GFP-SNC1-SUC2::URA3*	study	plasmid pCS30 was linearized with XbaI and integrated at the *SUC2* locus in BY4741 and its knockout derivatives.
Yeast Strain	HBY279	BY4741 *sla1Δ::KAN suc2::GFP-SNC1-SUC2::URA3*	This study	The GSS reporter plasmid pCS30 was linearized with XbaI and integrated at the *SUC2* locus in BY4741 and its knockout derivatives.
Yeast Strain	HBY281	BY4741 *vrp1Δ::KAN suc2::GFP-SNC1-SUC2::URA3*	This study	The GSS reporter plasmid pCS30 was linearized with XbaI and integrated at the *SUC2* locus in BY4741 and its knockout derivatives.
Yeast Strain	HBY284	BY4741 *yol098cΔ::KAN suc2::GFP-SNC1-SUC2::URA3*	This study	The GSS reporter plasmid pCS30 was linearized with XbaI and integrated at the *SUC2* locus in BY4741 and its knockout derivatives.
Yeast Strain	CSY452	BY4741 *crn1Δ::KAN suc2::GFP-SNC1-SUC2::URA3*	This study	The GSS reporter plasmid pCS30 was linearized with XbaI and integrated at the *SUC2* locus in BY4741 and its knockout derivatives.
Yeast Strain	CSY455	BY4741 *twf1Δ::KAN suc2::GFP-SNC1-SUC2::URA3*	This study	The GSS reporter plasmid pCS30 was linearized with XbaI and integrated at the *SUC2* locus in BY4741 and its knockout derivatives.
Yeast Strain	CSY449	BY4741 *rvs161Δ::KAN suc2::GFP-SNC1-SUC2::URA3*	This study	The GSS reporter plasmid pCS30 was linearized with XbaI and integrated at the *SUC2* locus in BY4741 and its knockout derivatives.

Type	Name	Description/Genotype	Source	Notes
Yeast Strain	CSY521	BY4741 *bbc1Δ::KAN suc2::GFP-SNC1-SUC2::URA3*	This study	The GSS reporter plasmid pCS30 was linearized with XbaI and integrated at the *SUC2* locus in BY4741 and its knockout derivatives.
Yeast Strain	CSY435	BY4741 *yap1802Δ::KAN suc2::GFP-SNC1-SUC2::URA3*	This study	The GSS reporter plasmid pCS30 was linearized with XbaI and integrated at the *SUC2* locus in BY4741 and its knockout derivatives.
Yeast Strain	CSY522	BY4741 *syp1Δ::KAN suc2::GFP-SNC1-SUC2::URA3*	This study	The GSS reporter plasmid pCS30 was linearized with XbaI and integrated at the *SUC2* locus in BY4741 and its knockout derivatives.
Yeast Strain	CSY523	BY4741 *cap1Δ::KAN suc2::GFP-SNC1-SUC2::URA3*	This study	The GSS reporter plasmid pCS30 was linearized with XbaI and integrated at the *SUC2* locus in BY4741 and its knockout derivatives.
Yeast Strain	CSY525	BY4741 *cap2Δ::KAN suc2::GFP-SNC1-SUC2::URA3*	This study	The GSS reporter plasmid pCS30 was linearized with XbaI and integrated at the *SUC2* locus in BY4741 and its knockout derivatives.
Yeast Strain	CSY444	BY4741 *yap1801Δ::KAN suc2::GFP-SNC1-SUC2::URA3*	This study	The GSS reporter plasmid pCS30 was linearized with XbaI and integrated at the *SUC2* locus in BY4741 and its knockout derivatives.
Yeast Strain	CSY462	BY4741 *suc2::GFP-snc1(V40A,M43A)-SUC2::URA3*	This study	The GSS EN- reporter plasmid pMD9 was linearized with XbaI and integrated at the SUC2 locus in BY4741
Yeast	MDY581	BY4741 *yap1801Δ::KAN*	This	The *YAP1802* ORF was

Type	Name	Description/Genotype	Source	Notes
Strain		*yap1802Δ::HPH*	study	replaced with the hygromycin resistance marker in BY4741 *yap1801*::KAN by transformation of a PCR fragment amplified from pFA6-hphNT1 (Janke et al., 2004)[h], generating MDY581.
Yeast Strain	HBY323	BY4741 *yap1801Δ::KAN yap1802Δ::HPH suc2::GFP-SNC1-SUC2::URA3*	This study	The GSS reporter plasmid pCS30 was linearized with XbaI and integrated at the *SUC2* locus in MDY581
Yeast Strain	MDY582	BY4741 *yap1801Δ::KAN yap1802ΔCBM-3HA::HIS3*	This study	The final 4 C-terminal residues of Yap1802 (564-568) were replaced with a 3xHA tag in BY4741 *yap1801*::KAN to make MDY582
Yeast Strain	MDY583	BY4741 *yap1801Δ::KAN YAP1802-3HA::HIS3*	This study	
Yeast Strain	CSY462	BY4741 *suc2*::GFP-SNC1(V40A,M43A)-SUC2::URA3	This study	The GSS EN- reporter plasmid pMD9 was linearized with XbaI and integrated at the *SUC2* locus in BY4741 to create CSY462
Yeast Strain	HBY333	BY4741 *suc2Δ::NAT-GFP-3xNPFxD-SSO1-SUC2*	This study	The 3xNGSS reporter was integrated at the *SUC2* locus in BY4741 and derivatives by transformation with a NotI/SnaBI fragment released from pMD69 to create strains HBY333-HBY338. Integration of reporters was confirmed by colony PCR.
Yeast Strain	HBY334	BY4741 *yap1801Δ::KAN suc2Δ::NAT-GFP-3xNPFxD-SSO1-SUC2*	This study	The 3xNGSS reporter was integrated at the *SUC2* locus in BY4741 and derivatives by transformation with a

Type	Name	Description/Genotype	Source	Notes
				NotI/SnaBI fragment released from pMD69 to create strains HBY333-HBY338. Integration of reporters was confirmed by colony PCR.
Yeast Strain	HBY335	BY4741 *yap1802Δ::KAN suc2Δ::NAT-GFP-3xNPFxD-SSO1-SUC2*	This study	The 3xNGSS reporter was integrated at the *SUC2* locus in BY4741 and derivatives by transformation with a NotI/SnaBI fragment released from pMD69 to create strains HBY333-HBY338. Integration of reporters was confirmed by colony PCR.
Yeast Strain	HBY336	BY4741 *yap1801Δ::KAN yap1802Δ::HPH suc2Δ::NAT-GFP-3xNPFxD-SSO1-SUC2*	This study	The 3xNGSS reporter was integrated at the *SUC2* locus in BY4741 and derivatives by transformation with a NotI/SnaBI fragment released from pMD69 to create strains HBY333-HBY338. Integration of reporters was confirmed by colony PCR.
Yeast Strain	HBY337	BY4741 *ldb17Δ::KAN suc2Δ::NAT-GFP-3xNPFxD-SSO1-SUC2*	This study	The 3xNGSS reporter was integrated at the *SUC2* locus in BY4741 and derivatives by transformation with a NotI/SnaBI fragment released from pMD69 to create strains HBY333-HBY338. Integration of reporters was confirmed by colony PCR.
Yeast	HBY338	BY4741 *sla1Δ::KAN*	This	The 3xNGSS reporter

Type	Name	Description/Genotype	Source	Notes
Strain		*suc2Δ::NAT-GFP-3xNPFxD-SSO1-SUC2*	study	was integrated at the *SUC2* locus in BY4741 and derivatives by transformation with a NotI/SnaBI fragment released from pMD69 to create strains HBY333-HBY338. Integration of reporters was confirmed by colony PCR.
Yeast Strain	LCY1785	BY4741 *LDB17-13MYC::KAN*	This study	C-terminal tag encoding a 13xmyc epitope was integrated at the LDB17 locus as previously described (Longtine et al., 1998)[i]
Yeast Strain	LCY1786	BY4741 *ldb17ΔPRD-13MYC::KAN*	This study	C-terminal tag encoding a 13xmyc epitope was integrated at the LDB17 locus before Pro475, truncating Ldb17 and removing the proline-rich domain (Longtine et al., 1998)[i]
Yeast Strain	LCY1797	BY4741 *LDB17-13MYC::KAN BZZ1-3HA::HIS3*	This study	C-terminal tag encoding a 3xHA epitope (Longtine et al., 1998)[i] was integrated at the BZZ1 locus in LCY1786
Yeast Strain	LCY1798	BY4741 *ldb17ΔPRD-13MYC::KAN BZZ1-3HA::HIS3*	This study	C-terminal tag encoding a 3xHA epitope (Longtine et al., 1998)[i] was integrated at the BZZ1 locus in LCY1786
Yeast Strain	CSY76	BY4741 *LDB17-GFP::HIS3*	This study	To create the control strains (CSY76 and CSY78), the GFP-*HIS3* cassette was integrated before the *LDB17* stop codon.
Yeast Strain	CSY80	BY4741 *ldb17ΔPRD-GFP::HIS3*	This study	Expression of Ldb17-PRDΔ in CSY80 and CSY79 was

Type	Name	Description/Genotype	Source	Notes
				accomplished by integration of a GFP-*HIS3* cassette pGFP+; (Scholz et al., 2000)[e] before Pro475, truncating Ldb17 and removing the proline-rich domain.
Yeast Strain	CSY78	BY4741 *bzz1Δ::KAN LDB17-GFP::HIS3*	This study	To create the control strains (CSY76 and CSY78), the GFP-*HIS3* cassette was integrated before the *LDB17* stop codon.
Yeast Strain	CSY79	BY4741 *bzz1Δ::KAN ldb17ΔPRD-GFP::HIS3*	This study	Expression of Ldb17-PRDΔ in CSY80 and CSY79 was accomplished by integration of a GFP-*HIS3* cassette pGFP+; (Scholz et al., 2000)[e] before Pro475, truncating Ldb17 and removing the proline-rich domain.
Yeast Strain	HBY377	CSY76 *suc2::GFP-SNC1-SUC2::URA3*	This study	The GSS reporter plasmid pCS30 was linearized with XbaI and integrated at the SUC2 locus in the indicated strain
Yeast Strain	HBY378	CSY80 *suc2::GFP-SNC1-SUC2::URA3*	This study	The GSS reporter plasmid pCS30 was linearized with XbaI and integrated at the SUC2 locus in the indicated strain
Yeast Strain	HBY379	CSY78 *suc2::GFP-SNC1-SUC2::URA3*	This study	The GSS reporter plasmid pCS30 was linearized with XbaI and integrated at the SUC2 locus in the indicated strain
Yeast Strain	HBY380	CSY79 *suc2::GFP-SNC1-SUC2::URA3*	This study	The GSS reporter plasmid pCS30 was linearized with XbaI and integrated at the SUC2 locus in the

Type	Name	Description/Genotype	Source	Notes
				indicated strain
Yeast Strain	MDY620	BY4741 *LDB17-4XGFP::NAT*	This study	MDY620 and MDY628 were constructed by transforming BY4741 and BY4741 *sla1Δ* with HpaI/XbaI digested pBW1427.
Yeast Strain	MDY628	BY4741 *sla1Δ::KAN LDB17-4XGFP::NAT*	This study	MDY620 and MDY628 were constructed by transforming BY4741 and BY4741 *sla1Δ* with HpaI/XbaI digested pBW1427.
Yeast Strain	CSY84	BY4741 *LDB17-GFP::NAT SLA1-RFP::HIS3*	This study	C-terminal tag encoding mRFP1.5 (Campbell et al., 2002)[j] was integrated as previously described (Longtine et al., 1998)[i]
Yeast Strain	CSY85	BY4741 *LDB17-GFP::NAT MYO5-RFP::HIS3*	This study	C-terminal tag encoding mRFP1.5 (Campbell et al., 2002)[j] was integrated as previously described (Longtine et al., 1998)[i]
Yeast Strain	CSY86	BY4741 *LDB17-GFP::NAT ABP1-RFP::HIS3*	This study	C-terminal tag encoding mRFP1.5 (Campbell et al., 2002)[j] was integrated as previously described (Longtine et al., 1998)[i]
Yeast Strain	SEY6210	MATa *leu2-3,112 ura3-52 his3-Δ200 trp1-Δ901 lys2-801 suc2-Δ9 Met-*	S. Emr	
Yeast Strain	BWY2563	SEY6210 *yap1801Δ::HIS3*	Wendland and Emr, 1998[k]	BY2563, BY2565 and BY2567 were backcrossed from strains described in (Wendland and Emr, 1998)[k]
Yeast Strain	BWY2565	SEY6210 *yap1802Δ::LEU2*	Wendland and Emr, 1998[k]	BY2563, BY2565 and BY2567 were backcrossed from strains described in (Wendland and Emr, 1998)[k]
Yeast Strain	BWY2567	SEY6210 *yap1801Δ::HIS3 yap1802Δ::LEU2*	Wendland and	BY2563, BY2565 and BY2567 were

Type	Name	Description/Genotype	Source	Notes
			Emr, 1998[k]	backcrossed from strains described in (Wendland and Emr, 1998)[k]
Yeast Strain	BWY2552	SEY6210 *ldb17Δ::NAT*	This study	*LDB17* was replaced by NAT^R MX4 amplified from p4339 (Tong and Boone, 2006)[l] in SEY6210 to create BWY2552
Yeast Strain	BWY2068	SEY6210 *end3Δ::KAN*	This study	*END3* was replaced by KAN^R MX6 amplified from pFA6a-KanMX6 (Longtine et al., 1998)[i] to create BY2068
Yeast Strain	HBY551	SEY6210 *ABP1-GFP::HIS3*	This study	C-terminal tag encoding an improved version of GFP (GFP+) (Scholz et al., 2000)[e] was integrated in SEY6210
Yeast Strain	HBY552	BWY2552 *ABP1-GFP::HIS3*	This study	C-terminal tag encoding an improved version of GFP (GFP+) (Scholz et al., 2000)[e] was integrated in WY2552
Yeast Strain	MDY562	SEY6210 *SLA1-RFP::HIS3*	This study	C-terminal tag encoding mRFP1.5 (Campbell et al., 2002)[j] was integrated as previously described (Longtine et al., 1998) in SEY6210
Yeast Strain	MDY564	SEY6210 *ldb17Δ::NAT SLA1-RFP::HIS3*	This study	C-terminal tag encoding mRFP1.5 (Campbell et al., 2002)[j] was integrated in BWY2552 as previously described (Longtine et al., 1998)[i]
Yeast Strain	PJ694a	MATa *trp1-901 leu2-3,112 ura3-52 his3-200 gal4Δ gal80Δ LYS::GAL1-HIS3 GAL2-ADE2 met2::GAL7-lacZ*	James et al., 1996[m]	
Yeast Strain	PJ694a	MATa *trp1-901 leu2-3,112 ura3-52 his3-200 gal4Δ*	James et al., 1996[m]	

Type	Name	Description/Genotype	Source	Notes
		gal80Δ LYS::GAL1-HIS3 GAL2-ADE2 met2::GAL7-lacZ		
Yeast Strain	Y2H-LDB17	PJ694a pOAD-*LDB17*	S. Fields	PJ69-4a containing pOAD-*LDB17* was obtained from the genome wide Y2H activation domain collection (gift from Stan Fields, U of Washington).
Yeast Strain	BMY102	PJ694a pOAD-*ldb17ΔPRD*	This study	PJ69-4a containing pOAD-*ldb17 ΔPRD* was generated by co-transformation of PJ694-a with an *LDB17* PCR fragment lacking the C-term PRD domain (Pro475-Lys491) and PvuII/NcoI-linearized pOAD, and was subsequently confirmed by sequencing and western blotting.
Yeast Strain	Y6613	MATa *his3Δ1 leu2Δ0 met15Δ0 ura3Δ0 lyp1Δ::STE3pr-LEU2 cyh*	C. Boone	gift from Charlie Boone.
Yeast Strain	MDY220	Y6613 *suc2::GFP-SNC1-SUC2::URA3*	This study	Synthetic genetic analysis (SGA) starting strains Y6613 (Tong and Boone, 2006)[g] and Y7043 (gift of C. Boone) were transformed with Xba1-linearized pCS30, yielding MDY220 and MDY519.
Yeast Strain	Y7043	MATa *his3Δ1 leu2Δ0 met15Δ0 ura3Δ0 can1::STE2pr-LEU2 lyp1 cyh2*	C. Boone	gift from Charlie Boone.
Yeast Strain	MDY519	Y7043 *suc2::GFP-SNC1-SUC2::URA3*	This study	Synthetic genetic analysis (SGA) starting strains Y6613 (Tong and Boone, 2006)[g] and Y7043 (gift of C. Boone) were

Type	Name	Description/Genotype	Source	Notes
				transformed with Xba1-linearized pCS30, yielding MDY220 and MDY519.
Yeast Strain	MDY525	Y7043 *suc2::GFP-SNC1-SUC2::NAT*	This study	Y7043 was transformed with pHB4 was digested with NotI and SnaB1
Yeast Strain	MDY59	Y7043 *suc2::GFP-SNC1(S59A)-SUC2::NAT*	This study	pHB4 was mutated to introduce the SNC1 S59A mutation, digested with NotI/SnaBI and transformed into Y7043
Yeast Strain	MDY79	Y7043 *suc2::GFP-SNC1(S59D)-SUC2::NAT*	This study	pHB4 was mutated to introduce the SNC1 S59D mutation, digested with NotI/SnaBI and transformed into Y7044
Yeast Strain	MDY324	Y7043 *suc2::GFP-SNC1(V40A,M43A)-SUC2::URA3 pNAT*	This study	The GSS EN- reporter plasmid pMD9 was linearized with XbaI and integrated at the *SUC2* locus in the indicated strain
Yeast Strain	MDY48	MDY519 *apm1Δ::NAT*	This study	Gene replacement with the NAT^R MX4 marker was accomplished by transformation of MDY519 with appropriate PCR products amplified from p4339 (Tong and Boone, 2006)[l].
Yeast Strain	MDY46	MDY519 *apm2Δ::NAT*	This study	Gene replacement with the NAT^R MX4 marker was accomplished by transformation of MDY519 with appropriate PCR products amplified from p4339 (Tong and Boone, 2006)[l].
Yeast Strain	MDY47	MDY519 *apl4Δ::NAT*	This study	Gene replacement with the NAT^R MX4 marker

Type	Name	Description/Genotype	Source	Notes
				was accomplished by transformation of MDY519 with appropriate PCR products amplified from p4339 (Tong and Boone, 2006)[l].
Yeast Strain	MDY35	MDY519 *yap1801Δ::NAT*	This study	Gene replacement with the NAT^R MX4 marker was accomplished by transformation of MDY519 with appropriate PCR products amplified from p4339 (Tong and Boone, 2006)[l].
Yeast Strain	MDY47	MDY519 *apl4Δ::NAT*	This study	Gene replacement with the NAT^R MX4 marker was accomplished by transformation of MDY519 with appropriate PCR products amplified from p4339 (Tong and Boone, 2006)[l].
Yeast Strain	MDY48	MDY519 *apm1Δ::NAT*	This study	Gene replacement with the NAT^R MX4 marker was accomplished by transformation of MDY519 with appropriate PCR products amplified from p4339 (Tong and Boone, 2006)[l].
Yeast Strain	MDY46	MDY519 *apm2Δ::NAT*	This study	Gene replacement with the NAT^R MX4 marker was accomplished by transformation of MDY519 with appropriate PCR products amplified from p4339 (Tong and Boone, 2006)[l].
Yeast Strain	MDY34	MDY519 *ent1Δ::NAT*	This study	Gene replacement with the NAT^R MX4 marker was accomplished by transformation of MDY519 with

Type	Name	Description/Genotype	Source	Notes
				appropriate PCR products amplified from p4339 (Tong and Boone, 2006)[l].
Yeast Strain	MDY35	MDY519 *ent2Δ::NAT*	This study	Gene replacement with the NAT^R MX4 marker was accomplished by transformation of MDY519 with appropriate PCR products amplified from p4339 (Tong and Boone, 2006)[l].
Yeast Strain	MDY36	MDY519 *ent4Δ::NAT*	This study	Gene replacement with the NAT^R MX4 marker was accomplished by transformation of MDY519 with appropriate PCR products amplified from p4339 (Tong and Boone, 2006)[l].
Yeast Strain	MDY53	MDY519 *glc8Δ::NAT*	This study	Gene replacement with the NAT^R MX4 marker was accomplished by transformation of MDY519 with appropriate PCR products amplified from p4339 (Tong and Boone, 2006)[l].
Yeast Strain	MDY43	MDY519 *inp52Δ::NAT*	This study	Gene replacement with the NAT^R MX4 marker was accomplished by transformation of MDY519 with appropriate PCR products amplified from p4339 (Tong and Boone, 2006)[l].
Yeast Strain	MDY37	MDY519 *prk1Δ::NAT*	This study	Gene replacement with the NAT^R MX4 marker was accomplished by transformation of MDY519 with appropriate PCR products amplified from p4339 (Tong and

Type	Name	Description/Genotype	Source	Notes
				Boone, 2006)[l].
Yeast Strain	MDY44	MDY519 *sec28Δ::NAT*	This study	Gene replacement with the NAT^R MX4 marker was accomplished by transformation of MDY519 with appropriate PCR products amplified from p4339 (Tong and Boone, 2006)[l].
Yeast Strain	MDY41	MDY519 *syp1Δ::NAT*	This study	Gene replacement with the NAT^R MX4 marker was accomplished by transformation of MDY519 with appropriate PCR products amplified from p4339 (Tong and Boone, 2006)[l].
Yeast Strain	MDY45	MDY519 *ubi4Δ::NAT*	This study	Gene replacement with the NAT^R MX4 marker was accomplished by transformation of MDY519 with appropriate PCR products amplified from p4339 (Tong and Boone, 2006)[l].
Yeast Strain	MDY52	MDY519 *vps13Δ::NAT*	This study	Gene replacement with the NAT^R MX4 marker was accomplished by transformation of MDY519 with appropriate PCR products amplified from p4339 (Tong and Boone, 2006)[l].
Yeast Strain	MDY33	MDY519 *yap1801Δ::NAT*	This study	Gene replacement with the NAT^R MX4 marker was accomplished by transformation of MDY519 with appropriate PCR products amplified from p4339 (Tong and Boone, 2006)[l].
Yeast Strain	MDY40	MDY519 *yap1802Δ::NAT*	This study	Gene replacement with the NAT^R MX4 marker

Type	Name	Description/Genotype	Source	Notes
				was accomplished by transformation of MDY519 with appropriate PCR products amplified from p4339 (Tong and Boone, 2006)[l].
Yeast Strain	MDY38	MDY519 *ydr348cΔ::NAT*	This study	Gene replacement with the NAT^R MX4 marker was accomplished by transformation of MDY519 with appropriate PCR products amplified from p4339 (Tong and Boone, 2006)[l].
Yeast Strain	MDY54	MDY519 *yvh1Δ::NAT*	This study	Gene replacement with the NAT^R MX4 marker was accomplished by transformation of MDY519 with appropriate PCR products amplified from p4339 (Tong and Boone, 2006)[l].
Yeast Strain	MDY88	MDY519 *apl6Δ::NAT*	This study	Gene replacement with the NAT^R MX4 marker was accomplished by transformation of MDY519 with appropriate PCR products amplified from p4339 (Tong and Boone, 2006)[l].
Yeast Strain	MDY14	MDY519 *atg20Δ::NAT*	This study	Gene replacement with the NAT^R MX4 marker was accomplished by transformation of MDY519 with appropriate PCR products amplified from p4339 (Tong and Boone, 2006)[l].
Yeast Strain	MDY87	MDY519 *ent5Δ::NAT*	This study	Gene replacement with the NAT^R MX4 marker was accomplished by transformation of MDY519 with

Type	Name	Description/Genotype	Source	Notes
				appropriate PCR products amplified from p4339 (Tong and Boone, 2006)[l].
Yeast Strain	MDY129	MDY519 *gga2Δ::NAT*	This study	Gene replacement with the NAT^R MX4 marker was accomplished by transformation of MDY519 with appropriate PCR products amplified from p4339 (Tong and Boone, 2006)[l].
Yeast Strain	MDY131	MDY519 *inp53Δ::NAT*	This study	Gene replacement with the NAT^R MX4 marker was accomplished by transformation of MDY519 with appropriate PCR products amplified from p4339 (Tong and Boone, 2006)[l].
Yeast Strain	MDY127	MDY519 *nhx1Δ::NAT*	This study	Gene replacement with the NAT^R MX4 marker was accomplished by transformation of MDY519 with appropriate PCR products amplified from p4339 (Tong and Boone, 2006)[l].
Yeast Strain	MDY10	MDY519 *snx4Δ::NAT*	This study	Gene replacement with the NAT^R MX4 marker was accomplished by transformation of MDY519 with appropriate PCR products amplified from p4339 (Tong and Boone, 2006)[l].
Yeast Strain	MDY169	MDY519 *snx41Δ::NAT*	This study	Gene replacement with the NAT^R MX4 marker was accomplished by transformation of MDY519 with appropriate PCR products amplified from p4339 (Tong and

Type	Name	Description/Genotype	Source	Notes
				Boone, 2006)[l].
Yeast Strain	MDY271	MDY519 *vam3Δ::NAT*	This study	Gene replacement with the NAT^R MX4 marker was accomplished by transformation of MDY519 with appropriate PCR products amplified from p4339 (Tong and Boone, 2006)[l].
Yeast Strain	MDY92	MDY519 *vps4Δ::NAT*	This study	Gene replacement with the NAT^R MX4 marker was accomplished by transformation of MDY519 with appropriate PCR products amplified from p4339 (Tong and Boone, 2006)[l].
Yeast Strain	MDY39	MDY519 *vps5Δ::NAT*	This study	Gene replacement with the NAT^R MX4 marker was accomplished by transformation of MDY519 with appropriate PCR products amplified from p4339 (Tong and Boone, 2006)[l].
Yeast Strain	MDY270	MDY519 *vps9Δ::NAT*	This study	Gene replacement with the NAT^R MX4 marker was accomplished by transformation of MDY519 with appropriate PCR products amplified from p4339 (Tong and Boone, 2006)[l].
Yeast Strain	MDY95	MDY519 *vps54Δ::NAT*	This study	Gene replacement with the NAT^R MX4 marker was accomplished by transformation of MDY519 with appropriate PCR products amplified from p4339 (Tong and Boone, 2006)[l].
Yeast Strain	CSY56	MDY519 *vps55Δ::NAT*	This study	Gene replacement with the NAT^R MX4 marker

Type	Name	Description/Genotype	Source	Notes
				was accomplished by transformation of MDY519 with appropriate PCR products amplified from p4339 (Tong and Boone, 2006)[l].
Yeast Strain	CSY57	MDY519 *vps68Δ::NAT*	This study	Gene replacement with the NAT^R MX4 marker was accomplished by transformation of MDY519 with appropriate PCR products amplified from p4339 (Tong and Boone, 2006)[l].
Yeast Strain	MDY125	MDY519 *yfr043cΔ::NAT*	This study	Gene replacement with the NAT^R MX4 marker was accomplished by transformation of MDY519 with appropriate PCR products amplified from p4339 (Tong and Boone, 2006)[l].
Yeast Strain	MDY170	MDY519 *ypt31Δ::NAT*	This study	Gene replacement with the NAT^R MX4 marker was accomplished by transformation of MDY519 with appropriate PCR products amplified from p4339 (Tong and Boone, 2006)[l].
Yeast Strain	MDY16	MDY519 *ypt35Δ::NAT*	This study	Gene replacement with the NAT^R MX4 marker was accomplished by transformation of MDY519 with appropriate PCR products amplified from p4339 (Tong and Boone, 2006)[l].
Yeast Strain	MDY292	MDY519 *trp1Δ::NAT*	This study	Gene replacement with the NAT^R MX4 marker was accomplished by transformation of MDY519 with

Type	Name	Description/Genotype	Source	Notes
				appropriate PCR products amplified from p4339 (Tong and Boone, 2006)[l].
Yeast Strain	MDY282	MDY519 *age2Δ::NAT*	This study	Gene replacement with the NAT^R MX4 marker was accomplished by transformation of MDY519 with appropriate PCR products amplified from p4339 (Tong and Boone, 2006)[l].
Yeast Strain	MDY171	MDY519 *cka1Δ::NAT*	This study	Gene replacement with the NAT^R MX4 marker was accomplished by transformation of MDY519 with appropriate PCR products amplified from p4339 (Tong and Boone, 2006)[l].
Yeast Strain	MDY280	MDY519 *ckb1Δ::NAT*	This study	Gene replacement with the NAT^R MX4 marker was accomplished by transformation of MDY519 with appropriate PCR products amplified from p4339 (Tong and Boone, 2006)[l].
Yeast Strain	MDY13	MDY519 *ent3Δ::NAT*	This study	Gene replacement with the NAT^R MX4 marker was accomplished by transformation of MDY519 with appropriate PCR products amplified from p4339 (Tong and Boone, 2006)[l].
Yeast Strain	MDY85	MDY519 *erg4Δ::NAT*	This study	Gene replacement with the NAT^R MX4 marker was accomplished by transformation of MDY519 with appropriate PCR products amplified from p4339 (Tong and

Type	Name	Description/Genotype	Source	Notes
				Boone, 2006)[l].
Yeast Strain	MDY133	MDY519 *fks1Δ::NAT*	This study	Gene replacement with the NAT^R MX4 marker was accomplished by transformation of MDY519 with appropriate PCR products amplified from p4339 (Tong and Boone, 2006)[l].
Yeast Strain	MDY279	MDY519 *gcs1Δ::NAT*	This study	Gene replacement with the NAT^R MX4 marker was accomplished by transformation of MDY519 with appropriate PCR products amplified from p4339 (Tong and Boone, 2006)[l].
Yeast Strain	MDY277	MDY519 *gef1Δ::NAT*	This study	Gene replacement with the NAT^R MX4 marker was accomplished by transformation of MDY519 with appropriate PCR products amplified from p4339 (Tong and Boone, 2006)[l].
Yeast Strain	MDY42	MDY519 *hul5Δ::NAT*	This study	Gene replacement with the NAT^R MX4 marker was accomplished by transformation of MDY519 with appropriate PCR products amplified from p4339 (Tong and Boone, 2006)[l].
Yeast Strain	MDY83	MDY519 *las21Δ::NAT*	This study	Gene replacement with the NAT^R MX4 marker was accomplished by transformation of MDY519 with appropriate PCR products amplified from p4339 (Tong and Boone, 2006)[l].
Yeast Strain	MDY82	MDY519 *lcb4Δ::NAT*	This study	Gene replacement with the NAT^R MX4 marker

Type	Name	Description/Genotype	Source	Notes
				was accomplished by transformation of MDY519 with appropriate PCR products amplified from p4339 (Tong and Boone, 2006)[l].
Yeast Strain	MDY265	MDY519 *sak1Δ::NAT*	This study	Gene replacement with the NAT^R MX4 marker was accomplished by transformation of MDY519 with appropriate PCR products amplified from p4339 (Tong and Boone, 2006)[l].
Yeast Strain	MDY268	MDY519 *scy1Δ::NAT*	This study	Gene replacement with the NAT^R MX4 marker was accomplished by transformation of MDY519 with appropriate PCR products amplified from p4339 (Tong and Boone, 2006)[l].
Yeast Strain	MDY284	MDY519 *vam7Δ::NAT*	This study	Gene replacement with the NAT^R MX4 marker was accomplished by transformation of MDY519 with appropriate PCR products amplified from p4339 (Tong and Boone, 2006)[l].
Yeast Strain	MDY283	MDY519 *vps8Δ::NAT*	This study	Gene replacement with the NAT^R MX4 marker was accomplished by transformation of MDY519 with appropriate PCR products amplified from p4339 (Tong and Boone, 2006)[l].
Yeast Strain	MDY286	MDY519 *vps17Δ::NAT*	This study	Gene replacement with the NAT^R MX4 marker was accomplished by transformation of MDY519 with

Type	Name	Description/Genotype	Source	Notes
				appropriate PCR products amplified from p4339 (Tong and Boone, 2006)[l].
Yeast Strain	MDY134	MDY519 *vps21Δ::NAT*	This study	Gene replacement with the NAT^R MX4 marker was accomplished by transformation of MDY519 with appropriate PCR products amplified from p4339 (Tong and Boone, 2006)[l].
Yeast Strain	MDY278	MDY519 *vps38Δ::NAT*	This study	Gene replacement with the NAT^R MX4 marker was accomplished by transformation of MDY519 with appropriate PCR products amplified from p4339 (Tong and Boone, 2006)[l].
Yeast Strain	MDY281	MDY519 *vps51Δ::NAT*	This study	Gene replacement with the NAT^R MX4 marker was accomplished by transformation of MDY519 with appropriate PCR products amplified from p4339 (Tong and Boone, 2006)[l].
Yeast Strain	MDY287	MDY519 *ykr078wΔ::NAT*	This study	Gene replacement with the NAT^R MX4 marker was accomplished by transformation of MDY519 with appropriate PCR products amplified from p4339 (Tong and Boone, 2006)[l].
Yeast Strain	MDY285	MDY519 *ypr097wΔ::NAT*	This study	Gene replacement with the NAT^R MX4 marker was accomplished by transformation of MDY519 with appropriate PCR products amplified from p4339 (Tong and

Type	Name	Description/Genotype	Source	Notes
				Boone, 2006)[l].
Yeast Strain	MDY80	MDY519 *ypt6Δ::NAT*	This study	Gene replacement with the NAT^R MX4 marker was accomplished by transformation of MDY519 with appropriate PCR products amplified from p4339 (Tong and Boone, 2006)[l].
Yeast Strain	MDY360	MDY519 *apm3Δ::NAT*	This study	Gene replacement with the NAT^R MX4 marker was accomplished by transformation of MDY519 with appropriate PCR products amplified from p4339 (Tong and Boone, 2006)[l].
Yeast Strain	MDY389	MDY519 *arf1Δ::NAT*	This study	Gene replacement with the NAT^R MX4 marker was accomplished by transformation of MDY519 with appropriate PCR products amplified from p4339 (Tong and Boone, 2006)[l].
Yeast Strain	MDY332	MDY519 *arr4Δ::NAT*	This study	Gene replacement with the NAT^R MX4 marker was accomplished by transformation of MDY519 with appropriate PCR products amplified from p4339 (Tong and Boone, 2006)[l].
Yeast Strain	MDY333	MDY519 *bsd2Δ::NAT*	This study	Gene replacement with the NAT^R MX4 marker was accomplished by transformation of MDY519 with appropriate PCR products amplified from p4339 (Tong and Boone, 2006)[l].
Yeast Strain	MDY415	MDY519 *hap4Δ::NAT*	This study	Gene replacement with the NAT^R MX4 marker

Type	Name	Description/Genotype	Source	Notes
				was accomplished by transformation of MDY519 with appropriate PCR products amplified from p4339 (Tong and Boone, 2006)[l].
Yeast Strain	MDY371	MDY519 *lsp1Δ::NAT*	This study	Gene replacement with the NAT^R MX4 marker was accomplished by transformation of MDY519 with appropriate PCR products amplified from p4339 (Tong and Boone, 2006)[l].
Yeast Strain	MDY413	MDY519 *mon2Δ::NAT*	This study	Gene replacement with the NAT^R MX4 marker was accomplished by transformation of MDY519 with appropriate PCR products amplified from p4339 (Tong and Boone, 2006)[l].
Yeast Strain	MDY357	MDY519 *mvp1Δ::NAT*	This study	Gene replacement with the NAT^R MX4 marker was accomplished by transformation of MDY519 with appropriate PCR products amplified from p4339 (Tong and Boone, 2006)[l].
Yeast Strain	MDY372	MDY519 *pil1Δ::NAT*	This study	Gene replacement with the NAT^R MX4 marker was accomplished by transformation of MDY519 with appropriate PCR products amplified from p4339 (Tong and Boone, 2006)[l].
Yeast Strain	MDY383	MDY519 *ptc1Δ::NAT*	This study	Gene replacement with the NAT^R MX4 marker was accomplished by transformation of MDY519 with

Type	Name	Description/Genotype	Source	Notes
				appropriate PCR products amplified from p4339 (Tong and Boone, 2006)[l].
Yeast Strain	MDY391	MDY519 *rav1Δ::NAT*	This study	Gene replacement with the NAT^R MX4 marker was accomplished by transformation of MDY519 with appropriate PCR products amplified from p4339 (Tong and Boone, 2006)[l].
Yeast Strain	MDY366	MDY519 *rts1Δ::NAT*	This study	Gene replacement with the NAT^R MX4 marker was accomplished by transformation of MDY519 with appropriate PCR products amplified from p4339 (Tong and Boone, 2006)[l].
Yeast Strain	MDY421	MDY519 *sft2Δ::NAT*	This study	Gene replacement with the NAT^R MX4 marker was accomplished by transformation of MDY519 with appropriate PCR products amplified from p4339 (Tong and Boone, 2006)[l].
Yeast Strain	MDY400	MDY519 *vrp1Δ::NAT*	This study	Gene replacement with the NAT^R MX4 marker was accomplished by transformation of MDY519 with appropriate PCR products amplified from p4339 (Tong and Boone, 2006)[l].
Yeast Strain	MDY51	MDY519 *akr1Δ::NAT*	This study	Gene replacement with the NAT^R MX4 marker was accomplished by transformation of MDY519 with appropriate PCR products amplified from p4339 (Tong and

Type	Name	Description/Genotype	Source	Notes
				Boone, 2006)[l].
Yeast Strain	MDY332	MDY519 *get3Δ::NAT*	This study	Gene replacement with the NAT^R MX4 marker was accomplished by transformation of MDY519 with appropriate PCR products amplified from p4339 (Tong and Boone, 2006)[l].
Yeast Strain	MDY393	MDY519 *stv1Δ::NAT*	This study	Gene replacement with the NAT^R MX4 marker was accomplished by transformation of MDY519 with appropriate PCR products amplified from p4339 (Tong and Boone, 2006)[l].
Yeast Strain	MDY398	MDY519 *ubp3Δ::NAT*	This study	Gene replacement with the NAT^R MX4 marker was accomplished by transformation of MDY519 with appropriate PCR products amplified from p4339 (Tong and Boone, 2006)[l].
Yeast Strain	MDY385	MDY519 *vps1Δ::NAT*	This study	Gene replacement with the NAT^R MX4 marker was accomplished by transformation of MDY519 with appropriate PCR products amplified from p4339 (Tong and Boone, 2006)[l].
Yeast Strain	MDY417	MDY519 *vps27Δ::NAT*	This study	Gene replacement with the NAT^R MX4 marker was accomplished by transformation of MDY519 with appropriate PCR products amplified from p4339 (Tong and Boone, 2006)[l].

Table A2. Full list of mutants with cell surface GSS levels greater to or equal to the median value for all strains.

Note that a low densitometry value indicates a high level of cell surface reporter. Densitometry values were subtracted from the median value for all strains to generate "SCORE".

Rank	ORF	Gene	Normalized densitometry values			SCORE
			MATa	MATalpha	average	
1	YCR009C	RVS161	0.11	0.04	0.07	0.93
2	YDR207C	UME6	0.05	0.10	0.07	0.93
3	YOR035C	SHE4	0.14	0.08	0.11	0.90
4	YLR337C	VRP1	0.14	0.12	0.13	0.87
5	YAL013W	DEP1	0.13		0.13	0.87
6	YPL045W	VPS16	0.13		0.13	0.87
7	YNL069C	RPL16B	0.03	0.24	0.13	0.87
8	YDR388W	RVS167	0.13		0.13	0.87
9	YMR198W	CIK1	0.14		0.14	0.87
10	YDL146W	LDB17		0.14	0.14	0.86
11	YKR094C	RPL40B	0.06	0.22	0.14	0.86
12	YBL007C	SLA1	0.14	0.15	0.15	0.86
13	YCR044C	PER1	0.10	0.20	0.15	0.86
14	YIL049W	DFG10	0.16		0.16	0.85
15	YKL002W	DID4	0.16		0.16	0.85
16	YIL154C	IMP2'	0.18		0.18	0.82
17	YDR276C	PMP3	0.07	0.35	0.21	0.80
18	YLR370C	ARC18	0.18	0.24	0.21	0.80
19	YLR056W	ERG3	0.21	0.22	0.21	0.79
20	YIL128W	MET18	0.32	0.13	0.23	0.78
21	YHR026W	PPA1	0.23		0.23	0.77
22	YER056C-A	RPL34A	0.23	0.24	0.23	0.77
23	YLR338W		0.28	0.19	0.24	0.77
24	YLR399C	BDF1	0.10	0.40	0.25	0.75
25	YMR311C	GLC8	0.14	0.36	0.25	0.75
26	YGR240C	PFK1		0.26	0.26	0.75
27	YDR442W		0.26		0.26	0.75
28	YOL004W	SIN3	0.26		0.26	0.75
29	YHR161C	YAP1801	0.06	0.45	0.26	0.75
30	YEL031W	SPF1	0.15	0.38	0.27	0.74
31	YBL047C	EDE1	0.21	0.33	0.27	0.74
32	YJL080C	SCP160		0.27	0.27	0.73
33	YNL215W	IES2	0.15	0.42	0.28	0.72
34	YMR091C	NPL6	0.29		0.29	0.71
35	YIL090W	ICE2	0.29		0.29	0.71
36	YDR364C	CDC40	0.29		0.29	0.71
37	YPL031C	PHO85	0.32	0.29	0.30	0.70

Rank	ORF	Gene	Normalized densitometry values			SCORE
			MATa	MATalpha	average	
38	YLR119W	SRN2	0.31		0.31	0.70
39	YDL081C	RPP1A	0.30	0.33	0.32	0.69
40	YNR006W	VPS27	0.43	0.21	0.32	0.69
41	YIL076W	SEC28	0.32		0.32	0.68
42	YGR241C	YAP1802	0.35	0.29	0.32	0.68
43	YLR025W	SNF7		0.33	0.33	0.68
44	YPR029C	APL4	0.23	0.44	0.33	0.67
45	YKL007W	CAP1	0.26	0.42	0.34	0.67
46	YIL093C	RSM25	0.34		0.34	0.66
47	YGL058W	RAD6	0.25	0.46	0.35	0.65
48	YJL176C	SWI3	0.71	0.00	0.35	0.65
49	YER074W	RPS24A	0.39	0.33	0.36	0.65
50	YBR127C	VMA2	0.36		0.36	0.64
51	YAL047C	SPC72	0.37		0.37	0.64
52	YNL079C	TPM1	0.50	0.24	0.37	0.63
53	YJR121W	ATP2	0.37		0.37	0.63
54	YCR088W	ABP1	0.32	0.42	0.37	0.63
55	YKL119C	VPH2		0.38	0.38	0.62
56	YGR242W		0.43	0.33	0.38	0.62
57	YPL178W	CBC2	0.38		0.38	0.62
58	YHL002W	HSE1	0.30	0.47	0.39	0.62
59	YHL025W	SNF6	0.39		0.39	0.62
60	YMR116C	ASC1	0.17	0.61	0.39	0.62
61	YMR109W	MYO5	0.35	0.43	0.39	0.61
62	YLR425W	TUS1	0.40	0.39	0.39	0.61
63	YNL105W		0.25	0.54	0.40	0.61
64	YBL027W	RPL19B	0.42	0.38	0.40	0.61
65	YDL002C	NHP10	0.26	0.56	0.41	0.59
66	YNR010W	CSE2	0.26	0.57	0.42	0.59
67	YIL084C	SDS3	0.43		0.43	0.58
68	YNL106C	INP52	0.29	0.56	0.43	0.58
69	YFL025C	BST1	0.35	0.51	0.43	0.58
70	YNR023W	SNF12	0.65	0.21	0.43	0.57
71	YNR052C	POP2	0.86	0.00	0.43	0.57
72	YGL168W	HUR1	0.36	0.51	0.43	0.57
73	YJL062W	LAS21	0.50	0.38	0.44	0.57
74	YIR034C	LYS1	0.57	0.31	0.44	0.56
75	YMR263W	SAP30	0.56	0.32	0.44	0.56
76	YGL084C	GUP1	0.38	0.51	0.44	0.56
77	YEL013W	VAC8	0.38	0.51	0.45	0.56
78	YIR003W		0.51	0.39	0.45	0.55
79	YKR035C		0.50	0.40	0.45	0.55
80	YLR171W		0.26	0.64	0.45	0.55
81	YPL002C	SNF8		0.45	0.45	0.55

Rank	ORF	Gene	Normalized densitometry values			SCORE
			MATa	MATalpha	average	
82	YCR028C-A	RIM1	0.45		0.45	0.55
83	YGR101W	PCP1	0.24	0.67	0.46	0.54
84	YLR200W	YKE2	0.46		0.46	0.54
85	YGL027C	CWH41	0.32	0.60	0.46	0.54
86	YDL243C	AAD4		0.47	0.47	0.53
87	YLR170C	APS1	0.27	0.67	0.47	0.53
88	YDL160C	DHH1		0.47	0.47	0.53
89	YOR209C	NPT1	0.34	0.61	0.48	0.53
90	YER092W	IES5	0.36	0.60	0.48	0.53
91	YAL068C		0.35	0.61	0.48	0.52
92	YGL219C	MDM34	0.53	0.43	0.48	0.52
93	YGR204W	ADE3	0.32	0.64	0.48	0.52
94	YLR169W		0.33	0.63	0.48	0.52
95	YGL066W	SGF73	0.43	0.54	0.48	0.52
96	YKR001C	VPS1	0.42	0.55	0.48	0.52
97	YOR275C	RIM20	0.39	0.59	0.49	0.51
98	YPL100W	ATG21	0.37	0.62	0.49	0.51
99	YPR067W	ISA2	0.50		0.50	0.51
100	YKL204W	EAP1	0.33	0.66	0.50	0.51
101	YNL219C	ALG9	0.55	0.45	0.50	0.51
102	YBL083C		0.50		0.50	0.51
103	YPL042C	SSN3	0.50		0.50	0.51
104	YJL175W		0.84	0.16	0.50	0.50
105	YNL197C	WHI3	0.97	0.04	0.51	0.50
106	YDR226W	ADK1		0.51	0.51	0.50
107	YOR126C	IAH1	0.19	0.83	0.51	0.50
108	YBL058W	SHP1		0.51	0.51	0.49
109	YOL129W	VPS68	0.39	0.64	0.52	0.49
110	YGR206W		0.51	0.53	0.52	0.48
111	YML019W	OST6	0.44	0.60	0.52	0.48
112	YDL194W	SNF3	0.54	0.51	0.52	0.48
113	YNR005C		0.66	0.39	0.52	0.48
114	YBL006C	LDB7	0.53		0.53	0.48
115	YKL041W	VPS24	0.53		0.53	0.48
116	YNL111C	CYB5	0.48	0.58	0.53	0.48
117	YFR031C-A	RPL2A	0.27	0.80	0.53	0.47
118	YBR095C		0.44	0.64	0.54	0.47
119	YBR156C	SLI15	0.84	0.23	0.54	0.47
120	YGR100W	MDR1	0.52	0.56	0.54	0.47
121	YBL082C	ALG3	0.52	0.56	0.54	0.46
122	YLL030C		0.06	1.03	0.55	0.46
123	YLR417W	VPS36		0.55	0.55	0.46

Rank	ORF	Gene	Normalized densitometry values			SCORE
			MATa	MATalpha	average	
124	YIL020C	HIS6	0.20	0.90	0.55	0.46
125	YNR030W	ALG12	0.53	0.57	0.55	0.45
126	YKR100C	SKG1	0.58	0.52	0.55	0.45
127	YIL034C	CAP2	0.46	0.64	0.55	0.45
128	YLR139C	SLS1	0.55		0.55	0.45
129	YIL163C		0.12	1.00	0.56	0.45
130	YPL256C	CLN2	0.62	0.50	0.56	0.45
131	YPR030W	CSR2	0.39	0.73	0.56	0.45
132	YHL019C	APM2	0.59	0.53	0.56	0.44
133	YML014W	TRM9	0.56		0.56	0.44
134	YJL153C	INO1	0.24	0.88	0.56	0.44
135	YHR030C	SLT2	0.64	0.48	0.56	0.44
136	YPR164W	MMS1	0.36	0.76	0.56	0.44
137	YPL179W	PPQ1	0.63	0.50	0.56	0.44
138	YDR006C	SOK1	0.53	0.60	0.56	0.44
139	YJR073C	OPI3		0.56	0.56	0.44
140	YML008C	ERG6	1.04	0.09	0.57	0.44
141	YER120W	SCS2	0.49	0.64	0.57	0.44
142	YKL073W	LHS1	0.67	0.47	0.57	0.44
143	YGL076C	RPL7A	0.52	0.62	0.57	0.43
144	YPR070W	MED1	0.73	0.41	0.57	0.43
145	YNL248C	RPA49	0.57		0.57	0.43
146	YPR024W	YME1	0.80	0.35	0.57	0.43
147	YKR099W	BAS1	0.53	0.62	0.58	0.43
148	YCL005W	LDB16	0.13	1.02	0.58	0.43
149	YDR074W	TPS2	0.64	0.52	0.58	0.43
150	YLR428C		0.64	0.52	0.58	0.43
151	YNL016W	PUB1	0.50	0.66	0.58	0.42
152	YIR023W	DAL81	0.14	1.02	0.58	0.42
153	YNL252C	MRPL17	0.58		0.58	0.42
154	YML048W	GSF2	0.49	0.68	0.58	0.42
155	YGR080W	TWF1	0.43	0.74	0.59	0.42
156	YNL269W	BSC4	0.13	1.04	0.59	0.42
157	YPL158C		0.59	0.59	0.59	0.42
158	YNL238W	KEX2	0.59		0.59	0.42
159	YER130C		0.60	0.57	0.59	0.42
160	YKL074C	MUD2	0.47	0.71	0.59	0.41
161	YBR289W	SNF5	0.59		0.59	0.41
162	YMR272C	SCS7	0.37	0.82	0.59	0.41
163	YCR063W	BUD31	0.57	0.62	0.59	0.41
164	YHL027W	RIM101	0.45	0.74	0.59	0.41
165	YPL057C	SUR1	0.46	0.73	0.60	0.41
166	YLR403W	SFP1	0.39	0.80	0.60	0.41
167	YPL118W	MRP51	0.60		0.60	0.41

Rank	ORF	Gene	Normalized densitometry values			SCORE
			MATa	MATalpha	average	
168	YGR256W	GND2	0.47	0.72	0.60	0.41
169	YLL033W		0.69	0.50	0.60	0.41
170	YNL097C	PHO23	0.61	0.59	0.60	0.41
171	YGR061C	ADE6	0.63	0.58	0.60	0.40
172	YCL007C		0.60		0.60	0.40
173	YJL183W	MNN11	0.88	0.33	0.60	0.40
174	YHR081W	LRP1	0.29	0.92	0.60	0.40
175	YDR448W	ADA2	0.57	0.64	0.61	0.40
176	YIL027C	KRE27	0.70	0.51	0.61	0.40
177	YGR157W	CHO2	0.65	0.57	0.61	0.40
178	YOL108C	INO4	0.61		0.61	0.40
179	YOR030W	DFG16	0.77	0.45	0.61	0.39
180	YOR008C	SLG1	0.73	0.49	0.61	0.39
181	YPR101W	SNT309	0.47	0.75	0.61	0.39
182	YGR056W	RSC1	0.56	0.67	0.61	0.39
183	YCR002C	CDC10	0.61		0.61	0.39
184	YDL176W		0.01	1.22	0.62	0.39
185	YEL036C	ANP1		0.62	0.62	0.39
186	YFR001W	LOC1	0.62		0.62	0.38
187	YJL060W	BNA3	0.81	0.43	0.62	0.38
188	YBR229C	ROT2		0.62	0.62	0.38
189	YLL038C	ENT4	0.66	0.58	0.62	0.38
190	YLL039C	UBI4	0.56	0.68	0.62	0.38
191	YOR026W	BUB3	0.70	0.54	0.62	0.38
192	YLR087C	CSF1	0.66	0.58	0.62	0.38
193	YOL036W		0.14	1.11	0.62	0.38
194	YGR122W		0.42	0.82	0.62	0.38
195	YBR097W	VPS15		0.62	0.62	0.38
196	YOR274W	MOD5	0.65	0.61	0.63	0.38
197	YJR075W	HOC1	0.66	0.59	0.63	0.38
198	YNL284C	MRPL10	0.63		0.63	0.38
199	YPL027W	SMA1	0.54	0.71	0.63	0.38
200	YNL220W	ADE12	0.52	0.74	0.63	0.38
201	YHR082C	KSP1	0.59	0.67	0.63	0.37
202	YJR034W	PET191	0.63		0.63	0.37
203	YNL280C	ERG24	1.09	0.18	0.63	0.37
204	YDL075W	RPL31A	0.61	0.66	0.63	0.37
205	YCR028C	FEN2	0.63		0.63	0.37
206	YLR069C	MEF1	0.64		0.64	0.37
207	YDL073W		0.22	1.05	0.64	0.37
208	YLR358C			0.64	0.64	0.37
209	YDR129C	SAC6	1.11	0.17	0.64	0.37
210	YPR052C	NHP6A	0.73	0.55	0.64	0.36
211	YIR026C	YVH1	0.91	0.38	0.64	0.36

Rank	ORF	Gene	Normalized densitometry values			SCORE
			MATa	MATalpha	average	
212	YMR023C	MSS1	0.26	1.02	0.64	0.36
213	YGL127C	SOH1	0.41	0.88	0.64	0.36
214	YLR382C	NAM2	0.64		0.64	0.36
215	YGL167C	PMR1	0.56	0.73	0.65	0.36
216	YCR030C	SYP1	0.51	0.78	0.65	0.36
217	YML017W	PSP2	0.69	0.60	0.65	0.36
218	YMR063W	RIM9	0.34	0.96	0.65	0.36
219	YBR255W		0.67	0.63	0.65	0.35
220	YOR141C	ARP8	1.03	0.28	0.65	0.35
221	YLR150W	STM1	0.63	0.67	0.65	0.35
222	YGL200C	EMP24		0.65	0.65	0.35
223	YGL014W	PUF4	0.65	0.66	0.65	0.35
224	YGL072C		0.34	0.97	0.65	0.35
225	YEL063C	CAN1	0.33	0.98	0.65	0.35
226	YAL055W	PEX22	0.72	0.58	0.65	0.35
227	YDR532C		1.22	0.09	0.65	0.35
228	YNL153C	GIM3	0.66		0.66	0.35
229	YJL124C	LSM1	0.68	0.64	0.66	0.35
230	YDR346C	SVF1	0.61	0.70	0.66	0.35
231	YJL020C	BBC1	0.75	0.57	0.66	0.35
232	YEL060C	PRB1	0.64	0.68	0.66	0.35
233	YJL128C	PBS2	0.59	0.73	0.66	0.34
234	YEL067C		0.53	0.80	0.66	0.34
235	YBR150C	TBS1	0.54	0.79	0.66	0.34
236	YKL081W	TEF4	0.43	0.90	0.66	0.34
237	YPL034W		0.66	0.68	0.67	0.34
238	YDL005C	MED2		0.67	0.67	0.34
239	YPR006C	ICL2	0.75	0.58	0.67	0.34
240	YGL016W	KAP122	0.50	0.83	0.67	0.34
241	YIR009W	MSL1	0.43	0.90	0.67	0.34
242	YJR116W		0.80	0.54	0.67	0.34
243	YLR412W		0.70	0.64	0.67	0.34
244	YPL129W	TAF14	0.67		0.67	0.33
245	YPL066W		0.93	0.41	0.67	0.33
246	YNR031C	SSK2	0.66	0.69	0.67	0.33
247	YJL067W		0.47	0.88	0.67	0.33
248	YBR144C		0.76	0.58	0.67	0.33
249	YJL068C		0.38	0.97	0.67	0.33
250	YFL013W-A		0.57	0.78	0.67	0.33
251	YMR031W-A		0.56	0.79	0.67	0.33
252	YLR149C		0.56	0.79	0.67	0.33
253	YIL116W	HIS5	0.25	1.10	0.68	0.33

Rank	ORF	Gene	Normalized densitometry values			SCORE
			MATa	MATalpha	average	
254	YLR113W	HOG1	0.75	0.60	0.68	0.33
255	YLR422W		0.65	0.70	0.68	0.33
256	YMR024W	MRPL3	0.34	1.01	0.68	0.33
257	YNL199C	GCR2	0.66	0.69	0.68	0.33
258	YHR092C	HXT4	0.85	0.51	0.68	0.32
259	YFL034W		0.70	0.66	0.68	0.32
260	YKL065C		0.72	0.64	0.68	0.32
261	YMR038C	CCS1	0.68		0.68	0.32
262	YGR160W		0.40	0.97	0.68	0.32
263	YOR067C	ALG8	0.65	0.72	0.68	0.32
264	YJL056C	ZAP1	0.51	0.85	0.68	0.32
265	YKL063C		0.68	0.69	0.68	0.32
266	YGR126W		0.92	0.45	0.68	0.32
267	YDR225W	HTA1	0.81	0.56	0.69	0.32
268	YBR106W	PHO88	0.75	0.62	0.69	0.32
269	YGR259C		0.58	0.80	0.69	0.32
270	YPL212C	PUS1	0.55	0.83	0.69	0.32
271	YDR233C	RTN1	0.54	0.84	0.69	0.32
272	YGL045W	RIM8	0.55	0.83	0.69	0.31
273	YIL130W		0.66	0.72	0.69	0.31
274	YOL009C	MDM12	0.53	0.85	0.69	0.31
275	YKR035W-A	DID2	0.66	0.73	0.69	0.31
276	YLR120C	YPS1	0.58	0.80	0.69	0.31
277	YJR055W	HIT1	0.42	0.96	0.69	0.31
278	YCR048W	ARE1	0.63	0.75	0.69	0.31
279	YGL149W		0.52	0.86	0.69	0.31
280	YJL120W		0.66	0.73	0.69	0.31
281	YDL161W	ENT1	0.66	0.73	0.69	0.31
282	YFL013C	IES1	0.79	0.59	0.69	0.31
283	YPR173C	VPS4	0.72	0.67	0.69	0.31
284	YML012W	ERV25	0.73	0.66	0.70	0.31
285	YIR005W	IST3	0.71	0.68	0.70	0.31
286	YHR079C	IRE1	0.79	0.60	0.70	0.31
287	YCL046W		0.66	0.73	0.70	0.31
288	YLR136C	TIS11	0.83	0.56	0.70	0.31
289	YPL036W	PMA2	0.57	0.83	0.70	0.31
290	YDR072C	IPT1	0.78	0.62	0.70	0.31
291	YCL008C	STP22	1.03	0.37	0.70	0.31
292	YDR335W	MSN5		0.70	0.70	0.31
293	YNL264C	PDR17	0.51	0.89	0.70	0.30
294	YOR189W	IES4	0.52	0.88	0.70	0.30
295	YPL227C	ALG5	0.73	0.68	0.70	0.30
296	YDR455C		0.44	0.97	0.70	0.30

Rank	ORF	Gene	Normalized densitometry values			SCORE
			MATa	MATalpha	average	
297	YMR032W	HOF1	0.70		0.70	0.30
298	YNL266W		0.70		0.70	0.30
299	YMR316C-A		0.47	0.94	0.70	0.30
300	YPL049C	DIG1	0.46	0.95	0.70	0.30
301	YLR262C	YPT6	0.54	0.87	0.70	0.30
302	YMR139W	RIM11	0.67	0.74	0.70	0.30
303	YCR060W	TAH1	0.47	0.94	0.71	0.30
304	YOR255W	OSW1	0.21	1.20	0.71	0.30
305	YDR414C	ERD1	0.75	0.67	0.71	0.29
306	YPL145C	KES1	0.73	0.69	0.71	0.29
307	YOR211C	MGM1	0.44	0.99	0.71	0.29
308	YOL007C		0.51	0.91	0.71	0.29
309	YAL010C	MDM10	0.71		0.71	0.29
310	YOR127W	RGA1	0.52	0.91	0.71	0.29
311	YGR078C	PAC10	0.61	0.82	0.71	0.29
312	YPL079W	RPL21B	0.14	1.28	0.71	0.29
313	YBL016W	FUS3	0.63	0.79	0.71	0.29
314	YER155C	BEM2	0.95	0.48	0.71	0.29
315	YNL084C	END3	1.20	0.23	0.71	0.29
316	YDL023C		0.70	0.73	0.71	0.29
317	YMR126C		0.71	0.72	0.72	0.29
318	YGR036C	CAX4	0.95	0.48	0.72	0.29
319	YPL101W	ELP4	0.71	0.72	0.72	0.29
320	YOR036W	PEP12	0.72		0.72	0.29
321	YGL012W	ERG4		0.72	0.72	0.29
322	YDR368W	YPR1	0.46	0.97	0.72	0.29
323	YOR016C	ERP4	0.69	0.74	0.72	0.29
324	YNL004W	HRB1	0.62	0.81	0.72	0.29
325	YPL239W	YAR1	0.64	0.79	0.72	0.29
326	YER154W	OXA1	0.75	0.69	0.72	0.29
327	YJR088C		0.64	0.80	0.72	0.28
328	YDR221W		0.79	0.65	0.72	0.28
329	YMR307W	GAS1	0.74	0.71	0.72	0.28
330	YNR050C	LYS9	0.72		0.72	0.28
331	YDR424C	DYN2	0.31	1.14	0.72	0.28
332	YDL231C	BRE4	0.86	0.58	0.72	0.28
333	YAL053W		0.56	0.89	0.72	0.28
334	YDL096C		0.68	0.76	0.72	0.28
335	YBR266C	SLM6	0.48	0.97	0.72	0.28
336	YKL001C	MET14	0.62	0.83	0.72	0.28
337	YJR106W	ECM27	0.58	0.86	0.72	0.28
338	YFR024C-A	LSB3	0.73	0.72	0.72	0.28

Rank	ORF	Gene	Normalized densitometry values			SCORE
			MATa	MATalpha	average	
339	YGL198W	YIP4	0.66	0.79	0.73	0.28
340	YBR248C	HIS7	0.41	1.04	0.73	0.28
341	YNL294C	RIM21	0.62	0.83	0.73	0.28
342	YGR143W	SKN1	0.64	0.82	0.73	0.28
343	YKL072W	STB6	0.73	0.73	0.73	0.28
344	YEL045C			0.73	0.73	0.28
345	YKL071W		0.72	0.73	0.73	0.28
346	YOL072W	THP1	1.01	0.45	0.73	0.28
347	YLR006C	SSK1	0.80	0.66	0.73	0.27
348	YJR082C	EAF6	0.71	0.75	0.73	0.27
349	YBR019C	GAL10	0.64	0.82	0.73	0.27
350	YLR371W	ROM2	0.73		0.73	0.27
351	YJR118C	ILM1	0.24	1.23	0.73	0.27
352	YPL193W	RSA1	0.26	1.21	0.73	0.27
353	YDR234W	LYS4	0.73		0.73	0.27
354	YER117W	RPL23B	1.04	0.43	0.73	0.27
355	YER087W		0.73		0.73	0.27
356	YJR010C-A	SPC1	0.53	0.94	0.73	0.27
357	YPR131C	NAT3	0.89	0.58	0.73	0.27
358	YFL016C	MDJ1	0.74		0.74	0.27
359	YGR058W		0.69	0.78	0.74	0.27
360	YKL139W	CTK1	0.74		0.74	0.27
361	YNL198C		0.73	0.74	0.74	0.27
362	YLR262C-A		0.58	0.89	0.74	0.27
363	YKL032C	IXR1	0.75	0.72	0.74	0.27
364	YOL006C	TOP1	0.45	1.03	0.74	0.27
365	YLR429W	CRN1	0.64	0.83	0.74	0.27
366	YNR021W		0.74	0.73	0.74	0.27
367	YML094W	GIM5	0.69	0.79	0.74	0.27
368	YMR092C	AIP1	0.72	0.75	0.74	0.27
369	YFL031W	HAC1	0.75	0.73	0.74	0.26
370	YGL109W		0.57	0.91	0.74	0.26
371	YJL095W	BCK1	0.71	0.77	0.74	0.26
372	YIR021W	MRS1	1.01	0.47	0.74	0.26
373	YER187W		0.52	0.96	0.74	0.26
374	YLR320W	MMS22	0.46	1.03	0.74	0.26
375	YNL050C		0.92	0.57	0.74	0.26
376	YPL226W	NEW1	0.52	0.96	0.74	0.26
377	YMR289W		0.97	0.52	0.74	0.26
378	YGR254W	ENO1	0.91	0.57	0.74	0.26
379	YGR138C	TPO2	0.89	0.59	0.74	0.26
380	YKL160W	ELF1	0.75	0.74	0.74	0.26
381	YMR074C		0.62	0.86	0.74	0.26

Rank	ORF	Gene	Normalized densitometry values			SCORE
			MATa	MATalpha	average	
382	YBR235W		0.85	0.63	0.74	0.26
383	YHR114W	BZZ1	0.79	0.70	0.74	0.26
384	YGR252W	GCN5	0.93	0.56	0.74	0.26
385	YIL085C	KTR7	0.85	0.64	0.75	0.26
386	YNL196C		0.51	0.98	0.75	0.26
387	YJR044C	VPS55	0.85	0.64	0.75	0.26
388	YNL123W		0.91	0.58	0.75	0.26
389	YER069W	ARG5,6	0.37	1.12	0.75	0.26
390	YJL121C	RPE1	0.75	0.74	0.75	0.26
391	YDL047W	SIT4	0.70	0.79	0.75	0.26
392	YJL215C		0.54	0.95	0.75	0.26
393	YJL038C		0.75		0.75	0.26
394	YCR017C	CWH43	0.76	0.74	0.75	0.26
395	YDR050C	TPI1	0.75		0.75	0.26
396	YOL100W	PKH2	0.75		0.75	0.26
397	YJL065C	DLS1	0.72	0.78	0.75	0.26
398	YGL256W	ADH4	0.61	0.89	0.75	0.25
399	YLL014W		0.66	0.84	0.75	0.25
400	YKL136W		0.66	0.84	0.75	0.25
401	YJL185C		0.94	0.56	0.75	0.25
402	YNL043C		1.03	0.47	0.75	0.25
403	YLR455W		0.64	0.86	0.75	0.25
404	YNL165W		0.75		0.75	0.25
405	YBR036C	CSG2	0.91	0.59	0.75	0.25
406	YBR114W	RAD16	1.02	0.48	0.75	0.25
407	YER175C	TMT1	0.56	0.94	0.75	0.25
408	YDR028C	REG1	0.82	0.69	0.75	0.25
409	YMR242C	RPL20A	0.60	0.90	0.75	0.25
410	YMR145C	NDE1	0.80	0.70	0.75	0.25
411	YGR135W	PRE9	0.89	0.62	0.75	0.25
412	YDL184C	RPL41A	0.53	0.97	0.75	0.25
413	YBR220C		0.79	0.71	0.75	0.25
414	YLL054C		0.69	0.81	0.75	0.25
415	YPL064C	CWC27	0.63	0.88	0.75	0.25
416	YDR329C	PEX3	0.98	0.53	0.75	0.25
417	YNL070W	TOM7	1.34	0.17	0.75	0.25
418	YPL061W	ALD6	0.65	0.86	0.76	0.25
419	YOL098C		0.66	0.85	0.76	0.25
420	YJL182C		0.67	0.84	0.76	0.25
421	YBR294W	SUL1	0.41	1.10	0.76	0.25
422	YOR128C	ADE2	0.64	0.87	0.76	0.25
423	YKR021W		1.00	0.52	0.76	0.25
424	YNL324W		0.71	0.81	0.76	0.25
425	YKR096W		0.75	0.77	0.76	0.25

Rank	ORF	Gene	Normalized densitometry values			SCORE
			MATa	MATalpha	average	
426	YOL028C	YAP7	0.81	0.71	0.76	0.25
427	YFL003C	MSH4	0.97	0.54	0.76	0.25
428	YGL231C		0.75	0.77	0.76	0.25
429	YPL165C	SET6	0.82	0.70	0.76	0.24
430	YAL035W	FUN12	0.60	0.92	0.76	0.24
431	YIL011W	TIR3	0.88	0.64	0.76	0.24
432	YKL213C	DOA1	0.77	0.75	0.76	0.24
433	YPR074C	TKL1	0.80	0.73	0.76	0.24
434	YJR010W	MET3	0.48	1.05	0.76	0.24
435	YNL148C	ALF1	0.76	0.76	0.76	0.24
436	YDR293C	SSD1	0.81	0.72	0.76	0.24
437	YBR059C	AKL1	0.72	0.81	0.76	0.24
438	YCL058C	FYV5	0.64	0.89	0.76	0.24
439	YGR023W	MTL1	0.76	0.77	0.76	0.24
440	YOR002W	ALG6	0.74	0.79	0.76	0.24
441	YML055W	SPC2	0.75	0.78	0.76	0.24
442	YKL064W	MNR2	0.81	0.72	0.76	0.24
443	YBL025W	RRN10	0.86	0.67	0.76	0.24
444	YPL240C	HSP82	0.49	1.04	0.76	0.24
445	YCR011C	ADP1	0.73	0.80	0.77	0.24
446	YOL076W	MDM20	0.77		0.77	0.24
447	YBR301W	DAN3	0.52	1.01	0.77	0.24
448	YOR345C		0.56	0.97	0.77	0.24
449	YMR317W		0.77		0.77	0.24
450	YLR099C	ICT1	0.56	0.97	0.77	0.24
451	YIL025C		0.85	0.68	0.77	0.24
452	YGR155W	CYS4	0.77	0.76	0.77	0.24
453	YCL045C		0.81	0.73	0.77	0.24
454	YOL059W	GPD2	0.80	0.74	0.77	0.24
455	YIL132C	CSM2	0.86	0.68	0.77	0.24
456	YMR275C	BUL1	0.82	0.72	0.77	0.24
457	YOL013C	HRD1	0.76	0.78	0.77	0.24
458	YDR011W	SNQ2	0.97	0.57	0.77	0.24
459	YMR148W		0.76	0.78	0.77	0.23
460	YDR265W	PEX10	0.66	0.88	0.77	0.23
461	YKL066W		0.77	0.77	0.77	0.23
462	YDL076C	RXT3	0.43	1.11	0.77	0.23
463	YMR179W	SPT21	0.83	0.71	0.77	0.23
464	YJR105W	ADO1		0.77	0.77	0.23
465	YDR071C	PAA1	0.60	0.94	0.77	0.23
466	YMR027W		0.67	0.88	0.77	0.23
467	YMR241W	YHM2	0.35	1.19	0.77	0.23
468	YLR386W	VAC14	0.73	0.81	0.77	0.23
469	YHR087W		0.50	1.04	0.77	0.23

Rank	ORF	Gene	Normalized densitometry values			SCORE
			MATa	MATalpha	average	
470	YOR130C	ORT1	0.56	0.99	0.77	0.23
471	YLL047W		0.95	0.60	0.77	0.23
472	YFL032W		0.80	0.75	0.77	0.23
473	YML084W		0.62	0.93	0.77	0.23
474	YPL041C		0.49	1.06	0.77	0.23
475	YOR378W		0.73	0.82	0.77	0.23
476	YGL015C		0.49	1.07	0.78	0.23
477	YNL089C		0.69	0.86	0.78	0.23
478	YCL074W		1.00	0.55	0.78	0.23
479	YPL017C		0.55	1.00	0.78	0.23
480	YNL255C	GIS2	0.93	0.62	0.78	0.23
481	YGR215W	RSM27	0.72	0.84	0.78	0.23
482	YEL054C	RPL12A	0.43	1.13	0.78	0.23
483	YER161C	SPT2	0.72	0.83	0.78	0.23
484	YPR053C		0.62	0.93	0.78	0.23
485	YDR010C		0.86	0.69	0.78	0.23
486	YMR031C		0.71	0.84	0.78	0.23
487	YPL077C		0.77	0.78	0.78	0.23
488	YGR130C		0.78	0.77	0.78	0.23
489	YPR065W	ROX1	0.81	0.74	0.78	0.23
490	YGL024W		0.92	0.63	0.78	0.23
491	YOL152W	FRE7	0.60	0.96	0.78	0.23
492	YMR252C		0.56	1.00	0.78	0.23
493	YNL042W	BOP3	1.20	0.36	0.78	0.22
494	YML029W	USA1	0.76	0.80	0.78	0.22
495	YDR209C		0.96	0.60	0.78	0.22
496	YOL001W	PHO80	0.48	1.08	0.78	0.22
497	YML083C		0.81	0.75	0.78	0.22
498	YNL192W	CHS1	0.78		0.78	0.22
499	YNL299W	TRF5	0.54	1.02	0.78	0.22
500	YPL139C	UME1	0.78	0.79	0.78	0.22
501	YKR097W	PCK1	0.77	0.79	0.78	0.22
502	YER068W	MOT2	0.58	0.98	0.78	0.22
503	YFL004W	VTC2	0.89	0.68	0.78	0.22
504	YGR069W		0.94	0.63	0.78	0.22
505	YJL127C	SPT10	0.76	0.80	0.78	0.22
506	YPL004C	LSP1	0.65	0.92	0.78	0.22
507	YLR152C		0.86	0.71	0.78	0.22
508	YPL102C		0.70	0.87	0.78	0.22
509	YNL316C	PHA2	0.54	1.03	0.78	0.22
510	YER122C	GLO3	0.52	1.05	0.78	0.22
511	YJL130C	URA2	0.78		0.78	0.22
512	YBR141C		0.84	0.73	0.78	0.22
513	YPL262W	FUM1	0.84	0.73	0.78	0.22

Rank	ORF	Gene	Normalized densitometry values			SCORE
			MATa	MATalpha	average	
514	YML099C	ARG81	0.65	0.92	0.78	0.22
515	YBR139W		0.82	0.75	0.79	0.22
516	YPL062W		0.82	0.75	0.79	0.22
517	YJR102C	VPS25	1.24	0.33	0.79	0.22
518	YPL056C		0.61	0.97	0.79	0.22
519	YJR122W	CAF17	0.79		0.79	0.22
520	YKL098W		0.67	0.90	0.79	0.22
521	YGL160W		0.78	0.80	0.79	0.22
522	YMR315W		0.59	0.99	0.79	0.22
523	YDR477W	SNF1	0.79		0.79	0.22
524	YOR331C		0.79		0.79	0.22
525	YGR020C	VMA7	0.79		0.79	0.22
526	YGR188C	BUB1	0.90	0.68	0.79	0.21
527	YJR052W	RAD7	0.67	0.91	0.79	0.21
528	YGL205W	POX1	0.79		0.79	0.21
529	YHR178W	STB5	0.68	0.91	0.79	0.21
530	YIL155C	GUT2	0.83	0.75	0.79	0.21
531	YDR192C	NUP42	0.93	0.66	0.79	0.21
532	YKL075C		0.87	0.72	0.79	0.21
533	YOR366W		0.72	0.86	0.79	0.21
534	YGR184C	UBR1	0.96	0.63	0.79	0.21
535	YPR069C	SPE3	0.77	0.82	0.79	0.21
536	YDR005C	MAF1	0.83	0.76	0.79	0.21
537	YHR110W	ERP5	0.88	0.71	0.79	0.21
538	YLR027C	AAT2	0.72	0.87	0.79	0.21
539	YMR251W		0.77	0.82	0.80	0.21
540	YGR208W	SER2	0.80	0.79	0.80	0.21
541	YBL044W		0.94	0.65	0.80	0.21
542	YCR053W	THR4	0.61	0.98	0.80	0.21
543	YNL246W	VPS75	0.84	0.75	0.80	0.21
544	YKL029C	MAE1	0.69	0.90	0.80	0.21
545	YPR063C		0.85	0.74	0.80	0.21
546	YDR241W	BUD26	0.85	0.75	0.80	0.21
547	YJL139C	YUR1	0.76	0.84	0.80	0.21
548	YKL174C	TPO5	0.81	0.78	0.80	0.21
549	YPR153W		0.84	0.76	0.80	0.21
550	YKL207W		0.83	0.76	0.80	0.21
551	YOR182C	RPS30B	0.73	0.87	0.80	0.21
552	YGR260W	TNA1	0.78	0.82	0.80	0.21
553	YHR003C		0.74	0.86	0.80	0.21
554	YJL071W	ARG2	0.76	0.84	0.80	0.21
555	YGR154C		0.73	0.87	0.80	0.20
556	YGL246C	RAI1	0.84	0.76	0.80	0.20
557	YMR154C	RIM13	0.72	0.88	0.80	0.20

Rank	ORF	Gene	Normalized densitometry values			SCORE
			MATa	MATalpha	average	
558	YDR525W	API2	0.67	0.93	0.80	0.20
559	YDR440W	DOT1		0.80	0.80	0.20
560	YPL234C	TFP3	0.80		0.80	0.20
561	YCR076C		0.86	0.74	0.80	0.20
562	YOL060C	MAM3	1.02	0.58	0.80	0.20
563	YER184C		0.89	0.71	0.80	0.20
564	YGR269W		0.90	0.70	0.80	0.20
565	YHR050W	SMF2	0.81	0.79	0.80	0.20
566	YPR091C		0.79	0.81	0.80	0.20
567	YER176W	ECM32	0.72	0.89	0.80	0.20
568	YNL250W	RAD50	0.83	0.77	0.80	0.20
569	YLR226W	BUR2	0.80		0.80	0.20
570	YBR023C	CHS3	0.66	0.94	0.80	0.20
571	YPR166C	MRP2	0.59	1.02	0.80	0.20
572	YLR354C	TAL1	0.74	0.87	0.80	0.20
573	YJL027C		1.02	0.59	0.80	0.20
574	YMR123W	PKR1	1.10	0.51	0.80	0.20
575	YBR201W	DER1	0.80	0.81	0.80	0.20
576	YGL161C	YIP5	0.87	0.74	0.80	0.20
577	YMR269W		0.96	0.65	0.80	0.20
578	YDR372C	VPS74	0.64	0.97	0.81	0.20
579	YOL104C	NDJ1	0.72	0.89	0.81	0.20
580	YNL325C	FIG4	0.79	0.83	0.81	0.20
581	YOR288C	MPD1	0.54	1.07	0.81	0.20
582	YOR285W		0.84	0.77	0.81	0.20
583	YGL174W	BUD13	0.76	0.85	0.81	0.20
584	YNL010W		0.73	0.88	0.81	0.20
585	YFR034C	PHO4	0.90	0.72	0.81	0.20
586	YMR316C-B		0.54	1.08	0.81	0.20
587	YLL002W	RTT109	0.67	0.94	0.81	0.20
588	YIL056W		0.79	0.83	0.81	0.20
589	YNR002C	ATO2	1.01	0.60	0.81	0.20
590	YOR239W	ABP140	0.68	0.94	0.81	0.20
591	YLR192C	HCR1	0.70	0.92	0.81	0.20
592	YGR153W		0.69	0.92	0.81	0.20
593	YDR466W	PKH3	0.79	0.83	0.81	0.20
594	YDR181C	SAS4	0.79	0.83	0.81	0.19
595	YGL105W	ARC1	1.07	0.55	0.81	0.19
596	YHR100C		0.81		0.81	0.19
597	YLR434C		0.61	1.01	0.81	0.19
598	YMR077C	VPS20	0.81		0.81	0.19
599	YJL212C	OPT1	0.67	0.95	0.81	0.19
600	YOR312C	RPL20B		0.81	0.81	0.19

Rank	ORF	Gene	Normalized densitometry values			SCORE
			MATa	MATalpha	average	
601	YFR011C		0.97	0.65	0.81	0.19
602	YNR022C	MRPL50	0.92	0.70	0.81	0.19
603	YDR360W		0.85	0.77	0.81	0.19
604	YOL016C	CMK2	0.75	0.87	0.81	0.19
605	YDR289C	RTT103	0.83	0.79	0.81	0.19
606	YJR131W	MNS1	0.92	0.71	0.81	0.19
607	YOR267C	HRK1	0.82	0.81	0.81	0.19
608	YLR325C	RPL38	0.82	0.80	0.81	0.19
609	YJR107W		0.74	0.88	0.81	0.19
610	YEL042W	GDA1	0.75	0.88	0.81	0.19
611	YNL009W	IDP3	0.80	0.83	0.81	0.19
612	YOL093W	TRM10	0.68	0.95	0.81	0.19
613	YDR315C	IPK1	0.70	0.93	0.81	0.19
614	YKL025C	PAN3	0.81	0.82	0.81	0.19
615	YPL070W	MUK1	0.82	0.81	0.81	0.19
616	YFR043C		0.70	0.92	0.81	0.19
617	YIL038C	NOT3	0.95	0.68	0.81	0.19
618	YLR207W	HRD3	0.82	0.81	0.81	0.19
619	YIL139C	REV7	1.05	0.58	0.81	0.19
620	YLR164W		0.90	0.73	0.81	0.19
621	YDR159W	SAC3	0.85	0.78	0.81	0.19
622	YPR009W	SUT2	1.09	0.54	0.81	0.19
623	YDR171W	HSP42	1.04	0.59	0.81	0.19
624	YOL126C	MDH2	0.68	0.95	0.82	0.19
625	YKL031W		0.84	0.79	0.82	0.19
626	YBR082C	UBC4	0.90	0.73	0.82	0.19
627	YNL268W	LYP1	0.76	0.88	0.82	0.19
628	YGR227W	DIE2	0.82	0.81	0.82	0.19
629	YOR043W	WHI2	0.74	0.90	0.82	0.19
630	YJL211C		0.74	0.90	0.82	0.19
631	YJL055W		0.67	0.97	0.82	0.19
632	YPR179C	HDA3	0.78	0.85	0.82	0.19
633	YJR108W	ABM1	0.78	0.85	0.82	0.19
634	YLR052W	IES3	0.89	0.75	0.82	0.19
635	YDR382W	RPP2B	0.62	1.02	0.82	0.19
636	YLR138W	NHA1	0.95	0.69	0.82	0.19
637	YGR228W		0.94	0.70	0.82	0.19
638	YKL003C	MRP17	0.82		0.82	0.19
639	YPL092W	SSU1	0.59	1.05	0.82	0.19
640	YGR263C		0.88	0.76	0.82	0.19
641	YLR133W	CKI1	0.34	1.30	0.82	0.19
642	YNL047C	SLM2	0.81	0.83	0.82	0.19
643	YBR125C	PTC4	1.00	0.64	0.82	0.19
644	YDR461W	MFA1		0.82	0.82	0.19

Rank	ORF	Gene	Normalized densitometry values			SCORE
			MATa	MATalpha	average	
645	YKR030W	GMH1	0.97	0.67	0.82	0.19
646	YLR432W	IMD3	0.71	0.93	0.82	0.18
647	YGL141W	HUL5	0.88	0.76	0.82	0.18
648	YDL162C		0.87	0.77	0.82	0.18
649	YJR109C	CPA2	0.85	0.79	0.82	0.18
650	YFR019W	FAB1	0.95	0.69	0.82	0.18
651	YGL146C		0.68	0.96	0.82	0.18
652	YMR312W	ELP6	0.77	0.87	0.82	0.18
653	YBR014C		0.68	0.96	0.82	0.18
654	YNL270C	ALP1	0.51	1.13	0.82	0.18
655	YEL007W		0.82		0.82	0.18
656	YOR273C	TPO4	1.08	0.56	0.82	0.18
657	YKL008C	LAC1	0.73	0.92	0.82	0.18
658	YLR356W		0.70	0.94	0.82	0.18
659	YDR444W		0.98	0.66	0.82	0.18
660	YDL197C	ASF2	1.01	0.64	0.82	0.18
661	YKL069W		0.86	0.79	0.82	0.18
662	YHR163W	SOL3	0.50	1.15	0.82	0.18
663	YDR057W	YOS9	0.78	0.87	0.82	0.18
664	YPL078C	ATP4	0.78	0.87	0.82	0.18
665	YMR044W	IOC4	1.02	0.63	0.82	0.18
666	YGL129C	RSM23	0.96	0.69	0.82	0.18
667	YBL033C	RIB1	0.49	1.16	0.82	0.18
668	YML128C	MSC1	0.78	0.87	0.83	0.18
669	YPL154C	PEP4	1.03	0.62	0.83	0.18
670	YBR286W	APE3	0.90	0.75	0.83	0.18
671	YNL121C	TOM70	0.94	0.71	0.83	0.18
672	YJL088W	ARG3	0.55	1.10	0.83	0.18
673	YJL216C		0.63	1.02	0.83	0.18
674	YDR063W		0.75	0.90	0.83	0.18
675	YIL005W	EPS1	0.88	0.78	0.83	0.18
676	YLR082C	SRL2	0.91	0.74	0.83	0.18
677	YHR151C		0.75	0.90	0.83	0.18
678	YOR270C	VPH1	0.93	0.73	0.83	0.18
679	YNL091W	NST1	0.83	0.83	0.83	0.18
680	YDL128W	VCX1	0.88	0.78	0.83	0.18
681	YIL133C	RPL16A	0.97	0.68	0.83	0.18
682	YNL164C	IBD2	0.83		0.83	0.18
683	YCL051W	LRE1	0.72	0.94	0.83	0.18
684	YGL108C		0.97	0.69	0.83	0.17
685	YOR271C		1.11	0.55	0.83	0.17
686	YOR124C	UBP2	0.79	0.87	0.83	0.17
687	YLR143W		0.84	0.82	0.83	0.17
688	YCL025C	AGP1	0.65	1.01	0.83	0.17

Rank	ORF	Gene	Normalized densitometry values			SCORE
			MATa	MATalpha	average	
689	YJL178C	ATG27	0.79	0.87	0.83	0.17
690	YLL053C		0.81	0.85	0.83	0.17
691	YOR333C		0.89	0.77	0.83	0.17
692	YNL214W	PEX17	0.89	0.77	0.83	0.17
693	YGR127W		1.03	0.63	0.83	0.17
694	YDL136W	RPL35B	0.59	1.07	0.83	0.17
695	YJL030W	MAD2	0.74	0.92	0.83	0.17
696	YJR087W		0.79	0.87	0.83	0.17
697	YEL015W	EDC3	1.00	0.67	0.83	0.17
698	YPR068C	HOS1	0.91	0.76	0.83	0.17
699	YAL016W	TPD3	0.83		0.83	0.17
700	YAL062W	GDH3	0.85	0.82	0.83	0.17
701	YDR330W	UBX5	0.94	0.73	0.83	0.17
702	YDR042C		0.83	0.84	0.83	0.17
703	YJL016W		0.84	0.83	0.83	0.17
704	YNL169C	PSD1	0.83		0.83	0.17
705	YGL107C	RMD9	0.93	0.74	0.83	0.17
706	YJR100C		0.74	0.92	0.83	0.17
707	YNL146W		0.95	0.72	0.83	0.17
708	YBL101C	ECM21	1.01	0.66	0.83	0.17
709	YBR128C	ATG14	0.88	0.79	0.84	0.17
710	YER177W	BMH1	0.84	0.83	0.84	0.17
711	YOR325W		0.86	0.81	0.84	0.17
712	YLR031W		0.87	0.80	0.84	0.17
713	YBR228W	SLX1	1.00	0.67	0.84	0.17
714	YEL056W	HAT2	0.69	0.99	0.84	0.17
715	YER179W	DMC1	0.79	0.88	0.84	0.17
716	YGL126W	SCS3	0.87	0.81	0.84	0.17
717	YNL040W		0.93	0.74	0.84	0.17
718	YLR384C	IKI3	0.86	0.81	0.84	0.17
719	YMR026C	PEX12	0.73	0.94	0.84	0.17
720	YHL011C	PRS3	0.84		0.84	0.17
721	YKR028W	SAP190	0.85	0.82	0.84	0.17
722	YGR261C	APL6	0.77	0.90	0.84	0.17
723	YER167W	BCK2	1.06	0.62	0.84	0.17
724	YHR015W	MIP6	0.95	0.73	0.84	0.17
725	YER119C-A		0.82	0.86	0.84	0.17
726	YNL008C	ASI3	0.77	0.91	0.84	0.17
727	YER085C		0.98	0.70	0.84	0.17
728	YML082W		0.69	0.99	0.84	0.16
729	YIL112W	HOS4	0.74	0.94	0.84	0.16
730	YNR074C	AIF1	0.65	1.03	0.84	0.16
731	YPL246C	RBD2	0.92	0.77	0.84	0.16

Rank	ORF	Gene	Normalized densitometry values			SCORE
			MATa	MATalpha	average	
732	YCL026C-A	FRM2	0.64	1.04	0.84	0.16
733	YDR247W	VHS1	0.84	0.84	0.84	0.16
734	YOL105C	WSC3	0.75	0.93	0.84	0.16
735	YLR151C	PCD1	0.94	0.74	0.84	0.16
736	YLR402W		0.86	0.82	0.84	0.16
737	YCL036W	GFD2	0.77	0.91	0.84	0.16
738	YNL045W		1.02	0.66	0.84	0.16
739	YBR233W	PBP2	1.01	0.68	0.84	0.16
740	YHR035W		1.21	0.48	0.84	0.16
741	YCR068W	ATG15	0.87	0.82	0.84	0.16
742	YLR450W	HMG2	0.75	0.93	0.84	0.16
743	YIL008W	URM1	0.97	0.72	0.84	0.16
744	YOR024W		1.01	0.68	0.84	0.16
745	YPR152C		0.85	0.83	0.84	0.16
746	YAL005C	SSA1	0.76	0.92	0.84	0.16
747	YNL259C	ATX1	0.70	0.99	0.84	0.16
748	YLL052C	AQY2	0.84	0.85	0.84	0.16
749	YGL210W	YPT32	1.07	0.62	0.84	0.16
750	YLR333C	RPS25B	0.70	0.98	0.84	0.16
751	YBR022W	POA1	0.66	1.03	0.84	0.16
752	YMR099C		0.86	0.83	0.84	0.16
753	YMR068W	AVO2	0.79	0.90	0.84	0.16
754	YMR067C	UBX4	0.96	0.73	0.84	0.16
755	YPL018W	CTF19	0.86	0.83	0.84	0.16
756	YPL059W	GRX5	0.84		0.84	0.16
757	YLR444C		1.10	0.59	0.85	0.16
758	YHR029C	YHI9	0.99	0.70	0.85	0.16
759	YDL189W	RBS1	0.65	1.04	0.85	0.16
760	YDR507C	GIN4		0.85	0.85	0.16
761	YAL061W		0.85	0.85	0.85	0.16
762	YPL230W		0.91	0.78	0.85	0.16
763	YOL058W	ARG1	0.88	0.81	0.85	0.16
764	YBR238C		0.77	0.92	0.85	0.16
765	YBR001C	NTH2	0.93	0.76	0.85	0.16
766	YER059W	PCL6	0.75	0.94	0.85	0.16
767	YNL099C	OCA1	0.59	1.10	0.85	0.16
768	YGR037C	ACB1	0.93	0.77	0.85	0.16
769	YML058W	SML1	0.75	0.94	0.85	0.16
770	YFL049W		0.84	0.86	0.85	0.16
771	YGL017W	ATE1	0.88	0.82	0.85	0.16
772	YDL072C		0.89	0.81	0.85	0.16
773	YMR172W	HOT1	0.68	1.02	0.85	0.16
774	YOL052C	SPE2	0.72	0.98	0.85	0.16

Rank	ORF	Gene	Normalized densitometry values			SCORE
			MATa	MATalpha	average	
775	YKL110C	KTI12	0.84	0.85	0.85	0.16
776	YNL241C	ZWF1	0.86	0.83	0.85	0.16
777	YJL172W	CPS1	0.92	0.78	0.85	0.16
778	YOR129C		0.80	0.89	0.85	0.16
779	YDR069C	DOA4	0.85		0.85	0.16
780	YDR273W	DON1	0.68	1.01	0.85	0.16
781	YBR224W		0.98	0.71	0.85	0.16
782	YNL273W	TOF1	0.85		0.85	0.16
783	YBL056W	PTC3	1.00	0.70	0.85	0.16
784	YDR127W	ARO1	0.76	0.93	0.85	0.16
785	YER080W		1.02	0.68	0.85	0.16
786	YDR017C	KCS1	1.04	0.65	0.85	0.16
787	YDR245W	MNN10	0.75	0.95	0.85	0.16
788	YGR200C	ELP2	1.00	0.70	0.85	0.16
789	YDR379W	RGA2	0.79	0.91	0.85	0.16
790	YBR219C		0.85	0.85	0.85	0.16
791	YEL018W	EAF5		0.85	0.85	0.15
792	YLR332W	MID2	0.97	0.73	0.85	0.15
793	YDL018C	ERP3	0.91	0.79	0.85	0.15
794	YJL122W		0.88	0.82	0.85	0.15
795	YLR263W	RED1	0.86	0.84	0.85	0.15
796	YMR302C	PRP12	1.02	0.68	0.85	0.15
797	YPL222W		0.69	1.01	0.85	0.15
798	YNL296W		0.57	1.13	0.85	0.15
799	YLR199C		0.88	0.82	0.85	0.15
800	YDR290W		0.88	0.82	0.85	0.15
801	YNR008W	LRO1	0.97	0.73	0.85	0.15
802	YPR026W	ATH1	0.92	0.78	0.85	0.15
803	YKL070W		0.86	0.84	0.85	0.15
804	YOR137C	SIA1	0.89	0.81	0.85	0.15
805	YKL168C	KKQ8	0.49	1.21	0.85	0.15
806	YDR313C	PIB1	0.83	0.87	0.85	0.15
807	YOR363C	$PI(4,5)P_2$	0.95	0.75	0.85	0.15
808	YOL116W	MSN1	0.89	0.81	0.85	0.15
809	YDL239C	ADY3	0.90	0.80	0.85	0.15
810	YGR125W		1.09	0.61	0.85	0.15
811	YDR015C		1.01	0.69	0.85	0.15
812	YOL064C	MET22	1.03	0.68	0.85	0.15
813	YBL107C		0.78	0.92	0.85	0.15
814	YGR212W	SLI1	0.85	0.86	0.85	0.15
815	YJR110W	YMR1	0.93	0.78	0.85	0.15
816	YDR043C	NRG1	0.86	0.84	0.85	0.15
817	YEL023C		0.96	0.75	0.85	0.15
818	YPR188C	MLC2	0.67	1.04	0.85	0.15

Rank	ORF	Gene	Normalized densitometry values			SCORE
			MATa	MATalpha	average	
819	YHR041C	SRB2	0.27	1.44	0.85	0.15
820	YKL047W		0.52	1.19	0.86	0.15
821	YFR010W	UBP6	0.99	0.72	0.86	0.15
822	YPR060C	ARO7	0.87	0.84	0.86	0.15
823	YGR229C	SMI1	1.00	0.71	0.86	0.15
824	YDR323C	PEP7	0.73	0.98	0.86	0.15
825	YLR242C	ARV1	0.79	0.92	0.86	0.15
826	YDL238C	GUD1	0.85	0.86	0.86	0.15
827	YNL155W		0.95	0.76	0.86	0.15
828	YLR146C	SPE4	1.04	0.67	0.86	0.15
829	YJL210W	PEX2	0.79	0.93	0.86	0.15
830	YDR470C	UGO1	0.71	1.00	0.86	0.15
831	YGR123C	PPT1	0.98	0.73	0.86	0.15
832	YLR191W	PEX13	0.90	0.81	0.86	0.15
833	YGL079W		0.89	0.83	0.86	0.15
834	YJL082W	IML2	0.84	0.88	0.86	0.15
835	YMR025W	CSI1	0.74	0.98	0.86	0.15
836	YPL054W	LEE1	0.68	1.03	0.86	0.15
837	YCR045C		0.97	0.74	0.86	0.15
838	YOL044W	PEX15	0.93	0.78	0.86	0.15
839	YDR048C		0.59	1.13	0.86	0.15
840	YGR163W	GTR2	0.84	0.87	0.86	0.15
841	YMR297W	PRC1	1.01	0.70	0.86	0.15
842	YOL099C		0.77	0.95	0.86	0.15
843	YKL027W		0.85	0.87	0.86	0.15
844	YGL133W	ITC1	0.81	0.91	0.86	0.15
845	YLR046C		0.92	0.80	0.86	0.15
846	YNL044W	YIP3	1.02	0.70	0.86	0.15
847	YMR316W	DIA1	0.74	0.97	0.86	0.15
848	YMR284W	YKU70	0.97	0.75	0.86	0.15
849	YEL062W	NPR2	0.84	0.88	0.86	0.15
850	YMR195W	ICY1	1.00	0.72	0.86	0.15
851	YDR099W	BMH2	0.89	0.83	0.86	0.14
852	YEL068C		0.67	1.05	0.86	0.14
853	YPR132W	RPS23B	0.91	0.81	0.86	0.14
854	YLL007C		1.07	0.65	0.86	0.14
855	YDR024W	FYV1	0.47	1.25	0.86	0.14
856	YJL161W		0.89	0.83	0.86	0.14
857	YER182W		0.98	0.74	0.86	0.14
858	YNL265C	IST1	0.86		0.86	0.14
859	YNL275W		0.72	1.01	0.86	0.14
860	YGL144C	ROG1	0.82	0.90	0.86	0.14
861	YDR257C	SET7	0.80	0.93	0.86	0.14
862	YGL244W	RTF1	0.86		0.86	0.14

Rank	ORF	Gene	Normalized densitometry values			SCORE
			MATa	MATalpha	average	
863	YER111C	SWI4	0.82	0.91	0.86	0.14
864	YJR084W	CSN12	0.69	1.03	0.86	0.14
865	YGL242C		0.99	0.73	0.86	0.14
866	YEL071W	DLD3	0.65	1.08	0.86	0.14
867	YHL017W		0.92	0.80	0.86	0.14
868	YCR024C-A	PMP1	0.78	0.95	0.86	0.14
869	YPR046W	MCM16	1.02	0.70	0.86	0.14
870	YEL009C	GCN4	0.72	1.00	0.86	0.14
871	YNL100W		0.58	1.15	0.86	0.14
872	YIL105C	SLM1	0.87	0.86	0.86	0.14
873	YLR351C	NIT3	0.95	0.78	0.86	0.14
874	YGR137W		1.10	0.63	0.86	0.14
875	YJR015W		0.91	0.82	0.86	0.14
876	YGR063C	SPT4	0.99	0.74	0.86	0.14
877	YFR032C		0.87	0.86	0.86	0.14
878	YOL057W		1.08	0.65	0.86	0.14
879	YDR264C	AKR1	0.87		0.87	0.14
880	YGR088W	CTT1	0.83	0.91	0.87	0.14
881	YER144C	UBP5	0.85	0.88	0.87	0.14
882	YGR170W	PSD2	0.84	0.90	0.87	0.14
883	YBR262C		0.88	0.85	0.87	0.14
884	YJR094W-A	RPL43B	1.16	0.57	0.87	0.14
885	YNL225C	CNM67	0.87		0.87	0.14
886	YEL025C		1.00	0.73	0.87	0.14
887	YLR296W		0.86	0.87	0.87	0.14
888	YJR031C	GEA1	0.86	0.88	0.87	0.14
889	YPL208W	RKM1	0.74	0.99	0.87	0.14
890	YOR078W	BUD21	0.72	1.01	0.87	0.14
891	YNL315C	ATP11	0.45	1.29	0.87	0.14
892	YIL140W	AXL2	0.97	0.77	0.87	0.14
893	YBR226C		0.91	0.82	0.87	0.14
894	YOR032C	HMS1	0.86	0.88	0.87	0.14
895	YDR184C	ATC1	0.98	0.76	0.87	0.14
896	YOL103W	ITR2	0.78	0.96	0.87	0.14
897	YGR223C	HSV2	0.90	0.83	0.87	0.14
898	YDR249C		0.73	1.00	0.87	0.14
899	YMR022W	QRI8	0.84	0.90	0.87	0.14
900	YJR119C		0.72	1.02	0.87	0.14
901	YOL125W		0.87		0.87	0.14
902	YCR089W	FIG2	0.80	0.94	0.87	0.14
903	YMR081C	ISF1	0.98	0.75	0.87	0.14
904	YFR040W	SAP155	0.88	0.85	0.87	0.14

Rank	ORF	Gene	Normalized densitometry values			SCORE
			MATa	MATalpha	average	
905	YPL223C	GRE1	0.75	0.99	0.87	0.14
906	YBR065C	ECM2	0.86	0.87	0.87	0.14
907	YLR154C	RNH203	0.97	0.77	0.87	0.14
908	YNR075W	COS10	0.74	1.00	0.87	0.14
909	YGR235C		0.76	0.98	0.87	0.14
910	YDR009W	GAL3	0.94	0.80	0.87	0.14
911	YPR079W	MRL1	0.91	0.83	0.87	0.13
912	YPL112C	PEX25	0.68	1.06	0.87	0.13
913	YKR041W		0.79	0.95	0.87	0.13
914	YEL066W	HPA3	0.78	0.96	0.87	0.13
915	YAL058W	CNE1	0.90	0.84	0.87	0.13
916	YNL136W	EAF7	0.67	1.07	0.87	0.13
917	YKL090W	CUE2	0.93	0.81	0.87	0.13
918	YDR479C	PEX29	0.81	0.93	0.87	0.13
919	YPL159C	PET20	0.96	0.78	0.87	0.13
920	YBR230C		1.06	0.68	0.87	0.13
921	YAL067C	SEO1	0.78	0.96	0.87	0.13
922	YLR098C	CHA4	0.83	0.91	0.87	0.13
923	YNL012W	SPO1	0.79	0.96	0.87	0.13
924	YER010C		0.63	1.11	0.87	0.13
925	YOR379C		0.85	0.90	0.87	0.13
926	YBR176W	ECM31	0.63	1.11	0.87	0.13
927	YKR007W	MEH1	0.95	0.79	0.87	0.13
928	YLR324W	PEX30	0.94	0.80	0.87	0.13
929	YOR028C	CIN5	0.95	0.79	0.87	0.13
930	YDR250C		0.70	1.04	0.87	0.13
931	YLL061W	MMP1	1.09	0.66	0.87	0.13
932	YER001W	MNN1	0.77	0.98	0.87	0.13
933	YEL014C		1.05	0.70	0.87	0.13
934	YDR443C	SSN2	0.52	1.23	0.87	0.13
935	YDR203W		1.15	0.60	0.87	0.13
936	YCL035C	GRX1	0.98	0.76	0.87	0.13
937	YLR353W	BUD8	0.68	1.07	0.87	0.13
938	YGL173C	KEM1	0.63	1.12	0.87	0.13
939	YFR044C		0.89	0.86	0.87	0.13
940	YGL059W		0.95	0.80	0.87	0.13
941	YDR421W	ARO80	0.80	0.95	0.87	0.13
942	YPL084W	BRO1	0.87		0.87	0.13
943	YPR156C	TPO3	0.92	0.83	0.87	0.13
944	YLR461W	PAU4	0.96	0.79	0.87	0.13
945	YLL056C		0.95	0.80	0.87	0.13
946	YIL162W	SUC2	0.88		0.88	0.13
947	YHR200W	RPN10	0.82	0.93	0.88	0.13
948	YDR539W		0.96	0.79	0.88	0.13

Rank	ORF	Gene	Normalized densitometry values			SCORE
			MATa	MATalpha	average	
949	YGR266W		0.96	0.79	0.88	0.13
950	YAL020C	ATS1	0.75	1.00	0.88	0.13
951	YOR276W	CAF20	0.67	1.08	0.88	0.13
952	YDR217C	RAD9	0.71	1.04	0.88	0.13
953	YGR164W		0.81	0.94	0.88	0.13
954	YPR151C	SUE1	0.78	0.97	0.88	0.13
955	YIL141W		1.01	0.74	0.88	0.13
956	YMR189W	GCV2	0.88	0.88	0.88	0.13
957	YKL026C	GPX1	0.89	0.87	0.88	0.13
958	YDL149W	ATG9	0.93	0.82	0.88	0.13
959	YMR062C	ECM40	0.88		0.88	0.13
960	YML075C	HMG1	0.86	0.89	0.88	0.13
961	YKL005C	BYE1	0.85	0.90	0.88	0.13
962	YMR262W		0.73	1.02	0.88	0.13
963	YOR292C		0.89	0.86	0.88	0.13
964	YHR184W	SSP1	0.76	1.00	0.88	0.13
965	YDR377W	ATP17	1.05	0.70	0.88	0.13
966	YNL291C	MID1	0.69	1.07	0.88	0.13
967	YGR248W	SOL4	0.92	0.84	0.88	0.13
968	YAL065C		0.84	0.91	0.88	0.13
969	YMR036C	MIH1	0.76	1.00	0.88	0.13
970	YGL025C	PGD1	0.95	0.81	0.88	0.13
971	YGR118W	RPS23A	0.84	0.92	0.88	0.13
972	YHR018C	ARG4	1.06	0.70	0.88	0.13
973	YML122C		0.88	0.88	0.88	0.13
974	YDL012C		0.87	0.89	0.88	0.12
975	YLR032W	RAD5	0.90	0.86	0.88	0.12
976	YBR084W	MIS1	0.76	1.00	0.88	0.12
977	YNL001W	DOM34	0.71	1.05	0.88	0.12
978	YIL002C	INP51	0.95	0.81	0.88	0.12
979	YKR044W	UIP5	0.93	0.83	0.88	0.12
980	YPL216W		0.89	0.88	0.88	0.12
981	YOR132W	VPS17	0.68	1.08	0.88	0.12
982	YJL170C	ASG7	1.07	0.70	0.88	0.12
983	YKL067W	YNK1	1.02	0.74	0.88	0.12
984	YER005W	YND1	0.75	1.01	0.88	0.12
985	YGL208W	SIP2	0.88	0.89	0.88	0.12
986	YGR015C		0.93	0.83	0.88	0.12
987	YGL261C		0.76	1.00	0.88	0.12
988	YIR004W	DJP1	0.88		0.88	0.12
989	YPL021W	ECM23	1.07	0.70	0.88	0.12
990	YDR239C		0.96	0.81	0.88	0.12
991	YPL111W	CAR1	0.80	0.96	0.88	0.12
992	YER097W		0.77	1.00	0.88	0.12

Rank	ORF	Gene	Normalized densitometry values			SCORE
			MATa	MATalpha	average	
993	YPL155C	KIP2	1.12	0.65	0.88	0.12
994	YJL214W	HXT8	0.72	1.04	0.88	0.12
995	YPL156C	PRM4	1.02	0.74	0.88	0.12
996	YLL055W		0.93	0.84	0.88	0.12
997	YFR038W		1.17	0.59	0.88	0.12
998	YAL060W	BDH1	0.95	0.82	0.88	0.12
999	YGL053W	PRM8	0.86	0.90	0.88	0.12
1000	YGL197W	MDS3	0.86	0.91	0.88	0.12
1001	YPL058C	PDR12	0.76	1.01	0.88	0.12
1002	YDR521W		0.90	0.86	0.88	0.12
1003	YOL063C		1.02	0.75	0.88	0.12
1004	YHR137W	ARO9	0.92	0.85	0.88	0.12
1005	YDL091C	UBX3	0.87	0.90	0.88	0.12
1006	YPR120C	CLB5	0.87	0.90	0.88	0.12
1007	YLR453C	RIF2	0.90	0.87	0.88	0.12
1008	YJL023C	PET130	1.06	0.70	0.88	0.12
1009	YCR106W	RDS1	0.91	0.86	0.88	0.12
1010	YDL167C	NRP1	0.92	0.85	0.88	0.12
1011	YLR427W	MAG2	0.79	0.98	0.88	0.12
1012	YOL055C	THI20	1.03	0.74	0.88	0.12
1013	YBR168W	PEX32	0.79	0.98	0.88	0.12
1014	YLR093C	NYV1	0.87	0.90	0.88	0.12
1015	YJL037W		0.85	0.92	0.88	0.12
1016	YGR159C	NSR1	0.69	1.08	0.89	0.12
1017	YKL077W		1.09	0.68	0.89	0.12
1018	YOR073W	SGO1	0.96	0.81	0.89	0.12
1019	YBL091C	MAP2	0.88	0.89	0.89	0.12
1020	YJR018W		0.89		0.89	0.12
1021	YGR168C		0.66	1.11	0.89	0.12
1022	YMR182C	RGM1	1.06	0.71	0.89	0.12
1023	YDL204W	RTN2	0.81	0.96	0.89	0.12
1024	YKL123W		0.69	1.08	0.89	0.12
1025	YDR193W		0.95	0.82	0.89	0.12
1026	YNL083W	SAL1	0.90	0.88	0.89	0.12
1027	YPR149W	NCE102	0.89	0.88	0.89	0.12
1028	YOR279C	RFM1	0.85	0.92	0.89	0.12
1029	YJR070C	LIA1	0.81	0.96	0.89	0.12
1030	YMR011W	HXT2	0.88	0.89	0.89	0.12
1031	YBR025C		0.93	0.85	0.89	0.12
1032	YJL134W	LCB3	0.84	0.94	0.89	0.12
1033	YLR421C	RPN13	0.85	0.93	0.89	0.12
1034	YLR258W	GSY2	0.99	0.79	0.89	0.12
1035	YJL043W		0.83	0.95	0.89	0.12
1036	YMR111C		0.95	0.82	0.89	0.12

Rank	ORF	Gene	Normalized densitometry values			SCORE
			MATa	MATalpha	average	
1037	YMR141C		1.08	0.70	0.89	0.12
1038	YLR219W	MSC3	0.93	0.85	0.89	0.12
1039	YGR192C	TDH3	0.96	0.82	0.89	0.12
1040	YLR074C	BUD20	0.72	1.06	0.89	0.12
1041	YJR050W	ISY1	0.74	1.04	0.89	0.12
1042	YJR062C	NTA1	0.85	0.93	0.89	0.12
1043	YJL177W	RPL17B	0.97	0.81	0.89	0.12
1044	YBL095W		0.87	0.91	0.89	0.12
1045	YER055C	HIS1	0.86	0.91	0.89	0.12
1046	YGR087C	PDC6	0.98	0.80	0.89	0.12
1047	YOR375C	GDH1	0.95	0.83	0.89	0.12
1048	YKR055W	RHO4	0.81	0.96	0.89	0.12
1049	YDR344C		0.90	0.88	0.89	0.12
1050	YMR016C	SOK2	0.85	0.93	0.89	0.12
1051	YNL293W	MSB3	0.87	0.91	0.89	0.12
1052	YKL184W	SPE1	1.01	0.77	0.89	0.12
1053	YFR013W	IOC3	0.91	0.87	0.89	0.11
1054	YMR243C	ZRC1	0.74	1.04	0.89	0.11
1055	YHL013C		0.85	0.93	0.89	0.11
1056	YDL127W	PCL2	0.92	0.86	0.89	0.11
1057	YML121W	GTR1	0.89	0.89	0.89	0.11
1058	YJR059W	PTK2	0.89	0.90	0.89	0.11
1059	YLR110C	CCW12	0.80	0.98	0.89	0.11
1060	YDR262W		0.88	0.91	0.89	0.11
1061	YIL160C	POT1	1.09	0.69	0.89	0.11
1062	YJL024C	APS3	1.02	0.77	0.89	0.11
1063	YDR073W	SNF11	0.93	0.85	0.89	0.11
1064	YLR456W		0.88	0.90	0.89	0.11
1065	YLR365W		0.72	1.06	0.89	0.11
1066	YJL007C		1.04	0.74	0.89	0.11
1067	YKL159C	RCN1	0.91	0.87	0.89	0.11
1068	YGL226C-A	OST5	0.94	0.84	0.89	0.11
1069	YPL213W	LEA1	0.89		0.89	0.11
1070	YPR150W		0.74	1.05	0.89	0.11
1071	YOL115W	PAP2	1.01	0.78	0.89	0.11
1072	YLR266C	PDR8	1.12	0.67	0.89	0.11
1073	YER123W	YCK3	0.81	0.98	0.89	0.11
1074	YJR039W		0.89	0.90	0.89	0.11
1075	YBL043W	ECM13	0.80	0.98	0.89	0.11
1076	YBR138C		0.95	0.84	0.89	0.11
1077	YIL156W	UBP7	0.92	0.87	0.89	0.11
1078	YJL137C	GLG2	1.05	0.74	0.89	0.11
1079	YOR263C		0.89	0.90	0.89	0.11

Rank	ORF	Gene	Normalized densitometry values			SCORE
			MATa	MATalpha	average	
1080	YLR280C		0.70	1.08	0.89	0.11
1081	YDR270W	CCC2	0.81	0.97	0.89	0.11
1082	YOR025W	HST3	0.99	0.80	0.89	0.11
1083	YBL063W	KIP1	0.96	0.82	0.89	0.11
1084	YHR158C	KEL1	0.93	0.86	0.89	0.11
1085	YKL091C		1.00	0.79	0.89	0.11
1086	YPR039W		1.00	0.79	0.89	0.11
1087	YBR005W	RCR1	1.05	0.74	0.89	0.11
1088	YGL218W		0.89		0.89	0.11
1089	YBR245C	ISW1	0.94	0.85	0.89	0.11
1090	YER156C		0.88	0.91	0.89	0.11
1091	YIL024C		0.99	0.80	0.89	0.11
1092	YJR021C	REC107	0.80	0.99	0.89	0.11
1093	YOR134W	BAG7	0.81	0.98	0.89	0.11
1094	YGR027C	RPS25A	1.04	0.74	0.89	0.11
1095	YBR287W		0.88	0.91	0.89	0.11
1096	YDR186C		0.96	0.83	0.90	0.11
1097	YOR229W	WTM2	0.95	0.84	0.90	0.11
1098	YJL012C	VTC4	0.99	0.80	0.90	0.11
1099	YPL127C	HHO1	0.90	0.89	0.90	0.11
1100	YGR124W	ASN2	1.03	0.76	0.90	0.11
1101	YCR077C	PAT1	1.01	0.78	0.90	0.11
1102	YOL065C	INP54	1.00	0.79	0.90	0.11
1103	YMR121C	RPL15B	0.90	0.90	0.90	0.11
1104	YOR290C	SNF2		0.90	0.90	0.11
1105	YBR204C		0.99	0.80	0.90	0.11
1106	YHL003C	LAG1	0.66	1.13	0.90	0.11
1107	YMR223W	UBP8	0.71	1.08	0.90	0.11
1108	YDR348C		0.83	0.97	0.90	0.11
1109	YOR286W		0.68	1.11	0.90	0.11
1110	YDR080W	VPS41	0.67	1.12	0.90	0.11
1111	YPR171W	BSP1	0.90	0.89	0.90	0.11
1112	YMR070W	MOT3	0.87	0.92	0.90	0.11
1113	YFR032C-A	RPL29	0.94	0.86	0.90	0.11
1114	YHR191C	CTF8	1.07	0.73	0.90	0.11
1115	YLR017W	MEU1	1.01	0.78	0.90	0.11
1116	YHR146W	CRP1	0.97	0.82	0.90	0.11
1117	YOL011W	PLB3	0.86	0.94	0.90	0.11
1118	YGR066C		1.02	0.78	0.90	0.11
1119	YDR269C		0.84	0.96	0.90	0.11
1120	YJL218W		0.75	1.04	0.90	0.11
1121	YLR426W		0.75	1.05	0.90	0.11
1122	YBL100C			0.90	0.90	0.11

Rank	ORF	Gene	Normalized densitometry values			SCORE
			MATa	MATalpha	average	
1123	YNL329C	PEX6	0.94	0.86	0.90	0.11
1124	YOR029W		1.05	0.74	0.90	0.11
1125	YNL208W		0.90		0.90	0.11
1126	YBR275C	RIF1	0.91	0.88	0.90	0.11
1127	YOR170W		0.96	0.84	0.90	0.11
1128	YMR078C	CTF18	0.95	0.85	0.90	0.11
1129	YNR032C-A	HUB1	1.04	0.76	0.90	0.11
1130	YPR092W		0.86	0.94	0.90	0.11
1131	YDR369C	XRS2	0.73	1.07	0.90	0.11
1132	YPR045C		1.09	0.70	0.90	0.11
1133	YKL170W	MRPL38		0.90	0.90	0.11
1134	YLR346C		0.98	0.81	0.90	0.11
1135	YOR192C		0.83	0.97	0.90	0.11
1136	YKL151C		0.83	0.97	0.90	0.11
1137	YCL047C		0.81	0.99	0.90	0.11
1138	YBL078C	ATG8	0.90	0.90	0.90	0.10
1139	YOR052C		0.92	0.88	0.90	0.10
1140	YOR111W		0.78	1.02	0.90	0.10
1141	YDR524C	AGE1	0.88	0.92	0.90	0.10
1142	YLR404W		0.91	0.89	0.90	0.10
1143	YPR109W		0.98	0.82	0.90	0.10
1144	YMR254C		0.75	1.05	0.90	0.10
1145	YNL029C	KTR5	0.97	0.83	0.90	0.10
1146	YML079W		0.68	1.12	0.90	0.10
1147	YCL010C	SGF29	0.82	0.99	0.90	0.10
1148	YLR142W	PUT1	0.96	0.84	0.90	0.10
1149	YOR044W		0.83	0.97	0.90	0.10
1150	YOR177C	MPC54	0.80	1.00	0.90	0.10
1151	YBL010C		0.90	0.90	0.90	0.10
1152	YHR176W	FMO1	0.81	1.00	0.90	0.10
1153	YBR197C		0.92	0.88	0.90	0.10
1154	YMR319C	FET4	0.83	0.98	0.90	0.10
1155	YNR027W	BUD17	0.92	0.88	0.90	0.10
1156	YGL021W	ALK1	0.95	0.85	0.90	0.10
1157	YCR105W	ADH7	1.06	0.74	0.90	0.10
1158	YIL059C		0.96	0.85	0.90	0.10
1159	YJR150C	DAN1	0.95	0.85	0.90	0.10
1160	YJR115W		1.00	0.80	0.90	0.10
1161	YOR293W	RPS10A	0.71	1.09	0.90	0.10
1162	YOR230W	WTM1	0.94	0.86	0.90	0.10
1163	YER180C	ISC10	1.03	0.78	0.90	0.10
1164	YKL179C	COY1	1.04	0.77	0.90	0.10
1165	YGL131C	SNT2	0.66	1.14	0.90	0.10

Rank	ORF	Gene	Normalized densitometry values			SCORE
			MATa	MATalpha	average	
1166	YMR251W-A	HOR7	0.81	1.00	0.90	0.10
1167	YJR035W	RAD26	1.00	0.81	0.90	0.10
1168	YGL202W	ARO8	0.90	0.91	0.90	0.10
1169	YGR239C	PEX21	0.95	0.86	0.90	0.10
1170	YGL140C		0.89	0.92	0.90	0.10
1171	YKL107W		0.97	0.84	0.90	0.10
1172	YGL157W		0.92	0.89	0.90	0.10
1173	YMR007W		0.92	0.89	0.90	0.10
1174	YOR245C	DGA1	0.88	0.93	0.90	0.10
1175	YOR184W	SER1	0.90	0.91	0.90	0.10
1176	YGL152C		0.88	0.93	0.90	0.10
1177	YGL181W	GTS1	0.85	0.96	0.90	0.10
1178	YGR133W	PEX4	1.02	0.79	0.90	0.10
1179	YDR497C	ITR1	0.96	0.84	0.90	0.10
1180	YOR306C	MCH5	0.97	0.84	0.91	0.10
1181	YDR173C	ARG82	0.91		0.91	0.10
1182	YDR058C	TGL2	0.96	0.85	0.91	0.10
1183	YEL041W		0.81	1.00	0.91	0.10
1184	YPL170W	DAP1	1.02	0.79	0.91	0.10
1185	YAR031W	PRM9	0.85	0.96	0.91	0.10
1186	YIL071C	PCI8	0.81	1.00	0.91	0.10
1187	YLR435W	TSR2	0.73	1.08	0.91	0.10
1188	YNR024W		0.96	0.85	0.91	0.10
1189	YDL039C	PRM7	0.93	0.88	0.91	0.10
1190	YMR303C	ADH2	1.11	0.70	0.91	0.10
1191	YLR410W	VIP1	0.85	0.96	0.91	0.10
1192	YML018C		1.02	0.80	0.91	0.10
1193	YPR018W	RLF2	0.76	1.06	0.91	0.10
1194	YOL041C	NOP12	0.81	1.01	0.91	0.10
1195	YER039C-A		1.20	0.62	0.91	0.10
1196	YBL104C		0.96	0.85	0.91	0.10
1197	YJL186W	MNN5	1.08	0.73	0.91	0.10
1198	YLL012W	YEH1	0.93	0.88	0.91	0.10
1199	YOR318C		1.00	0.82	0.91	0.10
1200	YLR104W		0.88	0.94	0.91	0.10
1201	YDL242W		1.05	0.77	0.91	0.10
1202	YBR147W		0.93	0.89	0.91	0.10
1203	YFR009W	GCN20	0.92	0.89	0.91	0.10
1204	YDR482C	CWC21	0.91	0.91	0.91	0.10
1205	YPL133C	RDS2	0.95	0.87	0.91	0.10
1206	YBR131W	CCZ1	0.91	0.91	0.91	0.10
1207	YHR021W	ECM12	1.00	0.82	0.91	0.10

Rank	ORF	Gene	Normalized densitometry values			SCORE
			MATa	MATalpha	average	
	-A					
1208	YBR227C	MCX1	0.96	0.85	0.91	0.10
1209	YGL170C	SPO74	0.90	0.92	0.91	0.10
1210	YOR280C	FSH3	0.98	0.84	0.91	0.10
1211	YBR276C	PPS1	0.94	0.88	0.91	0.10
1212	YBR222C	PCS60	0.87	0.95	0.91	0.10
1213	YBL062W		1.01	0.81	0.91	0.10
1214	YNL212W	VID27	0.95	0.87	0.91	0.10
1215	YER081W	SER3	0.99	0.83	0.91	0.10
1216	YKL216W	URA1	0.91		0.91	0.10
1217	YGR250C		1.03	0.79	0.91	0.10
1218	YDR261C	EXG2	0.85	0.97	0.91	0.10
1219	YIL012W		0.99	0.83	0.91	0.10
1220	YEL008W		0.82	1.00	0.91	0.10
1221	YLR225C		0.94	0.87	0.91	0.10
1222	YFL015C		0.80	1.02	0.91	0.09
1223	YER007W	PAC2	0.72	1.10	0.91	0.09
1224	YML022W	APT1	0.93	0.89	0.91	0.09
1225	YJR079W		1.25	0.58	0.91	0.09
1226	YDR378C	LSM6	0.44	1.39	0.91	0.09
1227	YPR022C		0.73	1.09	0.91	0.09
1228	YIL016W	SNL1	1.04	0.79	0.91	0.09
1229	YKR036C	CAF4	0.91	0.91	0.91	0.09
1230	YHR096C	HXT5	0.91		0.91	0.09
1231	YDL214C	PRR2	0.98	0.84	0.91	0.09
1232	YLR206W	ENT2	1.00	0.82	0.91	0.09
1233	YBR105C	VID24	0.94	0.89	0.91	0.09
1234	YDR272W	GLO2	0.79	1.03	0.91	0.09
1235	YFR014C	CMK1	0.87	0.96	0.91	0.09
1236	YLL021W	SPA2	0.64	1.19	0.91	0.09
1237	YHR183W	GND1	0.76	1.07	0.91	0.09
1238	YGR129W	SYF2	1.06	0.77	0.91	0.09
1239	YBL009W		0.99	0.83	0.91	0.09
1240	YDR371W	CTS2	0.87	0.96	0.91	0.09
1241	YDL086W		0.84	0.99	0.91	0.09
1242	YPL207W		0.93	0.90	0.91	0.09
1243	YMR259C		0.83	0.99	0.91	0.09
1244	YDL130W	RPP1B	0.95	0.88	0.91	0.09
1245	YML042W	CAT2	1.11	0.72	0.91	0.09
1246	YBR078W	ECM33	0.95	0.87	0.91	0.09
1247	YDL186W		0.70	1.13	0.91	0.09
1248	YDR007W	TRP1	0.98	0.85	0.91	0.09
1249	YHL039W		0.96	0.87	0.91	0.09
1250	YNL289W	PCL1	0.86	0.97	0.91	0.09

Rank	ORF	Gene	Normalized densitometry values			SCORE
			MATa	MATalpha	average	
1251	YNL190W		0.94	0.89	0.91	0.09
1252	YLR437C		1.01	0.82	0.91	0.09
1253	YDR363W-A	SEM1	0.90	0.92	0.91	0.09
1254	YBR046C	ZTA1	1.01	0.82	0.91	0.09
1255	YMR034C		0.77	1.06	0.91	0.09
1256	YLR299W	ECM38	0.75	1.07	0.91	0.09
1257	YDR251W	PAM1	0.99	0.84	0.91	0.09
1258	YDR003W	RCR2	1.02	0.81	0.91	0.09
1259	YHR086W	NAM8	0.93	0.90	0.91	0.09
1260	YPL152W	RRD2	0.98	0.85	0.91	0.09
1261	YGL071W	RCS1	0.89	0.94	0.91	0.09
1262	YML095C	RAD10	0.84	0.99	0.91	0.09
1263	YDL206W			0.91	0.91	0.09
1264	YDR283C	GCN2	0.84	0.99	0.91	0.09
1265	YLR213C	CRR1	1.03	0.80	0.92	0.09
1266	YJL208C	NUC1	0.79	1.04	0.92	0.09
1267	YNL125C	ESBP6	0.87	0.96	0.92	0.09
1268	YGR070W	ROM1	0.86	0.97	0.92	0.09
1269	YEL040W	UTR2	0.89	0.94	0.92	0.09
1270	YDR210W		1.12	0.71	0.92	0.09
1271	YBR169C	SSE2	0.80	1.03	0.92	0.09
1272	YPL130W	SPO19	0.97	0.86	0.92	0.09
1273	YKL121W		0.79	1.04	0.92	0.09
1274	YGR096W	TPC1	0.73	1.10	0.92	0.09
1275	YCL042W		0.97	0.86	0.92	0.09
1276	YLR220W	CCC1	0.94	0.89	0.92	0.09
1277	YFR012W		0.70	1.13	0.92	0.09
1278	YDR112W		0.79	1.04	0.92	0.09
1279	YNL015W	PBI2	0.75	1.09	0.92	0.09
1280	YDR486C	VPS60	0.78	1.05	0.92	0.09
1281	YLR454W		0.94	0.89	0.92	0.09
1282	YFL052W		0.81	1.03	0.92	0.09
1283	YDR271C		0.71	1.12	0.92	0.09
1284	YDR219C		0.97	0.87	0.92	0.09
1285	YJL064W		1.04	0.80	0.92	0.09
1286	YLR335W	NUP2	0.80	1.04	0.92	0.09
1287	YNL176C		0.77	1.07	0.92	0.09
1288	YNL028W		1.10	0.74	0.92	0.09
1289	YEL064C	AVT2	0.87	0.96	0.92	0.09
1290	YIL173W	VTH1	0.89	0.94	0.92	0.09
1291	YNL027W	CRZ1	1.06	0.78	0.92	0.09
1292	YLL060C	GTT2	1.08	0.75	0.92	0.09
1293	YHR123W	EPT1	0.83	1.00	0.92	0.09

Rank	ORF	Gene	Normalized densitometry values			SCORE
			MATa	MATalpha	average	
1294	YDR152W	GIR2	0.97	0.87	0.92	0.09
1295	YJR090C	GRR1		0.92	0.92	0.09
1296	YPL162C		1.04	0.79	0.92	0.09
1297	YJL217W		0.75	1.09	0.92	0.09
1298	YDR176W	NGG1	0.70	1.14	0.92	0.09
1299	YJL066C	MPM1	0.96	0.88	0.92	0.09
1300	YBR054W	YRO2	0.93	0.90	0.92	0.09
1301	YPR184W	GDB1	0.83	1.01	0.92	0.09
1302	YOR084W		0.99	0.85	0.92	0.09
1303	YLR072W		0.98	0.86	0.92	0.09
1304	YAL059W	ECM1	0.95	0.89	0.92	0.09
1305	YPL068C		0.88	0.95	0.92	0.08
1306	YOL107W		0.73	1.11	0.92	0.08
1307	YIR001C	SGN1	1.00	0.84	0.92	0.08
1308	YPR174C		0.77	1.07	0.92	0.08
1309	YEL003W	GIM4	0.93	0.91	0.92	0.08
1310	YOR108W	LEU9	1.03	0.81	0.92	0.08
1311	YBR107C	IML3	1.06	0.78	0.92	0.08
1312	YHL040C	ARN1	0.92	0.92	0.92	0.08
1313	YDL020C	RPN4	0.97	0.87	0.92	0.08
1314	YPR172W		0.77	1.07	0.92	0.08
1315	YKR105C		0.83	1.01	0.92	0.08
1316	YKL190W	CNB1	1.06	0.78	0.92	0.08
1317	YBR074W		0.97	0.87	0.92	0.08
1318	YLR372W	SUR4	0.84	1.00	0.92	0.08
1319	YML131W		1.04	0.80	0.92	0.08
1320	YDR408C	ADE8	0.92	0.92	0.92	0.08
1321	YLL059C		1.02	0.83	0.92	0.08
1322	YCR043C		0.93	0.91	0.92	0.08
1323	YHR033W		1.04	0.80	0.92	0.08
1324	YJR124C		1.04	0.81	0.92	0.08
1325	YOR231W	MKK1	0.96	0.88	0.92	0.08
1326	YGL243W	TAD1	0.91	0.94	0.92	0.08
1327	YDR185C		1.09	0.75	0.92	0.08
1328	YDR068W	DOS2	0.91	0.94	0.92	0.08
1329	YDR231C	COX20	0.70	1.14	0.92	0.08
1330	YJL135W		0.99	0.86	0.92	0.08
1331	YDL106C	PHO2	0.94	0.90	0.92	0.08
1332	YML047C	PRM6	0.95	0.89	0.92	0.08
1333	YJL184W	GON7	0.92		0.92	0.08
1334	YJR025C	BNA1	0.92	0.93	0.92	0.08
1335	YGR182C		0.91	0.93	0.92	0.08
1336	YMR310C		0.95	0.90	0.92	0.08
1337	YBR263W	SHM1	0.98	0.86	0.92	0.08

Rank	ORF	Gene	Normalized densitometry values			SCORE
			MATa	MATalpha	average	
1338	YGR011W		1.01	0.83	0.92	0.08
1339	YPL115C	BEM3	0.93	0.91	0.92	0.08
1340	YDR459C		0.89	0.95	0.92	0.08
1341	YBR225W		0.92	0.92	0.92	0.08
1342	YDR198C		1.05	0.80	0.92	0.08
1343	YMR214W	SCJ1	0.82	1.02	0.92	0.08
1344	YDR445C		0.90	0.95	0.92	0.08
1345	YLR118C		0.98	0.87	0.92	0.08
1346	YLL026W	HSP104	0.93	0.92	0.92	0.08
1347	YBR162C	TOS1	1.02	0.83	0.92	0.08
1348	YML013W	SEL1	1.04	0.80	0.92	0.08
1349	YDR370C		0.92	0.92	0.92	0.08
1350	YJL169W		0.93	0.91	0.92	0.08
1351	YHR113W		0.90	0.95	0.92	0.08
1352	YFL047W	RGD2	0.93	0.91	0.92	0.08
1353	YOL092W		0.81	1.04	0.92	0.08
1354	YEL011W	GLC3	0.83	1.02	0.92	0.08
1355	YER110C	KAP123	0.64	1.20	0.92	0.08
1356	YMR247C		0.90	0.94	0.92	0.08
1357	YMR161W	HLJ1	0.90	0.94	0.92	0.08
1358	YER044C	ERG28	0.92		0.92	0.08
1359	YMR226C		0.88	0.97	0.92	0.08
1360	YJL106W	IME2	1.03	0.82	0.92	0.08
1361	YLR111W		0.89	0.96	0.92	0.08
1362	YHR022C		1.06	0.79	0.92	0.08
1363	YPL026C	SKS1	0.74	1.11	0.92	0.08
1364	YER088C	DOT6	0.91	0.93	0.92	0.08
1365	YLR049C		0.94	0.91	0.92	0.08
1366	YDL095W	PMT1	0.72	1.13	0.92	0.08
1367	YMR144W		1.05	0.80	0.92	0.08
1368	YBR035C	PDX3	0.92		0.92	0.08
1369	YIL054W		1.05	0.80	0.92	0.08
1370	YBR291C	CTP1	0.89	0.96	0.92	0.08
1371	YMR205C	PFK2	0.93		0.93	0.08
1372	YOR058C	ASE1	0.98	0.87	0.93	0.08
1373	YMR053C	STB2	0.88	0.97	0.93	0.08
1374	YJR153W	PGU1	0.92	0.93	0.93	0.08
1375	YGL121C	GPG1	1.10	0.75	0.93	0.08
1376	YMR127C	SAS2	0.91	0.94	0.93	0.08
1377	YDR179C	CSN9	0.95	0.90	0.93	0.08
1378	YGR196C	FYV8	0.96	0.89	0.93	0.08
1379	YJL200C		0.76	1.09	0.93	0.08
1380	YNL234W		0.93		0.93	0.08
1381	YBR085W	AAC3	0.87	0.98	0.93	0.08

Rank	ORF	Gene	Normalized densitometry values			SCORE
			MATa	MATalpha	average	
1382	YMR175W	SIP18	0.89	0.96	0.93	0.08
1383	YCL040W	GLK1	0.97	0.88	0.93	0.08
1384	YNL326C	PFA3	0.91	0.94	0.93	0.08
1385	YLR304C	ACO1	1.02	0.84	0.93	0.08
1386	YFR026C		1.09	0.77	0.93	0.08
1387	YDL168W	SFA1	1.00	0.85	0.93	0.08
1388	YJR133W	XPT1	1.06	0.80	0.93	0.08
1389	YBR015C	MNN2	0.75	1.11	0.93	0.08
1390	YBR200W	BEM1	0.93	0.93	0.93	0.08
1391	YDR263C	DIN7	0.79	1.07	0.93	0.08
1392	YGR122C-A		1.13	0.73	0.93	0.08
1393	YDR326C		1.05	0.81	0.93	0.08
1394	YJL168C	SET2	0.89	0.96	0.93	0.08
1395	YMR258C		0.69	1.17	0.93	0.08
1396	YIL138C	TPM2	1.17	0.69	0.93	0.08
1397	YDR034C	LYS14	0.93		0.93	0.08
1398	YNL300W		0.74	1.12	0.93	0.08
1399	YLR137W		1.11	0.74	0.93	0.08
1400	YML003W		0.86	0.99	0.93	0.08
1401	YMR318C	ADH6	0.85	1.01	0.93	0.08
1402	YGR202C	PCT1	0.79	1.07	0.93	0.08
1403	YPL080C		0.75	1.11	0.93	0.08
1404	YGR017W		1.03	0.83	0.93	0.08
1405	YMR244W		0.79	1.06	0.93	0.08
1406	YEL016C	NPP2	1.03	0.83	0.93	0.08
1407	YGL235W		0.93	0.93	0.93	0.08
1408	YNR004W		1.07	0.79	0.93	0.07
1409	YDR253C	MET32	0.97	0.89	0.93	0.07
1410	YMR110C		1.00	0.86	0.93	0.07
1411	YLR228C	ECM22	0.93		0.93	0.07
1412	YKR098C	UBP11	0.94	0.92	0.93	0.07
1413	YDR333C		0.98	0.88	0.93	0.07
1414	YER075C	PTP3	1.14	0.72	0.93	0.07
1415	YER087C-A		1.10	0.76	0.93	0.07
1416	YIL013C	PDR11	1.10	0.76	0.93	0.07
1417	YJR024C		0.86	1.00	0.93	0.07
1418	YLR044C	PDC1	1.04	0.82	0.93	0.07
1419	YDR535C		0.90	0.96	0.93	0.07
1420	YKR092C	SRP40	0.59	1.27	0.93	0.07
1421	YOL061W	PRS5	0.95	0.92	0.93	0.07
1422	YLR265C	NEJ1	1.06	0.80	0.93	0.07
1423	YBR130C	SHE3	1.11	0.75	0.93	0.07

Rank	ORF	Gene	Normalized densitometry values			SCORE
			MATa	MATalpha	average	
1424	YGL086W	MAD1	0.92	0.94	0.93	0.07
1425	YDR096W	GIS1	0.87	0.99	0.93	0.07
1426	YKL076C	PSY1	1.06	0.80	0.93	0.07
1427	YOR018W	ROD1	0.82	1.04	0.93	0.07
1428	YEL017C-A	PMP2	1.07	0.79	0.93	0.07
1429	YPL257W		0.85	1.01	0.93	0.07
1430	YLR297W		0.88	0.98	0.93	0.07
1431	YDL022W	GPD1	0.91	0.96	0.93	0.07
1432	YBL068W	PRS4	0.91	0.95	0.93	0.07
1433	YIR016W		0.96	0.90	0.93	0.07
1434	YNL013C		0.77	1.09	0.93	0.07
1435	YGR268C	HUA1	1.09	0.77	0.93	0.07
1436	YAL036C	RBG1	0.87	1.00	0.93	0.07
1437	YJR135C	MCM22	0.79	1.07	0.93	0.07
1438	YLR224W		0.97	0.90	0.93	0.07
1439	YBR264C	YPT10	1.00	0.86	0.93	0.07
1440	YKR040C		0.93	0.93	0.93	0.07
1441	YKL146W	AVT3	0.98	0.88	0.93	0.07
1442	YAR029W		0.80	1.06	0.93	0.07
1443	YOR093C		0.79	1.07	0.93	0.07
1444	YDL190C	UFD2	0.71	1.16	0.93	0.07
1445	YLR352W		1.07	0.79	0.93	0.07
1446	YNL332W	THI12	1.02	0.84	0.93	0.07
1447	YHL035C		0.98	0.89	0.93	0.07
1448	YGR275W	RTT102	0.83	1.03	0.93	0.07
1449	YKR093W	PTR2	0.75	1.11	0.93	0.07
1450	YAL004W		0.86	1.01	0.93	0.07
1451	YDR380W	ARO10	1.00	0.87	0.93	0.07
1452	YLL023C		0.77	1.09	0.93	0.07
1453	YML102W	CAC2	0.84	1.02	0.93	0.07
1454	YNL055C	POR1	0.62	1.25	0.93	0.07
1455	YNL195C		0.84	1.03	0.93	0.07
1456	YOL075C		0.87	1.00	0.93	0.07
1457	YCR007C		0.96	0.90	0.93	0.07
1458	YNL304W	YPT11	0.86	1.01	0.93	0.07
1459	YKL044W		1.02	0.85	0.93	0.07
1460	YJL165C	HAL5	0.93	0.94	0.93	0.07
1461	YPR084W		0.69	1.17	0.93	0.07
1462	YLR433C	CNA1	0.82	1.05	0.93	0.07
1463	YER040W	GLN3	0.84	1.03	0.93	0.07
1464	YMR142C	RPL13B	0.73	1.14	0.94	0.07
1465	YOL136C	PFK27	0.94	0.93	0.94	0.07
1466	YGR053C		0.99	0.88	0.94	0.07

Rank	ORF	Gene	Normalized densitometry values			SCORE
			MATa	MATalpha	average	
1467	YLR034C	SMF3	0.95	0.92	0.94	0.07
1468	YDL171C	GLT1	0.85	1.03	0.94	0.07
1469	YOR296W		0.90	0.97	0.94	0.07
1470	YBR043C	QDR3	0.87	1.00	0.94	0.07
1471	YOL003C		1.02	0.85	0.94	0.07
1472	YFR035C		1.02	0.85	0.94	0.07
1473	YNR071C		0.72	1.16	0.94	0.07
1474	YPL033C		0.94	0.94	0.94	0.07
1475	YGR019W	UGA1	0.94	0.94	0.94	0.07
1476	YBL094C		0.96	0.92	0.94	0.07
1477	YDL054C	MCH1	0.94	0.94	0.94	0.07
1478	YOR059C		0.94	0.93	0.94	0.07
1479	YJL199C	MBB1	0.89	0.98	0.94	0.07
1480	YDR540C		0.95	0.92	0.94	0.07
1481	YEL047C		0.95	0.92	0.94	0.07
1482	YLR282C		1.02	0.85	0.94	0.07
1483	YEL037C	RAD23	0.98	0.90	0.94	0.07
1484	YLL058W		0.97	0.90	0.94	0.07
1485	YDR297W	SUR2	0.95	0.92	0.94	0.07
1486	YPL220W	RPL1A	0.89	0.99	0.94	0.07
1487	YMR238W	DFG5	0.92	0.95	0.94	0.07
1488	YJL052W	TDH1	0.97	0.90	0.94	0.07
1489	YKR091W	SRL3	0.80	1.08	0.94	0.07
1490	YHR207C	SET5	0.94	0.93	0.94	0.07
1491	YJL171C		1.06	0.82	0.94	0.07
1492	YMR155W		1.09	0.78	0.94	0.07
1493	YPR005C	HAL1	1.00	0.88	0.94	0.07
1494	YLL046C	RNP1	0.90	0.98	0.94	0.07
1495	YGL094C	PAN2	0.91	0.97	0.94	0.07
1496	YKL034W	TUL1	0.94	0.94	0.94	0.07
1497	YIL001W		1.01	0.87	0.94	0.07
1498	YDR467C		0.83	1.05	0.94	0.07
1499	YDR422C	SIP1	0.92	0.96	0.94	0.07
1500	YML002W		0.89	0.98	0.94	0.07
1501	YIL015W	BAR1	1.06	0.81	0.94	0.07
1502	YLL045C	RPL8B	0.79	1.08	0.94	0.07
1503	YDR405W	MRP20	0.94		0.94	0.07
1504	YGL199C		0.90	0.98	0.94	0.07
1505	YNR066C		0.97	0.91	0.94	0.07
1506	YBL003C	HTA2	0.88	1.00	0.94	0.07
1507	YOL106W		0.67	1.21	0.94	0.07
1508	YBR299W	MAL32	0.81	1.07	0.94	0.07
1509	YOL091W	SPO21	0.80	1.08	0.94	0.07
1510	YFR055W		0.98	0.90	0.94	0.07

Rank	ORF	Gene	Normalized densitometry values			SCORE
			MATa	MATalpha	average	
1511	YPR003C		0.97	0.91	0.94	0.07
1512	YPR141C	KAR3	1.03	0.85	0.94	0.06
1513	YLL005C	SPO75	0.85	1.03	0.94	0.06
1514	YOL025W	LAG2	0.81	1.07	0.94	0.06
1515	YMR294W-A		1.17	0.71	0.94	0.06
1516	YKR018C		0.79	1.09	0.94	0.06
1517	YMR255W	GFD1	0.74	1.14	0.94	0.06
1518	YAL051W	OAF1	0.92	0.96	0.94	0.06
1519	YNL187W		0.89	0.99	0.94	0.06
1520	YPR044C		0.72	1.16	0.94	0.06
1521	YPL053C	KTR6	0.70	1.18	0.94	0.06
1522	YJL206C		0.83	1.05	0.94	0.06
1523	YKL143W	LTV1	0.87	1.02	0.94	0.06
1524	YNL231C	PDR16	1.07	0.81	0.94	0.06
1525	YMR163C		0.80	1.08	0.94	0.06
1526	YGR057C	LST7	1.04	0.84	0.94	0.06
1527	YNL318C	HXT14	1.10	0.78	0.94	0.06
1528	YGR161C	RTS3	0.91	0.97	0.94	0.06
1529	YJL198W	PHO90	0.91	0.97	0.94	0.06
1530	YOR360C	PDE2	0.79	1.09	0.94	0.06
1531	YML038C	YMD8	0.99	0.89	0.94	0.06
1532	YGL158W	RCK1	0.95	0.93	0.94	0.06
1533	YHR016C	YSC84	0.99	0.89	0.94	0.06
1534	YNL120C		0.95	0.93	0.94	0.06
1535	YJR080C		0.73	1.15	0.94	0.06
1536	YNL046W		1.02	0.86	0.94	0.06
1537	YAR003W	SWD1	0.76	1.13	0.94	0.06
1538	YHR017W	YSC83	1.02	0.87	0.94	0.06
1539	YBR115C	LYS2	0.82	1.06	0.94	0.06
1540	YIL073C	SPO22	0.91	0.97	0.94	0.06
1541	YDR122W	KIN1	1.03	0.85	0.94	0.06
1542	YMR120C	ADE17	0.89	0.99	0.94	0.06
1543	YOL151W	GRE2	0.94	0.94	0.94	0.06
1544	YBR209W		0.81	1.07	0.94	0.06
1545	YDR031W		1.07	0.82	0.94	0.06
1546	YDR252W	BTT1	1.00	0.88	0.94	0.06
1547	YDL241W		1.03	0.85	0.94	0.06
1548	YGR234W	YHB1	0.92	0.97	0.94	0.06
1549	YNL140C		1.03	0.85	0.94	0.06
1550	YER070W	RNR1	0.53	1.35	0.94	0.06
1551	YPR054W	SMK1	0.83	1.06	0.94	0.06
1552	YJL132W		1.00	0.89	0.94	0.06
1553	YDR244W	PEX5	0.92	0.97	0.94	0.06

Rank	ORF	Gene	Normalized densitometry values			SCORE
			MATa	MATalpha	average	
1554	YLR414C		0.95	0.94	0.94	0.06
1555	YNL173C	MDG1	0.77	1.11	0.94	0.06
1556	YHR025W	THR1	1.00	0.89	0.94	0.06
1557	YOR380W	RDR1	0.96	0.92	0.94	0.06
1558	YLR234W	TOP3	0.90	0.99	0.94	0.06
1559	YIL037C	PRM2	0.91	0.97	0.94	0.06
1560	YNL271C	BNI1	0.94		0.94	0.06
1561	YIL030C	SSM4	0.97	0.92	0.94	0.06
1562	YBR295W	PCA1	0.89	1.00	0.94	0.06
1563	YOR021C		1.12	0.76	0.94	0.06
1564	YAL056W	GPB2	1.02	0.87	0.94	0.06
1565	YAL021C	CCR4	0.94		0.94	0.06
1566	YOR264W	DSE3	0.88	1.01	0.94	0.06
1567	YML053C		0.97	0.91	0.94	0.06
1568	YBR296C	PHO89	0.86	1.03	0.94	0.06
1569	YBR137W		1.00	0.89	0.94	0.06
1570	YGR136W	LSB1	0.97	0.92	0.94	0.06
1571	YPL253C	VIK1	1.00	0.89	0.94	0.06
1572	YOR076C	SKI7	0.88	1.01	0.94	0.06
1573	YLL057C	JLP1	1.17	0.72	0.94	0.06
1574	YIL060W		1.15	0.73	0.94	0.06
1575	YJR137C	ECM17	0.74	1.15	0.94	0.06
1576	YJL029C	VPS53	0.94		0.94	0.06
1577	YBR145W	ADH5	1.03	0.86	0.94	0.06
1578	YOL013W-A		0.82	1.07	0.94	0.06
1579	YJL192C	SOP4	0.90	0.99	0.94	0.06
1580	YPL221W		0.86	1.03	0.94	0.06
1581	YAL066W		0.80	1.09	0.94	0.06
1582	YPL167C	REV3	1.06	0.83	0.95	0.06
1583	YDR295C	HDA2	0.84	1.05	0.95	0.06
1584	YKL197C	PEX1	1.04	0.85	0.95	0.06
1585	YNL279W	PRM1	0.77	1.12	0.95	0.06
1586	YML057W	CMP2	1.15	0.74	0.95	0.06
1587	YOR381W	FRE3	0.92	0.97	0.95	0.06
1588	YOL081W	IRA2	1.00	0.89	0.95	0.06
1589	YGL214W		1.13	0.76	0.95	0.06
1590	YEL057C		0.87	1.02	0.95	0.06
1591	YLR443W	ECM7	1.05	0.84	0.95	0.06
1592	YLR131C	ACE2	0.86	1.03	0.95	0.06
1593	YNL292W	PUS4	0.93	0.96	0.95	0.06
1594	YPL267W		0.91	0.98	0.95	0.06
1595	YDL117W	CYK3	0.89	1.00	0.95	0.06
1596	YHR189W	PTH1	0.73	1.16	0.95	0.06

Rank	ORF	Gene	Normalized densitometry values			SCORE
			MATa	MATalpha	average	
1597	YLR438W	CAR2	1.02	0.87	0.95	0.06
1598	YOR365C		0.92	0.97	0.95	0.06
1599	YER181C		1.08	0.81	0.95	0.06
1600	YNL230C	ELA1	0.90	0.99	0.95	0.06
1601	YOR223W		0.96	0.94	0.95	0.06
1602	YER071C		0.92	0.97	0.95	0.06
1603	YKL101W	HSL1	0.95	0.94	0.95	0.06
1604	YDL085W	NDE2	0.98	0.92	0.95	0.06
1605	YLR187W	SKG3	0.97	0.93	0.95	0.06
1606	YLR364W		0.79	1.10	0.95	0.06
1607	YDL144C		0.95	0.94	0.95	0.06
1608	YKL086W	SRX1	1.09	0.81	0.95	0.06
1609	YDR392W	SPT3	0.63	1.26	0.95	0.06
1610	YOL124C	TRM11	0.94	0.96	0.95	0.06
1611	YGR221C	TOS2	1.00	0.89	0.95	0.06
1612	YFL053W	DAK2	0.93	0.97	0.95	0.06
1613	YOL056W	GPM3	1.04	0.86	0.95	0.06
1614	YNL335W		0.92	0.97	0.95	0.06
1615	YMR129W	POM152	1.04	0.86	0.95	0.06
1616	YLR108C		0.93	0.97	0.95	0.06
1617	YGR279C	SCW4	0.80	1.09	0.95	0.06
1618	YGR194C	XKS1	0.95	0.94	0.95	0.06
1619	YPL067C		0.79	1.10	0.95	0.06
1620	YMR105C	PGM2	0.94	0.95	0.95	0.06
1621	YCL064C	CHA1	0.84	1.05	0.95	0.06
1622	YDR518W	EUG1	0.90	1.00	0.95	0.06
1623	YEL017W	GTT3	1.04	0.86	0.95	0.06
1624	YJL152W		0.95	0.94	0.95	0.06
1625	YKL030W		0.96	0.94	0.95	0.06
1626	YNL249C	MPA43	0.93	0.97	0.95	0.06
1627	YPL149W	ATG5	0.74	1.15	0.95	0.06
1628	YDR026C		0.90	0.99	0.95	0.06
1629	YNL011C		1.05	0.85	0.95	0.06
1630	YNL057W		0.85	1.05	0.95	0.06
1631	YNL078W	NIS1	0.79	1.10	0.95	0.06
1632	YOR383C	FIT3	1.03	0.87	0.95	0.06
1633	YOL082W	ATG19	1.03	0.86	0.95	0.06
1634	YGR051C		0.94	0.96	0.95	0.06
1635	YBL065W		1.04	0.86	0.95	0.06
1636	YMR073C		0.93	0.97	0.95	0.06
1637	YKL120W	OAC1	0.92	0.97	0.95	0.06
1638	YDL135C	RDI1	0.91	0.98	0.95	0.06
1639	YGR003W	CUL3	1.01	0.89	0.95	0.06
1640	YGR093W		0.92	0.98	0.95	0.06

Rank	ORF	Gene	Normalized densitometry values			SCORE
			MATa	MATalpha	average	
1641	YFR006W		0.93	0.97	0.95	0.05
1642	YGL262W		1.07	0.83	0.95	0.05
1643	YMR231W	PEP5	0.95		0.95	0.05
1644	YLR181C	VTA1	0.96	0.94	0.95	0.05
1645	YJL213W		0.90	1.00	0.95	0.05
1646	YJL149W		0.94	0.96	0.95	0.05
1647	YGL033W	HOP2	0.82	1.08	0.95	0.05
1648	YOL122C	SMF1	0.78	1.12	0.95	0.05
1649	YFL030W	AGX1	0.86	1.04	0.95	0.05
1650	YDR484W	VPS52	0.91	0.99	0.95	0.05
1651	YGL175C	SAE2	0.84	1.06	0.95	0.05
1652	YHR181W	SVP26	0.91	0.99	0.95	0.05
1653	YBR260C	RGD1	1.00	0.90	0.95	0.05
1654	YNL237W	YTP1	0.99	0.91	0.95	0.05
1655	YPL269W	KAR9	0.93	0.97	0.95	0.05
1656	YPL125W	KAP120	1.00	0.90	0.95	0.05
1657	YDR439W	LRS4	0.94	0.96	0.95	0.05
1658	YAL007C	ERP2	0.92	0.98	0.95	0.05
1659	YGR004W	PEX31	0.99	0.91	0.95	0.05
1660	YIR039C	YPS6	1.02	0.88	0.95	0.05
1661	YPL071C		0.96	0.94	0.95	0.05
1662	YNL122C		1.07	0.83	0.95	0.05
1663	YKR051W		0.89	1.01	0.95	0.05
1664	YGL110C	CUE3		0.95	0.95	0.05
1665	YKL147C		0.95		0.95	0.05
1666	YNR013C	PHO91	0.92	0.98	0.95	0.05
1667	YCL014W	BUD3	1.10	0.81	0.95	0.05
1668	YGR139W		0.68	1.23	0.95	0.05
1669	YDR143C	SAN1	0.96	0.94	0.95	0.05
1670	YPL180W	TCO89	0.84	1.07	0.95	0.05
1671	YKL124W	SSH4	1.03	0.87	0.95	0.05
1672	YPR021C	AGC1	0.77	1.13	0.95	0.05
1673	YNL142W	MEP2	1.23	0.68	0.95	0.05
1674	YOL153C		0.78	1.12	0.95	0.05
1675	YPL119C	DBP1	0.97	0.93	0.95	0.05
1676	YDL114W		0.95		0.95	0.05
1677	YOR283W		0.99	0.92	0.95	0.05
1678	YKR043C		1.05	0.86	0.95	0.05
1679	YKR034W	DAL80	0.94	0.97	0.95	0.05
1680	YMR295C		1.15	0.75	0.95	0.05
1681	YNL129W	NRK1	1.04	0.86	0.95	0.05
1682	YOR096W	RPS7A	0.19	1.71	0.95	0.05
1683	YGR025W		0.95	0.96	0.95	0.05
1684	YKR078W		0.89	1.01	0.95	0.05

Rank	ORF	Gene	Normalized densitometry values			SCORE
			MATa	MATalpha	average	
1685	YNL157W		1.09	0.82	0.95	0.05
1686	YDR120C	TRM1	1.01	0.89	0.95	0.05
1687	YDR399W	HPT1	1.04	0.87	0.95	0.05
1688	YPL055C	LGE1	0.67	1.24	0.95	0.05
1689	YOR304W	ISW2	1.01	0.90	0.95	0.05
1690	YOR083W	WHI5	1.01	0.90	0.95	0.05
1691	YDR458C		0.89	1.02	0.95	0.05
1692	YHR028C	DAP2	0.96	0.95	0.95	0.05
1693	YAL017W	PSK1	0.89	1.02	0.95	0.05
1694	YIL094C	LYS12	0.95		0.95	0.05
1695	YHR142W	CHS7	0.92	0.98	0.95	0.05
1696	YOR080W	DIA2	0.92	0.99	0.95	0.05
1697	YJL103C		1.02	0.89	0.95	0.05
1698	YOR191W	RIS1	0.86	1.04	0.95	0.05
1699	YNL168C		0.82	1.09	0.95	0.05
1700	YBR278W	DPB3	0.93	0.98	0.95	0.05
1701	YGL028C	SCW11	0.86	1.05	0.95	0.05
1702	YPL090C	RPS6A	0.63	1.28	0.95	0.05
1703	YNL020C	ARK1	0.95	0.96	0.95	0.05
1704	YCR036W	RBK1	0.89	1.02	0.95	0.05
1705	YPR167C	MET16	0.79	1.12	0.95	0.05
1706	YNL086W		1.05	0.86	0.95	0.05
1707	YDR183W	PLP1	1.05	0.86	0.95	0.05
1708	YLR095C	IOC2	0.98	0.93	0.96	0.05
1709	YIR019C	MUC1	1.07	0.84	0.96	0.05
1710	YOR008C-A		0.84	1.07	0.96	0.05
1711	YBL019W	APN2	0.94	0.97	0.96	0.05
1712	YGL036W		0.97	0.94	0.96	0.05
1713	YGL196W		0.88	1.03	0.96	0.05
1714	YDR312W	SSF2	1.03	0.88	0.96	0.05
1715	YGL090W	LIF1	1.09	0.82	0.96	0.05
1716	YLR400W		0.94	0.97	0.96	0.05
1717	YBR108W		0.85	1.06	0.96	0.05
1718	YKL164C	PIR1	0.95	0.96	0.96	0.05
1719	YGL248W	PDE1	0.94	0.97	0.96	0.05
1720	YFL010C	WWM1	1.08	0.83	0.96	0.05
1721	YOR131C		0.90	1.01	0.96	0.05
1722	YKL171W		0.98	0.94	0.96	0.05
1723	YOL131W		0.94	0.97	0.96	0.05
1724	YNL025C	SSN8	0.96		0.96	0.05
1725	YDL130W-A	STF1	0.94	0.97	0.96	0.05
1726	YLR134W	PDC5	0.70	1.21	0.96	0.05

Rank	ORF	Gene	Normalized densitometry values			SCORE
			MATa	MATalpha	average	
1727	YDR340W		1.00	0.92	0.96	0.05
1728	YDR014W	RAD61	1.25	0.66	0.96	0.05
1729	YLR449W	FPR4	0.77	1.14	0.96	0.05
1730	YMR185W			0.96	0.96	0.05
1731	YLR179C		1.16	0.75	0.96	0.05
1732	YGR217W	CCH1	0.98	0.93	0.96	0.05
1733	YNL183C	NPR1	0.93	0.99	0.96	0.05
1734	YKL115C		1.07	0.85	0.96	0.05
1735	YPL247C		1.05	0.87	0.96	0.05
1736	YJL048C	UBX6	1.20	0.72	0.96	0.05
1737	YIL007C	NAS2	1.02	0.89	0.96	0.05
1738	YLR368W	MDM30	0.69	1.22	0.96	0.05
1739	YMR010W		0.62	1.29	0.96	0.05
1740	YOL150C		0.81	1.11	0.96	0.05
1741	YIL006W	YIA6	0.87	1.05	0.96	0.05
1742	YDR453C	TSA2	0.94	0.98	0.96	0.05
1743	YOR042W	CUE5	1.00	0.91	0.96	0.05
1744	YOR348C	PUT4	1.06	0.85	0.96	0.05
1745	YBR157C	ICS2	0.92	1.00	0.96	0.05
1746	YFL044C		0.94	0.97	0.96	0.05
1747	YKL140W	TGL1	0.95	0.96	0.96	0.05
1748	YOR101W	RAS1	0.93	0.98	0.96	0.05
1749	YCL048W	SPS22	0.95	0.96	0.96	0.05
1750	YHR031C	RRM3	0.95	0.97	0.96	0.05
1751	YJL157C	FAR1	1.05	0.87	0.96	0.05
1752	YDR435C	PPM1	0.87	1.04	0.96	0.05
1753	YKR104W		0.91	1.01	0.96	0.05
1754	YGR219W		0.89	1.02	0.96	0.05
1755	YDR537C		1.13	0.78	0.96	0.05
1756	YOR356W		1.11	0.81	0.96	0.05
1757	YMR294W	JNM1	1.16	0.76	0.96	0.05
1758	YMR305C	SCW10	0.86	1.06	0.96	0.05
1759	YKL218C	SRY1	0.90	1.01	0.96	0.05
1760	YDR321W	ASP1	0.89	1.03	0.96	0.05
1761	YGR039W		0.92	1.00	0.96	0.05
1762	YGR052W		1.00	0.92	0.96	0.05
1763	YFR036W	CDC26	1.10	0.82	0.96	0.05
1764	YGL007W			0.96	0.96	0.05
1765	YBL061C	SKT5	1.05	0.87	0.96	0.05
1766	YKL129C	MYO3	0.97	0.95	0.96	0.05
1767	YBR047W		0.99	0.93	0.96	0.05
1768	YOR173W	DCS2	0.94	0.98	0.96	0.05
1769	YER185W		0.89	1.03	0.96	0.05
1770	YPL225W		0.86	1.06	0.96	0.04

Rank	ORF	Gene	Normalized densitometry values			SCORE
			MATa	MATalpha	average	
1771	YLR401C	DUS3	0.94	0.98	0.96	0.04
1772	YJL078C	PRY3	0.90	1.02	0.96	0.04
1773	YMR173W	DDR48	1.00	0.92	0.96	0.04
1774	YMR114C		0.99	0.93	0.96	0.04
1775	YBL064C	PRX1	1.03	0.89	0.96	0.04
1776	YBR241C		0.98	0.94	0.96	0.04
1777	YBL096C		1.04	0.88	0.96	0.04
1778	YGR067C		0.97	0.95	0.96	0.04
1779	YDR480W	DIG2	0.93	0.99	0.96	0.04
1780	YNR061C		0.94	0.98	0.96	0.04
1781	YPL206C		0.94	0.98	0.96	0.04
1782	YNL145W	MFA2	1.09	0.83	0.96	0.04
1783	YKR009C	FOX2	0.96	0.96	0.96	0.04
1784	YEL059W		0.93	1.00	0.96	0.04
1785	YOL014W		0.91	1.01	0.96	0.04
1786	YOR175C		0.90	1.02	0.96	0.04
1787	YPL186C	UIP4	0.91	1.02	0.96	0.04
1788	YNL030W	HHF2	1.09	0.83	0.96	0.04
1789	YDL210W	UGA4	1.02	0.91	0.96	0.04
1790	YNL319W		0.95	0.98	0.96	0.04
1791	YOR308C	SNU66	0.97	0.96	0.96	0.04
1792	YGR199W	PMT6	0.99	0.93	0.96	0.04
1793	YER011W	TIR1	0.78	1.14	0.96	0.04
1794	YER044C-A	MEI4	1.09	0.84	0.96	0.04
1795	YMR119W	ASI1	0.97	0.96	0.96	0.04
1796	YCR083W	TRX3	0.96	0.97	0.96	0.04
1797	YBR071W		1.03	0.89	0.96	0.04
1798	YDR310C	SUM1	1.01	0.91	0.96	0.04
1799	YNL276C		0.71	1.22	0.96	0.04
1800	YOR010C	TIR2	0.96	0.97	0.96	0.04
1801	YJL126W	NIT2	0.97	0.95	0.96	0.04
1802	YBL046W		0.97	0.96	0.96	0.04
1803	YIR025W	MND2	1.07	0.86	0.96	0.04
1804	YPL166W		0.94	0.98	0.96	0.04
1805	YLR390W	ECM19	0.95	0.98	0.96	0.04
1806	YBR261C		0.96	0.96	0.96	0.04
1807	YPL171C	OYE3	1.06	0.87	0.96	0.04
1808	YDR035W	ARO3	1.00	0.92	0.96	0.04
1809	YLR024C	UBR2	0.85	1.07	0.96	0.04
1810	YML096W		1.00	0.93	0.96	0.04
1811	YNL253W	TEX1	0.94	0.99	0.96	0.04
1812	YLR042C		0.95	0.97	0.96	0.04
1813	YMR215W	GAS3	1.07	0.85	0.96	0.04

Rank	ORF	Gene	Normalized densitometry values			SCORE
			MATa	MATalpha	average	
1814	YMR264W	CUE1	0.93	1.00	0.96	0.04
1815	YGL263W	COS12	0.99	0.94	0.96	0.04
1816	YNL305C		0.81	1.11	0.96	0.04
1817	YFL063W		0.88	1.05	0.96	0.04
1818	YDL232W	OST4	0.96		0.96	0.04
1819	YOR328W	PDR10	0.95	0.98	0.96	0.04
1820	YJR049C	UTR1	1.02	0.91	0.96	0.04
1821	YPR062W	FCY1	0.92	1.01	0.96	0.04
1822	YKR039W	GAP1	0.98	0.95	0.96	0.04
1823	YNR062C		0.93	1.00	0.96	0.04
1824	YJR152W	DAL5	1.01	0.91	0.96	0.04
1825	YLR097C	HRT3	1.02	0.91	0.96	0.04
1826	YDR469W	SDC1	0.90	1.03	0.96	0.04
1827	YDL131W	LYS21	1.05	0.88	0.96	0.04
1828	YNL191W		0.95	0.98	0.96	0.04
1829	YLR331C		0.96	0.97	0.96	0.04
1830	YMR153C-A		1.11	0.82	0.96	0.04
1831	YKL175W	ZRT3	0.98	0.95	0.96	0.04
1832	YOR197W	MCA1	1.06	0.87	0.96	0.04
1833	YCR079W		0.97	0.96	0.96	0.04
1834	YKR033C		0.97	0.96	0.97	0.04
1835	YDR307W		0.96	0.98	0.97	0.04
1836	YOR166C		1.04	0.89	0.97	0.04
1837	YGL096W	TOS8	0.90	1.03	0.97	0.04
1838	YML021C	UNG1	0.86	1.07	0.97	0.04
1839	YOR147W	MDM32		0.97	0.97	0.04
1840	YER032W	FIR1	1.06	0.87	0.97	0.04
1841	YNL032W	SIW14	0.97	0.96	0.97	0.04
1842	YPL019C	VTC3	1.05	0.88	0.97	0.04
1843	YOR228C		0.92	1.01	0.97	0.04
1844	YBR018C	GAL7	0.87	1.06	0.97	0.04
1845	YGL228W	SHE10	0.94	0.99	0.97	0.04
1846	YGR008C	STF2	0.89	1.05	0.97	0.04
1847	YJR030C		1.00	0.93	0.97	0.04
1848	YOR302W		0.94	1.00	0.97	0.04
1849	YLR125W		1.10	0.84	0.97	0.04
1850	YKL092C	BUD2	1.16	0.77	0.97	0.04
1851	YGL077C	HNM1	0.97	0.97	0.97	0.04
1852	YNL180C	RHO5	1.08	0.86	0.97	0.04
1853	YNL322C	KRE1	0.97		0.97	0.04
1854	YHR014W	SPO13	1.18	0.76	0.97	0.04
1855	YER086W	ILV1	1.02	0.91	0.97	0.04
1856	YLL025W		0.95	0.98	0.97	0.04

Rank	ORF	Gene	Normalized densitometry values			SCORE
			MATa	MATalpha	average	
1857	YPL268W	PLC1	1.06	0.87	0.97	0.04
1858	YIL158W		0.94	1.00	0.97	0.04
1859	YMR204C	INP1	0.97	0.97	0.97	0.04
1860	YER007C-A		0.75	1.19	0.97	0.04
1861	YNR065C		1.04	0.90	0.97	0.04
1862	YDR083W	RRP8	0.95	0.98	0.97	0.04
1863	YLR084C	RAX2	0.98	0.95	0.97	0.04
1864	YHL047C	ARN2	0.84	1.10	0.97	0.04
1865	YGR173W	RBG2	1.14	0.80	0.97	0.04
1866	YOR311C	HSD1	1.02	0.92	0.97	0.04
1867	YHL033C	RPL8A	1.06	0.87	0.97	0.04
1868	YPL113C		0.97	0.96	0.97	0.04
1869	YOL039W	RPP2A	0.93	1.01	0.97	0.04
1870	YDR533C	HSP31	1.07	0.87	0.97	0.04
1871	YIR007W		1.01	0.93	0.97	0.04
1872	YGR092W	DBF2	1.08	0.86	0.97	0.04
1873	YCR020C	PET18	0.91	1.03	0.97	0.04
1874	YHL032C	GUT1	0.98	0.95	0.97	0.04
1875	YML100W-A		0.94	0.99	0.97	0.04
1876	YPL047W	SGF11	0.97	0.97	0.97	0.04
1877	YNL128W	TEP1	1.02	0.92	0.97	0.04
1878	YNL227C	JJJ1	0.99	0.94	0.97	0.04
1879	YPL163C	SVS1	1.12	0.82	0.97	0.04
1880	YBR244W	GPX2	0.97	0.97	0.97	0.04
1881	YOL128C	YGK3	0.92	1.01	0.97	0.04
1882	YLR294C		0.98	0.96	0.97	0.04
1883	YOL045W	PSK2	0.94	1.00	0.97	0.03
1884	YMR069W	NAT4	0.93	1.01	0.97	0.03
1885	YMR234W	RNH1	1.08	0.86	0.97	0.03
1886	YMR193W	MRPL24	1.02	0.92	0.97	0.03
1887	YHR136C	SPL2	0.99	0.95	0.97	0.03
1888	YBR203W	COS111	0.91	1.03	0.97	0.03
1889	YHR156C	LIN1	1.16	0.78	0.97	0.03
1890	YOR301W	RAX1	0.92	1.02	0.97	0.03
1891	YGR181W	TIM13	1.02	0.92	0.97	0.03
1892	YML072C	TCB3	0.86	1.08	0.97	0.03
1893	YOL158C	ENB1	0.90	1.04	0.97	0.03
1894	YOR190W	SPR1	0.94	1.00	0.97	0.03
1895	YNL072W	RNH201	1.03	0.91	0.97	0.03
1896	YKL105C		0.89	1.05	0.97	0.03
1897	YDR490C	PKH1	1.02	0.92	0.97	0.03
1898	YNL323W	LEM3	0.97	0.97	0.97	0.03

Rank	ORF	Gene	Normalized densitometry values			SCORE
			MATa	MATalpha	average	
1899	YOR183W	FYV12	0.84	1.10	0.97	0.03
1900	YOL132W	GAS4	0.95	0.99	0.97	0.03
1901	YER079W		1.00	0.95	0.97	0.03
1902	YDR084C	TVP23	0.99	0.95	0.97	0.03
1903	YPR128C	ANT1	0.95	0.99	0.97	0.03
1904	YFR015C	GSY1	0.96	0.98	0.97	0.03
1905	YNL211C		0.94	1.01	0.97	0.03
1906	YOR247W	SRL1	1.08	0.87	0.97	0.03
1907	YHR001W-A	QCR10	0.92	1.02	0.97	0.03
1908	YCL055W	KAR4	1.03	0.91	0.97	0.03
1909	YDL021W	GPM2	0.79	1.15	0.97	0.03
1910	YGL089C	MF(ALPHA)2	1.06	0.88	0.97	0.03
1911	YPL181W	CTI6	1.01	0.94	0.97	0.03
1912	YDL083C	RPS16B	0.93	1.02	0.97	0.03
1913	YBR052C		0.99	0.95	0.97	0.03
1914	YBR024W	SCO2	0.81	1.14	0.97	0.03
1915	YFR056C		1.02	0.92	0.97	0.03
1916	YPL096W	PNG1	0.90	1.05	0.97	0.03
1917	YML056C	IMD4	0.92	1.02	0.97	0.03
1918	YBR280C		0.98	0.97	0.97	0.03
1919	YLR246W	ERF2	1.04	0.90	0.97	0.03
1920	YMR194C-A		0.93	1.01	0.97	0.03
1921	YIL055C		1.07	0.87	0.97	0.03
1922	YIL009W	FAA3	0.98	0.97	0.97	0.03
1923	YKR069W	MET1	0.89	1.06	0.97	0.03
1924	YKL037W		0.93	1.02	0.97	0.03
1925	YCL034W	LSB5	0.94	1.00	0.97	0.03
1926	YAL028W	FRT2	1.04	0.90	0.97	0.03
1927	YIL096C		0.98	0.97	0.97	0.03
1928	YHL006C	SHU1	0.99	0.95	0.97	0.03
1929	YIL167W	SDL1	0.96	0.98	0.97	0.03
1930	YDR406W	PDR15	1.02	0.93	0.97	0.03
1931	YIL166C		0.93	1.02	0.97	0.03
1932	YKL202W		1.10	0.85	0.97	0.03
1933	YDR509W		0.95	1.00	0.97	0.03
1934	YNR067C	DSE4	1.01	0.94	0.97	0.03
1935	YBL051C	PIN4	0.95	1.00	0.97	0.03
1936	YOL147C	PEX11	0.96	0.99	0.97	0.03
1937	YIL014W	MNT3	0.97		0.97	0.03
1938	YIL102C		0.98		0.98	0.03
1939	YDR151C	CTH1	0.97	0.98	0.98	0.03

Rank	ORF	Gene	Normalized densitometry values			SCORE
			MATa	MATalpha	average	
1940	YMR178W		1.01	0.94	0.98	0.03
1941	YBR077C	SLM4	1.10	0.86	0.98	0.03
1942	YOR031W	CRS5	0.95	1.00	0.98	0.03
1943	YBR039W	ATP3	0.98		0.98	0.03
1944	YNL134C		0.99	0.97	0.98	0.03
1945	YLR065C		0.92	1.03	0.98	0.03
1946	YKR058W	GLG1	1.01	0.94	0.98	0.03
1947	YMR174C	PAI3	0.98	0.97	0.98	0.03
1948	YBR300C		0.86	1.09	0.98	0.03
1949	YHR209W		1.05	0.90	0.98	0.03
1950	YML101C	CUE4	1.06	0.89	0.98	0.03
1951	YMR246W	FAA4	0.90	1.05	0.98	0.03
1952	YLR311C		1.02	0.94	0.98	0.03
1953	YPR002W	PDH1	0.95	1.01	0.98	0.03
1954	YGR207C		1.02	0.93	0.98	0.03
1955	YPL188W	POS5	0.98		0.98	0.03
1956	YGR189C	CRH1	1.01	0.94	0.98	0.03
1957	YGR105W	VMA21	0.98		0.98	0.03
1958	YBR250W		0.98	0.97	0.98	0.03
1959	YFL056C	AAD6	0.98	0.97	0.98	0.03
1960	YER047C	SAP1	0.96	1.00	0.98	0.03
1961	YAL023C	PMT2	0.98	0.97	0.98	0.03
1962	YGL165C		0.94	1.02	0.98	0.03
1963	YOL163W		0.98	0.97	0.98	0.03
1964	YNL254C		1.00	0.95	0.98	0.03
1965	YNL301C	RPL18B	0.99	0.96	0.98	0.03
1966	YLR068W	FYV7	0.93	1.03	0.98	0.03
1967	YPL095C		0.93	1.03	0.98	0.03
1968	YPL014W		1.01	0.95	0.98	0.03
1969	YAL018C		1.10	0.85	0.98	0.03
1970	YDL088C	ASM4	0.94	1.02	0.98	0.03
1971	YPR160W	GPH1	1.01	0.95	0.98	0.03
1972	YDR374C		0.95	1.01	0.98	0.03
1973	YGR097W	ASK10	0.99	0.97	0.98	0.03
1974	YJR011C		0.83	1.12	0.98	0.03
1975	YLL051C	FRE6	0.97	0.99	0.98	0.03
1976	YLR385C	SWC7	1.02	0.93	0.98	0.03
1977	YMR017W	SPO20	0.99	0.97	0.98	0.03
1978	YDL066W	IDP1	1.06	0.90	0.98	0.03
1979	YBL060W		1.12	0.83	0.98	0.03
1980	YKL183W	LOT5	1.02	0.93	0.98	0.03
1981	YER164W	CHD1	1.14	0.82	0.98	0.03
1982	YDL188C	PPH22	0.99	0.97	0.98	0.03
1983	YNL074C	MLF3	0.92	1.03	0.98	0.03

Rank	ORF	Gene	Normalized densitometry values			SCORE
			MATa	MATalpha	average	
1984	YBL054W		1.03	0.93	0.98	0.03
1985	YKR026C	GCN3	1.12	0.84	0.98	0.03
1986	YBR073W	RDH54	1.00	0.96	0.98	0.03
1987	YDR206W	EBS1	1.10	0.86	0.98	0.03
1988	YJL079C	PRY1	0.98	0.97	0.98	0.03
1989	YOR342C		1.07	0.89	0.98	0.03
1990	YOR202W	HIS3	0.95	1.01	0.98	0.03
1991	YDR475C		0.99	0.97	0.98	0.03
1992	YDR536W	STL1	0.98		0.98	0.03
1993	YDR248C		0.94	1.01	0.98	0.03
1994	YDR538W	PAD1	1.01	0.94	0.98	0.03
1995	YGR213C	RTA1	0.80	1.16	0.98	0.03
1996	YMR086C-A		0.90	1.06	0.98	0.03
1997	YPL009C		0.99	0.97	0.98	0.03
1998	YPL008W	CHL1	1.09	0.86	0.98	0.03
1999	YDR483W	KRE2	0.99	0.96	0.98	0.03
2000	YOR051C		0.95	1.00	0.98	0.03
2001	YOR019W		1.21	0.75	0.98	0.03
2002	YOR359W	VTS1	1.13	0.83	0.98	0.03
2003	YJL163C		1.05	0.91	0.98	0.03
2004	YIR013C	GAT4	0.96	1.00	0.98	0.03
2005	YCR025C		0.91	1.05	0.98	0.03
2006	YLR227C	ADY4	0.91	1.05	0.98	0.03
2007	YER046W-A		0.90	1.06	0.98	0.03
2008	YDR500C	RPL37B		0.98	0.98	0.03
2009	YBR188C	NTC20	0.98	0.97	0.98	0.03
2010	YDL057W		1.01	0.95	0.98	0.03
2011	YBR298C	MAL31	1.05	0.91	0.98	0.03
2012	YGL258W		0.95	1.01	0.98	0.03
2013	YBR076W	ECM8	0.94	1.02	0.98	0.03
2014	YDR033W	MRH1	0.99	0.97	0.98	0.03
2015	YHR076W	PTC7	0.97	0.99	0.98	0.03
2016	YNL321W		1.04	0.92	0.98	0.03
2017	YDR142C	PEX7	1.04	0.92	0.98	0.02
2018	YKL211C	TRP3	1.05	0.91	0.98	0.02
2019	YML059C	NTE1	0.99	0.97	0.98	0.02
2020	YMR169C	ALD3	1.00	0.96	0.98	0.02
2021	YCL016C	DCC1	0.90	1.06	0.98	0.02
2022	YJR148W	BAT2	0.98	0.98	0.98	0.02
2023	YDR102C		1.03	0.93	0.98	0.02
2024	YLR313C	SPH1	0.98	0.98	0.98	0.02
2025	YLR357W	RSC2		0.98	0.98	0.02

Rank	ORF	Gene	Normalized densitometry values			SCORE
			MATa	MATalpha	average	
2026	YJL181W		1.03	0.93	0.98	0.02
2027	YNL295W		1.01	0.95	0.98	0.02
2028	YER170W	ADK2	1.19	0.77	0.98	0.02
2029	YDR336W		1.12	0.84	0.98	0.02
2030	YCL050C	APA1	0.97	0.99	0.98	0.02
2031	YMR300C	ADE4	1.29	0.67	0.98	0.02
2032	YDR061W		0.91	1.05	0.98	0.02
2033	YNL068C	FKH2	1.04	0.92	0.98	0.02
2034	YER073W	ALD5	0.96	1.00	0.98	0.02
2035	YMR219W	ESC1	1.00	0.96	0.98	0.02
2036	YBR270C		0.94	1.03	0.98	0.02
2037	YMR152W	YIM1	0.98	0.98	0.98	0.02
2038	YLL013C	PUF3	0.90	1.07	0.98	0.02
2039	YER046W	SPO73	1.00	0.96	0.98	0.02
2040	YMR273C	ZDS1	0.99	0.97	0.98	0.02
2041	YBR242W		0.92	1.05	0.98	0.02
2042	YPR038W		0.98	0.99	0.98	0.02
2043	YHR182W		0.88	1.09	0.98	0.02
2044	YER188W		1.09	0.88	0.98	0.02
2045	YER096W	SHC1	0.96	1.01	0.98	0.02
2046	YNR007C	ATG3	1.23	0.73	0.98	0.02
2047	YLR286C	CTS1	0.98	0.98	0.98	0.02
2048	YDR218C	SPR28	1.01	0.95	0.98	0.02
2049	YDR191W	HST4	1.13	0.83	0.98	0.02
2050	YMR002W		0.93	1.03	0.98	0.02
2051	YLR396C	VPS33	0.86	1.10	0.98	0.02
2052	YER169W	RPH1	1.17	0.80	0.98	0.02
2053	YNL143C		0.95	1.02	0.98	0.02
2054	YPL050C	MNN9	1.01	0.95	0.98	0.02
2055	YHR103W	SBE22	1.04	0.93	0.98	0.02
2056	YHR150W	PEX28	0.91	1.06	0.98	0.02
2057	YHR112C		0.96	1.01	0.98	0.02
2058	YKL017C	HCS1	0.98	0.99	0.98	0.02
2059	YBR030W		0.91	1.05	0.98	0.02
2060	YIR038C	GTT1	0.99	0.98	0.98	0.02
2061	YDR436W	PPZ2	0.96	1.01	0.98	0.02
2062	YDR134C		1.12	0.85	0.98	0.02
2063	YER141W	COX15	0.88	1.09	0.98	0.02
2064	YNL286W	CUS2	1.07	0.90	0.98	0.02
2065	YMR087W		0.91	1.06	0.98	0.02
2066	YOR185C	GSP2	1.00	0.97	0.98	0.02
2067	YLR016C	PML1	0.96	1.01	0.98	0.02
2068	YJL049W		1.01	0.95	0.98	0.02
2069	YJL141C	YAK1	1.01	0.96	0.98	0.02

Rank	ORF	Gene	Normalized densitometry values			SCORE
			MATa	MATalpha	average	
2070	YPR043W	RPL43A	0.78	1.19	0.98	0.02
2071	YER002W	NOP16	0.88	1.08	0.98	0.02
2072	YLR079W	SIC1	0.91	1.06	0.98	0.02
2073	YER051W		0.92	1.05	0.98	0.02
2074	YAL046C		0.90	1.06	0.98	0.02
2075	YJL075C		1.07	0.90	0.98	0.02
2076	YOL027C	MDM38	0.65	1.32	0.98	0.02
2077	YPR115W		1.06	0.91	0.99	0.02
2078	YBR173C	UMP1	0.98	0.99	0.99	0.02
2079	YJL201W	ECM25	1.00	0.97	0.99	0.02
2080	YKR029C	SET3	0.99	0.98	0.99	0.02
2081	YML123C	PHO84	0.96	1.01	0.99	0.02
2082	YBR068C	BAP2	0.96	1.01	0.99	0.02
2083	YIL135C	VHS2	1.13	0.84	0.99	0.02
2084	YDL052C	SLC1	0.97	1.00	0.99	0.02
2085	YKL201C	MNN4	1.10	0.87	0.99	0.02
2086	YJL191W	RPS14B	0.91	1.06	0.99	0.02
2087	YPR138C	MEP3	1.05	0.92	0.99	0.02
2088	YBR134W		1.06	0.91	0.99	0.02
2089	YDR345C	HXT3	1.06	0.91	0.99	0.02
2090	YOR324C	FRT1	0.95	1.02	0.99	0.02
2091	YCR090C		0.91	1.06	0.99	0.02
2092	YMR156C	TPP1	1.09	0.88	0.99	0.02
2093	YOR307C	SLY41	0.92	1.06	0.99	0.02
2094	YIL028W		0.95	1.02	0.99	0.02
2095	YLR330W	CHS5	1.03	0.94	0.99	0.02
2096	YNR063W		1.05	0.92	0.99	0.02
2097	YNL093W	YPT53	1.07	0.91	0.99	0.02
2098	YIL153W	RRD1	0.78	1.19	0.99	0.02
2099	YEL065W	SIT1	0.83	1.14	0.99	0.02
2100	YMR306W	FKS3	1.17	0.80	0.99	0.02
2101	YPL147W	PXA1	0.96	1.02	0.99	0.02
2102	YHL026C		0.99	0.99	0.99	0.02
2103	YIL170W	HXT12	1.06	0.92	0.99	0.02
2104	YPL199C		1.03	0.95	0.99	0.02
2105	YMR040W		1.03	0.95	0.99	0.02
2106	YIL064W		1.01	0.96	0.99	0.02
2107	YGR209C	TRX2	0.96	1.02	0.99	0.02
2108	YGR007W	MUQ1	1.05	0.92	0.99	0.02
2109	YOR049C	RSB1	0.98	0.99	0.99	0.02
2110	YLR036C		1.06	0.92	0.99	0.02
2111	YLR014C	PPR1	0.90	1.08	0.99	0.02
2112	YDR320C	SWA2	0.87	1.10	0.99	0.02
2113	YAL034C	FUN19	0.95	1.03	0.99	0.02

Rank	ORF	Gene	Normalized densitometry values			SCORE
			MATa	MATalpha	average	
2114	YCR085W		1.01	0.97	0.99	0.02
2115	YFR030W	MET10	0.95	1.03	0.99	0.02
2116	YDL133C-A	RPL41B	0.91	1.06	0.99	0.02
2117	YOL088C	MPD2	0.93	1.05	0.99	0.02
2118	YOR213C	SAS5	1.05	0.93	0.99	0.02
2119	YOR112W		0.93	1.05	0.99	0.02
2120	YBL075C	SSA3	1.02	0.96	0.99	0.02
2121	YNR068C			0.99	0.99	0.02
2122	YJL151C	SNA3	0.96	1.02	0.99	0.02
2123	YDR056C		0.99	0.99	0.99	0.02
2124	YDL123W	SNA4	0.99	0.99	0.99	0.02
2125	YLR431C	ATG23	0.79	1.19	0.99	0.01
2126	YLR287C-A	RPS30A		0.99	0.99	0.01
2127	YPL176C		1.09	0.89	0.99	0.01
2128	YHL041W		1.07	0.91	0.99	0.01
2129	YMR135C	GID8	1.16	0.82	0.99	0.01
2130	YPL182C		1.08	0.90	0.99	0.01
2131	YPL272C		0.99	0.99	0.99	0.01
2132	YPL052W	OAZ1	0.82	1.16	0.99	0.01
2133	YPL116W	HOS3	0.93	1.06	0.99	0.01
2134	YNL330C	RPD3	0.99		0.99	0.01
2135	YOL032W		0.90	1.08	0.99	0.01
2136	YER183C	FAU1	1.06	0.92	0.99	0.01
2137	YER089C	PTC2	1.04	0.94	0.99	0.01
2138	YGL114W		0.94	1.04	0.99	0.01
2139	YDR258C	HSP78	1.03	0.95	0.99	0.01
2140	YBR177C	EHT1	1.07	0.91	0.99	0.01
2141	YDR077W	SED1	1.00	0.98	0.99	0.01
2142	YJL051W		1.06	0.92	0.99	0.01
2143	YNL141W	AAH1	0.89	1.09	0.99	0.01
2144	YDL203C		0.92	1.06	0.99	0.01
2145	YOR225W		0.91	1.07	0.99	0.01
2146	YJL013C	MAD3	1.09	0.89	0.99	0.01
2147	YGL085W		0.98	1.00	0.99	0.01
2148	YLL042C	ATG10	0.86	1.12	0.99	0.01
2149	YPR071W		0.85	1.13	0.99	0.01
2150	YER045C	ACA1	0.96	1.02	0.99	0.01
2151	YGR021W		1.05	0.94	0.99	0.01
2152	YLL032C		0.98	1.00	0.99	0.01
2153	YOL084W	PHM7	0.98	1.00	0.99	0.01
2154	YOL042W	NGL1	0.97	1.02	0.99	0.01
2155	YHR125W		0.89	1.09	0.99	0.01

Rank	ORF	Gene	Normalized densitometry values			SCORE
			MATa	MATalpha	average	
2156	YIL121W	QDR2	0.82	1.17	0.99	0.01
2157	YER057C	HMF1	0.94	1.04	0.99	0.01
2158	YOR069W	VPS5	0.91	1.07	0.99	0.01
2159	YGR086C	PIL1	1.02	0.96	0.99	0.01
2160	YBR165W	UBS1	0.96	1.03	0.99	0.01
2161	YGR018C		1.17	0.82	0.99	0.01
2162	YPL105C		0.97	1.02	0.99	0.01
2163	YBR269C		1.02	0.96	0.99	0.01
2164	YCL069W	VBA3	0.90	1.09	0.99	0.01
2165	YOR079C	ATX2	0.93	1.06	0.99	0.01
2166	YBR239C		1.00	0.99	0.99	0.01
2167	YDR078C	SHU2	0.97	1.01	0.99	0.01
2168	YGL004C	RPN14	1.12	0.87	0.99	0.01
2169	YNL303W		0.91	1.08	0.99	0.01
2170	YPR125W		0.95	1.03	0.99	0.01
2171	YNR073C		1.03	0.96	0.99	0.01
2172	YEL046C	GLY1	0.88	1.11	0.99	0.01
2173	YHR127W		0.99	1.00	0.99	0.01
2174	YMR153W	NUP53	1.11	0.88	0.99	0.01
2175	YGR001C		0.99	1.00	0.99	0.01
2176	YCR098C	GIT1	0.87	1.12	0.99	0.01
2177	YDL079C	MRK1	1.02	0.97	0.99	0.01
2178	YBR133C	HSL7		0.99	0.99	0.01
2179	YER063W	THO1	0.96	1.03	0.99	0.01
2180	YNL193W		1.05	0.94	0.99	0.01
2181	YML108W		0.91	1.08	0.99	0.01
2182	YDR420W	HKR1	0.97	1.02	0.99	0.01
2183	YOR097C		0.94	1.05	0.99	0.01
2184	YLR406C	RPL31B	1.02	0.97	0.99	0.01
2185	YIL058W		1.05	0.94	0.99	0.01
2186	YIL040W	APQ12	0.94	1.04	0.99	0.01
2187	YMR201C	RAD14	1.00	0.99	0.99	0.01
2188	YHL007C	STE20		0.99	0.99	0.01
2189	YKR080W	MTD1	0.97	1.02	0.99	0.01
2190	YNL334C	SNO2	1.00	0.99	0.99	0.01
2191	YGR134W	CAF130	0.96	1.03	0.99	0.01
2192	YKR005C		1.05	0.94	0.99	0.01
2193	YGR193C	PDX1	1.12	0.87	0.99	0.01
2194	YDL049C	KNH1	1.01	0.98	0.99	0.01
2195	YDL065C	PEX19	1.08	0.91	0.99	0.01
2196	YDR220C		1.09	0.90	0.99	0.01
2197	YGL125W	MET13	0.99		0.99	0.01
2198	YDL124W		1.00	0.99	0.99	0.01
2199	YGR032W	GSC2	1.02	0.97	0.99	0.01

Rank	ORF	Gene	Normalized densitometry values			SCORE
			MATa	MATalpha	average	
2200	YPL177C	CUP9	1.17	0.82	0.99	0.01
2201	YLR020C	YEH2	0.99	1.00	0.99	0.01
2202	YBR099C		1.01	0.98	1.00	0.01
2203	YIR043C		0.93	1.06	1.00	0.01
2204	YOL089C	HAL9	1.02	0.97	1.00	0.01
2205	YLR344W	RPL26A	1.05	0.94	1.00	0.01
2206	YNL194C		0.97	1.02	1.00	0.01
2207	YLR376C	PSY3	0.89	1.10	1.00	0.01
2208	YGL159W		0.96	1.03	1.00	0.01
2209	YLR019W	PSR2	1.02	0.97	1.00	0.01
2210	YCR107W	AAD3	1.03	0.96	1.00	0.01
2211	YBR288C	APM3	0.91	1.09	1.00	0.01
2212	YDL040C	NAT1	0.98	1.01	1.00	0.01
2213	YPL098C	MGR2	0.93	1.06	1.00	0.01
2214	YDL240W	LRG1	1.04	0.95	1.00	0.01
2215	YDR285W	ZIP1	0.96	1.03	1.00	0.01
2216	YAL024C	LTE1	0.98	1.02	1.00	0.01
2217	YIR035C		0.98	1.01	1.00	0.01
2218	YBL066C	SEF1	1.00		1.00	0.01
2219	YOR015W		1.03	0.96	1.00	0.01
2220	YBR199W	KTR4	1.05	0.94	1.00	0.01
2221	YER049W		0.99	1.01	1.00	0.01
2222	YML011C		1.02	0.97	1.00	0.01
2223	YBR218C	PYC2	1.01	0.99	1.00	0.01
2224	YGL063W	PUS2	0.96	1.03	1.00	0.01
2225	YMR190C	SGS1	1.00		1.00	0.01
2226	YMR279C		1.07	0.92	1.00	0.01
2227	YDL094C		0.88	1.11	1.00	0.01
2228	YEL020C		1.14	0.86	1.00	0.01
2229	YDL125C	HNT1	0.99	1.00	1.00	0.01
2230	YIL052C	RPL34B	0.73	1.26	1.00	0.01
2231	YMR237W		1.06	0.93	1.00	0.01
2232	YDR502C	SAM2	1.15	0.85	1.00	0.01
2233	YDL019C	OSH2	1.01	0.99	1.00	0.01
2234	YOR222W	ODC2	0.97	1.02	1.00	0.01
2235	YGL050W		1.06	0.94	1.00	0.01
2236	YBR101C	FES1		1.00	1.00	0.01
2237	YGL132W		0.90	1.09	1.00	0.01
2238	YKR003W	OSH6	1.02	0.97	1.00	0.01
2239	YJR149W		1.11	0.89	1.00	0.01
2240	YER090W	TRP2	0.98	1.01	1.00	0.01
2241	YKL061W		1.01	0.98	1.00	0.01
2242	YDL074C	BRE1	1.00	0.99	1.00	0.01
2243	YDL089W		0.93	1.07	1.00	0.01

Rank	ORF	Gene	Normalized densitometry values			SCORE
			MATa	MATalpha	average	
2244	YOL037C		1.02	0.98	1.00	0.01
2245	YNR064C		0.99	1.00	1.00	0.01
2246	YHL012W		0.93	1.06	1.00	0.01
2247	YNL175C	NOP13	0.92	1.08	1.00	0.01
2248	YHR061C	GIC1	1.03	0.97	1.00	0.01
2249	YGR059W	SPR3	1.11	0.89	1.00	0.01
2250	YJL140W	RPB4	1.00		1.00	0.01
2251	YPR118W		0.99	1.01	1.00	0.01
2252	YOL029C		1.07	0.92	1.00	0.01
2253	YKL015W	PUT3	1.00	1.00	1.00	0.01
2254	YLR185W	RPL37A	0.90	1.10	1.00	0.01
2255	YKR010C	TOF2	0.91	1.08	1.00	0.01
2256	YKL161C		1.01	0.99	1.00	0.01
2257	YOR214C		1.09	0.91	1.00	0.01
2258	YDL027C		1.13	0.87	1.00	0.01
2259	YAR015W	ADE1	1.04	0.96	1.00	0.01
2260	YKL068W	NUP100	0.88	1.12	1.00	0.01
2261	YKR102W	FLO10	0.93	1.07	1.00	0.01
2262	YLR271W		1.01	0.98	1.00	0.01
2263	YNL139C	RLR1	1.00		1.00	0.01
2264	YBR195C	MSI1	1.02	0.97	1.00	0.01
2265	YBR016W		1.01	0.99	1.00	0.01
2266	YJL162C	JJJ2	1.00	0.99	1.00	0.01
2267	YLR077W		0.96	1.04	1.00	0.01
2268	YER135C		1.02	0.97	1.00	0.01
2269	YHR106W	TRR2	1.08	0.92	1.00	0.01
2270	YJL196C	ELO1	0.98	1.02	1.00	0.01
2271	YER035W	EDC2	0.99	1.01	1.00	0.01
2272	YJR020W		0.82	1.18	1.00	0.01
2273	YDR403W	DIT1	1.05	0.95	1.00	0.01
2274	YOR384W	FRE5	1.09	0.91	1.00	0.01
2275	YHR104W	GRE3	1.19	0.81	1.00	0.01
2276	YAL014C	SYN8	1.06	0.94	1.00	0.00
2277	YPL099C		0.92	1.08	1.00	0.00
2278	YOR248W		1.03	0.97	1.00	0.00
2279	YBR041W	FAT1	1.01	0.99	1.00	0.00
2280	YEL030W	ECM10	0.96	1.04	1.00	0.00
2281	YGL118C		1.13	0.87	1.00	0.00
2282	YHR057C	CPR2	0.96	1.04	1.00	0.00
2283	YLR334C		1.03	0.97	1.00	0.00
2284	YML051W	GAL80	0.86	1.14	1.00	0.00
2285	YIL149C	MLP2	0.98	1.02	1.00	0.00
2286	YER030W		1.09	0.91	1.00	0.00
2287	YOR133W	EFT1	0.90	1.10	1.00	0.00

Rank	ORF	Gene	Normalized densitometry values			SCORE
			MATa	MATalpha	average	
2288	YNL278W	CAF120	1.04	0.96	1.00	0.00
2289	YDR055W	PST1	1.10	0.90	1.00	0.00
2290	YER091C-A		1.07	0.93	1.00	0.00
2291	YPL123C	RNY1	1.07	0.93	1.00	0.00
2292	YJR130C	STR2	0.94	1.06	1.00	0.00
2293	YOR355W	GDS1	0.96	1.04	1.00	0.00
2294	YBR021W	FUR4	0.88	1.12	1.00	0.00
2295	YKR060W	UTP30	1.01	0.99	1.00	0.00
2296	YJL084C		1.06	0.94	1.00	0.00
2297	YJR038C		0.98	1.02	1.00	0.00
2298	YER062C	HOR2	0.99	1.02	1.00	0.00
2299	YOR092W	ECM3	0.94	1.07	1.00	0.00
2300	YHL028W	WSC4	0.97	1.03	1.00	0.00
2301	YPL040C	ISM1	1.04	0.96	1.00	0.00
2302	YLR363C	NMD4	0.82	1.19	1.00	0.00
2303	YEL010W		1.09	0.92	1.00	0.00
2304	YBR205W	KTR3	1.00	1.01	1.00	0.00
2305	YBR178W		1.15	0.86	1.00	0.00
2306	YKR012C		1.01	0.99	1.00	0.00
2307	YBR093C	PHO5	1.19	0.81	1.00	0.00
2308	YLR194C		0.94	1.07	1.00	0.00
2309	YBR187W		0.94	1.06	1.00	0.00
2310	YOR053W		1.08	0.93	1.00	0.00
2311	YGR286C	BIO2	0.97	1.03	1.00	0.00
2312	YNR060W	FRE4	0.93	1.07	1.00	0.00
2313	YDL115C	IWR1	1.08	0.92	1.00	0.00
2314	YBR056W		0.99	1.02	1.00	0.00
2315	YPL097W	MSY1	1.00		1.00	0.00
2316	YDR428C		1.08	0.92	1.00	0.00
2317	YML005W	TRM12	1.13	0.88	1.00	0.00
2318	YBR210W	ERV15	1.02	0.98	1.00	0.00
2319	YER132C	PMD1	1.02	0.99	1.00	0.00
2320	YOR322C	LDB19	1.07	0.94	1.00	0.00
2321	YDR488C	PAC11	1.03	0.98	1.00	0.00
2322	YEL028W		1.01	1.00	1.00	0.00
2323	YMR133W	REC114	1.13	0.87	1.00	0.00
2324	YNL031C	HHT2	1.06	0.95	1.00	0.00
2325	YGR012W		1.03	0.97	1.00	0.00
2326	YOL090W	MSH2	1.00		1.00	0.00
2327	YFR046C	CNN1	1.02	0.99	1.00	0.00
2328	YPL086C	ELP3	1.00		1.00	0.00
2329	YKL142W	MRP8	1.09	0.91	1.00	0.00
2330	YDR066C		1.08	0.92	1.00	0.00

Rank	ORF	Gene	Normalized densitometry values			SCORE
			MATa	MATalpha	average	
2331	YPR195C		1.02	0.99	1.00	0.00
2332	YDR135C	YCF1	1.08	0.93	1.00	0.00
2333	YBR297W	MAL33	1.02	0.98	1.00	0.00
2334	YPR076W		0.98	1.03	1.00	0.00
2335	YMR299C	DYN3	1.17	0.84	1.00	0.00
2336	YIL050W	PCL7	1.02	0.99	1.00	0.00
2337	YML007W	YAP1	0.94	1.06	1.00	0.00
2338	YHL030W	ECM29	0.95	1.06	1.00	0.00
2339	YMR210W		1.01	1.00	1.00	0.00
2340	YPL144W		1.11	0.90	1.00	0.00
2341	YGL232W	TAN1	1.03	0.98	1.00	0.00
2342	YCR027C	RHB1	0.94	1.07	1.00	0.00
2343	YGR236C	SPG1	1.00	1.01	1.00	0.00
2344	YMR015C	ERG5	0.90	1.11	1.00	0.00
2345	YDR046C	BAP3	1.02	0.99	1.00	0.00

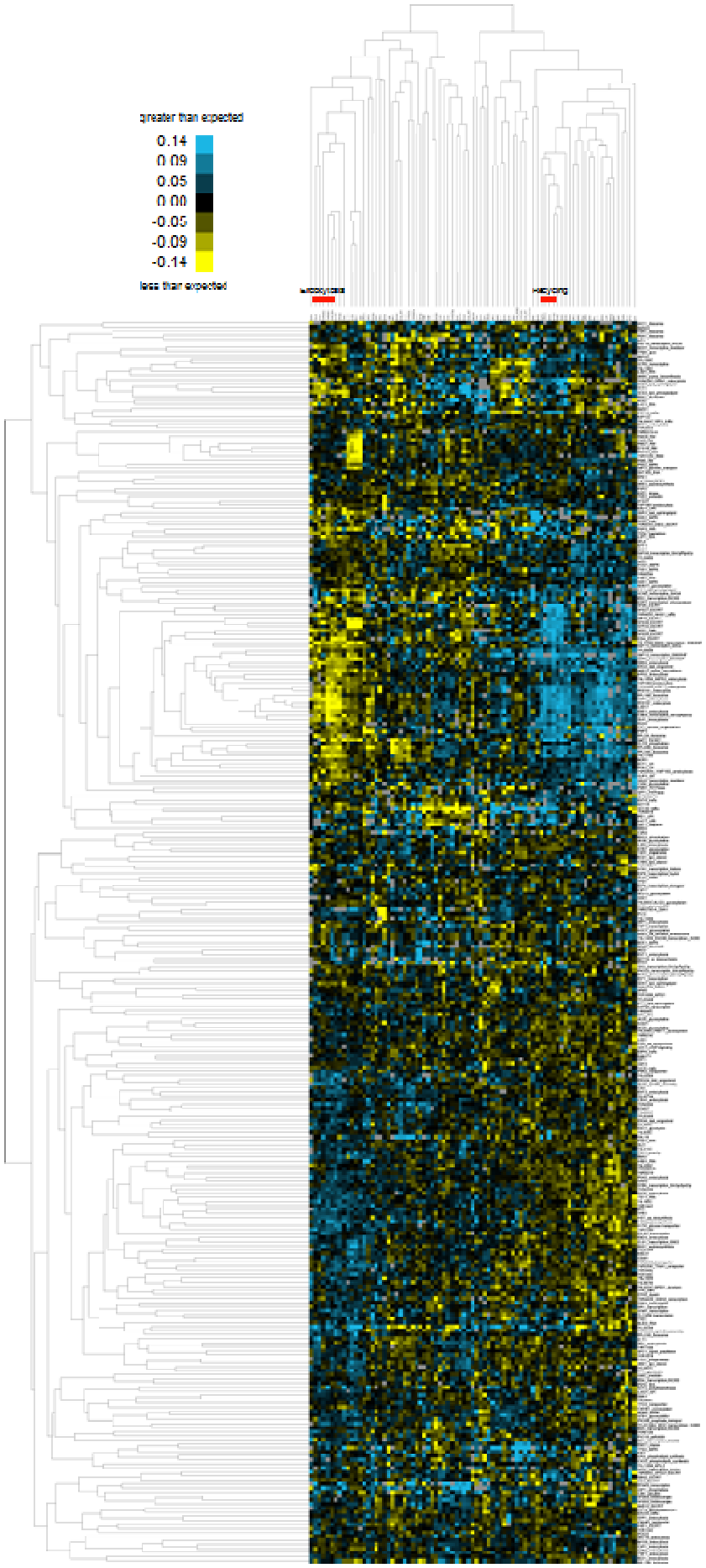
greater than expected
0.14
0.09
0.05
0.00
-0.05
-0.09
-0.14
less than expected
wood pulse
Heiyong

Figure A1. Full hierarchical clustering of the genetic interaction data.

Hierarchical clustering of normalized, median-centered invertase activity values of double mutant strains generated by crossing top-scoring mutants from the primary screen (array genes, y axis) to a diverse set of 81 trafficking mutants (query genes, x axis). Although 374 top-scoring mutants were used for the crosses, the heat map shows only the 307 array genes for which reliable double mutant data were obtained. Yellow indicates lower than expected levels of GSS at the cell surface, whereas blue indicates higher than expected levels. Red bars indicate representative query genes with known roles in endocytosis or recycling.

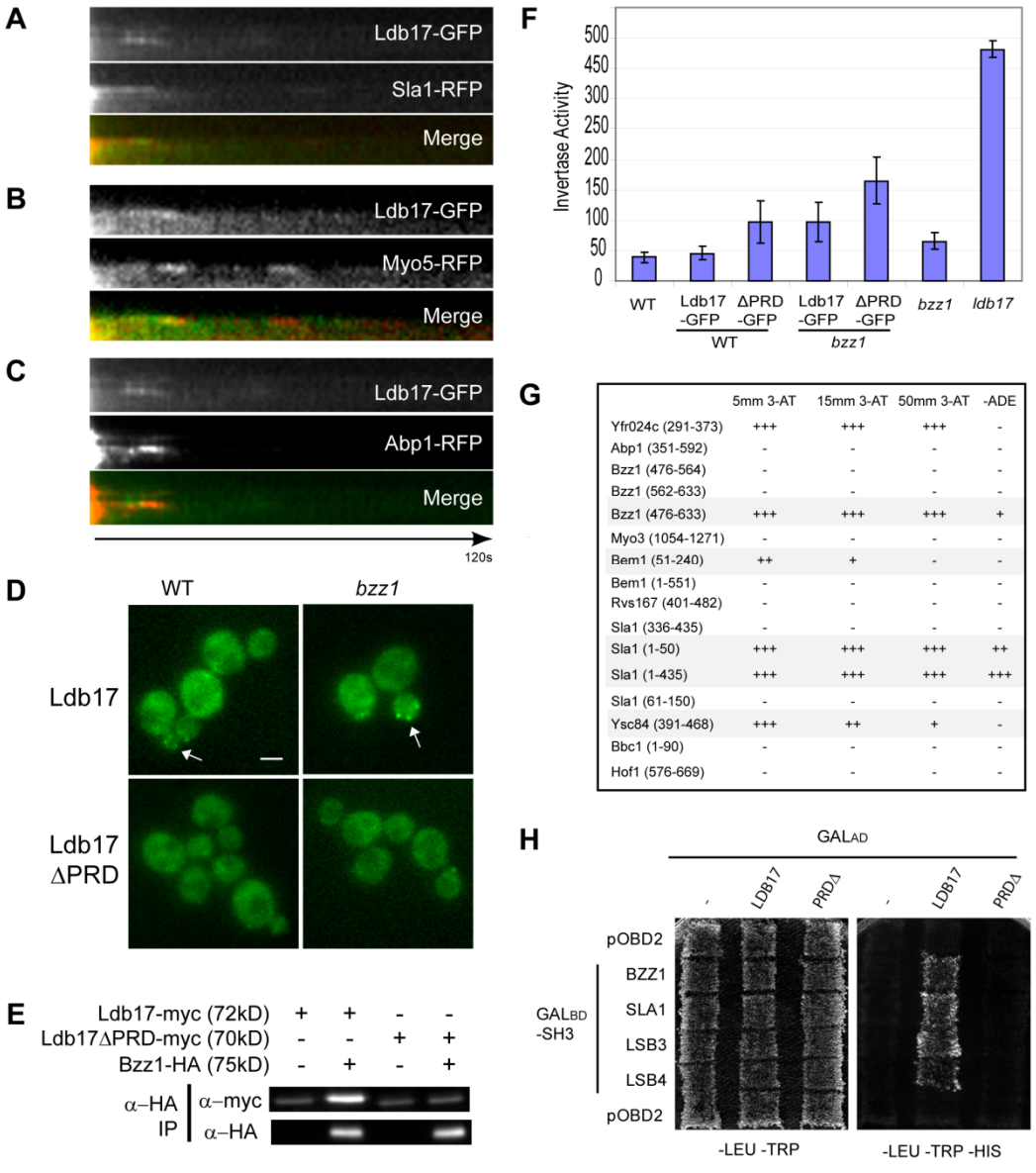

Figure A2. Characterization of LDB17 mutants and identification of Ldb17-interacting proteins. (A–C) Kymograph representations of Ldb17-GFP relative to markers Sla1-RFP **(A)**, Myo5-RFP **(B)**, and Abp1-RFP **(C)** at cortical patches over 120 s. **(D)** Localization of Ldb17-GFP and ldb17ΔPRD in wild-type (WT) and bzz1 cells. Bar, 2 µm. **(E)** Ldb17 interacts with the syndapin homologue Bzz1 through a C-terminal PRD. Proteins were immunoprecipitated from cells expressing Ldb17-myc, ldb17DPRD-myc, and/or Bzz1-HA with a-HA antibodies and detected by immunoblot analysis with either a-HA or a-myc. **(F)** Loss of the Ldb17 PRD or Bzz1 increases cell surface levels of the GSS reporter, as measured by liquid assay. Invertase activity is expressed as nanomole glucose

released per OD600 (mean of at least three experiments ± SD). **(G)** Summary of yeast two-hybrid interactions between Ldb17-GAL4AD and the 16 different SH3 domain–GAL4BD fusions. Interactions between Ldb17 and SH3 domains from Bzz1, Sla1, Ysc84/Lsb4, and Yfr024c/Lsb3 resulted in strong activation of the HIS3 reporter (resistant to 50 mM 3-AT). **(H)** PRD dependence of the yeast two-hybrid interactions. Diploid strains containing GALAD and GALBD plasmids are shown on the left; activation of the HIS3 reporter is shown on the right.

APPENDIX B: Supplemental material (chapter 3)

Table B.1. Plasmids and yeast strains used in this study

Type	Name	Description/Genotype	Source
yeast strain	LCY858	can1::SRE2pr-LEU2 *lyp1Δ cyh2 his3Δ1 leu2Δ0 ura3Δ0 met15Δ0* LYS2+	this study
yeast strain	LCY1156	LC858 *apm1Δ::NAT*	this study
yeast strain	LCY1154	LC858 *apm2Δ::NAT*	this study
yeast strain	LCY1155	LC858 *ap14Δ::NAT*	this study
yeast strain	LCY1141	LC858 *yap1801Δ::NAT*	this study
yeast strain	BY4741	MATa *his3-1 leu2-0 ura3-0*	this study
yeast strain	LC1994	BY4741 Apm2::GFP(HIS)	this study
yeast strain	LCY1979	BY4741 Apm4::GFP(HIS) Clc1::RFP(NAT)	this study
yeast strain	LCY1977	LCY1994 Clc1::RFP(NAT)	this study
yeast strain	HBY155	LC1979 *sla2Δ*	this study
yeast strain	LCY1978	LC1977 *sla2Δ*	this study
yeast strain	LCY1997	BY4741 Apm2::GFP(HIS3) Clc1::RFP(NAT)	this study
yeast strain	CTY708	BY4741 Apm1::RFP(KAN) Apm2::GFP(HIS3)	this study
yeast strain	CTY603	BY4741 Apm1::RFP(KAN) Ima1::GFP(HIS3)	this study
yeast strain	LCY2439	BY4741 Ima1::GFP(HIS3) Clc1::RFP(NAT)	this study
yeast strain	LCY1230	BY4741 *chs6Δ::NAT*	this study
yeast strain	LCY3168	1230 *apl2Δ::KAN*	this study
yeast strain	LCY3167	1230 *apm1Δ::KAN*	this study
yeast strain	LCY3170	1230 *apm2Δ::KAN*	this study
yeast strain	LCY3202	1230 *apm2Δ::KAN apm1Δ::URA*	this study
yeast strain	LCY3169	1230 *ima1Δ::KAN*	this study

Type	Name	Description/Genotype	Source
yeast strain	LCY3203	1230 *ima1Δ::KAN apm2Δ::URA*	this study
yeast strain	LCY3204	BY4741 + pNAT	this study
yeast strain	CTY301	Ima1-GFP(HIS3)	this study
yeast strain	CTY564	Ima1-GFP(HIS3) Apl4::3HA(KAN)	this study
yeast strain	CTY574	Ima1::GFP(HIS3) Apl4N::HA(KAN)	this study
yeast strain	CTY265	Ima1::GFP(HIS3) Apm1::3HA(KAN)	this study
yeast strain	CTY661	Ima1::GFP(HIS3) Apm2::3HA(KAN)	this study
yeast strain	pj694a	MAT**a** *trp1-901 leu2-3,112 ura3-52 his3-200 gal4Δ gal80Δ LYS::GAL1-HIS3 GAL2-ADE2 met2::GAL7-lacZ*	James et al., 1996[a]
yeast strain	pj694alpha	MATalpha *trp1-901 leu2-3,112 ura3-52 his3-200 gal4Δ gal80Δ LYS::GAL1-HIS3 GAL2-ADE2 met2::GAL7-lacZ*	James et al., 1996[a]
yeast strain	HBY536	pj694alpha pOBD2-Apm2	this study
yeast strain	HBY544	pj694alpha pOBD2-Apm2 (246-605)	this study
yeast strain	HBY625	pj694alpha pOBD2-Apm2 (391-605)	this study
yeast strain	NR	pj694alpha pOBD2-Apm2 (389-582)	this study
yeast strain	CTY188	pj694a pOAD-Apl4	this study
yeast strain	HBY539	pj694a pOAD-Ima1	this study
yeast strain	HBY626	pj694a pOAD-Mut5N (1-262)	this study
yeast strain	HBY463	LCY1994 *imaΔ::NAT*	this study
yeast strain	HBY567	BY4741 Apm2::3HA(KAN)	this study
yeast strain	HBY688	BY4741 Ima1::3HA(KAN)	this study
yeast strain	LCY2210	BY4741 Ima1::GFP(HIS3) *erg6Δ::NAT*	this study
yeast strain	CTY286	BY4741 Apl2::GFP(HIS3) *erg6Δ::NAT*	this study

Type	Name	Description/Genotype	Source
yeast strain	HB577	BY4741 + GFP-Snc1-Suc2::SUC2	The GSS reporter plasmid pCS30 was linearized with XbaI and integrated at the SUC2 locus.
yeast strain	SEY6210	MAT**a** *leu2-3,112 ura3-52 his3-Δ200 trp1-Δ901 lys2-801 suc2-Δ9 Met-*	S. Emr
yeast strain	HBY596	SEY6210 GFP::SNC1(URA)	this study
plasmid	pGST-Ima1		Open Biosystems
plasmid	pBG1805		Open Biosystems
plasmid	pNR1	pRS415-IMA1	this study
plasmid	pNR3	pRS415-IMA^{CM}	this study
plasmid	pLC1329	pSec7-DsRed(URA)	this study
plasmid	pOAD	Uetz et al., 2000	gift from Stan Fields
plasmid	pOBD2	Uetz et al., 2000	gift from Stan Fields
plasmid	pCS7	SNC1-GFP in pRS316	Schluter et al., 2008[b]
plasmid	pCS30	GFP-SNC1-SUC2 in pRS306 (GSS; TPI1 promoter)	Sequences from pGS (Lewis et al., 2000)[c] were PCR-amplified to introduce a SmaI site before the Snc1 stop codon, and subcloning this into XhoI/SmaI-digested pRS306. The resulting plasmid was digested with XbaI/SmaI, end-filled, and ligated to SUC2 sequences on a SmaI-HpaI fragment from pSEYC306 (Darsow et al., 2000)[d]
plasmid	pPPL92	pGST-SNC1	gift from Anne Spang

[a] James, P., Halladay, J. & Craig, E. A. (1996) Genomic libraries and a host strain designed for highly efficient two- hybrid selection in yeast. Genetics 144: 1425-1436

[b] Schluter et al. Global analysis of yeast endosomal transport identifies the vps55/68 sorting complex. Mol Biol Cell (2008) vol. 19 (4) pp. 1282-94

[c] Lewis et al. Specific retrieval of the exocytic SNARE Snc1p from early yeast endosomes. Mol.Biol.Cell (2000) vol. 11 (1) pp. 23-38

[d] Darsow et al. Invertase fusion proteins for analysis of protein trafficking in yeast. Meth Enzymol (2000) vol. 327 pp. 95-106